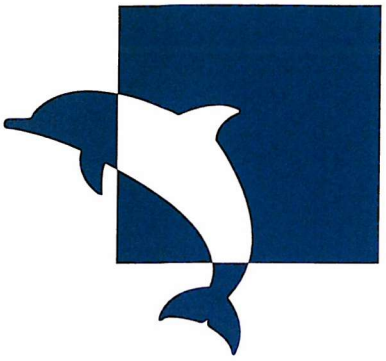

University of Southampton

An investigation into the surface properties and biological performance of treated Ti-6Al-4V alloy

PhD thesis

Ching-Hsin Ku

University of Southampton

SO17 1BJ, UK

Engineering Materials

Bioengineering Sciences Research Group

University of Southampton

Faculty of Engineering and Applied Science
Engineering Materials

Thesis submitted for the Degree of Doctor of Philosophy

An investigation into the surface properties and biological performance of treated Ti-6Al-4V alloy

By Ching-Hsin Ku

September 2001

UNIVERSITY OF SOUTHAMPTON

ABSTRACT

FACULTY OF ENGINEERING AND APPLIED SCIECNE

ENGINEERING MATERIALS

Doctor of Philosophy

AN INVESTIGATION INTO THE SURFACE PROPERTIES AND BIOLOGICAL PERFORMANCE OF TREATED Ti-6Al-4V ALLOY

By Ching-Hsin Ku

Previous research has demonstrated the effectiveness of applying a simple ageing treatment over the ASTM standard passivation treatment to reduce metal ion release from Ti-6Al-4V alloy into bovine serum solution. The present study aims to further understand the mechanisms behind the improved dissolution resistance exhibited by the aged Ti-6Al-4V alloy using a number of sophisticated surface analysis techniques, X-ray photoelectron spectroscopy and atomic force microscopy. Furthermore, osteoblastic cell culture and functional genomic studies have been employed to fully characterise the biological performance of the treated implants.

This study has demonstrated that the passivation treatment results in the elimination of vanadium from the oxide layer. The O/Ti ratio of the passivated sample significantly changes with immersion time in serum, indicating that further oxidation and dissolution processes were occurring. In contrast, the aged oxide surface is more stable and possesses hydroxylated groups, which are thought to play an important role in the reaction with serum proteins. In addition, this research has observed that the side effects of Al_2O_3 grit-blasting and heat treatment associated with the hydroxyapatite plasma-spraying coating cause the change in the Al% surface composition and the loss of chemisorbed H_2O groups; this in turn, affects the metal ion dissolution behaviour of the treated implant. Furthermore, a potentiodynamic test was used to assess the nature of the passive film; the aged surface showed better dissolution resistance and was less affected by bovine serum solution than other treatments.

No difference in cell viability/proliferation/morphology was apparent between the different surface treatments in a short-term test (less than 72 hours). In a long-term test (more than 72 hours up to 4 weeks), a higher cell proliferation was observed on the aged sample compared to the passivated and the control samples. In contrast, there was an accelerated alkaline phosphatase activity (ALP) on the control sample; this suggests that the early increase in ALP activity for the control sample could be a compensatory effect of decreased osteoblasts proliferation. Recent advances in functional genomic technology (cDNA microarray technology or called "genocompatibility") allow the investigation of gene regulation events from a great number of data to interpret the cell differentiation progression and the possible apoptotic pathways followed by metal ion release. It has been demonstrated that metal ion release delays the time course of gene expression in the focal adhesion kinase pathway and this may affect the cell proliferation and differentiation progression. Furthermore, it is proposed that the Bax pathway (via mitochondria) may play an important role in the apoptotic cell death, especially for metal ion release.

Based on the findings of this study the aged surface has demonstrated much improved dissolution resistance, which is reflected in its biological performance. Moreover, the genocompatibility test is introduced in this study to complement existing biocompatibility tests and to provide further detailed information on cell-implant interface reactions.

TABLE OF CONTENTS

LIST OF TABLES

LIST OF FIGURES

LIST OF APPENDICES

Acknowledgements

I would like to acknowledge the exceptional guidance, invaluable supervision and bountiful support given by Professor Peter J. Gregson, Dr. Martin Browne in the University of Southampton, Southampton, UK and Dr. Dominique P. Pioletti in EFPL, Lausanne, Switzerland (CH) as the supervisors and beyond. The advice of Dr. Julian Walton (Southampton) with the potentiodynamic tests is gratefully acknowledged. The technical assistance of Mr. Dave Beckett, Mr. Eric Bonner is also acknowledged. The helpful assistance of my colleagues Dr. Yigeng Xu, Mrs Sue Walker (Southampton), Mr. Martin Zulliger, Mr. Mathews Jacob, Mr. Bastian Peter, Mrs Arlette Kottelat (Lausanne, CH) on various matters is appreciated.

This research is supported by Taiwanese government scholarship for the graduated students of National Taiwan University studying in the University of Southampton, the faculty of Engineering and Applied Science, and Hôpital Orthopédique de la Suisse Romande, Switzerland for me, which is gratefully acknowledged.

I also would like to give my thanks to my friends Joyce, Doris, Pat, Diane, Dave & Ros, Eric & Lyne, Val (my landlady), Kunle, Vincent, Sam, Linda, Jessica, Yvonne (at Southampton), Anne (at Wellington), Nick & Ailie (at Gosport), Jonathon & Marie-Jeanne Castro (at Lausanne), John & Shirley (at Geneva) for your support and affection.

I also give my love and thanks to my parents, my brothers and sister-in-law. Thank you so much for your constant support and endless love. Without you, I cannot finish my study.

Indeed, I would like to give my blessing in Jesus Christ to you whosoever help me in visible or invisible way during the past years. "*The grace of the Lord Jesus Christ and the love of God and the fellowship of the Holy Spirit be with you all-2 Corinthians 13:14*".

Chapter 1 Introduction

1.1 Background

In 1975 Hench and Ethridge proposed [1] "An ideal implant material must have a dynamic surface chemistry that induces histological changes at the implant surface which normally occur if the implant were not present." According to this theory, there are two parallel directions of biomaterial research and development, which may be addressed: (1) Molecular tailoring of compositions and surfaces to match the biochemical requirements of the replaced tissues. (2) Microstructure design of materials to match the biomechanical requirements of natural host tissues. In order to fulfil these requirements, the following important items should be considered: mechanical characteristics, corrosion resistance and biocompatibility. Therefore, the choice of suitable metallic biomaterials is limited [2]. Of the currently used metallic materials such as CoCr-alloys, commercially pure (cp)-Ti, titanium alloys, cp-niobium, cp-tantalum, stainless steels, etc., titanium and its alloys can possibly offer the best combination of properties. Indeed, titanium and its alloys are finding increasing use in medical devices, including heart valves, cardiac pacemakers, bone plates, artificial joints, and dental implants [3].

In recent years, one of the major research areas in biomaterials has been in the area of surface science since it plays a fundamental role in controlling the biocompatibility of materials [4]. If we consider the biomaterial/tissue interface (Figure 1-1), the surface oxide layer provides a barrier between the biological system and the implant's metallic substrate. One of the problems associated with the implantation of a metallic component is metal ion release. This occurs due to a number of degradation processes that range from simple electrochemical dissolution to mechanical wear of articulating surfaces [5]. These problems are inherent due to the nature of use of metallic implants. Dissolution of the material becomes localised in nature and progresses at rates that

depend on the material's surface properties, composition, location and time of implantation. Since the oxide layer is the main barrier to attack, its characteristics are of great importance in the prevention of localised attack.

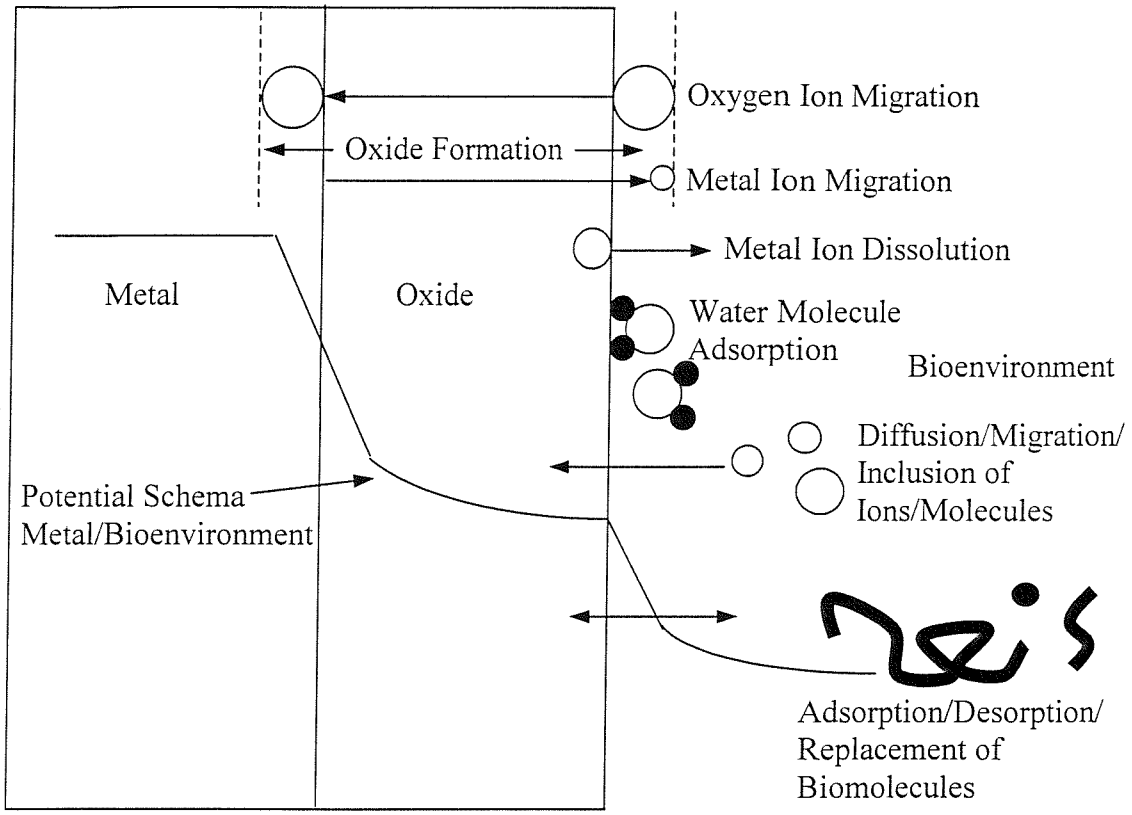

Figure 1-1 Processes and interactions occurring at the metal oxide/bioenvironment interface [6].

There are two possible ways in which the biocompatibility of titanium-based implants may be improved. One is to improve the stability of the oxide layer by creating inert oxide layers. The ASTM-F86 standard passivation (nitric acid) treatment has been used for this purpose. However, this treatment has actually been observed to increase Ti, Al, and V trace element release from Ti-6Al-4V[1] [7]. Previous work has investigated metal ion dissolution from Ti-6Al-4V implants in a simulated physiological environment (bovine serum solution); this has demonstrated that the passivated treatment followed by ageing in boiling distilled deionised water is an effective method for reducing metal

[1] Ti-6Al-4V: 90 wt% of Ti, 6 wt% of Al and 4 wt% of V.

ion release from a Ti-6Al-4V alloy implant surface [8]. Therefore, in controlling the characteristics of the surface oxide, the metal ion release behaviour of the materials may be optimised.

A second method of improving biocompatibility is to incorporate the main components of surrounding tissue, such as hydroxyapatite (HA) ($Ca_{10}(PO_4)_6(OH)_2$) on the implant surface. HA coatings have been shown to enhance osseointegration of metal prostheses [9] [10] [11] [12] and when applied onto metal substrates may also reduce the metal ion release, simply by acting as physical barriers [13]. However, it has been found that the HA-coating may alter the stability of the passivated film, the composition of metal surface and the metal ion release behaviour through the formation of the new compounds during plasma-spraying or via calcium and phosphate ion release as a result of degradation of the coating [13] [14] [15]. Therefore, through controlling the coating procedure, the stability of HA-coated Ti alloy may be improved.

In addition, electrochemical principles are very useful for understanding the factors affecting dissolution behaviour. The advantages of a technique such as polarisation curve measurement are its simplicity, time saving and the ability to measure the current density, which can address the nature of oxide layer. However, this provides only an indirect insight into the biocompatibility of the treated Ti-6Al-4V. Therefore, a complementary way of studying biocompatibility is through the use of cell culture techniques [16] [17]. Fundamental biochemical and biophysical studies are of paramount importance for investigating the biocompatibility of the treated Ti-6Al-4V surfaces. Moreover, in order to understand the role of metal ion dissolution in the biological mechanisms of osteoblast cells on the treated Ti-6Al-4V, newer experiments must be planned. Thus, functional genomic technology [18] [19] [20] is being developed as a novel and more quantitative and qualitative method for the investigation into gene modulation of implant surfaces.

1.2 Aim and objectives

This study focuses on two main areas; one is the examination of surface properties of the treated Ti-6Al-4V, the other is the examination of the biocompatibility of the treated Ti-6Al-4V. In the first objective of this thesis sophisticated surface analysis and potentiodynamic techniques are used to characterise the surface properties of treated Ti-6Al-4V and correlate them with the metal ion release behaviour. The second objective of this thesis uses the cell culture and functional genetic technologies to understand the osteoblastic cell behaviour and gene expression on the surface treated Ti-6Al-4V and evaluate the protein/gene regulation events in cell differentiation and cell death processes.

1.3 Structure of thesis

Chapter 2 gives an overview of the surface properties of the Ti alloys implant, the mechanism of metal ion dissolution, various techniques and methods to ascertain the surface properties, and the current state of the art for research on the biocompatibility of Ti alloys implant by using cell culture and functional genetic technologies.

Based on an established metal ion dissolution mechanism, this research aims to further visualise the change in the surface properties during immersion in bovine serum solution and understand the correlation between the surface properties and the kinetics of metal ion dissolution. Surface analysis techniques, X-ray photoelectron spectroscopy (XPS) and atomic force microscopy (AFM) are used to characterise chemical and morphological nature of the passive film of the treated Ti-6Al-4V prior to and after immersion are described in *Chapter 3*. This chapter also investigated the relationship between the change in Ti oxide layer surface chemistry during the HA plasma-spraying process and the resulting metal ion release behaviour, using XPS and SEM/EDS.

In *Chapter 4*, an anodic polarisation technique is used to interpret the dissolution behaviour of the treated Ti-6Al-4V and the effects of proteins (organic compounds) and of phosphate buffered saline (inorganic compounds) on the passive behaviour of the treated Ti-6Al-4V.

The combined methodologies employed in *Chapters 3* and *4* have resulted in a preliminary description of the mechanisms behind the improved dissolution behaviour of thermally treated Ti-alloy implants and of HA-coated Ti-alloy implants.

In *Chapter 5* osteoblastic cell cultures were performed to determine the effects of the treated Ti surfaces on cell viability, proliferation, cell morphology, and mineralisation in short-term (24 hours up to 72 hours) and long-term (72 hours up to 4 weeks) tests and gene expression (24, 48 and 120 hours). These tests are able to evaluate the host response to implants and to assess their ability to interact with biological systems. Moreover, a high-throughput technology, cDNA microarray, provides a comprehensive resource to survey thousands of genes in parallel, and examine the different gene expression associated with each surface treatment (referred to as "genocompatibility"). The advantage of this method is that it is able to examine large number of genes and target the significant roles or signalling pathways in cell growth, function or cell death. In particular, these findings have the potential for use in the diagnosis of orthopaedic diseases.

The main conclusions are described in *Chapter 6* and the recommended future work is given in *Chapter 7*.

To reflect the two different approaches upon which the thesis is based, references are arranged at the end of each chapter.

References

1. Hench, L.L. and E.C. Ethridge, *Biomaterials : an interfacial approach.* Biophysics and bioengineering series. 1982, New York: Academic Press. xii, 385.
2. Breme, J. and V. Wadewitz, *Comparison of titanium-tantalum and titanium-niobium alloys for application as dental implants.* Int J Oral Maxillofac Implants, 1989. **4**(2): p. 113-8.
3. Vannoort, R., *Titanium - the Implant Material of Today.* Journal of Materials Science, 1987. **22**(11): p. 3801-11.
4. Ratner, B.D., *New ideas in biomaterials science--a path to engineered biomaterials.* J Biomed Mater Res, 1993. **27**(7): p. 837-50.
5. Jacobs, J.J., J.L. Gilbert, and R.M. Urban, *Corrosion of metal orthopaedic implants.* Journal of Bone and Joint Surgery-American Volume, 1998. **80A**(2): p. 268-82.
6. Browne, M. and P.J. Gregson, *Surface modification of titanium alloy implants.* Biomaterials, 1994. **15**(11): p. 894-8.
7. Callen, B.W., et al., *Nitric acid passivation of Ti6Al4V reduces thickness of surface oxide layer and increases trace element release.* J Biomed Mater Res, 1995. **29**(3): p. 279-90.
8. Browne, M. and P.J. Gregson, *Effect of mechanical surface pretreatment on metal ion release.* Biomaterials, 2000. **21**(4): p. 385-92.
9. Chang, Y.L., et al., *Osteoblastic cell attachment to hydroxyapatite-coated implant surfaces in vitro.* Int J Oral Maxillofac Implants, 1999. **14**(2): p. 239-47.
10. Hing, K.A., et al., *Quantification of bone ingrowth within bone-derived porous hydroxyapatite implants of varying density.* Journal of Materials Science-Materials in Medicine, 1999. **10**(10-11): p. 663-70.
11. Lo, W.J. and D.M. Grant, *Hydroxyapatite thin films deposited onto uncoated and (Ti,Al,V)N-coated Ti alloys.* Journal of Biomedical Materials Research, 1999. **46**(3): p. 408-17.
12. Battistoni, C., et al., *Surface characterization of biocompatible hydroxyapatite coatings.* Surface and Interface Analysis, 2000. **29**(11): p. 773-81.

13. Sousa, S.R. and M.A. Barbosa, *Effect of hydroxyapatite thickness on metal ion release from Ti6Al4V substrates.* Biomaterials, 1996. **17**(4): p. 397-404.

14. Ducheyne, P. and K.E. Healy, *The effect of plasma-sprayed calcium phosphate ceramic coatings on the metal ion release from porous titanium and cobalt-chromium alloys.* J Biomed Mater Res, 1988. **22**(12): p. 1137-63.

15. Tufekci, E., et al., *Microstructures of plasma-sprayed hydroxyapatite-coated Ti-6Al-4V dental implants.* Int J Oral Maxillofac Implants, 1997. **12**(1): p. 25-31.

16. Wilke, A., et al., *Biocompatibility analysis of different biomaterials in human bone marrow cell cultures.* Journal of Biomedical Materials Research, 1998. **40**(2): p. 301-6.

17. Wilke, A., et al., *Human bone marrow cell culture: A sensitive method for determination of the biocompatibility of implant materials.* Atla-Alternatives to Laboratory Animals, 1999. **27**(1): p. 137-51.

18. Brazma, A., et al., *One-stop shop for microarray data - Is a universal, public DNA- microarray database a realistic goal?* Nature, 2000. **403**(6771): p. 699-700.

19. Brazma, A. and J. Vilo, *Gene expression data analysis.* Febs Letters, 2000. **480**(1): p. 17-24.

20. Celis, J.E., et al., *Gene expression profiling: monitoring transcription and translation products using DNA microarrays and proteomics.* Febs Letters, 2000. **480**(1): p. 2-16.

Chapter 2 Literature Review

2.1 The development of biomaterials

The development of biomaterials did not become practical until the advent of aseptic surgical techniques by Lister [1] in the 1880s. Earlier surgical procedures involving biomaterials were generally unsuccessful due to infection. The earliest successful implants were in the skeletal systems. Bone plates were introduced in the early 1900s to aid in the fixation of fractures. However, many of these plates failed due to poor design features, such as cross section area and stress concentrations at corners. The introduction of stainless steels and cobalt chromium alloys in the 1930s proved successful in fracture fixation, and the first joint replacement surgeries were carried out [2].

One of the most commonly used polymers was introduced into the field by chance rather than design. It was found that warplane pilots in World War II who were injured by fragments of plastic {polymethyl methacrylate (PMMA)} aircraft did not suffer adverse chronic reactions to the material in the body. PMMA became widely used after that time for corneal replacement and for replacement of sections of damaged skull bones. Following further advances in materials and in surgical techniques, blood vessel replacements were developed in the 1950s, and heart valves replacements and cemented joint replacements in the 1960s [3]. The CoCr alloy was used as the ball to combine with ultra-high molecular weight polyethene (UHMWPE) cup since the early 1960s. Titanium (Ti) has been used in the United States since 1951 and more commonly used in Great Britain since 1958 [4]. Hille [5] used Ti and Ti alloys as implant materials and has discussed their relevant metallurgy and properties. Ti was first introduced as a dental implant by Branemark et al in the early 1970s [6]. Until now, Ti and its alloys has become widely used in numerous surgical procedures in the

field of orthopaedic, cardiovascular and dental implantation. Hydroxyapatite (HA) has been used for over 20 years and is referred to as a bioactive ceramic because of the biological response it generates after implantation. Originally studied for dental and oral surgery applications, HA has been used to coat metal prostheses to encourage the formation of a chemical bond between the implant and bone [7].

2.2 Titanium and titanium alloys

Ti is an allotropic material that exists as a hexagonal closed-packed structure (α-Ti) up to 882°C and body-centred cubic structure (β-Ti) above that temperature. The fundamental effect of alloying additions to Ti is alteration of the transformation temperature and production of two phases, alpha (α) and beta (β) phases. Elements having extensive solubility in the α phase raise the transformation temperature and are called α stabilisers, e.g. aluminium (Al), oxygen (O), nitrogen (N), or carbon (C). Al is the α-stabilising metal used in commercially alloys. The α phase is also strengthened by addition of zirconium (Zr). Elements that depress the transformation temperature readily dissolve in and strengthen the β phase, and exhibit low α-phase solubility; there are known as β stabilisers, for example, vanadium (V). The relative amounts of α and β phases have a significant effect on the properties of the material in terms of tensile strength, ductility, creep properties, weld ability, and ease of formability [8].

The typical mechanical properties of Ti-6Al-4V alloy for medical application and cortical bone are given in Table 2-1 and Table 2-2, respectively [7] [9]. Ti and its alloys have some advantages over other commercially used metallic implants [9]. The lower density (Ti: 4.5 g/cm^3, cortical bone: 1.9 g/cm^3) reduces the patient's awareness of the implant, while the lower modulus reduces the stress discontinuity at the implant/cement interface. However, Ti has poor shear strength making it less desirable for bone screws, plates and similar applications.

Table 2-1 Mechanical properties of biomaterials [9]

	Ti-6Al-4V	cp-Ti	CoCrMo *cast*	CoNiCr *wrought*	CoCrMo *hip*	cp-Nb	cp-Ta	FeCrNiMo (316L)
Young's modulus (GPa)[1]	~110	~100	~200	~220	~330	~120	~200	~210
Yield strength (MPa)	~900	~300	~500	~850	~841	~250	~300	~250

1. Young's modulus (E) or tensile elsatic modulus ($\sigma = E\varepsilon$).
$\sigma(stress) = \frac{F(force)}{A(area)}$, $\varepsilon(strain) = \frac{(l_1 - l_0)}{l_0}$.

Table 2-2 Mechanical properties of a compact (cortical) human bone [7]

	Compression tests	Tensile tests
Young's modulus (GPa)	14.7-34.3 (average: 23 ± 4.8)	7.1-28.2 (average: 19.6 ± 6.2)
Yield strength (MPa)	133-295 (average: 200 ± 36)	92-188 (average: 141 ± 28)

2.2.1 Surface properties of titanium and titanium alloys

Ti and its alloys are characterised by excellent corrosion resistance, good mechanical properties and low density [10] [11]. Ti derives its resistance to corrosion by the formation of a tightly adherent oxide layer, which passivates the surface [12]. This oxide layer (about 20-30 Å) is formed immediately upon exposure to air. Its characteristics can be improved through different surface treatments, because the tianium dioxide (TiO_2) is a stable form under *in vivo* conditions. This oxide layer not only prevents metal ion release from Ti metal but it enhances specific protein absorption through hydrolysed TiO_2 surface groups. This accounts for the excellent biocompatibility of Ti [13].

2.2.2 Titanium oxides

It is the surface science of Ti and its alloys, which play a fundamental role in their biocompatibility. Simple surface treatments can be used to enhance the corrosion resistance and biocompatibility of this material. There are a number of different methods used to prepare the metal oxides on Ti surfaces, including clinical procedures (machining, solvent cleaning, sterilisation), electrochemical methods (electropolishing and anodic oxidation) [14] [15], thermal oxidation in air (ageing, heating) [16], and nitrogen-ion implantation [17]. The resulting oxide layer provides excellent corrosion resistance. An additional stabilisation procedure by immersion in boiling water was proposed to enhance the corrosion resistance of titanium oxide [18] [19] [20]. Browne [16] et al., demonstrated that ageing in boiling distilled deionised water reduced metal ion release from polished Ti-6Al-4V alloy implant stems into bovine serum by up to 80% compared to ASTM standard passivation procedures. The increase in corrosion resistance was attributed to conversion of the surface oxide to rutile, the most stable form of titanium oxide. In addition, the dielectric constant of TiO_2 is much higher than other metallic oxides and almost equal to that of water. There is a large scatter in dielectric constant valves for titanium oxide in the literature and it is known that this parameter depends strongly on the conditions under which the film is formed. A large dielectric constant results in a small electrostatic force at the surface and a small change in the conformation of a protein upon adsorption.

The main constituent of the surface oxide of Ti-6Al-4V is titanium dioxide, TiO_2. Titanium dioxide has two major forms, rutile and anatase. Both of them are tetragonal, rutile containing six atoms per unit cell and anatase twelve. The rutile TiO_2 (110) surface structure is believed to be close to the bulk truncated geometry. Figure 2-1 (a) shows the clean surface unit cell which consists of one six-fold co-ordinated Ti atom, one five-fold co-ordinated Ti atom, one two-fold co-ordinated bridging O atom above the (110) truncated plane, one three-fold co-ordinated bridging O atom below the plane, and two three-fold co-ordinated O's. Figure 2-1 (b) shows the hydroxylated surface based on a model by Kurtz et al [21]. According to this model, approximately half of the five-fold co-ordinated Ti atoms present at the clean surface are bonded to hydroxyl groups via water adsorption and dissociation. About half of the two-fold co-ordinated bridging O atoms at the surface become bonded to water derived hydrogen. The

dissociation of a water molecule at the surface results in two hydroxyl groups: one bonded to the previously five-fold co-ordinated Ti the basic site and the other formed by the bonding of a proton to the two-fold co-ordinated bridging O the acidic site. This can be proved by measuring the Ti2p spectrum using AlKα radiation [22]. This process increases the stabilisation of TiO_2 via the formation of hydroxylated TiO_2.

There are various descriptions about the nature of the passive film on Ti surface. Lausmaa [23] used Auger electron spectroscopy (AES) and X-ray photoelectron spectroscopy (XPS) to show that the surface oxide on Ti-6Al-4V contains several percent of oxidised Al, both at the outermost surface and in the interior of the oxide. The concentration of Al was higher at the surface than in the bulk alloy. Vanadium is not detected at the outermost surface by AES or XPS. Lee [24] et al investigated the properties of passivated films for Ti-6Al-4V alloy prepared by various methods (passivation and autoclaving). Passivation and autoclaving decreased the Ti to Ti^{4+} ratio by virtue of an increase in oxide thickness. One of the passivation treatments, a 400°C thermal treatment exhibited the lowest content of suboxides and metallic element. Pan [25] et al has suggested that this passive film exhibits a two-layer structure, *i.e.*, a dense inner layer and a porous outer layer. The outer layer possessed microscopic pores, which could be filled by either the solution or some hydrated/precipitated compounds depending on the exposure conditions. Other groups [26] [27] found that the surface of Ti is covered by a thin titanium oxide film composed of two areas: (1) a mixture of anatase and amorphous titanium oxide, (2) anatase. The relatively low crystallinity of the oxide facilitated the reaction with chemical species in a bioliquid.

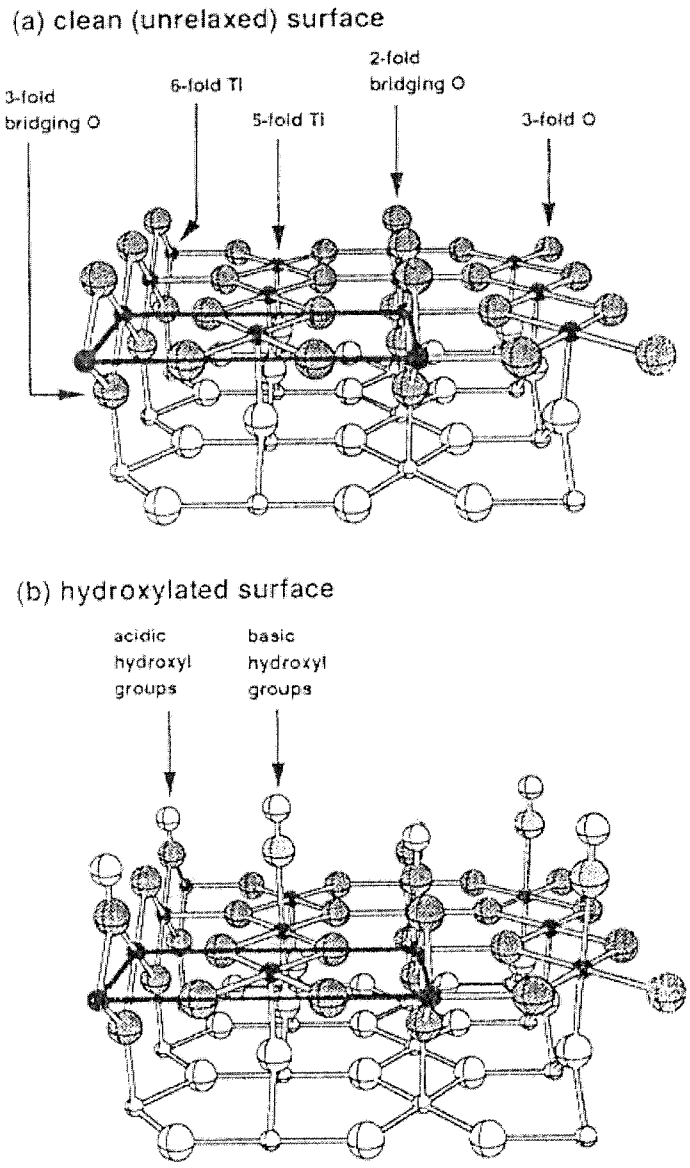

Figure 2-1 Cleaned and hydroxylated TiO_2 surface [22].

2.3 Metal oxide dissolution of titanium alloys

Metal ion release from implant alloys has become a source of concern in the orthopaedic industry. Implant degradation while in the human body results in the release of metallic and polymeric elements over time. Chemical interactions between the tissues and surface of the implants, and the mechanical friction of implants producing wear are responsible for the release of metal ions into the human body [28] [29]. When metal ions are released, some stay local to the implant while others are transported in the blood forming as metal ions/proteins complexes, accumulate in organs with potentially harmful effects, or are excreted [28]. Normally, vanadium is easily and rapidly excreted in urine. Aluminium ion (Al^{3+}) has been known as a detrimental metal to affect markedly a wide variety of biological systems and likely causes of a number of human diseases, such as osteomalacia and Alzheimer's disease [30]. It could be because Al^{3+} ions form complexes with organic substances, for example by reacting with the Ca-transporting system or iron-binding protein ferritin then transport into plasma [31]. It is also well known that titanium oxide binds cations, particularly polyvalent cations. The TiO_2 surface has a negative charge at a physiological pH. The binding of cations is based on electrostatic interactions between Ti-linked O^- on the implant and the cation. The oxide layer is highly polar and attracts water and water-soluble molecules [32]. Hydrolysis plays a significant role during stepwise anodic dissolution of metals, and the identity and stability of hydrolysis products must be carefully considered. In this regard, the most favoured species are electroneutral, such as $M(OH)_4$, because they have little affinity for reaction with organic molecules. Most of the Ti remains at local tissues. This behaviour may be explained in terms of the properties of the passive dissolution products of Ti. They have a limited co-ordinating capability with cellular chelators due to their high acidity, and form stable complexes, which are not freely transportable. Therefore, the measurement of Ti in body fluids (*in vivo*) has not been a good indicator of Ti alloy dissolution since so little is transported.

2.3.1 Metal oxide dissolution mechanisms

Several possible mechanisms have been proposed to explain metal oxide dissolution:

(1) Ducheyne and Healy [33] [34] have looked at the mechanisms of passive dissolution of titanium in a simulated physiological environment (Hanks' balanced salt solution, HBSS). They concluded that the mechanisms for passive dissolution *in vitro* could be separated into two phases. During the initial phase of dissolution (t<10d), equilibration of the oxide with the environment dominated. The growth kinetics were dependent on the electric field that developed across the oxide, which assists metal ion transport into the oxide lattice. When the immersion periods increased (t>15d), the differential dissolution rate slowed considerably. This is attributed to the increase in oxide thickness decreasing the electric field-assisted transport of ions into the oxide lattice, and thereby decreasing the driving force for dissolution.

(2) According to the works of Clark et al [35], the rate of corrosion of some metals (pure metal powders) can be markedly increased in the presence of protein solutions and different proteins produce different effects (Table 2-3).

Table 2-3 Analyses of metals in saline and protein solutions after 16 hours exposure (all concentrations are in ppm) [35]

Metal	Saline	Albumin	Fibrinogen
Aluminium (Al)	1.30	1.42	1.0
Chromium (Cr)	0.50	2.38	0.70
Cobalt (Co)	1.50	31.50	40.95
Copper (Cu)	3.72	169	96.60
Molybdenum (Mo)	514	390	355
Nickel (Ni)	4.80	7.70	9.5
Titanium (Ti)	0.2	0.2	0.2

For highly passivated metals such as Al and Ti, corrosion is negligible and proteins have no effect. For the transition metals, proteins can greatly enhance the rate of corrosion, by abstracting already oxidised metal from a protective oxide layer and

rendering the underlying material liable to attack. It is possible for proteins, such as albumin to act as a catalyst, oxidising the metal with internal disulphide groups, and forming a protein-metal complex, these disulphide bonds being subsequently reformed by oxidation with oxygen. However, Ti and Al are small multiple-charged ions with a high affinity for oxygen and a low affinity for nitrogen. The ionisable organic tissue sees the surface of Ti-based implant as an amphoteric, highly polar surface of hydroxylated TiO_2. It is known that the adsorption on such a surface is due to electrostatic attraction.

(3) The surface charge on the metal oxide is formed as a result of reactions between surface hydroxyl groups and electrolyte ions [36]. For aqueous solutions, hydrogen (hydroxide) ions and background electrolyte ions play an important role for surface charge formation. Hydrogen ions influence the surface charge through the acid-base reactions of surface hydroxyl groups (Eqs.2-1~2-3) [37]. Background electrolyte ions react with surface hydroxyl groups on the oxide, creating surface complexes. For example, the following reactions of complexation can take place in a system with NaCl as background electrolyte because sodium chloride makes up most of the ion concentration of body fluids (Eqs.2-3 ~ 2-5).

$$TiOH_2^+ \xleftrightarrow{K_1} TiOH + H_s^+ \qquad \text{(Equation 2-1)}$$

$$TiOH \xleftrightarrow{K_2} TiO^- + H_s^+ \qquad \text{(Equation 2-2)}$$

$$H_s^+ \longleftrightarrow H_b^+ \qquad \text{(Equation 2-3)}$$

$$TiOH_2^+Cl^- \longleftrightarrow TiOH + Cl^- + H^+ \qquad \text{(Equation 2-4)}$$

$$TiOH + Na^+ \longleftrightarrow TiO^-Na^+ + H^+ \qquad \text{(Equation 2-5)}$$

Where:
s and b stand for surface and bulk solution

Basic OH groups can adsorb H^+ according to the Eq.2-1, while acidic surface hydroxyls become deprotonated in Eq.2-2. Two acidity constants define the chemical equilibrium of the surface [38]. From the so-determined value of pK_1 and

pK_2 the value of the point of zero charge, PZC, (i.e. the pH value at which the electric charge of the surface is balanced) can be calculated using the standard equation:

$$PZC = \frac{(pk_1 + pk_2)}{2} \qquad \text{(Equation 2-6)}$$

The values of pK_1, pK_2, pzc for rutile are 3.90, 6.85, and 5.38, respectively [39]. The pKs values determine the amphoteric properties and the adsorption behaviour of this hydroxylated layer. The properties of these OH-groups as well as the charge of the oxide layer can be influenced by the pH of the electrolyte. When TiO_2 (rutile) immerses into the simulated body solution (pH=7.4~7.6, pH>PZC) and the surface of rutile will react with the simulated body solution [37]. This leads to negatively charged surfaces under physiological conditions. These properties are critical for the adsorption of biomolecules and therefore strongly influence the biocompatibility of the materials used [40]. Amino acids are also amphoteric and thus can act both as proton donors and acceptors. Amino acids exist in solution in the form of dipolar ions, i.e. zwitterions. The amino (NH_3^+) group and TiO^- surface species interact by chemisorption or surface complexation, where amino acid (cation) ions replace the surface H^+.

(4) A further possible mechanism for ion release involves chloride ion penetration into the oxide lattice. Oxide film rupture could occur maybe due to the presence of chloride ions at the metal-oxide interface [41] [42]. An accepted model for the charge (or ions) distribution in terms of a charge double-layer structure is used to explain this mechanism (Figure 2-2) [43]. This double layer[i] is present due to hydroxylated ions at the metal surface and charge transfer can occur within the layer depending on whether the metal oxide is stable (acting as a cathode) or whether it is passive up to and beyond removal of its protective oxide layer (as an anode). When the passive layer is broken metal ions release to solution until the passive layer is rebuilt (repassivated)[ii] [41] [44]. This rebuilding is combined with

[i] Please refer to *Appendices, double layer*.

[ii] Repassivation: Titanium develops a thin, tenacious and highly protective surface oxide film. The surface oxide of titanium will, if scratched or damaged, immediately reheal and restore itself in the

the reaction of anions, which come from the environment. Therefore, any anions in the environment may have a bearing on the final composition of the repassivated layer and its ability to reform.

presence of air or even very small amounts water. The corrosion resistance of titanium depends on a protective TiO_2 surface oxide film (http://www.titanium.org/).

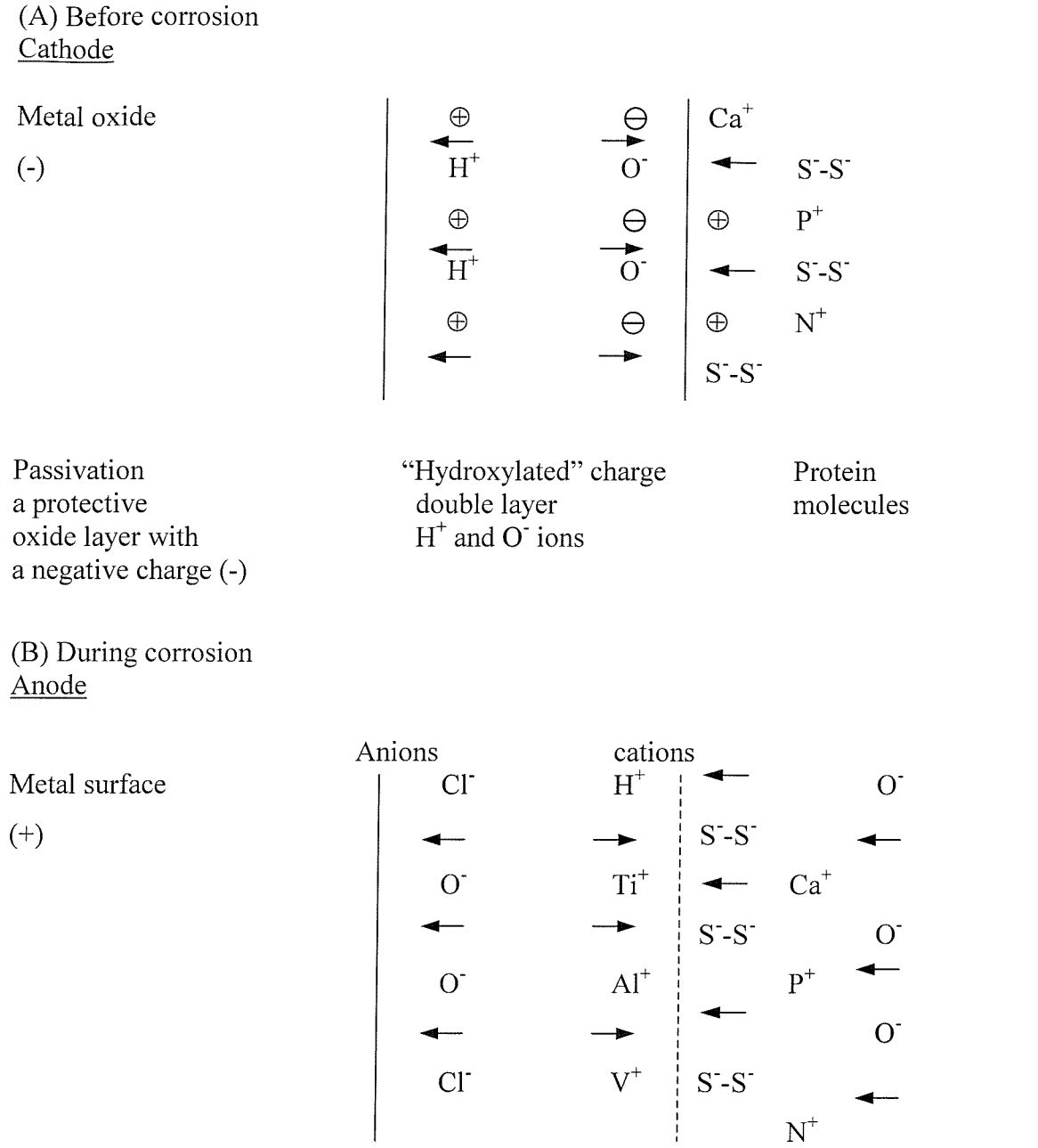

Figure 2-2 Theoretical model of charged double layer showing the transfer of charge at the metal/oxide/protein interfaces (A) before corrosion and (B) during corrosion [43].

2.3.2 HA-coating titanium alloy

Ti and its alloys are gaining increasing acceptance in the biomedical field. Various surface treatments of Ti have been attempted to improve its osseointegration[iii] [45]. The use of more biocompatible materials such as a calcium phosphate (Ca-P) coating to form a satisfactory biological coating nuclei for bone ingrowth and interfacial stability has therefore gained widespread acceptance [46] [47] [48] [49]. The chemical composition of a Ca-P material is considered to play an important role in the adhesion of bone cells as well as in the maturation of the extracellular matrix (ECM) [50]. It is thought that Ca^{2+} ions dissolve from the Ca-P surface and create an interfacial supersaturated condition, which in turn results in the precipitation of CO_3 apatite [51].

Plasma-spraying, the most common means of applying HA coatings to implant devices, employs a plasma, or ionised gas, to partially melt and transport the ceramic particulate onto the surface of the substrate [52] [53]. The carrier gas is usually argon, which is ionised as it passes within the high temperature discharge zone as the current arcs across the gap between the anode and the cathode. The nozzle of the plasma gun is kept from melting by water cooling, as temperatures developed in the plasma may exceed 30,000°C. As the ceramic particulate remains in the heated plasma zone for only a fraction of a second, usually only partial melting of the powder takes place. One advantage of the plasma spraying process is that during the coating process the substrate remains at a relatively low temperature (generally less than 300°C) so the mechanical properties of the metallic implant materials are not compromised.

However, the successful application of HA coatings to Ti is very difficult because the thermal expansion coefficient α of Ti is only 60% of that of HA [54]. The high shear strength required between the coating and the substrate can be achieved only by chemical bonding, which can be produced by diffusion during annealing of the coating implant composite. Because of the misfit of the expansion coefficients during cooling

[iii] Osseointegration is the procedure by which mature bone is deposited directly on implant materials without any intervening soft or fibrous tissue. For clinically successful implants, osseointegration is mandatory for secure association between bone and implant surface.

from the annealing temperature, tensile stresses will occur which will produce a cracking of the ceramic, causing a decrease in the adhesion strength.

A further complication is the decomposition of HA during plasma-spraying [55] [56]. Because the plasma-spraying parameters and starting powder properties such as initial stoichometry, particle size, lattice defects effect the decomposition of HA. During normal plasma-spraying, the underlying Ti has little or no influence on the decomposition of HA in the outer layer except in the region of the HA/Ti interface. Ti usually catalyses decomposition of HA into α-TCP ($Ca_3(PO_4)$, tricalcium phosphate) and TCPM ($Ca_4P_2O_9$, tetra calcium phosphate monoxide) plus a reaction with Ti dioxide, leads to α-TCP and $CaTiO_3$ because Ti ions diffuse into the coatings. The transport of ions is enhanced by pores and cracks in the coatings. Up to now, there have been few systematic investigations on the influence of underlying Ti upon decomposition of HA during plasma-spraying deposition, however, the use of post-heat-treatment in order to improve crystallinity and enhance chemical bonding at the coating/metal interface has been proposed [54] [57].

2.3.3 Corrosion studies of metal ion dissolution

Metallic corrosion is one of the main causes of metal ion release [58]. There is evidence that the insidious nature of fretting in Ti-6Al-4V often leads to other degradation mechanisms such as pitting corrosion and crevice corrosion[iv] [59] [60]. Metal ion release in the passive state and the film breakdown are important aspects of the corrosion phenomenon [35]. Corrosion is essentially an electrochemical process and is unavoidable. Metal dissolution (an oxidation reaction) occurs at the anode, and hydrogen reduction (a reduction reaction) occurs at the cathode. The potential difference between the anodic and cathodic reactions is the driving force for the metal ion dissolution or corrosion, while the current provides a measure of the rate at which the reactions are proceeding [61] [62].

[iv] Pitting corrosion: Pitting is localised corrosion which selectively attacks areas of a metal surface where there is a surface scratch or mechanically induced break in an otherwise protective film. Crevice corrosion: The attacked which occurs because part of a metal surface is in a shielded or restricted environment, compared to the rest of the metal which is exposed to a large volume of electrolyte.

Two essential factors determine how and why a metal corrodes [63]. The first characteristic is the thermodynamic driving force, which causes corrosion reactions and the second is the kinetics barrier, which limit the rate of these reactions. The thermodynamic driving force for the oxidation of metal atoms to ionic forms (Eq2-7) is the free energy (ΔG, Eq2-8),

$$M^{n+} + ne^{-} \longleftrightarrow M \qquad \text{(Equation 2-7)}$$

$$\Delta G_{red} = \Delta G^{0} + RT \ln \frac{[M]}{[M^{n+}][e^{-}]^{n}} \qquad \text{(Equation 2-8)}$$

Where:
ΔG_{red} is the free energy for the reduction reaction, $\Delta G°$ is the free energy of the reaction in a defined standard state, R is the gas constant, T is the temperature and the bracketed values are the activities of the species.

If the ΔG for oxidation is smaller than zero, the reaction occurs spontaneously.

There is another source of energy for the corrosion process. When positive and negative charges are separated from each other during corrosion, this separation between charges is known as the electrical double layer. It creates an electrical potential across the metal and solution interface, which may be expressed as:

$$\Delta G = -nF\Delta E \qquad \text{(Equation 2-9)}$$

Where:
n is the charge value of the ion, F is the Faraday constant, and ΔE is the voltage or potential across the interface between the metal and the solution.

The more negative the potential of a metal in solution, the more reactive it will tend to be. When it arrives at equilibrium, the chemical energy balances with the electrical energy and yields the Nernst equation:

$$\Delta E = \Delta E^0 + \frac{RT}{nF} \ln \frac{[M^{n+}]}{[M]} \qquad \text{(Equation 2-10)}$$

Which states that there is an electrical potential across the interface between the metal and the solution when metals are immersed in solution. From this equation, a scale of reactivity of the metal, known as the electrochemical series, can be established (Table 2-4). Ti has a very large negative potential, which means a large chemical driving force for corrosion (oxidation). It is this reactivity, which allows Ti to form a protective passive oxide film (passivation process) on exposure to air. This passivation process, or kinetic barrier, can prevent corrosion by physical limitation of the rate at which oxidation or reduction process can take place. For example, passive oxide films are the best-known forms of kinetic barriers to corrosion or other coatings.

Table 2-4 Standard electrochemical series for selected metals

	Reaction	Potential (*Volts*)
Noble[1]	$Au^{3+} + 3e^- \Leftrightarrow Au$	1.42
	$Pt^{2+} + 2e^- \Leftrightarrow Pt$	1.20
	$Ag^+ + e^- \Leftrightarrow Ag$	0.80
	$O_2 + 2H_2O + 4e^- \Leftrightarrow 4OH^-$	0.40
	$Ti(OH)^{3+} + H^+ + e^- \Leftrightarrow Ti^{3+} + H_2O$	0.06
	$2H_2O + 2e^- \Leftrightarrow 2OH^-$	-0.83
	$TiO_2 + 4H^+ + 4e^- \Leftrightarrow Ti + 2H_2O$	-0.86
Active	$Ti^{2+} + 2e^- \Leftrightarrow Ti$	-1.60

1. The more noble metals are less reactive, while the more active metals are more reactive and have a higher driving force for oxidation (corrosion).

However, these kinetic barriers can be removed through of improper use. Most of cases of implant failure were reported for Ti and its alloys have involved bio-corrosion or biodegradation, including mechanical damage or fretting corrosion. Such improper use of Ti-6Al-4V in cemented artificial hip implants caused a series of drastic failures by fretting corrosion and crevice corrosion [61]. Black et al. reported the clinical failure of a total hip-replacement prosthesis made of Ti-6Al-4V alloy and ultra-high molecular weight polyethylene [64]. The failure was due to excessive wear of the Ti-alloy femoral head. Willert et al reported crevice corrosion in twenty-eight Müller straight-stem

femoral components, made of Ti-6Al-4V or Ti-Al-Nb alloy, that had been implanted with bone cement during total hip replacement [65].

In a potential-pH equilibrium diagram (Figure 2-3) for a metal there are three major domains: immunity, passivity and corrosion. In the domain of immunity, the stable form of solid is the metal because the corrosion reaction is thermodynamically impossible. In the passivation domain, the solid stable form is an oxide, hydroxide, hydride or salt, which covers the surface and provides protection against corrosion by preventing contact between the metal and the electrolyte. In the domain of corrosion, the stable forms are soluble and corrosion proceeds without the formation of a passive surface film. A metal can be considered thermodynamically noble if its immunity domain coincides with the thermodynamic stability domain of water. The metal-solution potential difference and the pH determine whether aquocations or oxide will form [66] [67].

The rate of electrochemical film growth and dissolution is controlled by migration of charged species, such as metal cations (outward) and/or oxygen anions (inward) or, more likely, their vacancies. Therefore, the current density is also an important parameter for evaluating the rate of metal ion release when there is no significant dissolution of the film [25].

2.3.5 Potentiodynamic anodic polarisation

Potentiodynamic techniques are among the most reliable methods for characterisation of an electrochemical corrosion process. These methods allow the current (I) due to ion flow into the solution to be measured at a defined potential (E).

Most biomaterials for modern implants can not be differentiated or screened for corrosion by simple conventional immersion testing. If a test sample was placed in a physiologically relevant solution such as blood, salt-water etc., for 10 years, less than 0.1% weight change would occur during that entire period. Therefore, to screen

24

candidate materials in a reasonable period, corrosion must be accelerated in some way via electrochemical stimulation [68]. A typical anodic polarisation curve generally consists of an active state, a passive state and a transpassive state. In the active state, the current density increases rapidly with increasing potential; this results in the formation of an oxidised layer on the surface. In the passive state, the increase in current density is reduced and settles at a particular level due to the protective effect of the passive film. If the potential is increased further, the passive film starts to break down and the current density again increases steeply [69]. In practice ASTM G5, the electrochemical potential impressed upon a metallic specimen immersed in an acid solution is steadily increased until the protective oxide film on the metal surface breaks down and localised corrosion ensures. This breakdown is monitored by a sudden increase in the current flowing in the solution. The higher this potential, the more resistant the alloy is to passive film breakdown and to localised corrosion. Through such polarisation studies, it is possible to understand the nature of the passive film [17] [70].

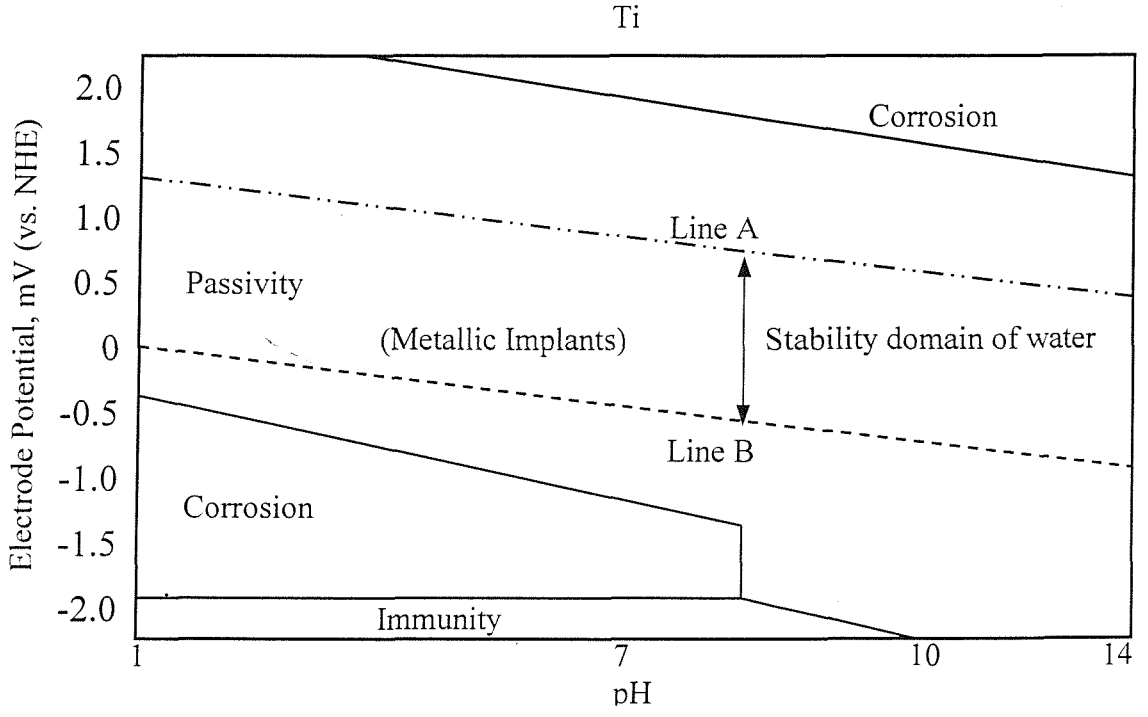

Above Line A (— · · —): $4OH^- \Leftrightarrow O_2 + 2H_2O + 4e^-$
Below Line B (- - - - -): $2H^+ + 2e^- \Leftrightarrow H_2$
NHE: normal hydrogen electrode

Figure 2-3 Simplified potential-pH equilibrium diagram for titanium.

2.4 Surface analysis techniques

There are several surface sensitive analytical techniques available for the study of biomaterials surface science [36]. These include X-ray photoelectron spectrometry (XPS) [71] [72], atomic force microscopy (AFM) [73], auger electron spectroscopy (AES), secondary ion mass spectrometry (SIMS) (Table 2-5). XPS and AFM have been applied in the present study, and are described below.

Table 2-5 Common techniques of characterising biomaterials surfaces [74]

Technique	Principle	Depth Resolution	Spatial resolution	Analytical sensitivity (Detection limits)	Cost[1]
XPS	X rays cause the emission of electrons of characteristic energy	10-250 Å	10-150 μm	0.1 atom%	$$$
STM/AFM	Measurement of the quantum tunnelling current between a metal tip and conductive surface	5 Å	1 Å	Single atoms	$$
AES[2]	A focused electron beam causes the emission of Auger electrons	50-100 Å	100 Å	0.1 atom%	$$$
SIMS	Ion bombardment leads to the emission of surface secondary ions	10 Å-1 μm	100 Å	Very high	$$

1. $, up to $5000; $$, $5000-$100,000; $$$, >$100,000.
2. AES is damaging to organic materials, and best used for inorganics.

2.4.1 X-ray photoelectron spectroscopy (XPS)

The biocompatibility of the material is directly related to the microstructure and the composition of the passive film. It is therefore necessary to characterise the film. XPS is a very useful method for determining the surface elemental and chemical composition of a material. A simple schematic diagram illustrating an XPS instrument is shown in Figure 2-4 (A) [74].

XPS provides quantitative compositional informational from the top 10 atomic layers of a sample surface for the elements lithium to uranium. Additionally, information regarding the chemical states of any elements present can also be obtained. Photoelectron spectroscopy is based on a single photon in/electron out process. In XPS the photon absorbed by an atom in a molecule or solid, leads to ionisation and the emission of a core (inner shell) electron (Figure 2-4 (B)).

The sample is irradiated with a beam of monochromatic soft x-rays and photoelectron emission results from the atoms in the specimen. The kinetic energies (KE) of these electrons relate to the atom and orbital from which they originated. The distribution of kinetic energies from a sample is then measured directly by the electron spectrometer. Atomic orbitals from atoms of the same element in different chemical environments are found to possess slightly different (but measurable) binding energies. These "chemical shifts" arise because of the variations in electrostatic screening experienced by core electrons as the valence and condition electrons are drawn towards or away from the specific atom. Differences in oxidation state, molecule environment and co-ordination number all provide different chemical shifts. Photoelectron binding energy (BE)[v] shifts are, therefore, the principal source of chemical information. It should be noted that these shifts can only be detected using a high performance instrument with suitable software [75].

[v] Typical XPS data for titanium oxide are described in *Appendices, XPS, Table 1.*

(A) Main compositions

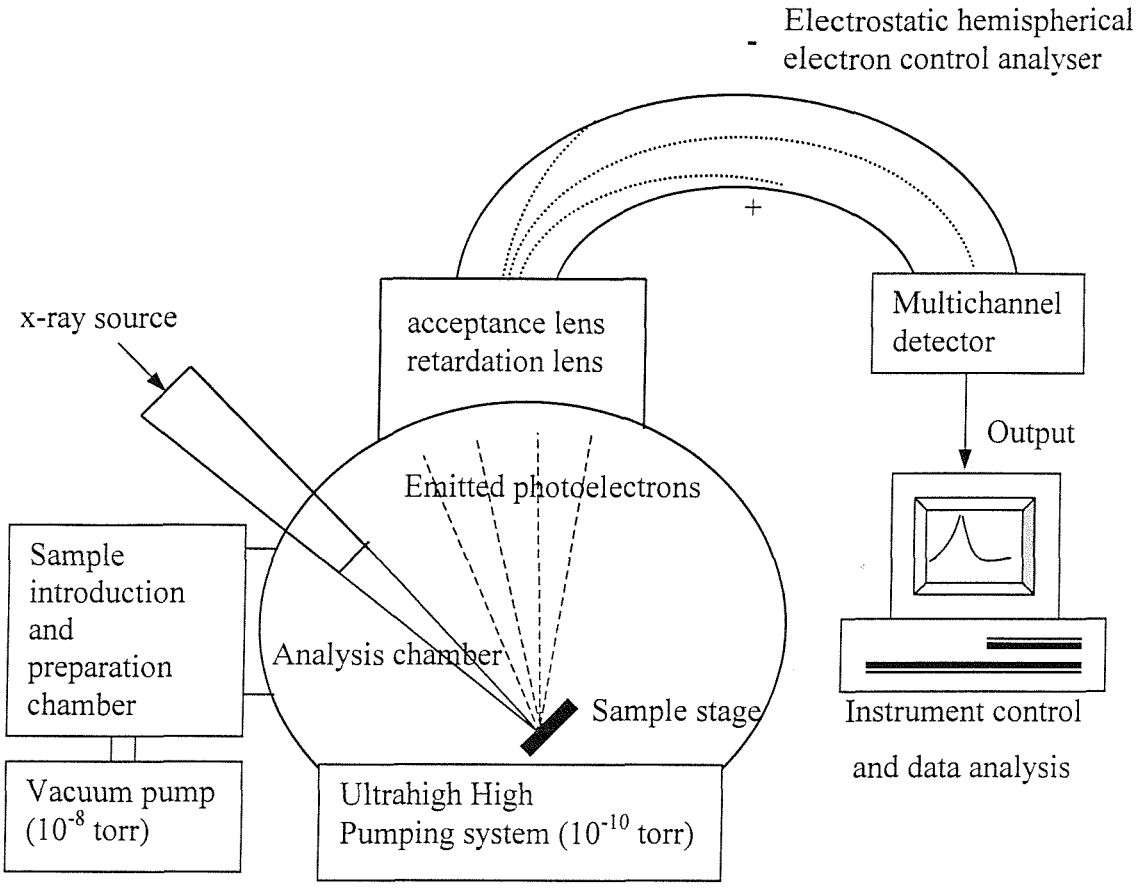

(B) Physical basis[vi]

The energy of photon is given by the Einstein relation:

$E = h\nu$

With:

h: Plank's constant (6.62×10^{-34} Js)
ν: frequency (Hz) of the radiation

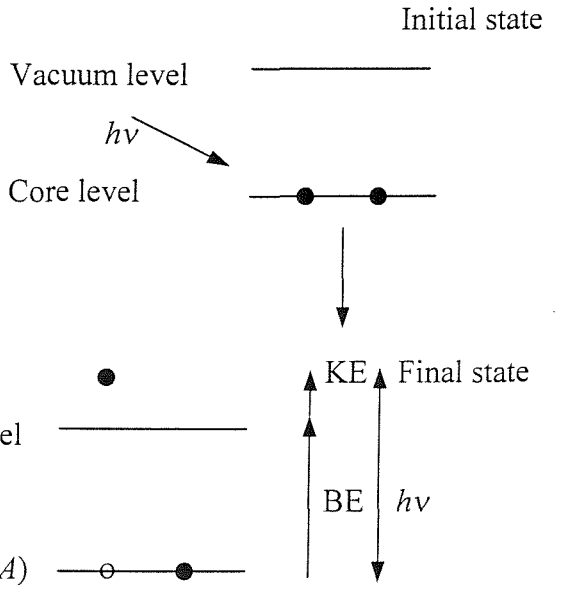

$A + h\nu \rightarrow A^+ + e^-$

$E(A) + h\nu = E(A^+) + E(e^-)$

$KE = h\nu - (E(A^+) - E(A))$

$KE = h\nu - BE$

Figure 2-4 (A) A schematic diagram of a monochromatized XPS instrument and (B) physical basis.

[vi] Figure and text are summarised from this website: http://www.chem.qmw.ac.uk/surfaces.

2.4.2 Atomic force microscopy (AFM)

The morphology of an implant surface can also affect its biocompatibility. *In vivo* studies have suggested that the roughness may control tissue healing and subsequent implant success [76] [77] [78]. In general, AFM enables one to detect surface morphology, nanoscale structure, and molecular- and atomic-scale lattices. AFM operates by measuring the forces between a probe and a sample in order to create an image (Figure 2-5). These forces depend on the nature of the samples, the distance between the probe and sample, the probe geometry, and any contamination on the sample surface. As the probe is brought close to the sample[vii], it is first attracted to the sample surface by a variety of long range attractive forces, such as van der Waals forces. When the probe gets very close to the surface, the electron orbitals of the atoms on the surface of the probe and samples start to repel each other. As the gap decreases, the repulsive forces neutralise the attractive forces, and then become dominant. The forces are then measured by the deflection of a spring cantilever, using Hook's Law: $F=-kx$, where k is the spring constant and x is the displacement of the cantilever. In the contact-mode AFM, which is used in this study, the repulsive force between the tip (located at the end of a cantilever) and samples is measured. The spatial variation of the tip-sample repulsive force or that of the tip height is converted into an image. Generally, the benefits of AFM are the better lateral resolution and the capability of making direct measurements e.g., height, widths, length, particle size and roughness [79].

[vii] Please refer to the *Appendices, AFM.*

(a) Main compositions

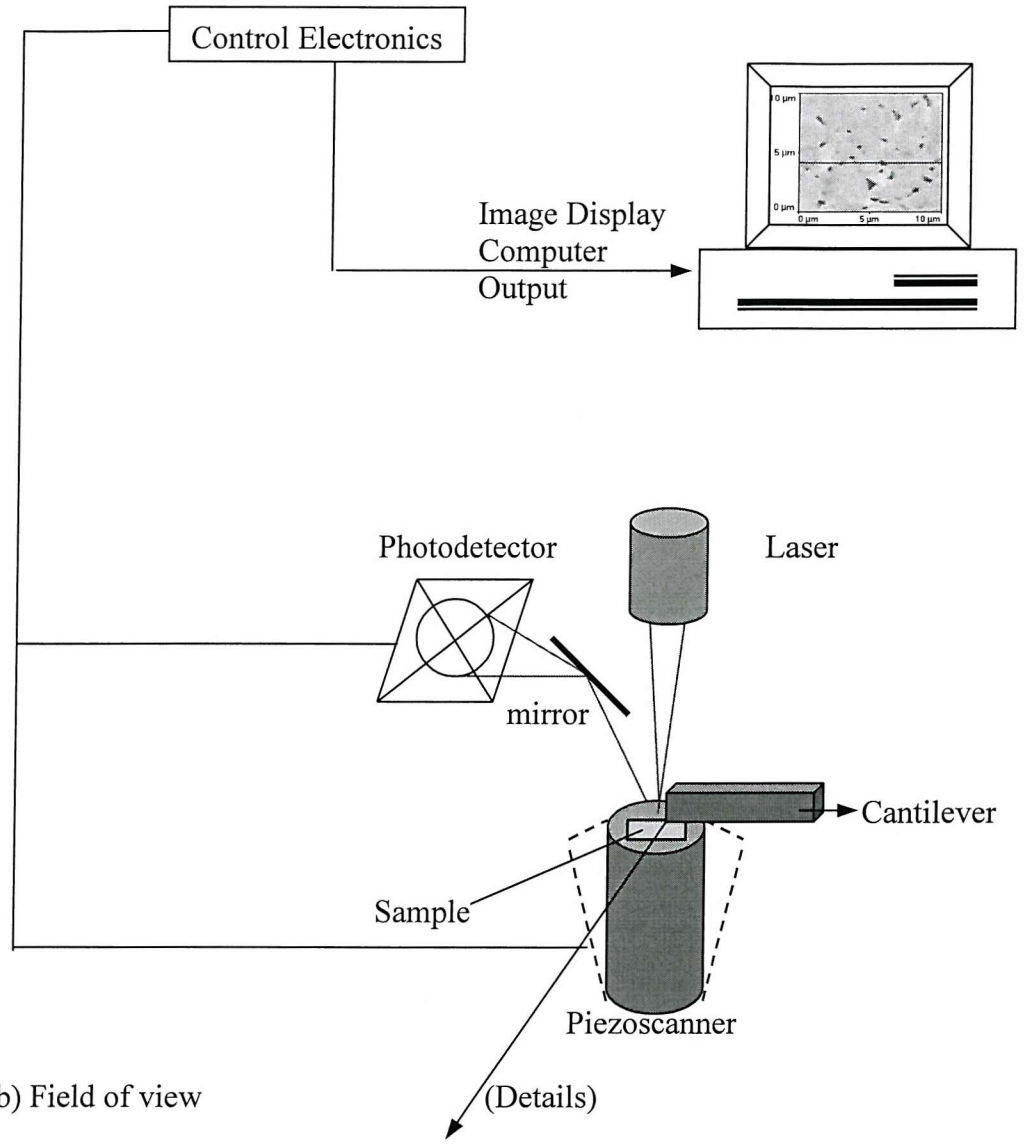

Figure 2-5 Schematic representation of an atomic force microscpoy (AFM). (A) The main compositions and (B) field of view.

2.5 Biological performance of Ti-6Al-4V oxides

Biocompatibility can be described as the ability of a material to perform with an appropriate host response in a specific application [80]. A specific application imposes demands on the properties of materials. Biomaterials have to be tested before they can be used in medical devices [81] [82]. Clinical success of the implant requires the simultaneous achievement of a stable interface with connective tissues (i.e. provide a chemical bond at the bone/implant interface) and a match of the mechanical behaviour of the implant with the tissue to be replaced (i.e. have a modulus similar to that of bone, as compared to other alloys, Table 2-1 and Table 2-2). In order to understand the host response to the implant, first of all, we must have the knowledge of osteoblastic biology, which is discussed in this section [83] [84] [85].

2.5.1 Osteoblastic biology

The cellular constituents of bone, primarily osteoblast and osteoclast, play a critical role in the overall survival of the implanted material. The function of osteoblasts is to form bone, which works in concert with osteoclasts that resorb bone surrounding the prosthesis [86]. There are four main types of bone cells: osteoblast, bone lining cells, osteocytes and osteoclasts - which are quite different geometrically and functionally. Osteoblasts are mononucleated cells that actively produce osteoid, which later mineralise. They are the only cells that produce bone tissue. Bone lining cells are dormant, flattened osteoblasts, which line 90% of the free surfaces within the microstructure of the bone tissue. Osteocytes are differentiated osteoblasts, which form an interconnected network within the bone tissue and are connected with the bone lining cells via gap junctions. For the cell culture experiments, osteoblasts have been investigated, but not osteocytes and osteoclasts because these cells have a low proliferation potential, i.e. they do not undergo cell division [87].

Normally a developmental sequence of bone cell differentiation is characterised by three principal periods: proliferation, extracellular matrix maturation and mineralisation. Changes in levels of expression of these osteoblast-associated

molecules and different combinations of several of the properties shown to be associated with osteoblast-like cells may be characteristic of cells at different development or maturational stages [88]. During the proliferation period, and fundamental to development of bone cell phenotype, several genes associated with formation of the extracellular matrix, such as collagen type I, fibronectin (FN), osteonectin (ON), osteopontin (OPN), bone sialoprotein (BSP), and osteocalcin (OC), are actively expressed. During the period of extracellular matrix maturation (from 12 to 18 d), the cell undergoes a series of modifications in composition and organisation that renders it competent for mineralisation. During the matrix maturation phase, the cell becomes alkaline phosphatase positive as the culture processes into the mineralisation stage (from 16 to 20 d) [89]. The osteoblast developmental sequence is given in Figure 2-6. It can be seen that over time the expression of collagen type I is relatively high and then decreases; ALP increases but decreases when mineralisation is well progressed. ALP is an early maker of osteroblast differentiation. This hallmark of the osteoblast phenotype is a widely accepted marker of new bone formation and osteoblast activity [90] [91]. In osteoblasts, the alkaline phosphatase protein and activity are sufficiently high to allow for histochemistry detection in cells associated with active formation of mineralised matrix [92]. OPN appears prior to certain other matrix proteins, such as BSP and OC, BSP is first detected in differentiated osteoblasts forming bone and OC appears with mineralisation [89].

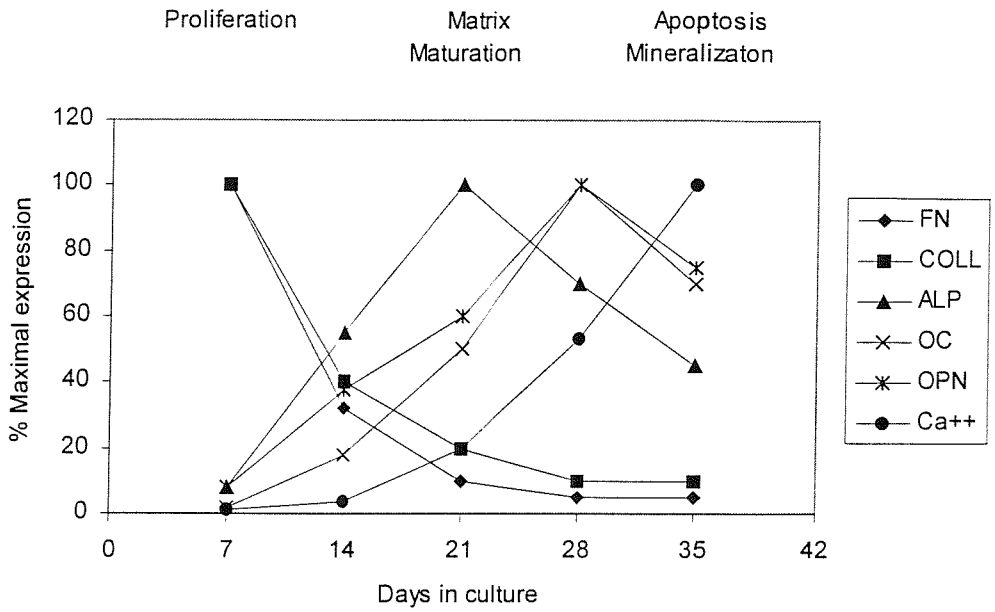

FN: fibronectin, COLL: collagen, ALP: alkaline phosphatase, OC: osteocalcin, and OPN: osteopontin.

Figure 2-6 The osteoblast developmental sequence [90].

2.5.2 Cell adhesion

The response of the body to a biomaterial is not merely confined to the surface chemistry and surface morphology. The biocompatibility of a biomaterial is also dependent on the cell behaviour on contact with its surface, in particular to cell adhesion [91]. The interaction of proteins with the implant surface is very important in the biological acceptance or rejection of artificial implants. For an implant to be successful, osseointegration is essential and closely associated with the phenomenological behaviour of cells (anchorage, attachment, adhesion and spreading). The formation and deposition of bone directly onto the implant requires a surface that is not only non-toxic but also allows or favours this behaviour [91] [93].

Cell adhesion comprises a sequence of four steps: initial cell attachment, cell spreading, organisation of actin cytoskeleton, and formation of focal adhesions [94]. Cells attach to proteins adsorbed on the surface through specific transmembrane adhesion molecules and to specific sites on these proteins [61]. Initial cell adhesion is a critical first step that determines the ultimate fate of the cell. Extracellualr matrix (ECM) components determine cell cycling, differentiation and maturation or apoptosis. A major synthetic ability of the bone-forming cell, the osteoblast, is the production of an ECM that matures and remodels into mineralised bone [95]. The ECM proteins adsorbed to the surface of the substrate bind to integrins through a specific peptide domain, e.g. the Arg-Gly-Asp (RGD) sequences in FN and vitronectin (VN) [96]. RGD may function as cell attachment signals. Focal adhesions consist of an assembly of transmembrane receptors, which are integrins [97] (Figure 2-7). Focal adhesion sites are where cells attach to substrates. They are characterised by 10-15 nm separation of the substrate from the cell surface where bundles of microfilaments terminate at the plasma membrane.

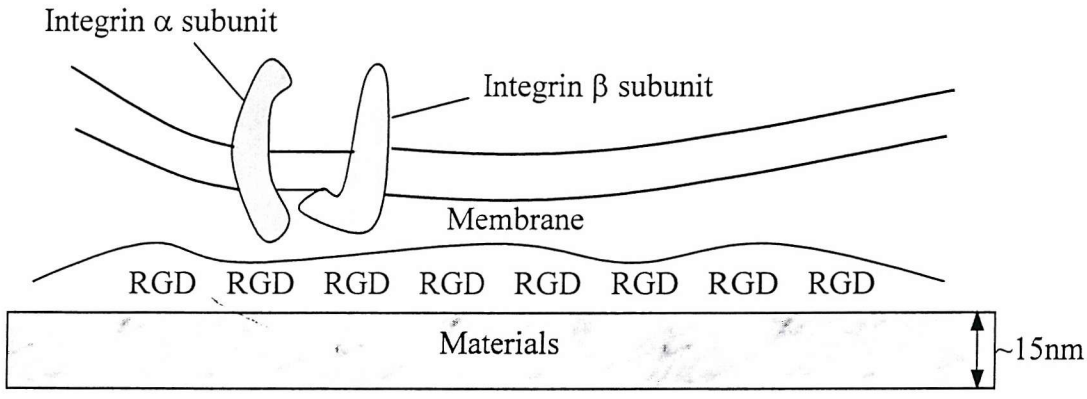

Figure 2-7 Diagrammatical representation of the structure of a focal adhesion plaque showing the position of fibronectin or vinculin in relation the cytoskeletal proteins and to cell membrane proteins: RDG, cell binding domain of proteins in conditioning layer [95].

The interrelation between the surface chemistry and morphology can be quite complex in terms of cell behaviour. Several aspects of the Ti surface have been reported or suspected to influence the body response, such as topography, composition and

roughness or surface energy [97] [98] [99] [100] [101]. Both the compositions of the alloy and the manufacturing process influence the properties of the oxide film and therefore play an important role in biocompatibility properties [102].

Davies et al. has confirmed that a collagen free proteoglycan layer of <500 Å thickness was found on the oxide of cpTi *in vivo* and *in vitro* [103]. He demonstrated the presence of an interfacial zone comprised of a noncollagenous, proteoglycan containing, cement-like material, between the metal substrate and mineralised extracellular matrix produced by the osteoblast-like cells in culture. Keller [104] et al conducted a series of surface characterisation techniques with short term *in vitro* biological assays to assess the effects of materials selection (cpTi and Ti-6Al-4V alloy) on osteoblast-like cell responses. Surface analysis indicated there was no significant difference in surface characteristics between the two implants besides the oxide thickness. According to their results, the levels of cell attachment and adaptation of the attached cell to the Ti surfaces were similar. This indicated that cpTi and Ti alloy are suitable and biologically compatible biomaterials.

Surface roughness has been reported to determine the shear strength of the implant/bone interface [105]. On the cellular level, surface topography influences cell adhesion, morphology, etc. For example the adsorption of specific cell-binding proteins is dependent on the surface energy and on the sign and density of the surface charges. The density of the surface charge of the oxide influences the amount of bovine serum albumin (BSA) on the surface. It is believed that carboxyl groups on the BSA molecule provide anchoring sites for the oxide during adsorption [106]. These dynamical adsorption and dissolution processes occur on the implant surface within a narrow interfacial zone of less than 1 nm [107]. These interactions are considered to play a significant role and may ultimately govern the nature of the tissue-biomaterial interface.

2.5.3 The effects of Ti-6Al-4V implants on biological expression

Under normal physical circumstances, bone repair and remodelling proceed in highly regulated cycles. However, this normal process may be affected due to the interaction

between the implants and surrounding physiological environment. It has been known that one of the major causes for early implant failures is prosthesis loosening due to osteolyisis. Osteolysis adjacent to an implant is believed to result mainly from release of wear particles or metal ions and the subsequent release of inflammatory mediators that stimulate pathological bone resorption [108] [109]. The presence of corrosion products may affect the systemic and local factors that regulate osteoblastic development and their function by promoting osteolysis [110]. Even among the variety of Ti alloys used in orthopaedics (Ti-6Al-4V alloy being a common choice), there are some concerns about the metal ion release in the tissues surrounding implants in humans. Although the toxicity of wear particles of Ti-6Al-4V at high concentration is less than that of the Co-Cr alloy wear particles, these particles release more inflammatory mediators, that is, prostaglandin E2, interleukin-1 (tumour necrosis factor) and interleukin-6 than the Co-Cr alloy wear particles [29].

For example, loose total hip replacements made of Ti-6Al-4V are known to produce increased Ti concentrations [63]. Recent work has shown that Ti or other metal ions affect apatite formation and growth, cell viability and proliferation, specific cellular function, such as ALP activity, extracellular mineralisation, and bone-related gene expression [111] [112]. The concentration of Al has well documented toxic effects in the serum or urine of patients who had a total hip-replacement component of Ti-based alloy. The presence and accumulation of Al in bone has been implicated in the development of bone lesions or osteolysis [113] [114] [115] [116]. Excess Al has been reported to cause either decreased or increased osteoblastic differentiation [117]. Maürer studied cellular uptake of Ti and V salts during fretting corrosion *in vitro* [118]. Vanadium exhibited toxicity at levels greater than 10 μg/ml. The vanadium content of the Ti-6Al-4V alloy may cause some difficulties, because vanadium was regarded as tumorigenic [119]. Vanadium in the +5 oxide state is also known to affect cell proliferation [114].

Therefore, in order to identify a material as biocompatible to bone, it is more important to measure several significant proteins or enzymes (markers), which express during the osteoblast developmental sequence than to evaluate general cytotoxicity [29]. Moreover, recent developmental in the field of genomic study have resulted in a novel method for characterising the implant/cell interaction. The cDNA microarray is a state

of the art technology used to evaluate the gene expression [120] [121]. This should lead to a better understanding of the regulatory events and the pathways controlling osteoblast developmental processes and further highlight the molecular mechanisms involved [122]. The following section discusses this new technology and the genes to be assessed.

2.5.4 Functional genomics-cDNA microarray technology

The field of genomics includes studies of genome mapping, gene sequencing, gene function and gene expression. The advent of high-throughput, genome-scale technologies is revolutionising biology. These technologies allow novel approaches to complex biomedical problems ranging from basic research in fundamental cellular structure and processes to applied research in pathogenesis, and therapy, including genetic determinants of the differences in treatment responses [123] [124] [120] [121].

High-density microarrays using cDNA or oligonucleotide probes can analyse the expression levels of tens of thousands of human genes simultaneously and quantitatively both in health and disease. Single nucleotide polymorphism [121] can be readily interrogated by array technology, enabling linkage studies to determine the role of specific genes in complex phenotypes. As the DNA sequences of more and more organisms have been decoded, researchers have begun to realise that at least as much information in genomes is devoted to controlling where and at what level genes are expressed as is devoted to defining proteins.

This form of investigation could lead to the tailoring of treatment according to the patient's genetic constitution by studying genetic polymorphism in drug-metabolising enzymes, transporters, receptors, and other drug targets that have been linked to inter individual differences in the efficacy and toxicity of many medications.

This "discovery-driven" approach to research contrasts with the more traditional hypothesis-driven approach that has characterised much biological research. The two approaches are complementary and potentially synergistic. Phenomena documented by hypothesis-driven research can be exploited using genomic approaches to define

mechanisms and interactions. Data obtained from the genomic approach spawns additional hypotheses [125] [126] [127] [128] [129] [130] [131].

2.5.5 Gene analyses

The following genes are investigated in our present research. There is a brief description of their role in the osteoblast developmental sequence. Most of the following information is summarised from these references [90] [132] [133] [134].

The osteoblast development sequence of gene expression can be categorised in to the following 4 developmental periods [90]:

Stage 1 (Cell proliferation):

Initially, proliferation supports expansion of the osteoblast cell population to form a multilayered cellular nodule, and biosynthesis of the type I collagen found in bone extracellular matrix (ECM). At this time, genes requisite for activation of proliferation (e.g., c-*myc*, c-*fos*, c-*jun*) and cell cycle progression (e.g. histones, cyclins) are expressed together with expression of genes encoding growth factors (e.g., fibroblast growth factor (FGF), insulin-like growth factor (IGF)-1) cell adhesion proteins (e.g., fibronectin) and others associated with the regulation of ECM biosynthesis (e.g., TGF β, type I collagen). The details are described in follows:

Bone extracellular matrix (ECM): cell proliferation supports expansion of the osteoblast cell population to form a multilayered cellular nodule and biosynthesis of Type I collagen can be found in ECM. Type I collagen is the most abundant extracellular protein of bones (90% of the matrix) and is critical for mineralisation [135]. Collagen is defined as structural proteins of the extracellular matrix. Each molecule of type I collagen is typically composed of two α1 chains and one α2 chain coiled around each other in a characteristic triple helix.

Bone morphogenetic proteins (BMPs): BMPs involved in determining parameters of size and shape during mesenchymal cell condensation and are important regulators of bone repair processes. BMPs are part of a large multigene family, the transforming

growth factor β (TGF-β) family. The relationships of the members of the TGF-β/BMP gene family, BMP-2 and BMP-4 and *Drosophila* (*Dpp*) show a higher degrees of sequence similarities [133]. BMP-2 directs cells to osteoblast differentiation.

Transforming growth factor (TGF) β superfamily (cytokines): The TGF β superfamily provides significant contributions to skeletal development, a well-known modulator of cell proliferation and extracellular matrix biosynthesis. Transforming growth factor (TGF) β family consists of three members, TGF-β1, TGF-β2 and TGF-β3, which have similar biological effects. It also contains proteins such as bone morphogenetic proteins. *In vivo*, the highest levels of TGF-β are found in platelets and bone. It has been demonstrated that subcutaneous injections of platelet-derived TGF-β in newborn mice increase type I collagen synthesis by dermal fibroblasts with formation of granulation tissue. It has been shown that BMP-2, like TGF-β1 upregulates the expression of the type I α1 collagen gene. The actions of TGF-β1 and BMP-2 on the expression of the early marker of osteoblast differentiation are both mediated by transcriptional events [136].

Platelet-derived growth factor (PDGF) (cytokines): PDGF is synthesised by normal and malignant skeletal cells, and osteosarcoma cell lines express both the PDGF A and B genes. PDGF stimulates bone cell replication and DNA synthesis, both in intact calvaria and isolated rat osteoblasts. It appears that the primary effect of PDGF in bone is related to its mitogenic activity. It also induces the transcriptional activation of proto-oncogenes, such as c-*fos* and c-*jun* in the osteoblast-like MC3T3-E1 cells [137].

Growth factors-Insulin-like growth factors (IGF) and Fibroblastic growth factors (FGFs): IGF-1 is synthesised by many cells, including bone cells. It can simulate osteoblast and fibroblast proliferation and increase type I collagen production by these cells. IGF-2 produced by bone cells, which is one of the most abundant growth factors found in bone extracellular matrix, can also stimulate type I collagen synthesis by osteoblastic cells, with an increase in corresponding mRNA transcripts. FGF and FGF receptors are involved in cartilage formation and skeletal development [138]. Although there are nine FGFs, but only FGF-1 and FGF-2 (= bFGF, basic fibroblast growth factor) have been studied in bone, which are found in the bone matrix. FGF-1 and FGF-

2 have also been found to stimulate bone cell replication and cell proliferation. However, FGF-2 inhibits type I collagen and ALP synthesis in osteoblastic cells, affects production of IGF-1 and IGF-2 and their binding proteins in osteoblasts, and *in vitro* FGFs inhibit markers of the osteoblast phenotype. FGF-2 is also a potent stimulator of osteoclast formation and bone resorption. Thus, FGF-2 should be considered as an important regulator of osteoclastic-osteoblastic interaction or coupling.

Interleukin 1 (IL-1), IL-6 and Prostaglandin E-2 (PGE_2) (cytokines): IL-1 has an inhibitory effect on type I collagen production by osteoblasts and this inhibitory effect is due to an inhibition of type I collagen genes transcription. IL-6 is well known to induce osteoclastogenesis and to directly stimulate bone resorption [139]. PGF_2 was shown to stimulate cyclic AMP production and bone resorption in organ cultures.

Protein tyrosine kinases (PTKs): Protein kinases are involved in most of the cytokine signalling pathways[viii] [140]. Therefore, there were several protein kinase inhibitors, for example genistein, to assess the role of protein tyrosine kinase (PTK) and protein kinase c (PKC) activities in the up-regulation of type I α1 collagen mRNA expression by transforming growth factor β1 (TGF-β1) and bone morphogenetic protein 2 (BMP-2). Mitogen-activated protein kinase (MAPK) pathway participated in the upregulation of type I α1 collagen gene expression by TGF-β1 and BMP-2 [136].

Homo sapiens serine/threonine kinase (stem cell tyrosine kinase 1, STK-1): Protein serine/threonine kinases are the most common type of cytosolic kinases, and are responsible for the vast majority of phosphorylation events in the cells [134]. STK-1 is a member of the type m receptor tyrosine kinase family that includes KIT (steel factor receptor), FMS (colony-stimulating factor 1R), and platelet derived growth factor receptor. STK-1, the human homolog of Flk-2/Flt-3, is selectively expressed in CD34+

[viii] Cytokines, casually called growth factors; cytokines are soluble mediators of intercellular communication. They contribute to a chemical signalling language that regulates development, tissue repair, haemopoiesis, inflammation and the immune response. They act in a complex network where one cytokine can influence the production of, and response to, many other cytokines. Protein kinases: The basic activity is the ability to add a phosphate group to amino acid in a target protein.

human bone marrow cells and is involved in the proliferation of early progenitor/stem cells [141].

c-*mys*, **c-*fos*** [142] and **c-*jun*** [143]: These are cell-growth regulated genes, for activation of proliferation. These genes encode proteins that support proliferation by functioning as transactivation factors in the case of c-*myc* and c-*fos* and as proteins that play a primary role in packaging newly replicated DNA into chromatin in the case of histones. Expression of c-*fos* and c-*jun* has been shown to occur primarily during the proliferation period of the osteoblast developmental sequence. The *fos-jun* complex may suppress osteocalcin gene transcription when proliferation is underway by directly or indirectly modulating sequence-specific interactions at the vitamin D receptor binding domain.

RGD-containing proteins–Fibronectin (FN) and vitronectin (VN): These are cell adhesion proteins (non-collagenous). FN is synthesised by many connective tissue cells and is a major component of serum. It is likely that cell-matrix interactions mediated by fibronectin-$\alpha_5\beta_1$ binding play a role in the maturation sequence of cells in the osteoblastic lineage. VN is a serum protein found at low levels in mineralised matrix. Its cell surface receptor-$\alpha_v\beta_3$ is broadly distributed throughout bone tissue.

Integrin: A heterodimeric glycoprotein consisting of α and β subunits that noncovalently interact to form adhesion receptors with defined specificities (Table 2-6) [144]. To date, 16 α different mammalian and 8 β subunits have been identified, forming 22 distinct heterodimers. Integrin can be found in osteoblasts and osteoclasts with different roles, which are listed in Table 2-7.

Table 2-6 Simplified classification of integrins based on binding characteristics

Submit	Ligands
Integrins that bind primarily to basement membrane proteins	
$\alpha_1\beta_1$ $\alpha_2\beta_2$ $\alpha_3\beta_1$ $\alpha_6\beta_1$ $\alpha_6\beta_4$	Laminin/collagen Collagen/laminin Laminin/collagen/fibronectin Laminin Laminin
Integrins that bind primarily to matrix proteins of inflammation, would healing and development	
$\alpha_4\beta_1$	Fibronectin (CSII site)
$\alpha_5\beta_1$	Fibronectin (RGD site)
$\alpha_v\beta_1$	Fibronectin, vitronectin, fibrinogen, thrombospondin, von Willebrand factor, osteopontin, bone sialoprotein
$\alpha_v\beta_3$	Fibronectin
$\alpha_v\beta_5$	Vitronectin
$\alpha_v\beta_6$	Fibronectin
$\alpha_v\beta_8$	?

Table 2-7 Possible roles of adhesion receptors (integrin) in osteoblasts and osteoclasts [133]

Osteoblasts (and osteocytes)
Transducation of mechanical signals within skeleton to regulate cell function
Adhesion to bone matrix, including unmineralised osteoid
Regulation of osteoblast maturation
Regulation of mature cell function (matrix synthesis, protease secretion, etc)
Interaction with other bone cells (e.g., osteoclasts) and cells in the bone marrow compartment (e.g., marrow stroma, leucocytes)
Osteoclasts
Migration of committed osteoclast progenitors/precursors from the bone marrow to sites of future resorption exiting via specialised endothelial barriers
Homing to bone (using chemo-, hapto-tatic signals) and ingress across vascular endothelium
Recognition of, adhesion to, and migration upon bone matrix proteins
Fusion of postmitotic osteoclast precursors
Regulatory intercellular interactions with osteoblasts, leucocytes, and other cell types in marrow space; presentation of growth factors from extracellular matrix stores
Signal transduction (and control of osteoclast function) by interaction with matrix (via RGD and other sequences)
Cellular polarisation, tight sealing zone formation, and bone resorption
Cessation of resorption by detachment from matrix, cell migration, and regulation of osteoclast survival versus apoptosis

Stage 2 (Down-regulation of proliferation, 12-18 days):

Following the initial proliferation period, expression of genes associated with the maturation and organization of the bone ECM are upregulated, contributing to rendering the extracellular matrix competent for mineralisation (e.g., alkaline phosphatase). Collagen synthesis continues and undergoes cross-link maturation. The details are described in follows:

Alkaline phosphatase (ALP) (noncollagenous glycoproteins): For mineralisation, A(L)P-1 binding activity is observed primarily in proliferating osteoblasts and dramatically decreases after the down-regulation of proliferation and the initiation of extracellular matrix maturation and mineralisation.

Stage 3 (Mineralisation, 16-20 days):

The third developmental period involves gene expression related to the accumulation of hydroxyapatite in the ECM. Genes encoding several proteins with mineral binding properties, e.g., osteopontin, osteocalcin, and bone sialoprotein, exhibit maximal expression at this time when mineralisation of bone tissue-like organised matrix is ongoing. This profile suggests functional roles for these proteins in regulation of the ordered deposition of hydroxyapatite.

Bone matrix glycoproteins (noncollagenous proteins)–Osteonectin /SPARC (secreted protein, acidic and rich in cysteine); osteopontin (OPN)/bone sialoprotein (BSP); bone matrix proteoglycans-biglycan/decorin and osteocalcin (OC): While the organic matrix of bone is composed primarily of collagen, it may not be the direct nucleator of hydroxyapatite deposition; therefore the existence of noncollagenous components (bone-synthesised proteins) associated with the mineralised matrix, in regulation of the ordered deposition of hydroxyapatite (HA), is important in bone physiology. In other words, there are a large number of matrix proteins that have been found bind to collagen thereby forming fibrils, and it is probable that collagen serves as a scaffolding upon which nucleators are oriented.

Osteonectin stimulates the binding of both of Ca^{2+}-HA and Ca^{2+} to insoluble collagen in a dose-dependent manner, and may play a role in the initiation of bone mineralisation. There is also evidence that osteonectin interacts with other extracellular

matrix components. For example, binding activity of bovine bone osteonectin to type I collagen has been demonstrated by Romberg [145]. Although osteonectin is highly enriched in bone, it is also expressed in a variety of other connective tissues at specific points during development, maturation, or repair process in *vivo*.

OPN and **BSP** are RGD-containing glycoproteins characterised by the relatively large amounts of sialic acid, localised in mineralising matrix. At the transcriptional level [146] [147], these proteins are regulated at multiple levels with respect to induction and enhancement by hormones, growth factors (Table 2-8). OPN also plays a role in the early stages of osteogenesis by attachment of osteoblasts to the extracellular matrix that they are synthesizing, be involved in attachment of osteoclasts during bone resorption. It is likely that OPN participates in intracellular signalling via interaction of in GRGD (Gly-Arg-Gly-Asp) sequences with $\alpha_v\beta_3$ integrins.

Osteocalcin (γ-carboxy glutamin acid-containing proteins) is a marker of the mature osteoblast, which may regulate activity of osteoclasts and their precursors, and may mark the turning point between bone formation and resorption. Retinoic acid can be used to exhibit potent growth inhibitory and cell differentiation activities that account for their beneficial effects in treating hyperproliferative diseases [148].

Stage 4 (Apoptosis):

Apoptotic activity occurs. A fourth developmental period follows in mature cultures during which time collagenase is elevated, and apoptotic activity and collagen expression is evident.

Tumour necrosis factor (TNF) (cytokine) contains TNFα and TNFβ, which have similar biological activities, are both potent stimulators of bone resorption and inhibitors of bone collagen synthesis. TNF-related apoptosis-inducing ligand (TRAIL) is a member of the TNF superfamily of cytokines, which have been shown to induce apoptosis in a variety of cancer cells [149].

Table 2-8 Growth factor and hormonal regulation of osteopontin (OPN) and bone sialoprotein (BSP)

Factor	RNA	Protein
Transforming growth factor β	↑ OPN MC3T3-E1	↑ OPN MC3T3-E1
	↑ OPN ROS 17/2.8	↑ OPN ROS 17/2.8
	— OPN ROS 17/2.8	↓ OPN ROS 17/2.8
	↑ OPN rat calvaria	↑ OPN rat calvaria
Platelet-derived growth	—	↑ OPN rat calvaria
Leukemia-inhibitory factor	↑ OPN MC3T3-E1	—
Interleukin 1	↑ OPN MC3T3-E1	↑ OPN MC3T3-E1
	↑ OPN mouse calvaria	—
Dexamethasone	↓ OPN ROS 17/2.8	—
	↓ OPN rat calvaria	—
	↑ OPN rat marrow stroma	↑ OPN rat marrow stroma
	↑ BSP ROS 17/2.8	
	↑ BSP rat calvaria	
1,25-dihydroxyvitamin D_3	↑ OPN ROS 17/2.8	↑ OPN ROS 17/2.8
	↑ OPN MC3T3-E1	—
	↑ OPN mouse calvaria	—
	↑ OPN rat calvaria	↑ OPN rat calvaria
	↑ OPN rat marrow stroma	↑ OPN mouse JB6 cells
	↓ BSP ROS 17/2.8	—
	↓ BSP rat calvaria cells	—
Transformation	↑ OPN mouse epidermis ↑ OPN mouse JB6 cells ↑ OPN 3T3 cells ↑ OPN rat kidney line	↑ OPN mouse epidermis
		↑ OPN mouse JB6 cells
		↑ OPN 3T3 cells
		↑ OPN rat kidney line
		↑ OPN human osteosarcoma
		↑ OPN human fibrosarcoma
		↑ OPN human cervix
		↑ OPN human colon
		↑ OPN human ovary
		↑ OPN human bladder
		↑ OPN human macrophage
		↑ OPN hamster fibroblast
		↑ OPN rat fibroblast
		↑ OPN mouse fibroblast
		↑ OPN rabbit fibroblast
		↑ OPN rat liver epithelia

Human nuclear transcription factor-kappa B (NF-κB): NF-κB is a key transcription factor which is involved in the transcription of a wide array of genes that are involved

in immune and inflammatory responses, and also contribute to the regulation of cellular proliferation and apoptosis. A large and continuously expanding range of pathogens has been shown to induce NF-κB activation and in many cases, a participation of NF-κB in the pathogenesis of the diseases caused by these infectious agents is suspected. The expression of p50 (NF-κB) and p52 (NF-κB) activity is investigated in this study. Recent work has suggested that p50 play an important role in skin carcinogenesis [150]. Generally speaking, NF-κB plays an early, critical role in the carcinogen-driven transformation of mammary glands [151].

Colony-stimulating factor (CSF)-1 and **macrophage CSF** (M-CSF): Osteoclast formation in bone is supported by osteoblasts expressing the receptor activator of the NF-kappa B ligand (RANKL) and macrophage colony-stimulating factor (M-CSF) expression [152] [153].

Caspase-like apoptosis regulatory protein, apoptosis specific protein (ASP) and human Bcl-2 family and Bcl-xL: Caspases which play crucial roles during apoptosis are activated from their inactive performs in a sequence of cleavage by other members of the caspase family. Apoptosis specific protein was observed to expression high levels when human and rodent cells undergoing apoptosis [154] [155] [156]. Bcl-xL an antiapoptotic member of the Bcl-2 family and prevents activation of caspases *in vitro* [157]. Bcl-xL can block cytochromate c release from mitochondria, which play an essential role in apoptosis by releasing apoptogenic molecules such as cytochrome c and some caspases, which are regulated by Bcl-2 family proteins [158].

Summary

The current literature survey has mainly focussed on two areas: (1) *the mechanism of metal ion release and the factors, which may influence the dissolution process*. These factors include the surface properties and chemical composition of the oxide, the electrochemical behaviour of the alloy, coating effects and biological interactions, and the literature has focused on some key *in vitro* and *in vivo* studies. Biocompatibility tests of materials without an understanding of their surface properties would serve little

purpose, therefore a number of appropriate analytical tools have been described. Analysis of the surface characterisation and composition of biomaterials is critical to allow a better understanding of the interactions between the host and implant. (2) *Quantification of the implant-host interaction.* The characterisation of the surface treated alloy in the initial part of this study has been approached from materials science perspective. However, ultimately, it is the biological performance of the treated implant, which is crucial to its acceptance or rejection *in vivo*. Therefore, a thorough understanding of the host tissue biology and biocompatibility methodologies, such as cell culture and functional genomic studies are required. It is through such an understanding that the improved dissolution behaviour and biocompatibility exhibited by the ageing treatment may be understood. Moreover, studies of this nature will further help in the design of specific surfaces tailored to provide improved biocompatibility.

References

1. Lister, J., Br Med J, 1883. **2**: p. 855.
2. Smith-Peterson, M.N., Journal of bone and Joint Surgery, 1939. **21**: p. 269.
3. Park, J.B. and R.S. Lakes, *Biomaterials-An Introduction.* 1992, London: Plenum Press.
4. Laing, P.G., *Compatibility of biomaterials.* Orthopedic Clinics of North America, 1973. **4**: p. 249.
5. Hille, G.H., *Titanium for surgical implants.* J. Mater., 1966. **1**: p. 373-83.
6. Branemark, P.I., et al., Scand J Plast Reconstr Surg, 1977. **11**: p. 39-94.
7. An, Y.H. and R.A. Draughn, *Mechanical testing of bone and the bone-implant interface*. 2000, London: CRC press.
8. Duncan, R.M. and B.H. Hanson, *The selection and use of titanium, Materials Engineering Design Guides; 39.* 1980, United Kingdom: Oxford University Press.
9. Breme, J., *Titanium and Titanium-Alloys, Biomaterials of Preference.* Memoires Et Etudes Scientifiques De La Revue De Metallurgie, 1989. **86**(10): p. 625-37.
10. Okazaki, Y., et al., *Corrosion resistance, mechanical properties, corrosion fatigue strength and cytocompatibility of new Ti alloys without Al and V.* Biomaterials, 1998. **19**(13): p. 1197-215.
11. Niinomi, M., *Mechanical properties of biomedical titanium alloys.* Materials Science and Engineering a-Structural Materials Properties Microstructure and Processing, 1998. **243**(1-2): p. 231-6.
12. Syrett, B.C. and A. Acharya, *Corrosion and degradation of implant materials, ASTM STP 684.* 1979, Pennsylvania: American Society for Testing and Materials.
13. Boulton, L.H. and A.J. Betts, *Corrosion performance of titanium and titanium stabilised stainless steels.* Br Corros, 1991. **26**(4): p. 287-92.
14. Evans, S.L., *Adhesively bonded hydroxyapatite coatings*, in *Department of Engineering Materials*. 1992, University of Southampton: Southampton, UK. p. 12.

15. Liu, J.Q., et al., *High-resolution transmission electron microscopy investigations of a highly adhesive hydroxyapatite coating/titanium interface fabricated by ion-beam-assisted deposition.* J Biomed Mater Res, 2000. **52**(1): p. 115-8.

16. Browne, M., P.J. Gregson, and R.H. West, *Characterization of titanium alloy implant surfaces with improved dissolution resistance.* Journal of Materials Science-Materials in Medicine, 1996. **7**(6): p. 323-9.

17. Sundararajan, T., et al., *Surface characterization of electrochemically formed passive film on nitrogen ion implanted Ti6Al4V alloy.* Materials Transactions Jim, 1998. **39**(7): p. 756-61.

18. Wisbey, A., et al., *Effect of surface-treatment on the dissolution of titanium-based implant materials.* Biomaterials, 1999. **12**(5): p. 470-3.

19. Pouilleau, J., et al., *Structure and composition of passive titanium oxide films.* Materials Science and Engineering B-Solid State Materials for Advanced Technology, 1997. **47**(3): p. 235-43.

20. Pouilleau, J., et al., *Surface study of a titanium-based ceramic electrode material by X-ray photoelectron spectroscopy.* Journal of Materials Science, 1997. **32**(21): p. 5645-51.

21. Kurtz, R.L., et al., *Synchrotron Radiation Studies of H2O Adsorption on TiO2(110).* Surface Science, 1989. **218**(1): p. 178-200.

22. Bullock, E.L., L. Patthey, and S.G. Steinemann, *Clean and hydroxylated rutile TiO2(110) surfaces studied by X- ray photoelectron spectroscopy.* Surface Science, 1996. **352**: p. 504-10.

23. Lausmaa, J., *Surface spectroscopic characterization of titanium implant materials.* Journal of Electron Spectroscopy and Related Phenomena, 1996. **81**(3): p. 343-61.

24. Lee, T.M., E. Chang, and C.Y. Yang, *A comparison of the corrosion behaviour and surface characteristics of vacuum-brazed and heat-treated Ti6Al4V alloy.* Journal of Materials Science-Materials in Medicine, 1998. **9**(8): p. 429-37.

25. Pan, J., D. Thierry, and C. Leygraf, *Electrochemical impedance spectroscopy study of the passive oxide film on titanium for implant application.* Electrochimica Acta, 1996. **41**(7-8): p. 1143-53.

26. Sundgren, J.E., et al., *Adsorption of Fibrinogen on Titanium and Gold Surfaces Studied by Esca and Ellipsometry.* Journal of Colloid and Interface Science, 1986. **113**(2): p. 530-43.

27. Hanawa, T., et al., *Surface modification of titanium in calcium-ion-containing solutions.* Journal of Biomedical Materials Research, 1997. **34**(3): p. 273-8.

28. Ektessabi, A.M., et al., *Application of synchrotron radiation in investigation of metal- ion release from a hip replacement prosthesis.* Journal of Synchrotron Radiation, 1998. **5**: p. 1136-8.

29. Okazaki, Y., et al., *Effects of Ti, Al and V concentrations on cell viability.* Materials Transactions Jim, 1998. **39**(10): p. 1053-62.

30. Nelson, D.J., *Aluminum complexation with nucleoside di-and triphosphates and implication in nucleoside binding proteins.* Coordination chemistry reviews, 1996. **149**: p. 95-111.

31. Berthon, G., *Chemical speciation studies in relation to aluminium metabolism and toxicity.* Coordination chemistry reviews, 1996. **149**: p. 241-80.

32. Ellingsen, J.E., *A Study on the Mechanism of Protein Adsorption to Tio2.* Biomaterials, 1991. **12**(6): p. 593-6.

33. Ducheyne, P. and K.E. Healy, *The Effect of Plasma-Sprayed Calcium-Phosphate Ceramic Coatings on the Metal-Ion Release from Porous Titanium and Cobalt- Chromium Alloys.* Journal of Biomedical Materials Research, 1988. **22**(12): p. 1137-63.

34. Healy, K.E. and P. Ducheyne, *Passive Dissolution Kinetics of Titanium Invitro.* Journal of Materials Science-Materials in Medicine, 1993. **4**(2): p. 117-26.

35. Clark, G.C.F. and D.F. Williams, *The Effects of Proteins on Metallic Corrosion.* Journal of Biomedical Materials Research, 1982. **16**(2): p. 125-34.

36. Prutton, M., *Introduction to surface physics.* 1994, Oxford: Oxford Science Productions.

37. Janusz, W., et al., *Investigation of the electrical double layer in a metal oxide/monovalent electrolyte solution system.* Journal of Colloid and Interface Science, 1997. **187**(2): p. 381-7.

38. Gold, J.M., M. Schmidt, and S.G. Steinemann, *Xps Study of Amino-Acid Adsorption to Titanium Surfaces.* Helvetica Physica Acta, 1989. **62**(2-3): p. 246-9.

39. Spanos, N., I. Georgiadou, and A. Lycourghiotis, *Investigation of Rutile, Anatase, and Industrial Titania Water Solution Interfaces Using Potentiometric Titration and Microelectrophoresis.* Journal of Colloid and Interface Science, 1995. **172**(2): p. 374-82.

40. Born, R., et al., *Surface analysis of titanium based biomaterials.* Fresenius Journal of Analytical Chemistry, 1998. **361**(6-7): p. 697-700.

41. Burstein, G.T. and R.M. Souto, *Observations of Localized Instability of Passive Titanium in Chloride Solution.* Electrochimica Acta, 1995. **40**(12): p. 1881-8.

42. Souto, R.M. and G.T. Burstein, *A preliminary investigation into the microscopic depassivation of passive titanium implant materials in vitro.* Journal of Materials Science-Materials in Medicine, 1996. **7**(6): p. 337-43.

43. Khan, M.A., R.L. Williams, and D.F. Williams, *The corrosion behaviour of Ti-6Al-4V, Ti-6Al-7Nb and Ti-13Nb- 13Zr in protein solutions.* Biomaterials, 1999. **20**(7): p. 631-7.

44. Souto, R.M. and G.T. Burstein, *Study of corrosion processes with electrochemical noise measurements.* Electrochemical Methods in Corrosion Research Vi, Pts 1 and 2, 1998. **289-2**: p. 799-806.

45. Morris, H.F. and S. Ochi, *Hydroxyapatite-coated implants: A case for their use.* Journal of Oral and Maxillofacial Surgery, 1998. **56**(11): p. 1303-11.

46. Marra, K.G., et al., *In vitro analysis of biodegradable polymer blend/hydroxyapatite composites for bone tissue engineering.* Journal of Biomedical Materials Research, 1999. **47**(3): p. 324-35.

47. Narasaraju, T.S.B. and D.E. Phebe, *Some physico-chemical aspects of hydroxylapatite.* Journal of Materials Science, 1996. **31**(1): p. 1-21.

48. Han, Y., et al., *Characterization and stability of hydroxyapatite coatings prepared by an electrodeposition and alkaline-treatment process.* Journal of Biomedical Materials Research, 2001. **54**(1): p. 96-101.

49. Cook, S.D., et al., *Hydroxylapatite Coating of Porous Implants Improves Bone Ingrowth and Interface Attachment Strength.* Journal of Biomedical Materials Research, 1992. **26**(8): p. 989-1001.

50. Hulshoff, J.E.G., et al., *Interfacial phenomena: An in vitro study of the effect of calcium phosphate (Ca-P) ceramic on bone formation.* Journal of Biomedical Materials Research, 1998. **40**(3): p. 464-74.

51. Ong, J.L., et al., *Osteoblast precursor cell activity on HA surfaces of different treatments.* Journal of Biomedical Materials Research, 1998. **39**(2): p. 176-83.

52. Ellies, L.G., D.G.A. Nelson, and J.D.B. Featherstone, *Crystallographic Changes in Calcium Phosphates During Plasma- Spraying.* Biomaterials, 1992. **13**(5): p. 313-6.

53. Cheang, P. and K.A. Khor, *Addressing processing problems associated with plasma spraying of hydroxyapatite coatings.* Biomaterials, 1996. **17**(5): p. 537-44.

54. Weng, J., et al., *Integrity and thermal decomposition of apatite in coatings influenced by underlying titanium during plasma spraying and post-heat-treatment.* Journal of Biomedical Materials Research, 1996. **30**(1): p. 5-11.

55. Liu, D.M., H.M. Chou, and J.D. Wu, *Plasma-Sprayed Hydroxyapatite Coating - Effect of Different Calcium-Phosphate Ceramics.* Journal of Materials Science-Materials in Medicine, 1994. **5**(3): p. 147-53.

56. Albrektsson, T., *Hydroxyapatite-coated implants: A case against their use.* Journal of Oral and Maxillofacial Surgery, 1998. **56**(11): p. 1312-26.

57. Zyman, Z., et al., *Phase and Structural-Changes in Hydroxyapatite Coatings under Heat-Treatment.* Biomaterials, 1994. **15**(2): p. 151-5.

58. Cortada, M., et al., *Metallic ion release in artificial saliva of titanium oral implants coupled with different metal superstructures.* Bio-Medical Materials and Engineering, 1997. **7**(3): p. 213-20.

59. Elliott, C.B. and D.W. Hoeppner, *The importance of wear and corrosion on the fretting fatigue behavior of two aluminum alloys.* Wear, 1999. **236**(1-2): p. 128-33.

60. Hoeppner, D.W. and V. Chandrasekaran, *Fretting in Orthopedic Implants - a Review.* Wear, 1994. **173**(1-2): p. 189-97.

61. Helsen, J.A. and H.J. Breme, *Metals as Biomaterials, Biomaterials Science and Engineering Series*. 1998, London: Wiley.

62. Trethewey, K.R. and J. Chamberlain, *Corrosion for science and engineering.* 1996, Essex: Longman.

63. Jacobs, J.J., J.L. Gilbert, and R.M. Urban, *Corrosion of metal orthopaedic implants.* Journal of Bone and Joint Surgery-American Volume, 1998. **80A**(2): p. 268-82.

64. Black, J., et al., *Metallosis Associated with a Stable Titanium-Alloy Femoral Component in Total Hip-Replacement - a Case-Report.* Journal of Bone and Joint Surgery-American Volume, 1990. **72A**(1): p. 126-30.

65. Willert, H.G., et al., *Crevice corrosion of cemented titanium alloy stems in total hip replacements.* Clinical Orthopaedics and Related Research, 1996(333): p. 51-75.

66. Brown, S.A. and J.E. Lemons, *Medical applications of titanium and its alloys the material and biological issues.* 1996, Pennsylvania, USA: ASTM.

67. Diggle, J.W., *The anodic behaviour of metals and semiconductors series, in Oxides and oxide films, vol.1.* 1972, New York: Marcel Dekker.

68. ASTM, *Standard test method for pitting or crevice corrosion of metallic surgical implant materials-F746-87.* Vol. 03.02. 1998, Pennsylvania, USA: American Society for Testing and Materials.

69. Jones, D.A., *Principles and Prevention of Corrosion.* 1992, London: Prentice-Hall.

70. Sundararajan, T., et al., *Electrochemical studies on nitrogen ion implanted Ti6Al4V alloy.* Anti-Corrosion Methods and Materials, 1998. **45**(3): p. 162-+.

71. Sutherland, D.S., et al., *Surface-Analysis of Titanium Implants.* Biomaterials, 1993. **14**(12): p. 893-9.

72. Woodruff, D.P. and T.A. Delchar, *Modern techniques of surface science,solid state science series.* 1994, Cambridge: Cambridge press. xxi, 567.

73. Magonov, S.N. and M.H. Whangbo, *Surface analysis with STM and AFM.* 1994: VCH.

74. Ratner, B.D., et al., *Biomaterials science An introduction to materials in Medicine.* 1996, San Diego: Academic Press. xxi, 567.

75. Briggs, D. and M.P. Seah, *Auger and X-ray photoelectron spectroscopy*, ed. n. ed. Vol. 1. 1990, London: Wiley.

76. Placko, H.E., et al., *Surface characterization of titanium-based implant materials.* International Journal of Oral & Maxillofacial Implants, 2000. **15**(3): p. 355-63.

77. Anselme, K., et al., *The relative influence of the topography and chemistry of TiAl6V4 surfaces on osteoblastic cell behaviour.* Biomaterials, 2000. **21**(15): p. 1567-77.

78. Baleani, M., M. Viceconti, and A. Toni, *The effect of sandblasting treatment on endurance properties of titanium alloy hip prostheses.* Artificial Organs, 2000. **24**(4): p. 296-9.

79. Jalava, J.P., et al., *Structural investigation of hydrous TiO2 precipitates and their aging products by X-ray diffraction, atomic force microscopy, and transmission electron microscopy.* Industrial & Engineering Chemistry Research, 1998. **37**(4): p. 1317-23.

80. Williams, D.F., *Definitions in Biomaterials, Progress in Biomedical Engineering, 4.* 1987, London: Elsevier Press.

81. Kirkpatrick, C.J., et al., *Current trends in biocompatibility testing.* Proceedings of the Institution of Mechanical Engineers Part H- Journal of Engineering in Medicine, 1998. **212**(H2): p. 75-84.

82. Hanks, C.T., J.C. Wataha, and Z.L. Sun, *In vitro models of biocompatibility: A review.* Dental Materials, 1996. **12**(3): p. 186-93.

83. Ratner, B.D., *Molecular design strategies for biomaterials that heal.* Macromolecular Symposia, 1998. **130**: p. 327-35.

84. Suchanek, W. and M. Yoshimura, *Processing and properties of hydroxyapatite-based biomaterials for use as hard tissue replacement implants.* Journal of Materials Research, 1998. **13**(1): p. 94-117.

85. Ratner, B.D., *New Ideas in Biomaterials Science - a Path to Engineered Biomaterials.* Journal of Biomedical Materials Research, 1993. **27**(7): p. 837-50.

86. Ahmad, M., M. McCarthy, and G. Gronowicz, *An in vitro model for mineralization of human osteoblast-like cells on implant materials.* Biomaterials, 1999. **20**(3): p. 211-20.

87. Nauman, E.A., et al., *Microscale engineering applications in bone adaptation.* Microscale Thermophysical Engineering, 1998. **2**(3): p. 139-72.

88. Aubin, J.E., et al., *Osteoblast and Chondroblast Differentiation.* Bone, 1995. **17**(2): p. S77-S83.

89. Lian, J.B. and G.S. Stein, *Concepts of Osteoblast Growth and Differentiation - Basis for Modulation of Bone Cell-Development and Tissue Formation.* Critical Reviews in Oral Biology & Medicine, 1992. **3**(3): p. 269-305.

90. Lian, J.B. and G.S. Stein, *Osteoblast biology.* Osteoporosis, ed. R. Marcus, D. Feldman, and J. Kelsey. 1996, San Diego: Academic Press. xxiv, 1373.

91. Ahmad, M., et al., *Differential response of human osteoblast-like cells to commercially pure (cp) titanium grades 1 and 4.* Journal of Biomedical Materials Research, 1999. **46**(1): p. 121-31.

92. Sanderson, C., *Entering the realm of mineralized bone processing: A review of the literature and techniques.* Journal of Histotechnology, 1997. **20**(3): p. 259-66.

93. Goldberg, V.M. and T. Jinno, *The bone-implant interface: A dynamic surface.* Journal of Long-Term Effects of Medical Implants, 1999. **9**(1-2): p. 11-21.

94. Lebaron, R.G. and K.A. Athanasiou, *Extracellular matrix cell adhesion peptides: Functional applications in orthopedic materials.* Tissue Engineering, 2000. **6**(2): p. 85-103.

95. Shah, A.K., et al., *Mechanism of BMP-2 stimulated adhesion of osteoblastic cells to titanium alloy.* Biology of the Cell, 1999. **91**(2): p. 131-42.

96. MacDonald, D.E., et al., *Surface analysis of human plasma fibronectin adsorbed to commercially pure titanium materials.* Journal of Biomedical Materials Research, 1998. **41**(1): p. 120-30.

97. Hunter, A., et al., *Attachment and Proliferation of Osteoblasts and Fibroblasts on Biomaterials for Orthopedic Use.* Biomaterials, 1995. **16**(4): p. 287-95.

98. Kirkpatrick, C.J., et al., *The cell and molecular biological approach to biomaterial research: A perspective.* Journal of Materials Science-Materials in Medicine, 1997. **8**(3): p. 131-41.

99. Giacomelli, C.E., M.J. Avena, and C.P. DePauli, *Adsorption of bovine serum albumin onto TiO2 particles.* Journal of Colloid and Interface Science, 1997. **188**(2): p. 387-95.

100. Anselme, K., *Osteoblast adhesion on biomaterials.* Biomaterials, 2000. **21**(7): p. 667-81.

101. D'Lima, D.D., et al., *Bone response to implant surface morphology.* Journal of Arthroplasty, 1998. **13**(8): p. 928-34.

102. Sittig, C., et al., *Surface characterization of implant materials cp Ti, Ti-6Al-7Nb and Ti-6Al-4V with different pretreatments.* Journal of Materials Science-Materials in Medicine, 1999. **10**(1): p. 35-46.

103. Davies, J.E., B. Lowenberg, and A. Shiga, *The Bone Titanium Interface Invitro.* Journal of Biomedical Materials Research, 1990. **24**(10): p. 1289-306.

104. Keller, J.C., et al., *Characterizations of Titanium Implant Surfaces .3.* Journal of Biomedical Materials Research, 1994. **28**(8): p. 939-46.

105. Wen, X.J., X.X. Wang, and N. Zhang, *Microrough surface of metallic biomaterials: A literature review.* Bio-Medical Materials and Engineering, 1996. **6**(3): p. 173-89.

106. Urano, H. and S. Fukuzaki, *Influence of anionic compounds on adsorption behavior of bovine serum albumin at oxide-water interfaces.* Journal of Fermentation and Bioengineering, 1997. **83**(3): p. 261-6.

107. Kasemo, B. and J. Lausmaa, *Surface Science Aspects on Inorganic Biomaterials.* Crc Critical Reviews in Biocompatibility, 1986. **2**(4): p. 335-80.

108. Schroeder, A., et al., *Titanium containing amorphous hydrogenated carbon films (a-C : H/Ti): surface analysis and evaluation of cellular reactions using bone marrow cell cultures in vitro.* Biomaterials, 2000. **21**(5): p. 449-56.

109. Pioletti, D.P., et al., *The cytotoxic effect of titanium particles phagocytosed by osteoblasts.* Journal of Biomedical Materials Research, 1999. **46**(3): p. 399-407.

110. Morais, S., et al., *In vitro osteoblastic differentiation of human bone marrow cells in the presence of metal ions.* Journal of Biomedical Materials Research, 1999. **44**(2): p. 176-90.

111. Liao, H.H., T. Wurtz, and J.G. Li, *Influence of titanium ion on mineral formation and properties of osteoid nodules in rat calvaria cultures.* Journal of Biomedical Materials Research, 1999. **47**(2): p. 220-7.

112. Nichols, K.G. and D.A. Puleo, *Effect of metal ions on the formation and function of osteoclastic cells in vitro.* Journal of Biomedical Materials Research, 1997. **35**(2): p. 265-71.

113. Bellows, C.G., J.E. Aubin, and J.N. Heersche, *Aluminum inhibits both initiation and progression of mineralization of osteoid nodules formed in differentiating rat calvaria cell cultures.* J Bone Miner Res, 1995. **10**(12): p. 2011-6.

114. Thompson, G.J. and D.A. Puleo, *Effects of Sublethal Metal-Ion Concentrations on Osteogenic Cells Derived from Bone-Marrow Stromal Cells.* Journal of Applied Biomaterials, 1995. **6**(4): p. 249-58.

115. Merklein, F., et al., *Standardised testing of bone-implant surfaces using an osteoblast cell culture system. Part I: Standard materials in orthopaedic surgery.* Biomedizinische Technik, 1998. **43**(12): p. 354-9.

116. Martin, R.B., *Aluminum Speciation in Biology.* Ciba Foundation Symposia, 1992. **169**: p. 5-25.

117. Bellows, C.G., J.N.M. Heersche, and J.E. Aubin, *Aluminum accelerates osteoblastic differentiation but is cytotoxic in long-term rat calvaria cell cultures.* Calcified Tissue International, 1999. **65**(1): p. 59-65.

118. Maurer, A.M., K. Merritt, and S.A. Brown, *Cellular Uptake of Titanium and Vanadium from Addition of Salts or Fretting Corrosion in-Vitro.* Journal of Biomedical Materials Research, 1994. **28**(2): p. 241-6.

119. Manlapaz, M., W.J. Maloney, and R.L. Smith, *In vitro activation of human fibroblasts by retrieved titanium alloy wear debris.* Journal of Orthopaedic Research, 1996. **14**(3): p. 465-72.

120. Brazma, A. and J. Vilo, *Gene expression data analysis.* Febs Letters, 2000. **480**(1): p. 17-24.

121. Celis, J.E., et al., *Gene expression profiling: monitoring transcription and translation products using DNA microarrays and proteomics.* Febs Letters, 2000. **480**(1): p. 2-16.

122. Kiberstis, P., O. Smith, and C. Norman, *Bone health in the balance.* Science, 2000. **289**(5484): p. 1497.

123. Ducy, P., T. Schinke, and G. Karsenty, *The osteoblast: A sophisticated fibroblast under central surveillance.* Science, 2000. **289**(5484): p. 1501-4.

124. Teitelbaum, S.L., *Bone resorption by osteoclasts.* Science, 2000. **289**(5484): p. 1504-8.

125. Gerstein, M., *Measurement of the effectiveness of transitive sequence comparison, through a third 'intermediate' sequence.* Bioinformatics, 1998. **14**(8): p. 707-14.

126. Brazma, A., et al., *One-stop shop for microarray data - Is a universal, public DNA- microarray database a realistic goal?* Nature, 2000. **403**(6771): p. 699-700.

127. Streicher, J., et al., *Computer-based three-dimensional visualization of developmental gene expression.* Nature Genetics, 2000. **25**(2): p. 147-52.

128. Cho, R.J. and M.J. Campbell, *Transcription, genomes, function.* Trends in Genetics, 2000. **16**(9): p. 409-15.

129. Cummings, C.A. and D.A. Relman, *Using DNA microarrays to study host-microbe interactions.* Emerging Infectious Diseases, 2000. **6**(5): p. 513-25.

130. Ghosh, D., *High throughput and global approaches to gene expression.* Combinatorial Chemistry & High Throughput Screening, 2000. **3**(5): p. 411-20.

131. Gerstein, M. and R. Jansen, *The current excitement in bioinformatics - analysis of whole- genome expression data: how does it relate to protein structure and function?* Current Opinion in Structural Biology, 2000. **10**(5): p. 574-84.

132. Noda, M., *Cellular and molecular biology of bone.* 1993, San Diego: Academic Press.

133. Bilezikian, J.P. and L.G. Raisz, *Principles of bone biology.* 1996, San Diego: Academic Press. xxi, 567.

134. Benjamin, L., *Genes VII.* 7th ed ed. 2000, Oxford: Oxford University Press.

135. Anselme, K., et al., *Qualitative and quantitative study of human osteoblast adhesion on materials with various surface roughnesses.* Journal of Biomedical Materials Research, 2000. **49**(2): p. 155-66.

136. Palcy, S. and D. Goltzman, *Protein kinase signalling pathways involved in the up- regulation of the rat alpha 1(I) collagen gene by transforming growth factor beta(1) and bane morphogenetic protein 2 in osteoblastic cells.* Biochemical Journal, 1999. **343**: p. 21-7.

137. Martelli, A.M., et al., *Phosphatidylinositol 3-kinase translocates to the nucleus of osteoblast-like MC3T3-E1 cells in response to insulin-like growth factor I and platelet-derived growth factor but not to the proapoptotic cytokine tumor necrosis factor alpha.* Journal of Bone and Mineral Research, 2000. **15**(9): p. 1716-30.

138. Montero, A., et al., *Disruption of the fibroblast growth factor-2 gene results in decreased bone mass and bone formation.* J Clin Invest, 2000. **105**(8): p. 1085-93.

139. Takei, H., et al., *Combined effect of titanium particles and TNF-alpha on the production of IL-6 by osteoblast-like cells.* Journal of Biomedical Materials Research, 2000. **52**(2): p. 382-7.

140. Balkwill, F., *The Cytokine Network.* 2000, Oxford: Oxford University Press.

141. Small, D., et al., *Stk-1, the Human Homolog of Flk-2/Flt-3, Is Selectively Expressed in Cd34(+) Human Bone-Marrow Cells and Is Involved in the Proliferation of Early Progenitor Stem-Cells.* Proceedings of the National Academy of Sciences of the United States of America, 1994. **91**(2): p. 459-63.

142. Grigoriadis, A.E., et al., *C-Fos - a Key Regulator of Osteoclast-Macrophage Lineage Determination and Bone Remodeling.* Science, 1994. **266**(5184): p. 443-8.

143. Rabbani, S.A., et al., *Induction in human osteoblastic cells (SaOS(2)) of the early response genes fos, jun, and myc by the amino terminal fragment (ATF) of urokinase.* Journal of Cellular Physiology, 1997. **172**(2): p. 137-45.

144. Saito, T., S.M. Albelda, and C.T. Brighton, *Identification of Integrin Receptors on Cultured Human Bone- Cells.* Journal of Orthopaedic Research, 1994. **12**(3): p. 384-94.

145. Romberg, R.W., et al., *Isolation and Characterization of Native Adult Osteonectin.* Journal of Biological Chemistry, 1985. **260**(5): p. 2728-36.

146. DeRisi, J.L., V.R. Iyer, and P.O. Brown, *Exploring the metabolic and genetic control of gene expression on a genomic scale.* Science, 1997. **278**(5338): p. 680-6.

147. Iyer, V.R., et al., *The transcriptional program in the response of human fibroblasts to serum.* Science, 1999. **283**(5398): p. 83-7.

148. DiSepio, D., et al., *Identification and characterization of a retinoid-induced class II tumor suppressor growth regulatory gene.* Proceedings of the National Academy of Sciences of the United States of America, 1998. **95**(25): p. 14811-5.

149. Griffith, T.S., et al., *Adenoviral-mediated gene transfer of trail induces tumor cell apoptosis.* Faseb Journal, 2000. **14**(6): p. A1003-A1003.

150. Budunova, I.V., et al., *Increased expression of p50-NF-kappa B and constitutive activation of NF-kappa B transcription factors during mouse skin carcinogenesis.* Oncogene, 1999. **18**(52): p. 7423-31.

151. Kim, D.W., et al., *Activation of NF-kappa B/Rel occurs early during neoplastic transformation of mammary cells.* Carcinogenesis, 2000. **21**(5): p. 871-9.

152. Quinn, J.M.W., et al., *Fibroblastic stromal cells express receptor activator of NF- kappa B ligand and support osteoclast differentiation.* Journal of Bone and Mineral Research, 2000. **15**(8): p. 1459-66.

153. Dunn, S.M., et al., *Requirement for Nuclear Factor (Nf)-Kappa-B P65 and Nf-Interleukin-6 Binding-Elements in the Tumor-Necrosis-Factor Response Region of the Granulocyte-Colony-Stimulating Factor Promoter.* Blood, 1994. **83**(9): p. 2469-79.

154. Bjorkerud, S. and B. Bjorkerud, *Apoptosis is abundant in human atherosclerotic lesions, especially in inflammatory cells (macrophages and T cells), and may contribute to the accumulation of gruel and plaque instability.* American Journal of Pathology, 1996. **149**(2): p. 367-80.

155. Hammond, E.M., et al., *Homology between a human apoptosis specific protein and the product of APG5, a gene involved in autophagy in yeast.* Febs Letters, 1998. **425**(3): p. 391-5.

156. Grand, R.J.A., et al., *A Novel Protein Expressed in Mammalian-Cells Undergoing Apoptosis.* Experimental Cell Research, 1995. **218**(2): p. 439-51.

157. Fujita, E., et al., *Detection of caspase-9 activation in the cell death of the Bcl- x-deficient mouse embryo nervous system by cleavage sites- directed antisera.* Developmental Brain Research, 2000. **122**(2): p. 135-47.

158. Shimizu, S., Y. Shinohara, and Y. Tsujimoto, *Bax and Bcl-x(L) independently regulate apoptotic changes of yeast mitochondria that require VDAC but not adenine nucleotide translocator.* Oncogene, 2000. **19**(38): p. 4309-18.

Chapter 3 Characterisation and Performance of Metal Oxides

Part A. Uncoated Ti-6Al-4V

3.1 Introduction

Implants made from cp.-Ti or Ti-6Al-4V are customarily subjected to passivation treatments to produce a more inert surface by increasing the thickness of the spontaneously produced oxide layer. The ASTM-F86 standard is used for this purpose [1]. However, this treatment has actually been observed to increase Ti, Al, and V trace elements release from the Ti-6Al-4V alloy due to the formation of a less stable outer oxide layer [2] [3].

Previous work has investigated metal ion dissolution from Ti-6Al-4V implants in two simulated physiological environment (Ringer's solution[i] and bovine serum solution). It has been demonstrated that a simple thermal treatment, ageing in deionised distilled boiling water, is an effective method for reducing ion release from the passivated surface [4] [5] and improving biocompatibility[ii] [6]. In addition, previous TEM results[iii] have showed that the passivated structure consisted of a heterogeneous surface, including amorphous oxide and the anatase form of TiO_2 [7]. The aged oxide structure is more homogeneous, consisting of distinct crystalline phases corresponding to the rutile form of TiO_2, which is thicker, denser and more stable than the active passivated

[i] Ringer's solution: 9 kg/m^3 NaCl, 0.43 kg/m^3 KCl, 0.24 kg/m^3 $CaCl_2$ and 0.2 kg/m^3 $NaHCO_3$.
[ii] Please see *Chapter 5*.
[iii] Please see *Chapter 4, Table 4-3*.

surface oxide [8]. In particular, the passivated and the aged oxide surfaces produced different metal ion dissolution kinetics [9].

It has been shown that the surface properties of a biomaterial influence the nature of the adsorbed protein layers, cellular ingrowth, and ultimately biocompatibility [10] [11]. When immersed in a physiological environment, three mechanisms may occur at the materials/bio-environment interface: (1) metal ion dissolution [7] [9] (2) adsorption and desorption of biomolecules [12] [13] and (3) metal oxide formation [14] [15] [16]. Metal ion release can affect the stability of the interface between the solution and the oxide layer and in turn to induce side affects, such as abnormal cell growth or matrix (or fibre) formation events *in vitro* or *in vivo* [17].

Therefore this phase of the research attempts to determine: (1) the surface properties of the treated Ti-6Al-4V alloys using state of the art surface analytical techniques, (2) the change in the surface properties of various treated surfaces during immersion in bovine serum solution to further understand the correlation between the surface properties and metal ion release kinetics, and (3) the interface reaction between a solid surface and an adsorbed protein film.

3.2 Materials and Methods

3.2.1 Ti alloy surface preparation

Distal sections of forged Ti-6Al-4V alloy femoral stems from the Ti-Mod Freeman hip replacement were supplied by Finsbury Instruments (Leatherhead, Surrey, UK). The hip stems were cut into discs in 10 mm^2 and 1 mm thickness. The samples were first wet-ground with 120, 600, 1200, 2400 and 4000 grit silicon carbide abrasive paper (Struers, UK) at approximately 150 rpm, then polished with 6, 3 and 1 μm diamond solution (Microcloth Buehler, UK) on a clean polishing cloth (Microcloth Buehler, UK) and finally with colloidal silica polishing suspension (0.06 μm, Mastermet Buehler, UK). Following polishing, the samples were cleaned in 1% Triton solution for 1 hour and rinsed in deionised distilled water (MilliQ water, 18 MOhm water). This treatment

was used as a control (C). The practice for surface preparation of surgical implants involves a nitric acid passivation treatment (P) based on the ASTM F86 protocol using 30% nitric acid for 1 hour [1]. A third treatment (the ageing treatment, A) consisted of the passivated treatment followed by ageing in boiling deionised distilled water (MilliQ water) for 10 hours. The successive steps of the three surface treatments are shown in Table 3-1. The treated Ti-6Al-4V samples were then placed in bovine serum solution (Batch No. SBS 2117, First Link Ltd., UK) (Table 3-2) and incubated under a humidified 5% CO_2/air atmosphere at 37°C±0.1°C.

Table 3-1 The successive steps of surface treatments for the control, the passivated and the ageing Ti-6Al-4V

	Control (C)	Passivated (P)	Aged (A)
Surface preparation	-Polished -Cleaning in 1% Triton for 1 hour -Rinsing in deionised distilled water (MilliQ water)	-Polished -Cleaning 1% Triton for 1 hour -Rinsing in deionised distilled water -30% nitric acid for 1 hour -Rinsing in deionised distilled water	-Polished -Cleaning 1% Triton for 1 hour -Rinsing in deionised distilled water -30% nitric acid for 1 hour -Rinsing in deionised distilled water -10 hours in boiling deionised distilled water
Sterilisation	-Immersed in 100% ethanol for 10 min -Air-dried -Exposed under UV light for 30 min on each side -Rinsing in phosphate buffered solution (PBS) before immersion		

Table 3-2 Analysis of sterile adult bovine serum solution

Biophysical Assay:	**Concentration**
Density	1.023 b/ml at 24.1°C
Osmolarity	279 mOsmol/kg
pH	7.89
Proteins:	
Total protein	86.88 mg/ml
IgG (Mancini)	18.5 mg/ml
Albumin (Mancini) (MW: 67,000, isoelectric point: 4.7)	48 mg/ml
Globulin (MW: 2 x 53,000 + 2 x 23,000, isoelectric point: 7.2)	41 mg/ml
Haemoglobin	318.2 mg/l
Biochemcial Profile:	
Sodium (Na)	142 mmol/l
Potassium (K)	N/A mmol/l
Urea ($(NH_2)_2$-CO)	4.5 mmol/l
Creatinine ($C_4H_7N_3O$)	144 umol/l
Bilirubin ($C_{33}H_{36}N_4O_6$)	N/A umol/l
Aspartate transferase	69 U/l
Alkaline phosphatase	189 U/l
Calcium (Ca)	2.45 mmol/l

3.2.2 Surface examination

Two non-destructive characterisation techniques were used to assess the surface topography and the chemical nature of the passive film of Ti-6Al-4V, (1) atomic force microscopy (AFM) [18] [19] and (2) X-ray photoelectron spectroscopy (XPS) [20] [21]. All disc samples were approximately 10 mm^2 diameter and 1 mm thickness.

3.2.2.1 Atomic force microscopy (AFM) analysis

Topographic images of all treated samples prior to and after immersion in bovine serum solution for 1, 10 and 240 hours were analysed at 3 random surface locations in duplicates using a Topometrix TMX-3000 atomic force microscope (Santa Clara, CA) in contact mode. After immersion, samples were carefully rinsed in deionised distilled

water (MQ H_2O) to remove the unattached proteins or contamination before analyses. The samples were scanned using Si_3N_4 tips. The scan ranges were from 10 μm to 1 μm. The scan rate (μm/s) was adjusted to produce the best image. Generally, the maximum scan rate was twice the scan range. For the image and data analyses, TopoMetrix Software options to display the image, to calculate the surface roughness (R_a)[iv] and the line measurement (cross section profiles) were used. The average surface roughness is presented at each point corresponding to the mean ± standard deviation of three independent analyses (Table 3-3).

3.2.2.2 X-ray photoelectron spectroscopy (XPS) analysis

XPS measurements were performed on all treated samples prior to and after immersion for 1, 10 and 240 hours using a Surface Science Instruments (SSI) M-Probe Spectrometer operating at a base pressure of $3x10^{-9}$ torr. The instrument energy scale was calibrated using the Au($4f_{7/2}$) and Cu($2p_{3/2}$) peaks at 83.93 and 932.67 eV respectively. After immersion, samples were carefully rinsed in deionised distilled water (MQ H_2O) to remove the unattached proteins or contamination before analyses. Ion etching was not used to remove the adventitious carbon on the surface, because the experimental purpose was to examine the effects of immersion on the surface properties [22]. The samples were irradiated with a monochromatic Al Kα X-ray source (1486.6 eV) with a spot size of 1000 μm x 400 μm and ~180W power. Survey spectra were recorded with a pass energy of 150 eV, from which the surface chemical compositions were determined. The survey range was –10 to 1100 eV. The result was presented by value (at%) not by original spectra in order to evaluate the chemical compositions and each point corresponds to the average of the three random points. Three different take-off angles (angle resolved)[v], 15°, 35° and 90° correpsonding to analysis depths of about 1-3 nm, 3-5 nm and 5-9 nm, respectively, were also used to obtain depth resolutions of the passivated and the aged samples. In addition, the selected high-resolution spectra were recorded with a pass energy of 50 eV, from which

[iv] The definition of *Ra* is described in *Appendices, roughness (R_a)*.
[v] The physical basis is described in *Appendices, XPS*.

the chemical states of specific elements (O, C and N) were determined. The binding energy (BE) shifts due to surface charging were corrected using the C 1s peak at 285 eV as a standard.

3.3 Results

3.3.1 Surface morphology prior to immersion

Figure 3-1 shows the topography of the surface treated alloy as revealed using AFM in contact mode. The image of the control (C) sample clearly shows the expected duplex microstructure (α and β phases) of Ti-6Al-4V (Figure 3-1 (a)). The β-phase is harder than α-phase[vi]. On the polished samples, with the β phases protruding slightly out of the surface compared to the α-phases according to the line scan measurements. The distances from peaks to valleys were from 3.63 nm to 4.85 nm (Figure 3-1 (a)). Image (b) shows a change in morphology after the passivation (P) treatment, due to the preferential dissolution of the vanadium rich β-phases. Several small pores were displayed on the surface and by the line scan (cross section) measurement. The aged (A) sample also exhibited a similar morphology on the same scale (10 μm^2, image not shown). The difference in roughness (R_a) between the passivated and the aged samples can be observed at a small scale (1 μm^2) (Figure 3-1 (c) and (d)). The area R_a was about 1.29 nm and 0.56 nm, respectively. The passivated surface showed obvious peaks and valleys from the line scan measurement, the distances between peaks and valleys were from 5.55 nm to 8.12 nm (Figure 3-1 (c)). Interestingly, the aged surface was granular in appearance (Figure 3-1 (d)).

3.3.2 Surface morphology after immersion

The topography of the samples after one hour immersion in bovine serum solution is shown in Figure 3-2. For the passivated sample, the originally identified β phase was

[vi] Hardness (Vickers): pure Ti: 970 MN/m^2, pure Al: 167 MN/m^2 and pure V: 628 MN/m^2 (http://www.webelements.com/).

covered by protein, and the outline of this phase can be recognised using a line scan measurement (Figure 3-2(a)). Some precipitates were clearly seen on the aged samples on a 5 μm^2 scan size (Figure 3-2(b)). However, the passivated sample, compared to the aged sample (Figure 3-2(b)), did not show obvious precipitates on the surface. On an 1 μm^2 scan area, the aged surface (R_a = 7.62 nm) showed higher surface roughness than the passivated surface (R_a = 1.57 nm) (Figure 3-2(c)).

The surface average roughness (R_a) values after immersion in bovine serum solution are shown in Table 3-3. For the surface roughness on an 1 μm^2 scan area, the aged sample immediately increased from the original average value of 0.60 nm to approximately 6.03 nm at 1 hour immersion, then gradually decreased to a steady value of 1.37 nm after 10 hours immersion. In contrast, the average R_a of the passivated sample slightly increased from the original average value of 1.14 nm to 1.87 nm at one hour immersion then gradually decreased to 0.77 nm at 240 hours.

(a) C (area *Ra* = 0.99 nm)

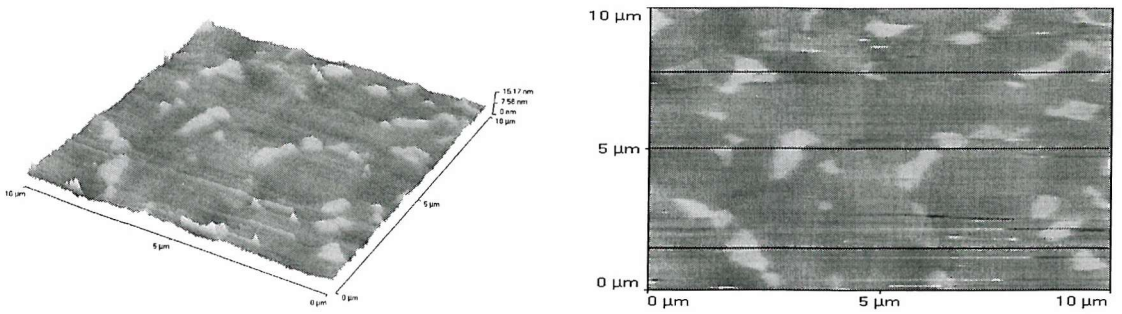

C (line scan measurement)

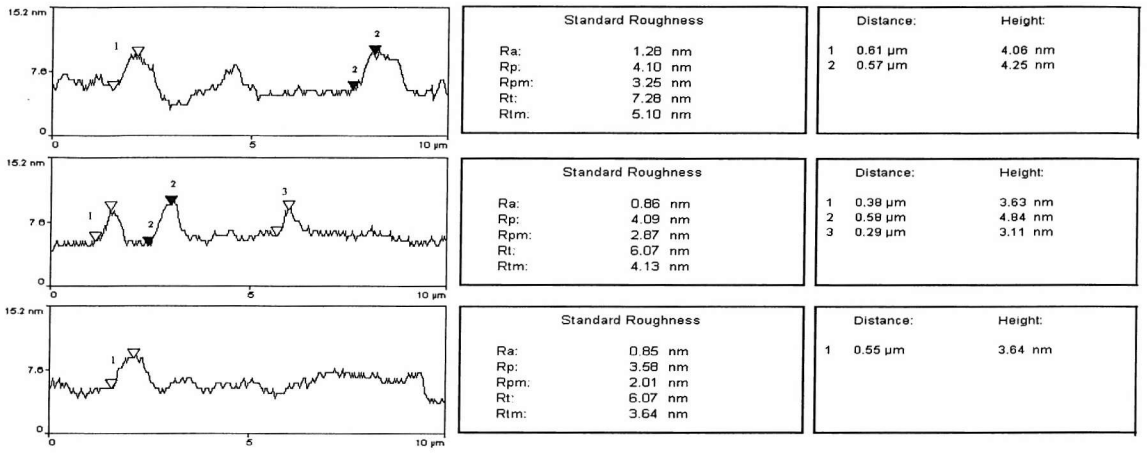

(b) P (area *Ra* = 1.01 nm)

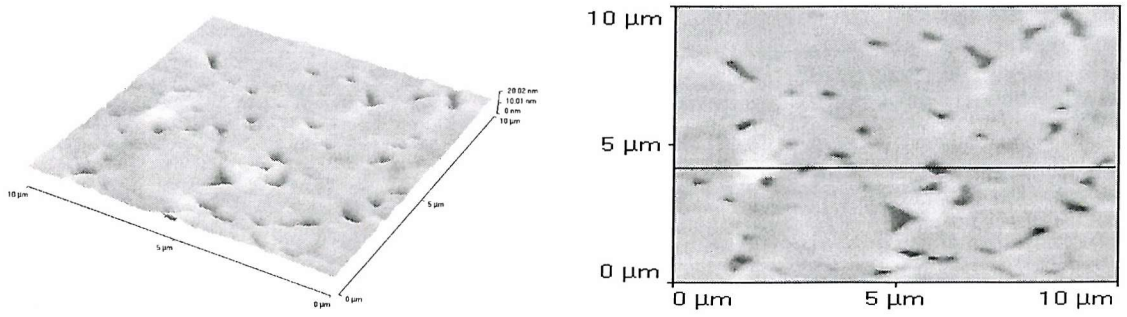

P (line scan measurement)

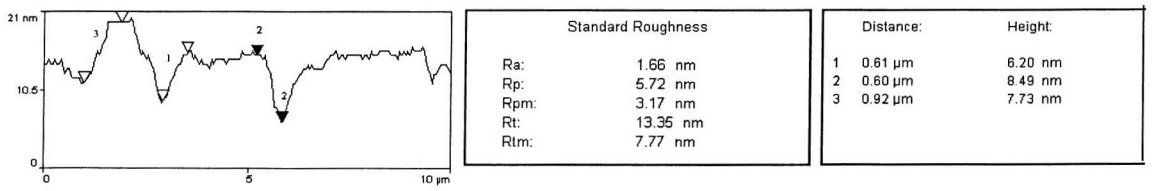

Figure 3-1 AFM images of the control (C), the passivated (P) and the aged (A) Ti-6Al-4V prior to immersion.

(c) P (area *Ra* = 1.29 nm)

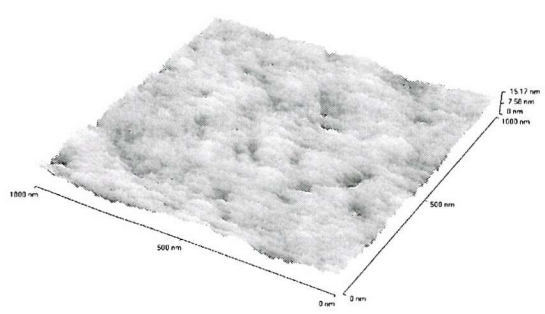

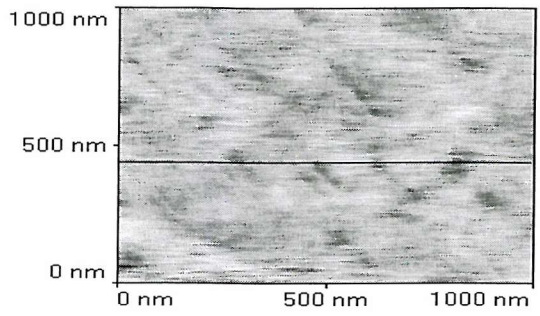

P (line scan measurement)

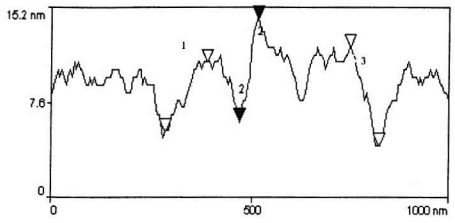

Standard Roughness	
Ra:	1.43 nm
Rp:	5.01 nm
Rpm:	2.34 nm
Rt:	10.31 nm
Rtm:	5.58 nm

	Distance:	Height:
1	105.99 nm	5.55 nm
2	46.08 nm	8.12 nm
3	73.73 nm	7.89 nm

(d) A (area *Ra* = 0.56 nm)

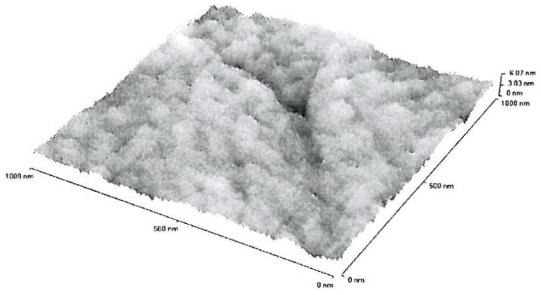

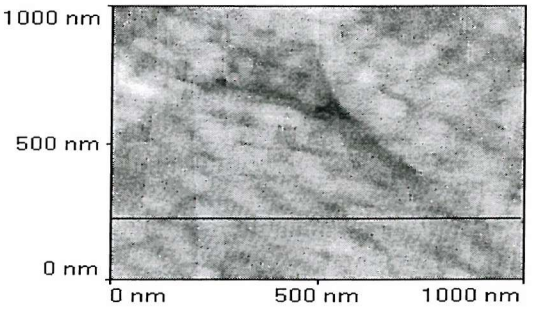

A (line scan measurement)

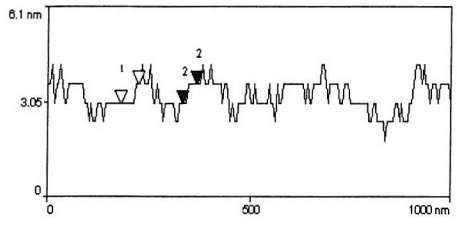

Standard Roughness	
Ra:	0.42 nm
Rp:	0.98 nm
Rpm:	0.98 nm
Rt:	2.43 nm
Rtm:	1.94 nm

	Distance:	Height:
1	44.55 nm	0.61 nm
2	33.79 nm	0.61 nm

Figure 3-1 (*continued*)

(a) P (area *Ra* = 2.17 nm)

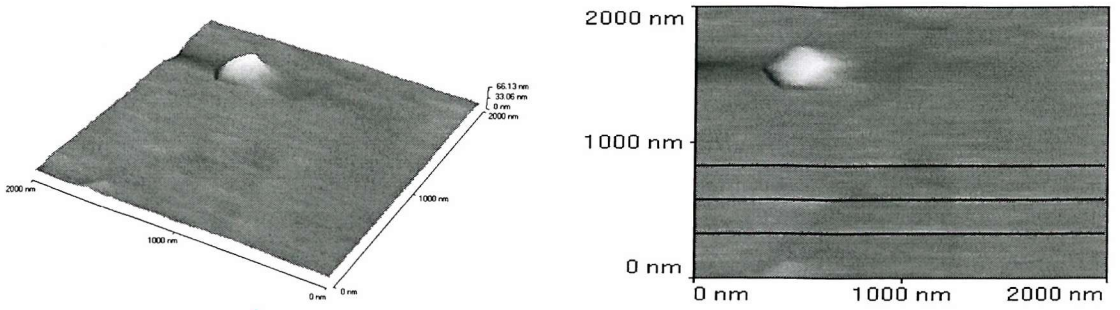

P (line scan measurement)

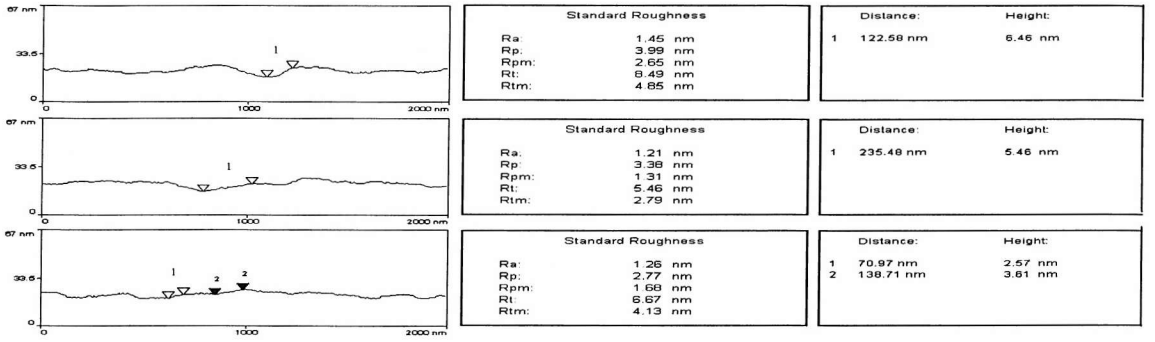

(b) A (area *Ra* = 6.56 nm)

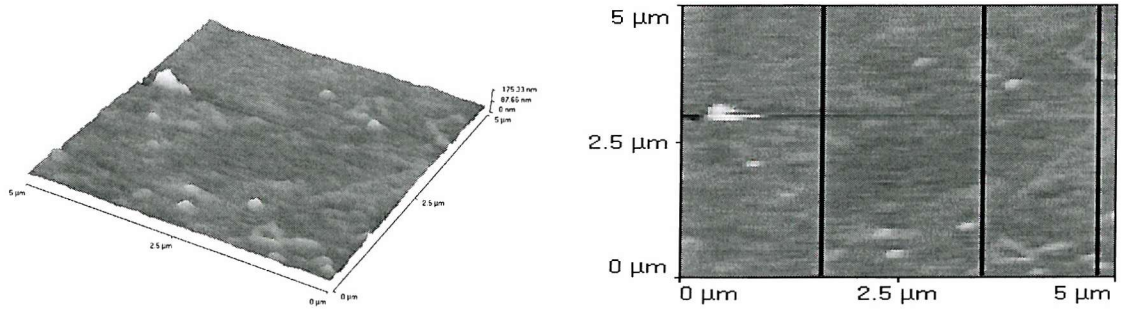

A (line scan measurement)

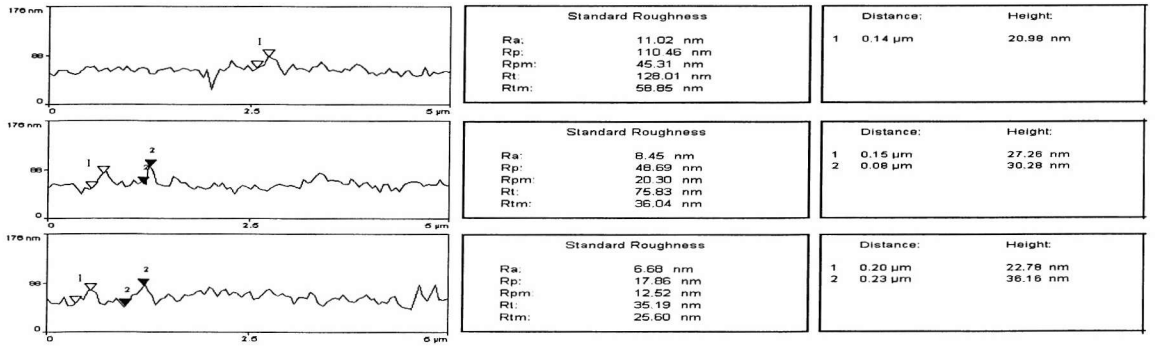

Figure 3-2 AFM images of the passivated (P) and the aged (A) Ti-6Al-4V after one hour immersion.

(c) P (area *Ra* = 1.57 nm)

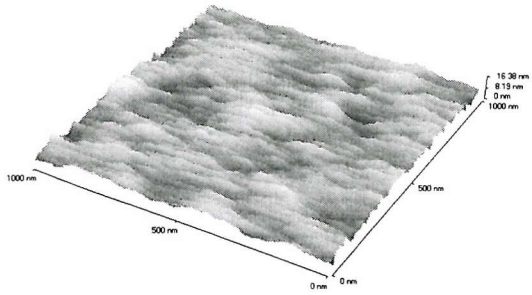

A (area *Ra* = 7.62 nm)

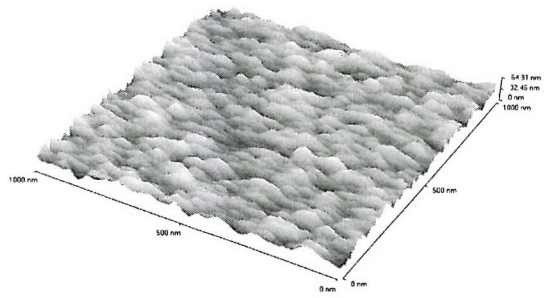

Figure 3-2 (*Continued*)

Table 3-3 Surface average roughness (R_a) of various treated Ti-6Al-4V prior and after immersion

Sample	P			
Immersion time (h)	0	1	10	240
Average R_a (nm) : Mean values (±stdev)	1.14 (±0.092)	1.87 (±0.302)	3.51 (±0.288)	0.77 (±0.127)
Sample	A			
Immersion time (h)	0	1	10	240
Average R_a (nm) : Mean values (±stdev)	0.60 (±0.174)	6.03 (±1.906)	1.37 (±0.242)	0.81 (±0.311)

3.3.3 XPS survey spectra and depth resolution analysis

The investigation of the treated surface involved recording survey scans to determine the elemental composition. The depth resolution was used to identify the oxide layers of the treated surfaces in different depths.

The XPS survey spectra showed that titanium (Ti, BE: ≈ 458 eV), aluminium (Al, BE: ≈ 118 eV), oxygen (O, BE: ≈ 530 eV), carbon (C, BE: ≈ 285 eV) and nitrogen (N, BE: ≈ 400 eV) were present in all samples before immersion (Table 3-4). Ti was mainly in the oxidised state in the form of TiO_2 (458 eV) for both samples. Al could only be

detected in a significantly quantity on the passivated surface prior to immersion. Vanadium (V) was not observed in the surface oxide film on the passivated (P) and the aged (A) surfaces. This has also been demonstrated in the previous study in our group [7]. The level of N, C and sulphide (S) were enhanced after immersion in bovine serum solution, indicating it was biological in origin. In contrast, the content of Ti and O decreased after immersion. Most of samples after immersion did not have detectable level of Al, except P-10 h (90°) and A-240 h (35°) with less than 1% Al observed.

Table 3-4 Surface compositions of the passivated (P) and the aged (A) Ti-6Al-4V alloys prior to and after immersion

	Prior to immersion	After immersion								
Samples	P	P-1 h			P-10 h			P-240 h		
Take-off angles / Element (at%)	35	15	35	90	15	35	90	15	35	90
Ti 2p	11.40	0.15	0.45	0.81	0.36	0.91	2.40	0.72	2.20	3.73
Al 3s	3.70	-	-	-	-	-	0.86	-	-	-
O 1s	39.70	15.58	18.29	19.31	20.40	21.64	24.93	18.03	21.81	28.32
C 1s	42.40	72.96	67.58	67.34	66.82	63.62	59.39	68.95	62.63	55.71
N 1s	2.60	8.99	12.07	10.68	12.42	13.13	12.39	11.38	12.78	11.60
S 2p	-	0.50	0.42	0.81	-	0.71	-	0.92	0.59	0.64
Si 2p	-	1.82	1.21	1.04	-	-	-	-	-	-
	Prior to immersion	After immersion								
Samples	A	A-1 h			A-10 h			A-240 h		
Take-off angles / Element (at%)	35	15	35	90	15	35	90	15	35	90
Ti 2p	7.62	1.34	1.77	3.35	1.74	2.70	4.23	1.69	2.70	4.56
Al 3s	0.67	-	-	-	-	-	-	-	0.82	-
O 1s	34.59	20.62	21.46	27.11	22.96	25.38	30.09	21.80	25.39	29.32
C 1s	52.69	65.22	63.66	56.35	62.59	58.37	53.88	62.90	58.30	54.05
N 1s	3.39	12.34	12.56	13.19	11.83	13.00	11.79	12.58	11.73	11.62
S 2p	-	0.48	0.55	-	0.88	0.55	-	1.02	1.05	0.45
Si 2p	-	-	-	-	-	-	-	-	-	-

Concerning the different immersion times and the various take-off angles (the depth profile), the content (at%) of Ti% and O% of the passivated sample increased with immersion time for each take-off angle (Table 3-4). For the aged sample, the content of Ti% and O% reached a plateau after 10 hours immersion for each take-off angle. In addition, the Ti% and O% of the aged sample were generally higher than that of the passivated sample.

For both treatments, the depth profile also showed that the content of carbon decreased with increasing depth for each time scale. It is also interesting to note that the N% content of the passivated sample increased from a 15° take-off angle to a 35° take-off angle, then decreased for a 90° take-off angle, i.e. at the greatest depth. However, the N% content of the aged sample remained relatively constant (range of 11-13%) for all immersion times (Figure 3-3). In addition, inorganic elements, Ca and P were not detected and less than 1% S was detected for most of the samples.

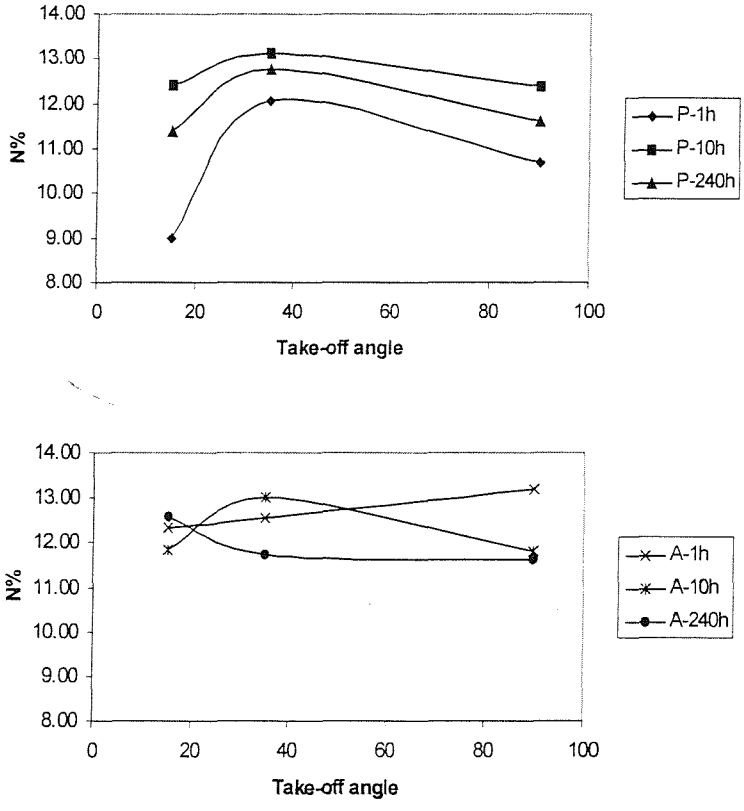

Figure 3-3 XPS-depth profile analyses showing N content of the immersed treated samples for different time scales.

By calculating the O/Ti ratio at each depth profile, it has been found that an O/Ti ratio higher than 2 indicated less TiO_2 amount than expected (Figure 3-4). For the passivated samples, the O/Ti ratio remarkably decreased with the increasing depth (1-7 nm) and also with the increasing immersion time. For the aged samples, the O/Ti ratio gradually decreased with the increasing depth, also with the increasing immersion time, and reached a stable state (O/Ti ratio: 9.4 at 3-5 nm of depth) after 10 hours immersion [23]. The O/Ti ratio of the aged sample was also lower than the passivated sample.

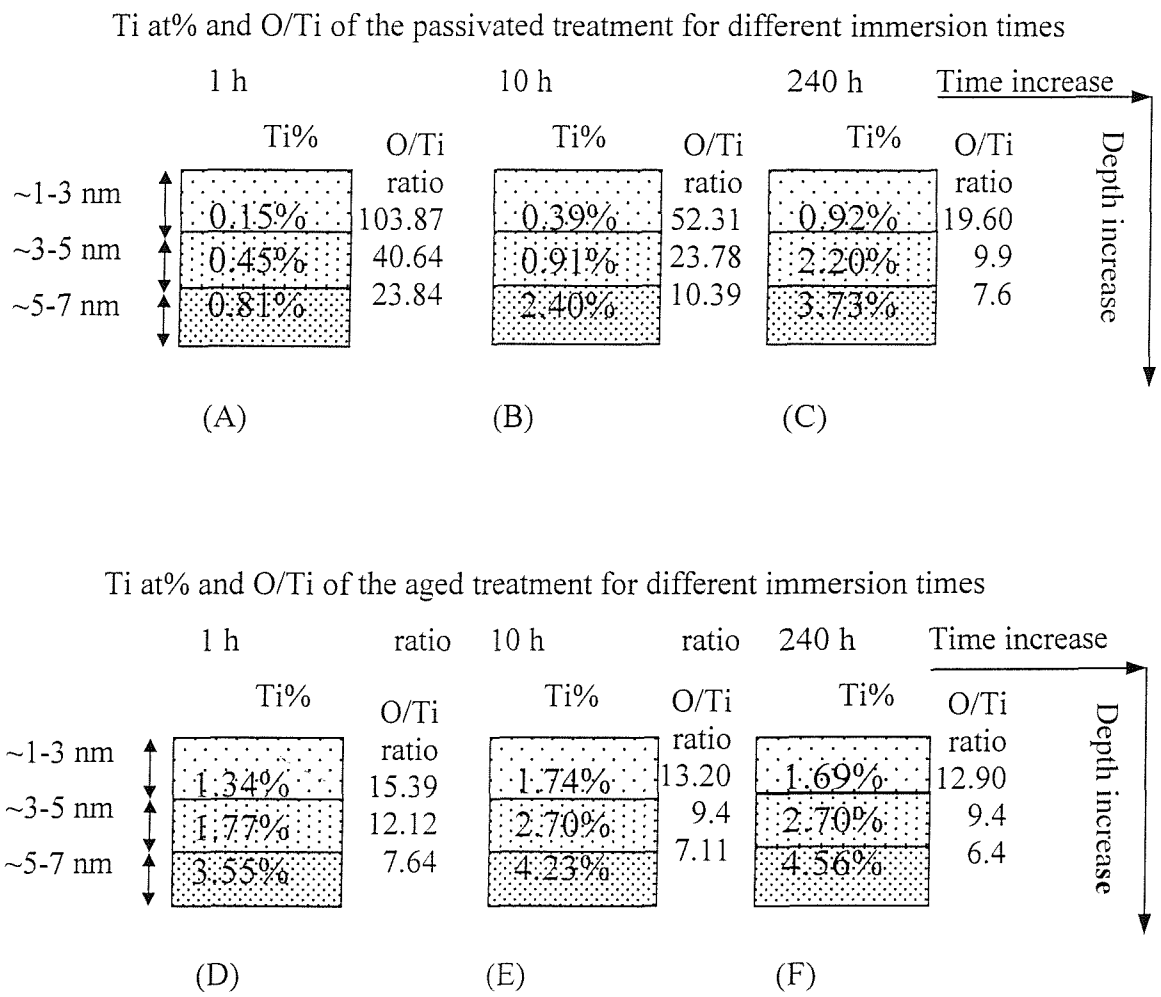

O/Ti ratio before immersion: the passivated sample: 3.38 and the aged sample: 4.54

Figure 3-4 Ti% depth profile and O/Ti ratios in the oxide layers of the passivated and the aged samples.

3.3.4 XPS high-resolution analysis

High-resolution spectra were acquired for the O 1s, C 1s and N 1s components of the passivated and the aged samples at 240 hours immersion in bovine serum solution (Table 3-5).

Table 3-5 XPS high-resolution analysis of the passivated (P) and the aged (A) samples after 240 h immersion (at a 35° take-off angle)

P											
O 1s				C 1s				N 1s			
BE (eV)	%	Chemical state	FWHM	BE (eV)	%	Chemical state	FWHM	BE (eV)	%	Chemical state	FWHM
530.88	25.0	TiO_2	1.55	285.67	55.3	C-H or C-C	1.48	400.91	100	N-C	1.58
532.47	55.9	C=O and C-OH	1.50	287.04	25.9	C-O	1.44				
533.78	19.1	Chemisorbed H_2O	1.52	288.88	18.7	O-C=O	1.46				
A[1]											
O 1s				C 1s				N 1s			
BE (eV)	%	Chemical state	FWHM	BE (eV)	%	Chemical state	FWHM	BE (eV)	%	Chemical state	FWHM
530.66	30.1	TiO_2	1.55	285.61	50.6	C-H or C-C	1.49	400.83	100	N-C	1.63
532.38	52.5	C=O and C-OH	1.53	286.92	28.3	C-O	1.43				
533.72	17.4	Chemisorbed H_2O	1.51	288.78	21.1	O-C=O	1.47				

1. According to the previous work in our group, the aged surface is consisted of 45.4% TiO_2, 28.2% C=O and C-OH and 26.4% chemisorbed H_2O before immersion [24].

The binding energy (BE), the difference of the peak positions (BE difference) and equal full width at half-maximum (FWHM) were utilised to identify the chemical

state[vii] [25] [26]. The O 1s peak was resolved into three individual peaks, the oxygen species O^{2-}, OH and chemisorbed water (from the lowest to the highest binding energy), each with an approximate 1.5 eV spacing at FWHM. In addition, for the passivated sample, the BE differences between the oxide species (O^{2-}) and the hydroxyl oxygen (OH), and between the hydroxyl oxygen (OH) and chemisorbed water were 1.59 eV and 1.31 eV, respectively. The BE differences were 1.72 eV and 1.34 eV for the aged sample. It is worthy to notice that after immersion the aged surface showed the increase in the amount of C=O and C-OH and the decrease in TiO_2 and chemisorbed H_2O (basic OH). The binding energies resolved for the C 1s peak were ~285.57 eV, ~287.04 eV and ~288.88 eV corresponding to (C-H and C-C), (C-O) and (O-C=O), respectively. The FWHM is approximate 1.4-1.5 eV. The C-H and C-C bond were most predominant in all cases. Two other components (C-O and O-C=O) at higher binding energies were approximately 45-50% of total carbon observed which indicated it was biological in origin. The high-resolution N 1s peak at ~400.91 eV was identified as C-N. The FWHM was approximately 1.6 eV.

3.4 Discussion

In this study, the surface analytical techniques, AFM and XPS, provided detailed information on the treated Ti-6Al-4V alloys prior to and after immersion. These high sensitivity, high-resolution and non-damaging techniques, allowed topography, elemental composition, chemical state and chemical depth profile of surface oxides to be qualified.

In order to understand how the treated surface affected the behaviour of proteins or cells [27], it was necessary to characterise the physical and chemical properties of the sample prior to immersion. AFM and XPS analyses of the passivated surface showed that the β-phase was attacked (AFM), resulting in the elimination of detectable vanadium (XPS). Similar results have also been found in the literature [22] [28]. The calculated Ti-6Al-4V atomic ratio excluding contamination of O and C is 24/2.8/1

[vii] The definitions of BE, BE difference and FWHM are described in *Appendices, XPS.*

(Ti/Al/V bulk). The atomic ratio of the oxides (TiO_2, Al_2O_3 and V_2O_5) is about 16.94/3.31/1[viii]. A published data also showed the atomic ratio (oxides) of 14.29/2.43/1 [29]. 11.40% Ti and 7.62% Ti were detected on the passivated and the aged samples prior to immersion, respectively, suggesting values of V are 0.67% and 0.45% on P and A oxide surfaces calculated according to this atomic ratio (16.94/3.31/1). It has been demonstrated that V was lower at the surface as compared with the Ti-6Al-4V bulk and showed 0.54 % V for the passivated surface [28]. This value and our calculated one are above the detection limit of XPS (0.1%). Therefore, the absence of vanadium suggests that vanadium was removed from the surface during the nitric acid treatment and ageing treatment. Vanadium, unlike many transition metals, has an active dissolution behaviour with a limited tendency for passivation [30]. The formed oxide film represented a non-stoichometric oxidation state of the metal (Eq.3-1) or mixture of oxides of varying valences. In acid solution where an excess of hydrogen ions is present, the interaction between the non-stoichometric oxide film and the hydrogen ion will take place resulting in the removal of this film (Eq.3-2).

$$2V + xO_2 \rightarrow 2VO_x \qquad \text{(Equation 3-1)}$$

$$V - O_x + 2xH^+ + 2xe^- \rightarrow V + xH_2O \qquad \text{(Equation 3-2)}$$

$$k = Ae^{\frac{-Ea}{RT}} \qquad \text{(Equation 3-3)}$$

Arrhenius equation (Eq.3-3)

Where,
k: rate constant
R: gas constant
T: absolute temperature
A: pre-exponential factor
Ea: experimental activation energy

[viii] The elemental composition data from native oxides: Ti: (17 at% Ti, 40 at% O, 39 at% C), Al (28 at% Al, 44 at% O, 28 at% C), and V: (24 at% V, 46 at% O, 28 at% C) (website: http://www.xpsdata.com). The atomic ratio of the bulk Ti-6Al-4V is different from the atomic ratio of the oxides (TiO_2, Al_2O_3 and V_2O_5). The atomic ratio (oxides) of Ti/Al/V is approximate 16.94/3.31/1 ($=\frac{90}{48}\times 17\% : \frac{6}{27}\times 28\% : \frac{4}{51}\times 24\%$).

The 10 hours ageing treatment may also encourage further vanadium ion release into solution. It has been found that the rate constant of a reaction can usually be related to the temperature by (Eq.3-3). Normally, the reaction rates increase by a factor of 2 to 3 for each 10°C rise in temperature [31].

In addition, the change in morphology of the aged surface compared to the passivated surface is thought to be due to the increased concentration of hydroxylated groups [5] [32]. During ageing in deionised distilled boiling water, the oxide layer induced dissociative decomposition of water molecules, resulting in the formation of hydroxyl groups. These hydroxyl groups are both acidic and basic in native and are termed TiOH and Ti-OH groups, respectively [33] [34]. These titanium oxides can change to either a positive or a negative charge on a surface depending on its environment [8]. The hydroxylated groups are able to enhance the reaction between Ti oxide and organic compounds [35] [36]. This will be discussed later in this chapter.

Examination of the surface properties of the samples after immersion is able to determine the interface reaction between surface and proteins, and to build up the correlation between the surface properties and metal ion kinetics. After one hour immersion, the surface roughness (R_a) values of both surfaces increased, indicative of protein adsorption process from the bovine serum solution. The aged sample had a higher R_a value than the passivated sample at the first hour, this suggested that the aged surface with the hydroxylated groups may be more biocompatible than the passivated sample to enhance increased cell adhesion [37]. With increasing immersion time, more proteins were adsorbed on the surface and a large-scale agglomerate precipitate structure developed; consequently the surface roughness decreased with time [38]. One possible interfacial reaction is that the adsorption occurs predominantly within the acidic pH range[ix] [39] and this adsorption behaviour could involve the basic hydroxyl (Ti-OH) groups reacting with the deprotonated carboxyl groups ($-COO^-$) of an amino acid (Figure 3-5) [35] [40]. Our results have demonstrated that after immersion the

[ix] Some researches have suggested that the pH level decreased to approximately 5.2 caused by local inflammation at the initial reaction in interface. This value approaches the "equilibrium" physiological value of 7.35 within approximately ten days. However, the pH of the implant site has been shown to fluctuate to lower values (as lower as approximately 4) in cases of loosening or infection (http://www.engr.sjsu.edu/). The hydroxyls of titania are protonated and positively charged below PZC of pH 5.38.

amounts of TiO_2 and chemisorbed H_2O (basic OH groups) decreased while the amount of C=O and C-OH increased. It is because the deprotonated carboxyl groups replace the basic OH groups. Indeed, the hydroxylated groups (or surface properties) play a critical role in cell/implant reaction during immersion.

After ageing surface treatment ⇒ Immersion in bovine serum solution

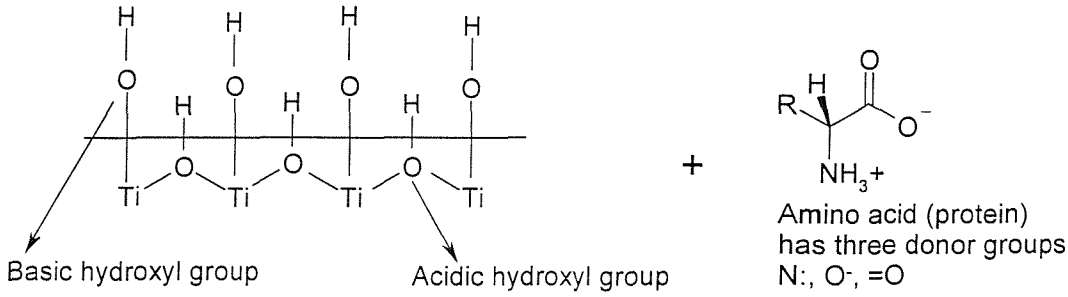

⇒ Protein adsorption (or dissolution)

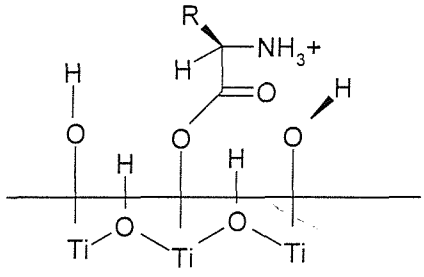

Figure 3-5 Reaction between proteins and oxide layers.

Considering the reaction between the surface oxide and the biomolecules, the XPS analysis showed that content of carbon decreased with increasing depth for both treatments. This is probably because proteins, i.e. amino acid chains consisting of hydrocarbon, could not penetrate into the inner oxide layer easily. Interestingly, there

was a noticeable difference in nitrogen depth profile between the passivated and the aged surface. It is thought that the passivated surface consists of three layers: an inner compact, stable layer (corresponding to the 90° take-off angle), an intermediate layer (corresponding to the 35° take-off angle) and an outer porous less stable layer (corresponding to the 15° take-off angle) [41] [42] [43]. It is possible that small organic nitrogen compounds entering the active passivated oxide layer and aggregating in the intermediate larger were available for further chemical reactions [44]. In addition, the passivated sample had a higher R_a value (the greater distances from peaks to valleys) than the aged sample prior to immersion; thus proteins are able to embed in these valleys for more reaction with oxide layers. This may explain the different N% tendency between the passivated and the aged samples. No Ca and P was detectable from our result, this may be due to the protein adsorption in turn to affect the formation of HA on the surface. The two major factors that may cause the inhibition of HA formation (or calcification) on substrate in serum are the presence of albumin (negatively charged protein) and those of the other major species found in serum [45] [46].

The surface O/Ti ratio after one hour immersion was greater than would be expected from the theoretically ratio value of two for TiO_2. This may be due to the incorporation of biomolecules in TiO_2 matrix. With increasing time, metal ion, oxygen ion or oxide-containing species migration actively cause further oxide formation; therefore the ratio of O/Ti decreased, particularly for the passivated samples, suggesting that further dissolution and oxidation processes may keep occurring even after 240 hours immersion. Similarly Ong et al have also observed a change in the relative distribution of O 1s with time in solution for passivated Ti (ASTM F76) surfaces (Table 3-6) [47]. For the aged surface, the reaction between the solution and oxide layer appears to reach a stable state after 10 hours; therefore the O/Ti ratio did not alter significantly from 10 hours to 240 hours. Nevertheless, the O/Ti ratio of the passivated surface changed significantly with time. This observation is consistent with the metal ion release kinetics exhibited during long-term immersion according to the previous work in our group[x] [5]. The higher oxide formation rate in the passivated surface may therefore be explained in terms of a higher metal dissolution rate, and the reaction between proteins

[x] The details are described in *Appendices, metal ion release kinetics.*

and oxide layers. The reaction between proteins and oxide layers; this in turn alters the oxide layer chemistry during immersion [23] [48].

Based on the present findings and previous results in our groups, the ASTM-F86 passivation procedure has been found to produce the adverse effects for Ti alloys in terms of metal ion release. However, a suitable adjunct in the form of an ageing treatment has been shown to enhance the passivated surface by producing a more stable and inert oxide layer. This treatment is simple, inexpensive and produces a stable homogenesis surface oxide.

In this study, the great advantage of the surface analytical techniques is able to interpret the surface properties and explain the interface reaction between bovine serum solution and the oxide layer. The aged surface with its high degree of crystallinity, the relative freedom from defects or a heterogeneous surface and the hydroxylated groups encourages protein adhesion, reduces the tendency towards increased metal ion dissolution [34] [49] [50]. It is therefore evident, that for the development of new biomaterials with biocompatible surfaces, it is very important to synthesize a specific surface, which is able to control the precise reaction between the adsorption of protein and the metal oxide surface.

Table 3-6 Relative distributions (± 1 SD) of different components for O 1s over time in solution [47]

Relative distribution of O 1s concentration (%)			
Ti samples	Component A[5] (529.8 eV)	Component B (531.0 eV)	Component C (532.3 eV)
TiO_2 single crystal[1]	66.5	5.28	28.24
Samples[2] prior to immersion[3]	70.4±0.6	12.6±0.3	16.9±0.9
3 hours immersion	60.6±0.4	25.5±4.8	13.9±4.4
3 days immersion	48.0±9.2	34.0±12.5	18.1±3.3
6 days immersion	49.9±13.3	34.6±12.6	15.5±0.7
9 days immersion	32.0±7.4	46.4±11.4	21.6±4.1
P 10 days immersion[4]	**25.0**	**55.9**	**19.1**
A 10 days immersion[4]	**30.1**	**52.5**	**17.4**
12 days immersion	12.1±6.7	67.5±3.6	20.4±3.0

1. One TiO_2 rutile single crystal standard analysed.
2. ASTM F86-76 passivation procedure (40% nitric acid at room temperature for 30min).
3. Samples were immersed in a rat bone marrow cell culture system (α-MEM: with Earle's salts, L-glutamine and non-essential amino acids without sodium bicarbonate).
4. These are our results from Table 3-5, samples were immersed in bovine serum solution.
5. A: TiO_2, B: C=O and C-OH, C: chemisorbed H_2O.

Part B. HA-coated Ti-6Al-4V

3.5 Introduction

Most load bearing orthopaedic implants today are made from either titanium-based alloys or cobalt-chromium alloys. These materials possess excellent mechanical properties and corrosion resistance. However, their ability to bond with bone is limited [35] [51]. Titanium based alloys however, have shown some potential for "osseointegration"[xi] [52] with bone on account of its oxide layer, which possesses a distinct surface chemistry [51].

There has been a trend in orthopaedics to apply a biologically active coating to enhance the ability of a load bearing implant to bond directly to bone, and potentially extend the lifetime of these devices significantly [51]. This coating can incorporate the main constituents of the surrounding tissue [53]. A good example of such a coating is hydroxyapatite (HA, $Ca_{10}(PO_4)_6(OH)_2$) [54], which is used extensively used to encourage bone/implant osseointegration [55] because of its chemical stability [56] and biocompatibility for circumferential osseous apposition [18]. In addition to the aforementioned biocompatibility considerations, the coating can form a protective barrier and therefore improve the dissolution resistance of metallic implants.

Among the various coating methods available, plasma-spraying has become one of the most common methods for applying the HA coating [57] [58]. Prior to coating, a number of surface roughening techniques, e.g. grit-blasting, may be used to enhance the anchorage of the HA coating to the implant surface. The HA, in turn, encourages osteoprogenitor cell adhesion [59] [60]. However, there are two potential weaknesses

[xi] Osseointegration is the procedure by which mature bone is deposited directly on implant materials without any intervening soft or fibrous tissue. For clinically successful implants, osseointegration is mandatory for secure association between the bone and implant surface.

caused during the process, which need to be addressed, namely, the interface strength between the HA and the metal substrate [61] [62] [63] and the long-term stability of the sprayed HA coatings [64] [65].

In the case of Ti and its alloys, the problems are in part due to the difference in the coefficients of thermal expansion (CTE) (HA is higher than Ti; Ti is about 60% of HA) [66] [67], the reaction between HA and titanium alloy [68], and the associated underlying substrate deformation [69], and the decomposition of HA [67]. These problems may in turn cause increased metal ion release or in severe cases, cause loosening of the implant. However, the effect of plasma-spraying on the titanium alloy surface science and associated metal ion release is still unclear [70] [71].

Previous work in this group has investigated the effects of the HA coating process on the stability of the oxide layer in terms of metal ion release. It has been found that the application of the HA coating decreased the metal ion release from the nitric acid passivated samples (compared to the uncoated Ti alloys) and unexpectedly there was an increase in metal ion release from the aged samples [9]. It was proposed that the high temperature process might alter the nature of the aged oxide. This hypothesis has yet to be confirmed. In addition, Park et al also found that the microstructure of Ti-6Al-4V near the interface has been affected by the heat generated during plasma-spraying [66].

Therefore this research attempts to relate the effect of the plasma-spraying on titanium alloy surface with the metal ion release kinetics [18]. In particular it will focus on three issues: (1) The effect of the high temperature produced during plasma-spraying on the treated titanium surfaces, (2) The effect of the grit-blasting on the treated titanium and (3) The properties of the HA coated surface.

3.6 Materials and Methods

3.6.1 Ti alloy surface preparation

Distal sections of forged Ti-6Al-4V alloy femoral stems from the Ti-Mod Freeman hip replacement were supplied by Finsbury Instruments (Leatherhead, Surrey, UK). The hip stems were cut into discs in 10 mm^2 and 1 mm thickness, polished to 1 μm and give a final polish with 0.06 μm colloidal silica polishing suspension. The successive steps of the nitric acid passivation (P) and the ageing (A) treatments are described in Table 3-1. The treated samples (two samples for each treatment) were subjected to grit-blasting using high-purity alumina (Al_2O_3: 99.7%, Fe_2O_3: 0.04%, Na_2O: 0.18%; grit size: 14) at high pressure in order to roughen the surface. Surface roughness profiles of grit-blasted and polished specimens were made on a Talysurf Series 10 profilometer. The polished specimens and the corundum (Al_2O_3) blasted specimens had a surface roughness R_a = 0.1 μm and R_a = ~15 μm, respectively [9]. A HA coating was then plasma sprayed onto the discs (two samples for each treatment) to an average thickness of 75-150 μm (Plasma Biotal Ltd., Derbyshire). The plasma spraying process is that HA powder is fed into a high temperature gas flame to form a plasma then it is accelerated to the substrate [72].

Additionally, the passivated and aged samples (two samples for each treatment) were subjected to the equivalent heat cycle treatment[xii] without blasting or coating to assess the effect on Ti-6Al-4V implant surfaces due to the high temperature of the plasma-spraying process alone. During the plasma-spraying process, the Ti alloy substrate remains at a relatively low temperature (generally less than 300°C) so the mechanical properties of the metallic implant materials are not compromised.

The treated Ti-6Al-4V samples (P-B, P-T, A-B and A-T) were cleaned, then placed in bovine serum solution (Table 3-2) for 240 hours and incubated under a humidified 5% CO_2 air atmosphere at 37°C±0.1°C to examine the difference in surface properties from the sample prior to and after immersion. The details and the nomenclature of each treatment are shown in Table 3-7.

[xii] Due to the commercial reason, the degree of temperature performed does not be given here.

Table 3-7 Symbols for various surface treatments

Symbols	Treatments
C	Control, as received followed by polishing and cleaning procedure
P	C followed by 30% nitric acid passivation treatment
P-B	P followed by blasting treatment
P-T	P followed by heat treatment (time/temperature heat cycle)
P-B-HA	P followed by blasting treatment and HA-coated
A	P followed by 10 h boiling deionised distilled water treatment
A-B	A followed by blasting treatment
A-T	A followed by heat treatment (time/temperature heat cycle)
A-B-HA	A followed by blasting treatment and HA-coated

3.6.2 Surface examination

3.6.2.1 Surface morphology-SEM/EDS analysis

The surface morphology (secondary electron image, SEI) of the grit-blasted and the HA-coated surface was examined by SEM (JEOL JSM 6400) with a 15~20 kV accelerating voltage, which was adjusted to produce the best image. Carbon was coated on samples before SEM-EDS analysis. The Energy Dispersive Spectroscopy (EDS) and IMIX (Integrated Microanalyser for Images and X-rays) microanalysis software systems (Princeton Gamma-Tech, Princeton, NJ) were used to identify and quantify the elemental composition of the sample areas by analysing the characteristic X-rays produced from the material.

3.6.2.2 X-ray photoelectron spectroscopy (XPS) analysis

XPS measurements were performed on the heat-treated passivated (P-T) and the heat-treated aged (A-T) samples prior to and after immersion using a Surface Science Instruments (SSI) M-Probe Spectrometer. Survey spectra were used to determine the surface chemical compositions. The result was presented by value (at%) and not by

original spectra in order to evaluate the chemical compositions. In addition, the selected high-resolution spectra were recorded with a pass energy of 50 eV, from which the chemical states (O, C, N and Ti) of specific elements were determined. The standard electron take-off angle used for analysis was 35°.

3.7 Results

3.7.1 SEM/EDS analysis-the grit-blasted samples

The SEM images of the grit-blasted samples were shown in Figure 3-6. The grit-blasted passivated (P-B) and the grit-blasted aged (A-B) surfaces showed irregular surfaces. The contamination of Al_2O_3 particles (about 150μm in width) as a result of the girt-blasting treatment was clearly shown in Figure 3-6 (a, point 1) and (c, point 3). The composition of the particle confirmed by EDS analyses was Al_2O_3 (Table 3-8). A high-magnification (x 4,000) image of this Al_2O_3 particle surface was shown in Figure 3-6 (e).

EDS analyses showed that most of the grit-blasted surfaces consisted of metals (Ti, Al and V in bulk) and metal oxides (TiO_2, Al_2O_3 and V_2O_3 in surface) (Table 3-8). For both of treatments prior to immersion, Al-rich phases (could be α-phase) and V-rich phases (could be β-phases) can be detected from the point scan. Most interestingly, the Ti/Al atomic ratio (area scan: 1.16 for P-B; 2.08 for A-B) demonstrated that the amount of Al% increased after immersion for both treatments. The values were smaller than the values from the point scan before immersion or the theoretical level, 8.6 (Ti-6Al-4V bulk) or 5.12 (native oxides).

Table 3-8 EDS analyses of the grit-blasted samples prior to and after 240 hours immersion (corresponding to Figure 3-6 (a)-(d))

	Prior to immersion			After immersion	
Sample	(a) P-B			(b) P-B	
Scan type[1]	Point scan			Area scan	Point scan
Element (at%)	Point 1	Point 2 (V rich phase)	Al rich phase		
Ti	0.23	29.46	26.39 (±1.814)	18.84 (±1.379)	17.06 (±2.722)
Al	39.70	1.69	6.67 (±2.476)	16.18 (±1.640)	20.06 (±5.834)
V	0.02	2.94	1.67 (±0.323)	1.23 (±0.021)	1.58 (±0.389)
O	60.04	65.90	65.27 (±0.366)	63.77 (±0.276)	53.42(±14.672)
P	0.00	0.00	0.00 (-)	0.00 (-)	0.00 (-)
Na	0.00	0.00	0.00 (-)	0.00 (-)	0.00 (-)
Possible Metal oxides	Al_2O_3	TiO_2 V_2O_3 Al_2O_3	TiO_2 Al_2O_3 V_2O_3 or V_2O_5	TiO_2 Al_2O_3 V_2O_3 or V_2O_5	TiO_2 Al_2O_3 V_2O_3 or V_2O_5
Ti/Al/V ratio[2]	≈ 100% Al_2O_3	10/0.6/1	15.8/4/1	15.3/13.2/1	10.8/12.7/1
Ti/Al ratio	-	10/0.6	3.95	1.16	0.85
	Prior to immersion			After immersion	
Sample	(c) A-B			(d) A-B	
Scan type	Point scan			Area scan	Point scan
Element (at%)	Point 3	Point 4 (V rich phase)	Point 5 (Al rich phase)		
Ti	0.14 (±0.041)	29.65	28.10	22.57 (±3.077)	19.65 (±8.311)
Al	39.83 (±0.058)	1.43	4.56	10.83 (±4.137)	14.45(±10.607)
V	0.01 (±0.01)	2.99	1.72	1.32 (±0.411)	1.27(±0.601)
O	60.03 (±0.008)	65.93	65.62	64.05 (±0.623)	63.50 (±1.569)
P	0.00 (-)	0.00	0.00	0.03 (±0.036)	0.03 (±0.034)
Na	0.00 (-)	0.00	0.00	1.20 (±0.033)	1.11 (±0.297)
Possible Metal oxides	Al_2O_3	TiO_2 V_2O_3 Al_2O_3	TiO_2 Al_2O_3 V_2O_3 or V_2O_5	TiO_2 Al_2O_3 V_2O_3 or V_2O_5	TiO_2 Al_2O_3 V_2O_3 or V_2O_5
Ti/Al/V ratio	≈ 100% Al_2O_3	9.9/0.5/1	16.3/2.7/1	17.1/8.2/1	15.5/11.4/1
Ti/Al ratio	-	9.9/0.5	6.04	2.08	1.36

1. 3 different point (scan) scans in duplicates for each treatment. The data presented in (mean values ± stdev).
2. Ti/Al/V (Ti-6Al-4V bulk) atomic ratio: 24/2.8/1, Ti/Al: 8.6; Ti/Al/V (native oxides) atomic ratio: 16.94/3.31/1, Ti/Al: 5.12 (The detailed calculation is described in *footnote viii*). The analytical depth of EDS covers about 1 μm, therefore it includes not only surface oxides but also bulk compositions.

3.7.2 XPS survey spectra analysis-the heat treated samples

The XPS survey spectra of the heat-treated passivated (P-T) and the heat-treated aged (A-T) samples prior to immersion are shown in Table 3-9. The amount of surface carbon and nitrogen on the samples, which may be due to contamination from exposure to atmosphere, decreased after heat treatment. The Ti/Al ratios were similar (≈ 3.08) for samples P and P-T. Vanadium was detected only on sample P-T, which was 0.57% less than 1%. There was no obvious difference in Al% between samples P and P-T. In contrast, the Al% of sample A-T increased after the heat treatment compared to the aged sample (A). Interestingly, the Ti/Al ratio of the aged surface significantly decreased from 11.37 to 1.45 after the heat treatment. After immersion, C and N increased, while Ti, Al and O content decreased for most of treatments. Only the aged sample showed slight increase in Al%.

Table 3-9 XPS analyses for different surface treatments prior to and after 240 h immersion (at a 35° take-off angle)

	Prior to immersion				After immersion			
Elements (at%)	P	P-T	A	A-T	P	P-T	A	A-T
Ti 2p	11.40	11.52	7.62	6.86	2.20	0.94	2.70	-
Al 3s	3.70	3.73	0.67	4.61	-	-	0.82	-
V 2p3	-	0.57	-	-	-	-	-	-
O 1s	39.70	41.34	34.59	42.43	18.03	20.84	25.39	20.42
C 1s	42.40	38.17	52.69	35.09	68.95	64.22	58.30	64.31
N 1s	2.60	1.07	3.39	1.66	11.38	11.74	11.73	12.19
S 2p	-	-	-	-	0.92	-	1.05	-
Ti/Al ratio[1]	3.08	3.09	11.37	1.45	-	-	-	-

1. Ti/Al/V (Ti-6Al-4V bulk) atomic ratio: 24/2.8/1, Ti/Al: 8.6; Ti/Al/V (native oxides): 16.94/3.31/1, Ti/Al: 5.12 (The detailed calculation is described in *footnote viii*).

3.7.3 XPS high-resolution analysis-the heat treated samples

The high-resolution spectra of the heat-treated passivated and the heat-treated aged samples were shown in Table 3-10. The O 1s high-resolution spectra of the heat-treated

surface prior to immersion showed that chemisorbed H_2O was not detected on the P-T surface, but 15.7% chemisorbed H_2O was detected on the A-T surface. After immersion, the amount (at%) of the lower binding energy (BE) O 1s peak (~530 eV, equivalent to TiO_2) decreased for both treatments (P-T and A-T). The two higher BE of O 1s components (~532 eV and ~533 eV, equivalent to C=O and C-OH, and chemisorbed H_2O) increased. The high-resolution C 1s spectra showed that the amount of (C-O) and (O-C=O) increased, and the amount of (C-H or C-C) decreased after immersion. The binding energy of N was around 400 eV, which corresponds to N-C. The Ti 2p spectra of P-T and A-T prior to immersion and A-T after immersion were deconvoluted into two peaks and identified as the Ti $2p_{3/2}$ of TiO_2 at 458.88 eV and the Ti $2p_{1/2}$ peak of TiO_2 at 464.56 eV. The BE difference was 5.68 eV. Sample P-T showed 4 peaks after immersion suggesting the existence of additional Ti containing species. The Ti $2p_{1/2}$ was at 465.46 eV and the Ti $2p_{3/2}$ was at 459.02 eV, and the BE difference was 6.44 eV indicated TiO_2. However, another two Ti 2p peaks found at 457.83 eV and 464.02 eV are unable to be identified as a certain state from present data.

3.7.4 SEM/EDS analysis-the HA-coated samples

The SEM images of the HA-coated blasted samples were shown in Figure 3-7. There was no observable difference between the HA-coated passivated (P-B-HA) and the HA-coated aged (A-B-HA) samples. Both showed a typical HA-coated morphology with plate like regions where the HA has spread on implant. The small discontinuities (cracks) in the coating were in the order of ~1 μm. These cracks could be due to the contraction on cooling. EDS analyses also showed that the atomic ratio of Ca/P, which was 2.23 and 2.28 for P-B-HA and A-B-HA higher than the theoretical value, 1.67. The compositions (at%) of Ca, P and O for P-B-HA prior to immersion were 27.60 ± 1.01, 12.36 ± 2.05 and 59.53 ± 0.58, respectively. The compositions (at%) of Ca, P and O for A-B-HA prior to immersion were 26.78 ± 1.81, 13.07 ± 1.07 and 59.92 ± 0.78, respectively (the data presented in mean values ± stdev).

(a) P-B (x 150, scale bar: 100 μm)

(b) P-B (x 1,000, scale bar: 10 μm)

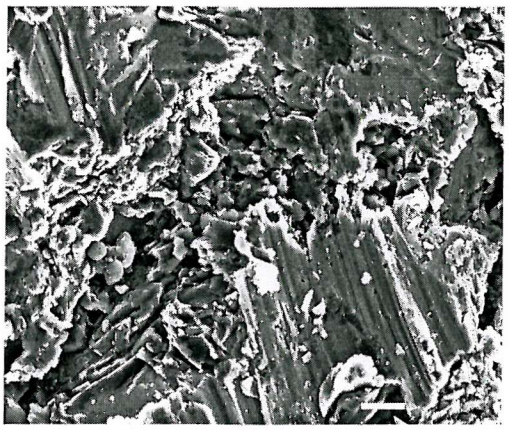

(c) A-B (x 1,000, scale bar: 10 μm)

(d) A-B (x 1,000, scale bar: 10 μm)

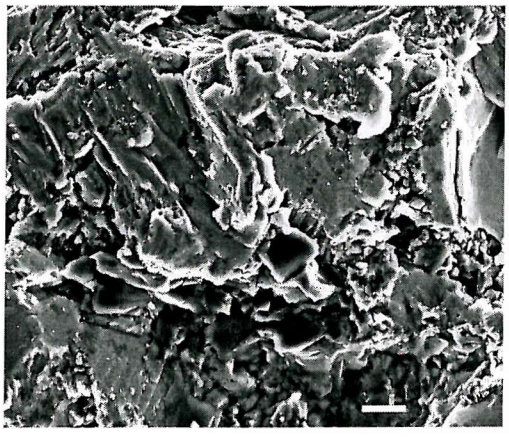

(e) P-B (x 4,000, scale bar: 1 μm)

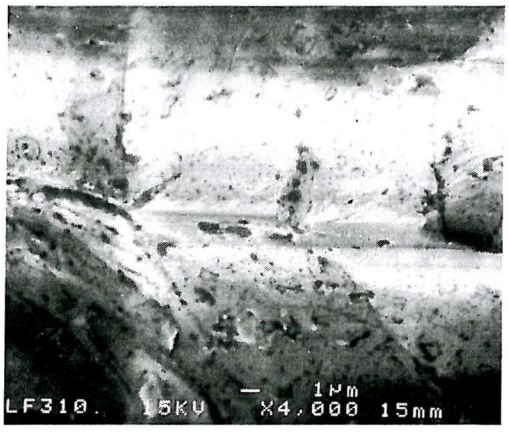

Figure 3-6 SEM images (secondary electron image) of the grit-blasted samples.
(a) and (c) prior to immersion, numbers 1 and 3: Al_2O_3 particle, numbers 2 and 4: V-rich phase, number 5: Al-rich phase.
(b) and (d) after immersion for 240 hours.
(e) High magnification (x 4,000) of Al_2O_3 particle shown in (a).

Table 3-10 XPS high-resolution analysis of P-T and A-T prior to and after immersion (at a 35° take-off angle)

P-T prior to immersion											
O 1s			C 1s			N 1s			Ti 2p		
BE (eV)	%	Chemical state	BE (eV)	%	Chemical state	BE (eV)	%	Chemical state	BE (eV)	%	Chemical state
530.36	78.0	TiO_2 (O^{2-})	285.09	77.5	C-H or C-C	401.40	100	N-C	458.88	67.0	TiO_2 (Ti $2p_{3/2}$)
532.24	22.0	C=O and C-OH	286.40	17.0	C-O				464.57	33.0	TiO_2 (Ti $2p_{1/2}$)
-	0.0	Chemisorbed H_2O	288.92	5.4	O-C=O						
P-T after immersion											
O 1s			C 1s			N 1s			Ti 2p		
BE (eV)	%	Chemical state	BE (eV)	%	Chemical state	BE (eV)	%	Chemical state	BE (eV)	%	Chemical state
530.27	20.1	TiO_2 (O^{2-})	285.07	58.6	C-H or C-C	400.35	100	N-C	457.83	9.8	Ti_2O_3 or Ti-N-O (?)
531.82	59.0	C=O and C-OH	286.47	24.8	C-O				459.02	54.2	TiO_2 (Ti $2p_{3/2}$)
533.24	20.9	Chemisorbed H_2O	288.30	16.6	O-C=O				464.02	19.7	?
									465.46	16.2	TiO_2 (Ti $2p_{1/2}$)
A-T prior to immersion											
O 1s			C 1s			N 1s			Ti 2p		
BE (eV)	%	Chemical state	BE (eV)	%	Chemical state	BE (eV)	%	Chemical state	BE (eV)	%	Chemical state
530.28	56.1	TiO_2 (O^{2-})	285.05	78.7	C-H or C-C	400.20	100	N-C or N-O	458.88	68.9	TiO_2 (Ti $2p_{3/2}$)
531.91	28.2	C=O and C-OH	286.66	12.8	C-O				464.56	31.1	TiO_2 (Ti $2p_{1/2}$)
533.09	15.7	Chemisorbed H_2O	288.67	8.5	O-C=O						
A-T after immersion											
O 1s			C 1s			N 1s			Ti 2p		
BE (eV)	%	Chemical state	BE (eV)	%	Chemical state	BE (eV)	%	Chemical state	BE (eV)	%	Chemical state
530.28	0.0	TiO_2 (O^{2-})	285.02	56.2	C-H or C-C	400.21	100	N-C	458.88	68.9	TiO_2 (Ti2 $p_{3/2}$)
531.33	82.6	C=O and C-OH	286.44	26.1	C-O				464.56	31.1	TiO_2 (Ti2 $p_{1/2}$)
533.19	17.4	Chemisorbed H_2O	288.26	17.7	O-C=O						

(a) P-B-HA

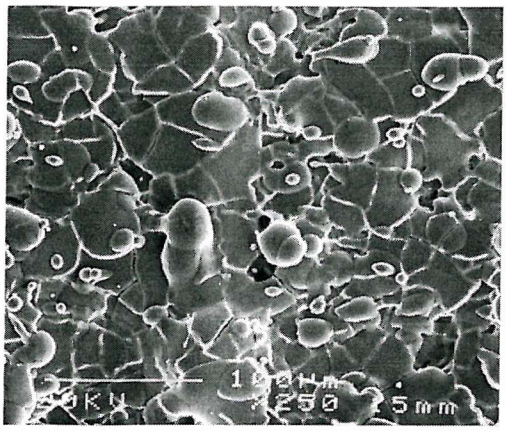

(b) A-B-HA

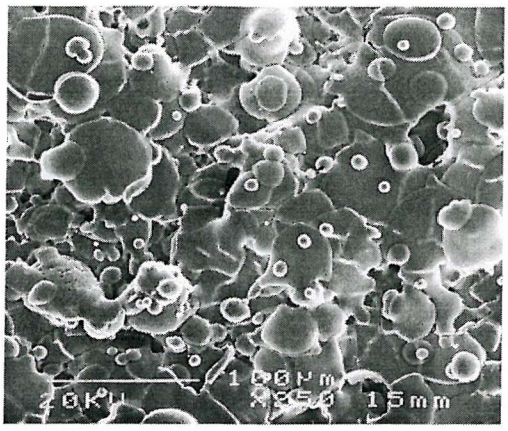

(c) P-B-HA

(Area scan, Ca: P: O = 2.23: 1: 4.82)

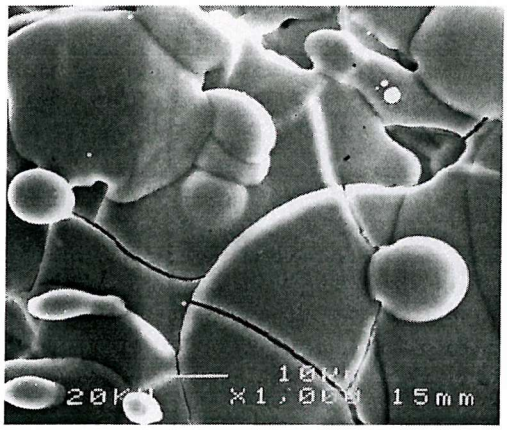

(d) A-B-HA

(Area scan, Ca: P: O = 2.28: 1: 4.82)

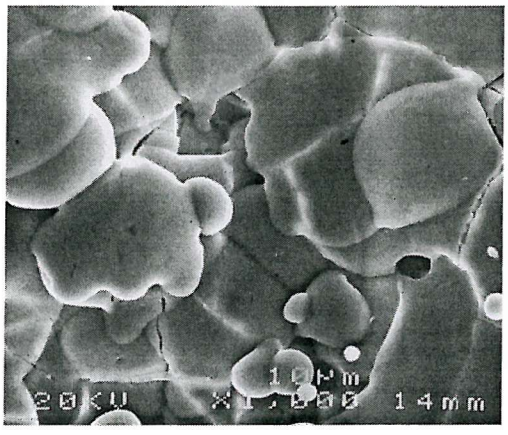

(e) A-B-HA

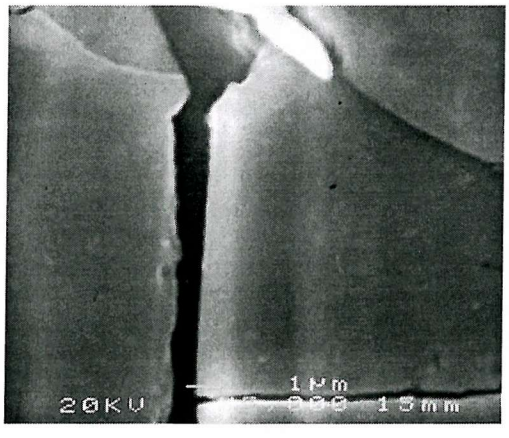

P-B-HA (Ca%: 27.60 ± 1.01, P: 12.36 ± 2.05, O: 59.53 ± 0.58)
A-B-HA (Ca%: 26.78 ± 1.81, P: 13.07 ± 1.07, O: 59.92 ± 0.78)
Data presented in (mean values ± stdev), 3 different area scans in duplicates

Figure 3-7 SEM images (secondary electron image) of the HA-coated samples without immersion.

3.8 Discussion

In this study, XPS and SEM/EDS have provided qualitative and quantitative information about how the HA plasma-spraying coating procedures (grit-blasting, heat cycling and HA-coating) affect the properties of the treated Ti-6Al-4V substrate and the HA layer. This information can now be used to explain the metal ion release kinetic behaviour observed for each treatment.

According to the result in Table 3-9, the grit-blasting and the high-temperature (heat treatment) associated with the plasma-spraying process may change the structure and surface composition. In order to interpret the surface properties of the grit-blast samples, SEM and EDS analyses were utilised in this study. SEM images showed the Al_2O_3 particles (~150 μm in length) embedded in the surface after the blasting process. These Al_2O_3 particles may involve in the degradation of the interfacial bond strength. A similar finding has been demonstrated by other researchers [66]. In addition, the roughened surface consisted of metals and their oxides, TiO_2, V_2O_3 and Al_2O_3 or Al_2O_5. The emergence of Al and V oxides on the grit-blasted surfaces constitute a potential risk for long-term implantation in terms of metal ion release. An AlO_x-enriched layer has also been observed on Ti-6Al-4V alloy surfaces, which was treated by sand-blasting method (500 μm or 3 mm alumina particles) [65].

Moreover, it is interesting to notice that the amount of Al increased on the P-B and A-B surfaces after immersion. During immersion, the metal ions are released into the region surrounding the implant/solution interface (so-called "double layer"). When the concentration of metal ions reaches a saturation point, they are deposited onto the surface. The metal ions may also react with organic compounds to form the complexes before deposition and in turn alter the chemical structure of the oxide layer [23]. It is reasonable to assume that the grit-blasted surface will produce a higher metal ion release rate than P or A due to the increased surface roughness (R_a). It has been proved that the higher metal dissolution rate in the passivated surface induced the higher metal oxide formation rate [48]. Therefore, the increasing Al% on the surface after immersion may be because not only the Al from the bulk but also the Al_2O_3 particles contamination dissolved then deposited onto the surface. Our result indicates that the

mechanical process induced the rearrangement of the surface structure in turn to cause the change in the surface composition presented in the increasing Al% after immersion. This presents a potential risk to increase the metal ion release, which will affect osteoblastic cell proliferation and adhesion (in *Chapters 5*).

After the heat treatment alone, no obvious difference in surface composition between P and P-T was found. Indeed, the Al% and the ratio Ti/Al of the passivated surface were similar to that of the heat-treated passivated surface, although 0.57% V was detected. This suggests that the heat treatment did not significantly change the chemical surface composition of the passivated surface. On the contrary, the amount of Al% of the heat-treated aged (A-T) sample increased compared to the aged (A) sample. The ratio Ti/Al of A-T was also lower than 5.12 (calculated from native oxides, TiO_2 and Al_2O_3) or 8.6 (calculated from bulk Ti-6Al-4V). Thus, the heat treatment increased the surface Al concentration. The increase in Al concentration in the outer layers of air-heated oxides (400°C for 45min) has also been confirmed in literature [5] [73]. It is possible that the heat treatment causes hydroxylated groups to vaporize from the aged surface and extensively transform the chemical surface composition. Thus the effective oxide layer thickness would consist mostly of aluminium containing TiO_2 [74] [75]. Interestingly, V was not found in the heat-treated aged (A-T) sample. This appears to agree with the result of Eq. 3-1 to 3-3, because most of vanadium has been removed during the passivation and ageing treatments.

Interestingly, chemisorbed H_2O was not detected on P-T surface (Table 3-10) from the XPS high-resolution analysis. It has been found that the passivated surface consists of less hydroxylated groups [33]. However, 15.7% chemisorbed H_2O (or basic OH) was remained on the surface of A-T. The previous study showed that the aged surface consists of 45.4% O^{2-}, 28.2% acidic OH and 26.4% basic OH (chemisorbed H_2O) [7]. This suggests that the heat treatment [8] removed part of the hydroxylated groups (loss of chemisorbed H_2O) from the surface formed during ageing thus altering the surface structure. Moreover, from the view of biocompatibility, the loss of basic OH (chemisorbed H_2O) may affect the reaction between the surface oxides and amino acids (proteins) because the protein adsorption behaviour could involve the basic hydroxyl (Ti-OH) groups reacting with the deprotonated carboxyl group ($-COO^-$) of an amino acid (Figure 3-5) [35] [40].

After immersion, the binding energy O 1s components (~532 eV, C=O and C-OH) increased for all samples; this corresponds to the C 1s high-resolution spectra increase in (C-O) and (O-C=O), indicating that the carbon is organic nature. Nevertheless, it decreased in (C-H or C-C). N% increased for all samples after immersion and the binding energy of N 1s at 400 eV also confirmed that this is organic in origin (C-N). The main chemical state of Ti was TiO_2 for all samples. However, after immersion the P-T revealed four peaks, two peaks were unidentified. The peak at 457.83 eV is not TiN (BE: 397 eV), Ti-N-O (BE: 457.0 eV, Ti2P3/2), metallic Ti (BE: 453.8 eV), TiO (BE: between 454.8 eV to 456.0eV) or TiC (455.1 eV) [76]. Even though Ti $2p_{3/2}$ peak of Ti-N-O was at 457.0 eV, the Ti $2p_{1/2}$ peak of Ti-N-O at 461.7eV was not detected [77]. Therefore, it is very difficult to prove that the peak at 457.83 eV was contributed by Ti-N-O. The unidentified peaks may be related to the reaction between bovine serum solution and reconstructed titanium oxide surface as a result of the metal ion release behaviour exhibited by the passivated oxides. This indicates that a complicated reaction involving metal ions and organic species is occurring at the interface of bio-environment and sample P-T. This needs to be confirmed before any conclusion can be drawn.

The SEM images of the HA-coated samples showed that pores and cracks in the coatings result in recesses approximately 1 μm in width. These cracks could be due to thermal expansion mismatch between the coating and the substrate, or to the release of thermal stress generated on cooling. These cracks may become channels to allow metal ions to be leached into the physiological environment [66].

The EDS results also showed that the Ca/P atomic ratio is higher than the theoretical level, 1.67, indicative of newly formed phases. A similar result was also found by Oh et al. who observed an increase in the Ca/P atomic ratio from 1.67 in the powder state to about 2.17-2.48 in the coating; CaO and $Ca_4P_2O_9$ were identified in the coating layer [78]. It is possible therefore, that CaO and $Ca_4P_2O_9$ may partly constitute the HA-coated film in our sample surfaces since they have a similar atomic ratio. The decomposition or transformation for HA during the plasma-spraying into the newly formed phases may be explain in terms of the following reactions (Rx 3-1 and 3-2) [78] [79]:

$$Ca_{10}(PO_4)_6 \rightarrow 2Ca_3(PO_4)\ (\beta\ form) + Ca_4P_2O_9 + H_2O\ (above\ 1050\ °C,\ decomposition)$$

(Reaction 3-1)

Where:

$Ca_3(PO_4)$: tricalcium phosphate (TCP)

$Ca_4P_2O_9$: tetra calcium phosphate monoxide (TCPM)

$$2Ca_3(PO_4)\ (\beta\ form) \rightarrow 2Ca_3(PO_4)\ (\alpha\ form)\ (phase\ transformation)$$

$$Ca_4P_2O_9 \rightarrow Ca_3(PO_4) + CaO\ (above\ 1350\ °C,\ decomposition)$$

(Reaction 3-2)

From these two reactions, we can assume that as soon as the HA particles are injected into a plasma flame (range around 30,000°C), the particle reaches a temperature of more than 1350 °C facilitating the formation of CaO, α-$Ca_3(PO_4)$ and $Ca_4P_2O_9$ in the coating in our results.

Any amorphous layers in the coating may cause the resorption and mechanical failure of the coating because a resorption will produce a considerable increase in *in vitro* dissolution rates at physiological pH [80] [81]. Alternatively, it can be beneficial because a resorbable coating can degrade with time and partly be replaced by bone ingrowth [82]. In general, as much as 20% of coating might be removed within 2 years because these coatings are susceptible to resorption by osteoclast-like cells [83].

Overall the contamination of Al_2O_3 during the blasting process, the increased Al% on the heat-treated aged surface, the changes of the chemical state and any amorphous phases of the HA-coated surface may alter the metal ion dissolution behaviour of all the samples. These results can be used to explain our previous work [9]. The change in the heat-treated aged surface properties, such as its surface composition and the loss of chemisorbed H_2O may cause the surface properties of A-T to appear to be closely related to that of the passivated, and would explain why the metal ion dissolution rate constant (R) of the HA-coated aged sample ($R = 1.8 \times 10^{-4}\ \mu g/cm^2/s^{1/2}$) was on the same scale to that of the HA-coated passivated sample ($R = 2.43 \times 10^{-4}\ \mu g/cm^2/s^{1/2}$) [9]. In addition, the increased Al% on the surface due to the heat treatment and the blasting

process may explain why the application of a HA-coating increases the metal ion dissolution from the HA-coated aged sample (R = 1.8 x 10^{-4} $\mu g/cm^2/s^{1/2}$) compared to the uncoated sample (R = 7.17 x 10^{-5} $\mu g/cm^2/s^{1/2}$). The HA-coated passivated sample (R = 2.43 x 10^{-4} $\mu g/cm^2/s^{1/2}$) decreases the metal ion release compared to the uncoated sample (R = 2.54 x 10^{-4} $\mu g/cm^2/s^{1/2}$), suggesting that the HA-coating treatment acts a barrier for metal ion release from the passivated surface, as would be expected.

Furthermore, the plasma-spraying process requires a substantial dissipation of thermal and kinetic energy at the time of impact of the calcium-phosphate particle on the metal surface. It has been suggested that this energy is released in part to the oxide, by either promoting diffusion of ions of the ceramic into the metal surface or by modifying the defect density of the oxide crystal structure. Both of them have an effect on the ion diffusion kinetics from the bulk through the oxide of the surface metal. Such effects are significant with respect to the ion release from titanium alloys [61]. The possible transport pathway for metal ion releasing from the HA-coated surface to the bio-environment could be due to the cracks in the HA-coated surface. The cracks, and the resorbable amorphous phases may enhance the metal ion release with increasing time [79].

Summary

The first part of the present work (Part A) has explained the metal ion release behaviour *in vitro* of surface treated Ti-6Al-4V in terms of its surface chemistry and morphology. The passivated sample exhibited continued dissolution and oxidation processes during 240 hours immersion. This is thought to be due to its open, porous, less stable structure. The aged surface is more stable and has an increased concentration of hydroxylated groups, which in turn inhibit metal ion dissolution and enhance protein adsorption reactions. The ASTM-F86 passivation procedure alone may therefore not be appropriate for Ti and its alloys; the addition of a simple inexpensive ageing treatment can improve the dissolution resistance of the native oxide layer on Ti alloys. Furthermore, in order to be accepted into clinical practice, the examination of the biocompatibility of the aged oxide surface is necessary. This forms the subject of *Chapters 5*.

The second part of this work (Part B) has examined that the interfacial changes which occur due to the HA plasma-spraying treatment. It has been known a mechanically weak phase exists at the HA/metal interface and several works have been conducted which however mainly focus on the decomposition of HA or the interface fracture between HA and titanium alloy substrate [66]. Few works have examined the possible side effects the plasma-spraying program on the substrate and how it affects the metal ion release kinetics. In this work, grit-blasting treatment and the heat treatment seems to modify the Ti-6Al-4V surface properties and in terms to affect metal ion release behaviour. The results have shown that the grit-blasting causes the contamination of Al_2O_3 on the surface. The heat treatment changes the Al% surface composition of the aged surface and causes the loss of chemisorbed H_2O groups. These processes are likely to increase Al metal ion release into the biological fluids, which can significantly alter cell behaviour. In addition, the cracks may also enhance the metal ion release by forming channels for ion transport. Consequently, the application of a plasma-sprayed coating does not produce the desired reduction in metal ion release for the aged samples. However, from the view of long-term implantation, the ageing treatment is still necessary to improve the surface stability of the passivated surface because the chemisorbed H_2O on the surface may play an important role in stabilising the surface properties and enhancing the reaction between protein and substrate. Therefore, it is very important to control carefully the spray parameters in order to maintain the stability of the oxide layer (substrate), reduce surface cracks and increase in crystallinity.

References

1. ASTM, *Medical devices; Emergency medical services.* Vol. 13.01. 1999, Pennsylvania, USA: American Society for Testing and Materials.
2. Callen, B.W., et al., *Nitric acid passivation of Ti6Al4V reduces thickness of surface oxide layer and increases trace element release.* J Biomed Mater Res, 1995. **29**(3): p. 279-90.
3. Lowenberg, B.F., et al., *ASTM-F86 passivation increases trace element release from Ti6Al4V into culture medium.* J Mater Sci Mater Med, 1994. **5**: p. 467-72.
4. Wisbey, A., *The TiN coating of surgical implant materials*, in *Engineering Materials*. 1990, University of Southampton: Southampton.
5. Browne, M., P.J. Gregson, and R.H. West, *Characterization of titanium alloy implant surfaces with improved dissolution resistance.* J Mater Sci Mater Med, 1996. **7**: p. 323-9.
6. Ku, C.-H., et al., *Osteoblast differentiation on various Ti-6Al-4V surface treatments (accepted to Biomaterials).* 2001.
7. Browne, M. and P.J. Gregson, *Surface modification of titanium alloy implants.* Biomaterials, 1994. **15**(11): p. 894-8.
8. Kim, M.S. and J.G. Chung, *A study on the adsorption characteristics of orthophosphates on rutile-type titanium dioxide in aqueous solutions.* Journal of Colloid and Interface Science, 2001. **233**(1): p. 31-7.
9. Browne, M. and P.J. Gregson, *Effect of mechanical surface pretreatment on metal ion release.* Biomaterials, 2000. **21**(4): p. 385-92.
10. Kasemo, B., *Biocompatibility of titanium implants: surface science aspects.* J Prosthet Dent, 1983. **49**(6): p. 832-7.
11. McAlarney, M.E., M.A. Oshiro, and L.P. Huang, *Effects of titanium oxide properties on biocompatibility. A preliminary study.* N Y State Dent J, 1993. **59**(9): p. 45-8.
12. Jackson, D.R., S. omanovic, and S.G. Roscoe, *Electrochemical studies of the adsorption behavior of serum proteins on titanium.* Langmuir, 2000. **16**: p. 5449-57.
13. Eliades, G., G. Palaghias, and G. Vougiouklakis, *Effect of acidic conditioners on dentin morphology, molecular composition and collagen conformation in situ.* Dental Materials, 1997. **13**(1): p. 24-33.

14. Keller, J.C., et al., *Characterizations of titanium implant surfaces. III.* J Biomed Mater Res, 1994. **28**(8): p. 939-46.

15. Muster, D., et al., *The surface finishing of surgical and dental implants (value and difficulties).* Rev Stomatol Chir Maxillofac, 1992. **93**(3): p. 198-200.

16. Eliades, T., *Passive film growth on titanium alloys: Physicochemical and biologic considerations.* International Journal of Oral & Maxillofacial Implants, 1997. **12**(5): p. 621-27.

17. Puleo, D.A. and A. Nanci, *Understanding and controlling the bone-implant interface.* Biomaterials, 1999. **20**(23-4): p. 2311-21.

18. Campbell, P.A., et al., *Vacuum plasma sprayed hydroxyapatite coatings on titanium alloy substrates: surface characterization and observation of dissolution processes using atomic force microscopy.* J Vac Sci Technol B, 1996. **14**(2): p. 1167-72.

19. Zhang, F., et al., *Microstructure of titanium oxide films investigated by atomic force microscopy and transmission electron microscopy.* Nuclear Instruments and Methods Physical Research B, 1998. **142**: p. 61-6.

20. Gold, J.M., M. Schmidt, and S.G. Steinemann, *XPS study of amino acid adsorption to titanium surfaces.* Helvetica Physica Acta, 1989. **62**: p. 246-9.

21. Leitao, E., M.A. Barbosa, and K. de Groot, *XPS characterization of surface films formed on surface-modified implant materials after cell culture.* J Mater Sci Mater Med, 1997. **8**(7): p. 423-6.

22. Milosev, I., M. Metikos-Hukovic, and H.H. Strehblow, *Passive film on orthopaedic TiAlV alloy formed in physiological solution investigated by X-ray photoelectron spectroscopy.* Biomaterials, 2000. **21**(20): p. 2103-13.

23. Effah, E.A., P.D. Bianco, and P. Ducheyne, *Crystal structure of the surface oxide layer on titanium and its changes arising from immersion.* J Biomed Mater Res, 1995. **29**(1): p. 73-80.

24. Browne, M., *Surface modification of titanium alloy implants*, in *Department of Engineering Materials*. 1995, University of Southampton: Southampton, UK. p. 80.

25. Briggs, D. and M.P. Seah, *Practical surface analysis*. 2nd ed. 1990, Chichester; New York: Wiley. 2 v.

26. McCafferty, E. and J.P. Wightman, *Determination of the concentration of surface hydroxyl groups on metal oxide films by a quantitative XPS method.* Surface and Interface Analysis, 1998. **26**(8): p. 549-64.

27. Cooper, L.F., *A role for surface topography in creating and maintaining bone at titanium endosseous implants.* Journal of Prosthetic Dentistry, 2000. **84**(5): p. 522-34.

28. Sittig, C., et al., *Surface characterization of implant materials c.p. Ti, Ti-6Al-7Nb and Ti-6Al-4V with different pretreatments.* J Mater Sci Mater Med, 1999. **10**(1): p. 35-46.

29. Ask, M., J. Lausmaa, and B. Kasemo, *Preparation and Surface Spectroscopic Characterization of Oxide-Films on Ti6al4v.* Applied Surface Science, 1989. **35**(3): p. 283-301.

30. Al-Kharafi, F.M. and W.A. Badawy, *Electrochemical behaviour of vanadium in aqueous solutions of different pH.* Electrochimica Acta, 1997. **42**(4): p. 579-86.

31. Pataki, L. and E. Zapp, *Basic analytical chemistry.* 1980, Oxford: Pergamon.

32. Lee, T.M., E. Chang, and C.Y. Yang, *Surface characteristics of Ti6Al4V alloy: effect of materials, passivation and autoclaving.* J Mater Sci Mater Med, 1998. **9**(8): p. 439-48.

33. Mao, C., et al., *Oriented growth of phosphates on polycrystalline titanium in a process mimicking biomineralization.* J Crystal Growth, 1999. **206**: p. 308-21.

34. Wang, L.Q., et al., *Interactions of liquid and vapor water with stoichiometric and defective TiO2(100) surfaces.* Surf Sci, 1999. **440**: p. 60-8.

35. Helsen, J.A. and H.J. Breme, *Metals as Biomaterials, Biomaterials Science and Engineering Series.* 1998, London: Wiley.

36. Lima, J., et al., *Interactions between calcium, phosphate, and albumin on the surface of titanium.* Journal of Biomedical Materials Research, 2001. **55**(1): p. 45-53.

37. Urano, H. and S. Fukuzaki, *Influence of anionic compounds on adsorption behaviour of bovine serum albumin at oxide-water interface.* J Ferment Bioeng, 1997. **83**(3): p. 261-6.

38. Williams, R.L. and D.F. Williams, *Albumin adsorption on metal surfaces.* Biomaterials, 1988. **9**(5): p. 206-12.

39. Fonseca, C. and M.A. Barbosa, *Corrosion behaviour of titanium in biofluids containing H2O2 studied by electrochemical impedance spectroscopy.* Corrosion Science, 2001. **43**(3): p. 547-59.

40. Healy, K.E. and P. Ducheyne, *The Mechanisms of Passive Dissolution of Titanium in a Model Physiological Environment.* Journal of Biomedical Materials Research, 1992. **26**(3): p. 319-38.

41. Pan, J., D. Thierry, and C. Leygraf, *Hydrogen peroxide toward enhanced oxide growth on titanium in PBS solution: Blue coloration and clinical relevance.* Journal of Biomedical Materials Research, 1996. **30**(3): p. 393-402.

42. Pan, J., et al., *Variation of oxide films on titanium induced by osteoblast-like cell culture and the influence of an H2O2 pretreatment.* Journal of Biomedical Materials Research, 1998. **40**(2): p. 244-56.

43. Pouilleau, J., et al., *Structure and composition of passive titanium oxide films.* Mater Sci Eng B, 1997. **47**: p. 235-43.

44. Schubert, U., et al., *Metal-complexes in inorganic matrices .13. nickel-complexes with lysinate-substituted titanium alkoxides as ligands-X-ray structure-analysis of [(Eto)(3)Ti(Glycinate)](2).* Inorganic chemistry, 1995. **34**(4): p. 995-7.

45. Martin, R.I. and P.W. Brown, *Formation of hydroxyapatite in serum.* J Mater Sci Mater Med, 1994. **5**: p. 96-102.

46. Meyer, J.L. and H. Fleisch, *Calcification Inhibitors in Rat and Human-Serum and Plasma.* Biochimica Et Biophysica Acta, 1984. **799**(2): p. 115-21.

47. Ong, J.L., et al., *Spectroscopic characterization of passivated titanium in a physiologic Response of titanium surfaces to simulated biological environments.* J Mater Sci Mater Med, 1995. **6**: p. 113-9.

48. Sundgren, J.E., P. Bodo, and I. Lundstrom, *Auger electron spectroscopic studies of the interface between human tissue and implants of titanium and stainless steel.* J Colloid Interface Sci, 1986. **110**(1): p. 9-20.

49. Kumar, P.M., S. Badrinarayanan, and M. Sastry, *Nanocrystalline TiO2 studied by optical, FTIR and X-ray photoelectron spectroscopy: correlation to presence of surface states.* Thin solid films, 2000. **358**: p. 122-30.

50. Ratner, B.D., *New ideas in biomaterials science--a path to engineered biomaterials [see comments].* J Biomed Mater Res, 1993. **27**(7): p. 837-50.

51. Morris, H.F. and S. Ochi, *Hydroxyapatite-coated implants: A case for their use.* Journal of Oral and Maxillofacial Surgery, 1998. **56**(11): p. 1303-11.

52. Ahmad, M., M. McCarthy, and G. Gronowicz, *An in vitro model for mineralization of human osteoblast-like cells on implant materials.* Biomaterials, 1999. **20**(3): p. 211-20.

53. Chang, Y.L., et al., *Osteoblastic cell attachment to hydroxyapatite-coated implant surfaces in vitro.* Int J Oral Maxillofac Implants, 1999. **14**(2): p. 239-47.

54. Narasaraju, T.S.B. and D.E. Phebe, *Review some physical-chemical aspects of hydroxyapatite.* J Mater Sci, 1996. **31**: p. 1-21.

55. Ding, S.J., C.P. Ju, and J.H. Lin, *Characterization of hydroxyapatite and titanium coatings sputtered on Ti-6Al-4V substrate.* J Biomed Mater Res, 1999. **44**(3): p. 266-79.

56. Leitao, E., M.A. Barbosa, and K. de Groot, *Influence of substrate material and surface finishing on the morphology of the calcium-phosphate coating.* J Biomed Mater Res, 1997. **36**(1): p. 85-90.

57. Cook, S.D., et al., *Hydroxylapatite Coating of Porous Implants Improves Bone Ingrowth and Interface Attachment Strength.* Journal of Biomedical Materials Research, 1992. **26**(8): p. 989-1001.

58. Khor, K.A., C.S. Yip, and P. Cheang, *Ti-6Al-4V/hydroxyapatite composite coatings prepared by thermal spray techniques.* Journal of Thermal Spray Technology, 1997. **6**(1): p. 109-15.

59. Svehla, M., et al., *Morphometric and mechanical evaluation of titanium implant integration: comparison of five surface structures.* J Biomed Mater Res, 2000. **51**(1): p. 15-22.

60. Piveteau, L.D., B. Gasser, and L. Schlapbach, *Evaluating mechanical adhesion of sol-gel titanium dioxide coatings containing calcium phosphate for metal implant application.* Biomaterials, 2000. **21**(21): p. 2193-201.

61. Ducheyne, P. and K.E. Healy, *The effect of plasma-sprayed calcium phosphate ceramic coatings on the metal ion release from porous titanium and cobalt-chromium alloys.* J Biomed Mater Res, 1988. **22**(12): p. 1137-63.

62. Liu, J.Q., et al., *High-resolution transmission electron microscopy investigations of a highly adhesive hydroxyapatite coating/titanium interface fabricated by ion-beam-assisted deposition.* J Biomed Mater Res, 2000. **52**(1): p. 115-8.

63. Lo, W.J., et al., *Physical, chemical, and biological characterization of pulsed laser deposited and plasma sputtered hydroxyapatite thin films on titanium alloy.* J Biomed Mater Res, 2000. **50**(4): p. 536-45.

64. Ogiso, M., Y. Yamashita, and T. Matsumoto, *The process of physical weakening and dissolution of the HA-coated implant in bone and soft tissue.* J Dent Res, 1998. **77**(6): p. 1426-34.

65. Albrektsson, T., *Hydroxyapatite-coated implants: A case against their use.* Journal of Oral and Maxillofacial Surgery, 1998. **56**(11): p. 1312-26.

66. Park, E.J., R.A. Condrate, and D.T. Hoelzer, *Interfacial characterization of plasma-spray coated calcium phosphate on Ti-6Al-4V.* J mater Sci Mater Med, 1998. **9**(11): p. 643-9.

67. Weng, J., et al., *Integrity and thermal decomposition of apatite in coatings influenced by underlying titanium during plasma spraying and post-heat-treatment.* J Biomed Mater Res, 1996. **30**(1): p. 5-11.

68. Ji, H.X., C.B. Ponton, and P.M. Marquis, *Microstructural characterization of hydroxyapatite coating on titanium.* J Mater Sci Mater Med, 1992. **3**(4): p. 283-7.

69. Zhang, C.G., Y. Leng, and J.Y. Chen, *Elastic and plastic behavior of plasma-sprayed hydroxyapatite coatings on a Ti-6Al-4V substrate.* Biomaterials, 2001. **22**(11): p. 1357-63.

70. Ducheyne, P., P.D. Bianco, and C. Kim, *Bone tissue growth enhancement by calcium phosphate coatings on porous titanium alloys: the effect of shielding metal dissolution product [published erratum appears in Biomaterials 1992;13(11):800].* Biomaterials, 1992. **13**(9): p. 617-24.

71. Sousa, S.R. and M.A. Barbosa, *Effect of hydroxyapatite thickness on metal ion release from Ti6Al4V substrates.* Biomaterials, 1996. **17**(4): p. 397-404.

72. Degroot, K., et al., *Plasma Sprayed Coatings of Hydroxylapatite.* Journal of Biomedical Materials Research, 1987. **21**(12): p. 1375-81.

73. Vogt, K.W., et al., *Characterization of thin titanium oxide adhesion layers on gold: resistivity, morphology, and composition.* Surface Science, 1994. **301**(1-3): p. 203-13.

74. Crowell, J.E., et al., *The Adsorption and Thermal-Decomposition of Water on Clean and Oxygen-Predosed Al(111).* Journal of Chemical Physics, 1987. **86**(10): p. 5804-15.

75. Batra, I.P. and L. Kleinman, *Chemisorption of Oxygen on Aluminum Surfaces.* Journal of Electron Spectroscopy and Related Phenomena, 1984. **33**(3): p. 175-241.

76. Schroeder, A., et al., *Titanium containing amorphous hydrogenated carbon films (a-C: H/Ti): surface analysis and evaluation of cellular reactions using bone marrow cell cultures in vitro.* Biomaterials, 2000. **21**(5): p. 449-56.

77. Sundararajan, T., et al., *Surface characterization of electrochemically formed passive film on nitrogen ion implanted Ti6Al4V alloy.* Materials Transactions Jim, 1998. **39**(7): p. 756-61.

78. Oh, K.T. and Y.S. Park, *Plasma-sprayed coating of hydroxylapatite on super austenitic stainless steels.* Surface & Coatings Technology, 1998. **110**(1-2): p. 4-12.

79. Radin, S.R. and P. Ducheyne, *Plasma Spraying Induced Changes of Calcium-Phosphate Ceramic Characteristics and the Effect on Invitro Stability.* Journal of Materials Science-Materials in Medicine, 1992. **3**(1): p. 33-42.

80. Vogel, J., et al., *Structural changes in plasma sprayed hydroxyapatite.* Cfi-Ceramic Forum International, 1999. **76**(3): p. 28-32.

81. MacDonald, D.E., et al., *Physicochemical study of plasma-sprayed hydroxyapatite-coated implants in humans.* Journal of Biomedical Materials Research, 2001. **54**(4): p. 480-90.

82. Soballe, K., et al., *A review of ceramic coatings for implant fixation.* J Long Term Eff Med Implants, 1999. **9**(1-2): p. 131-51.

83. Capello, W.N., et al., *Hydroxyapatite-coated total hip femoral components in patients less than fifty years old - Clinical and radiographic results after five to eight years of follow-up.* Journal of Bone and Joint Surgery-American Volume, 1997. **79A**(7): p. 1023-9.

Chapter 4 Dissolution of Metal Oxides

4.1 Introduction

The previous chapter has examined and described the surface properties of the treated Ti-6Al-4V samples using XPS and SEM/EDS. It is well known that the surface properties determine the overall corrosion behaviour [1] [2]. Medical devices temporarily or indefinitely exposed *in vivo* or *in vitro* to quite aggressive biological fluids [3] are subjected to corrosion and degradation. Corrosion products[i] [4] can be transported around the body through the circulation of blood with potentially harmful effects [5]. Therefore it is very important to study the corrosion resistance (properties) of the surface treated Ti-6Al-4V *in vitro* to consider the various phenomena of metal ion release *in vivo*.

Titanium is reported to be a corrosion resistant metal due to its stable passive oxide surface layer. Several surface oxidation techniques, like ageing or nitrogen ion implantation [6] may be used to produce relatively thick oxide layers in order to improve corrosion resistance [7]. The ability of repassivation[ii] is also an important property for protecting the substrate Ti from corrosion [8]. Even though titanium has a passivated oxide layer and considerably high breakdown potentials more than 2 V (saturated calomel electrode, SCE) [9], this is not to say that titanium is totally inert in the body. The passive state is not entirely stable and metal ions, like titanium may be

[i] For the typical metallic femoral component of a total hip replacement, the total metal ion release is 11 to 22 mg/yr. The total body burden for a 70 kg man for most of the metals involved is below 10 mg, and normal concentrations in body fluids and tissues are probably in the 0.1 to 1.0 ng/ml range.

[ii] Repassivation: Titanium develops a thin, tenacious and highly protective surface oxide film. The surface oxide of titanium will, if scratched or damaged, immediately re-heal and restore itself in the presence of air or even very small amounts water. The corrosion resistance of titanium depends on a protective TiO_2 surface oxide film (http://www.titanium.org/).

released into the test environment. For example in the presence of chloride, localised breakdown on a highly microscopic scale has been found and this process can occur readily in pH 2.5 at 0.5 V (SCE) *in vitro* [5] [10] [11].

In addition, proteins such as albumin can affect the corrosion behaviour of some metals and their presence can either inhibit or accelerate the corrosion phenomena [12]. Proteins behave differently with different metals, since their role in a corrosion environment is governed by many factors such as surface properties, proteins adsorption, interaction of proteins with other ions present in solution to form organic complexes, and the transport of anionic and cathodic charge around and away from the local environment [13]. The spontaneous adsorption of organic material from the aqueous phase alters the interfacial free energy of the solid, as well as the corrosion potential of metal surfaces. If micro-roughness of the metal surface is considered, corrosion current can flow between the peaks and valleys of the roughness elements [14].

Due to the high breakdown potential of Ti alloy, it is unlikely that the passive layers will be broken down in the physiological environment. Therefore, the examination of the breakdown potential would serve little purpose. Nevertheless, the aim of the present work is to detect the effects of bovine serum solution and phosphate buffered saline (PBS) on corrosion behaviour of the treated Ti-6Al-4V by using a potentiodynamic study. The polarisation curves are particularly valuable in quantifying the corrosion behaviour of the treated Ti-6Al-4V.

4.2 Materials and Methods

4.2.1 Ti alloy surface preparation

Three sets of surface-treated Ti-6Al-4V alloy samples were prepared; the control (C), the nitric acid passivation (P) and ageing (A) in discs form. The surface preparation

was described in *Chapter 3, 3.2.1 Ti alloy surface preparation.* All tests were performed in duplicates.

4.2.2 Potentiodynamic tests

The test samples subjected to the control, the passivation and aged treatment were immersed in bovine serum solution or in PBS (PBS-14200, Gibco, UK) incubated under a humidified 5% CO_2/air atmosphere at 37°C±0.1°C. They were immersed in the simulated physiological environments for either a short-term test (10 hours) or long-term test (240 hours) to investigate any changes in the corrosion behaviour. The treated samples (C, P and A), which did not undergo immersion, were used as references for each group. The compositions of bovine serum solution and PBS are summarised in Table 4-1. The details and the nomenclature of each treatment are in Table 4-2. After immersion, samples were carefully cleaned by using deionised distilled water (MilliQ water, 18 MOhm water) then a surface area of 1.1 cm^2 (= $\pi \times (1.186/2)^2$) was exposed in a PBS electrolyte (pH = 7.4±0.2) for 10 minutes to establish a steady state open circuit potential for potentiodynamic studies. The experimental system is illustrated in Figure 4-1. Experiments were conducted in with de-aerated solutions; oxygen may affect the potential curve, therefore nitrogen was bubbled for 30 minutes through the solution to remove any oxygen. Anodic potentiodynamic polarisations were undertaken by using a potentiostat (EG&G Applied Research 263A potentiostat, Princeton, NJ) at a potential voltage range of between –0.5 V and +1.0 V and the scan rate was 0.5 mV/s. The electrolyte cell was made of glass and had a capacity of 200 ml. The specimen acted a working electrode (anode) and was placed in the cell facing a graphite rod, auxiliary electrode (cathode). A silver/silver chloride electrode (SSC) was used as a reference electrode. The potentiodynamic experiments were performed at ambient temperature.

Table 4-1 Analyses of sterile adult bovine serum solution and PBS

Bovine serum solution		PBS	
Biophysical Assay	Concentration	Biophysical Assay	Concentration
Density	1.023 b/ml at 24.1°C	-	-
Osmolarity	279 mOsmol/kg	-	-
pH	7.89	pH	7.4
Proteins		Proteins	
Total protein	86.88 mg/ml	-	-
IgG (Mancini)	18.5 mg/ml	-	-
Albumin (Mancini)	48 mg/ml	-	-
Globulin	41 mg/ml	-	-
Haemoglobin	318.2 mg/l	-	-
Biochemcial Profile		Component	10X liquid (g/l)
Sodium	142 mmol/l	KCl	2.00
Potassium	N/A mmol/l	KH_2PO_4	2.00
Urea	4.5 mmol/l	NaCl	80.00
Creatinine	144 umol/l	$Na_2HPO_4 \cdot 7H_2O$	21.60
Bilirubin	N/A umol/l	-	-
Aspt. Transferase	69 U/l	-	-
Alk. Phosphatase	189 U/l	-	-
Calcium	2.45 mmol/l	-	-

Table 4-2 Symbols for potentiodynamic tests

Symbols	Treatments
C	Control, received followed by polishing and cleaning procedure
P	C followed by 30% nitric acid passivation treatment
A	P followed by 10 h boiling deionised distilled water treatment
C (or A or P) bovine serum 10 h	C (or A or P) immersion in bovine serum for 10 h before potentiodynamic tests
C (or A or P) PBS 10 h	C (or A or P) immersion in PBS for 10 h before potentiodynamic tests
C (or A or P) bovine serum 240 h	C (or A or P) immersion in bovine serum for 240 h before potentiodynamic tests
C (or A or P) PBS 240 h	C (or A or P) immersion in PBS for 240 h before potentiodynamic tests

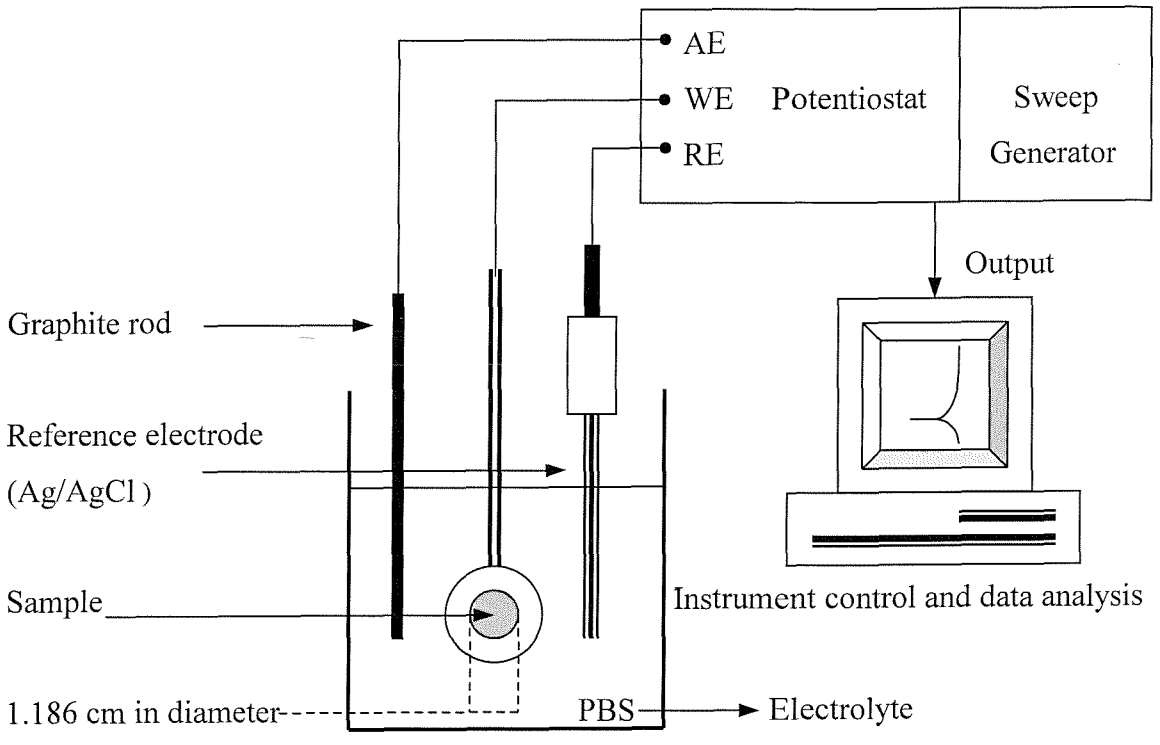

Figure 4-1 Schematic illustration of the experimental set-up for potentiodynamic test.

4.3 Results

The potentiodynamic (anodic polarisation) test is a method to evaluate the corrosion properties of a metal from the relation between the current density per unit surface area and the scanning potential. The current density indicates the dissolution kinetics of metallic ions from the metal surface into the electrolyte, namely the state of corrosion [15]. This study has assessed the passive behaviour of the treated Ti-6Al-4V alloy using an anodic polarisation technique, scanning potentials to +1000 mV (SSC). The breakdown potential was not reach for all samples, as the breakdown potential for Ti alloys is difficult to assess owing to the instability of the aqueous electrolytes at the high potentials required. Consequently, in this set of experiments there was no pit formation.

4.3.1 The corrosion behaviour of the control samples (C)

For the control (C) sample without immersion, the open circuit potential (E_{corr}) of the control was –256 mV. The current densities of the passive region were around 0 to 2 $\mu A/cm^2$ and the current density increased after ~ 452 mV (Figure 4-2 (a)). After immersion in PBS or bovine serum solution, the current density of the passive region increased. The sample immersed in bovine serum solution for 240 hours (C Bovine serum 240h) showed a clear increase in current density above a potential of ~320 mV which was lower than the other control samples (C, C Bovine serum 10h, C PBS 10h and C PBS 240h).

4.3.2 The corrosion behaviour of the passivated samples (P)

For the passivated sample (P) without immersion, the E_{corr} was –258 mV. The current densities of the passive region were around 1 to 3 $\mu A/cm^2$ and the current density increased after ~ 342 mV (Figure 4-2 (b)). After immersion in PBS or bovine serum solution, the current density of passive region decreased. The sample immersed in bovine serum solution for 240 hours showed a clear increase in current density above

potential of ~ 250 mV which was lower than the other passivated samples (P, P Bovine serum 10h, P PBS 10h and P PBS 240h).

4.3.3 The corrosion behaviour of the aged samples (A)

For the aged sample (A) without immersion, the E_{corr} was –248 mV. The current densities of the passive region were around 0 to 3 $\mu A/cm^2$ and the current density increased after ~ 562 mV (Figure 4-2 (c)). The aged sample (A) had a broader passive region compared to the passivated sample and the control sample. The aged sample prior to and after immersion in PBS or bovine serum solution had similar current densities. The sample immersion in bovine serum solution for 240 hours showed an obvious increase in current density above potential of ~ 360 mV which was lower than the other treated samples (A, A Bovine serum 10h, A PBS 10h and A PBS 240h).

It is interesting to notice that the significant differences in current density between the samples immersed in bovine serum solution and samples immersed in PBS for 240 hours. The current densities of the samples in bovine serum increased at a lower potential than that in PBS. With increasing potential, the current density became constant until reaching the end point of +1,000 mV. This was due to the growth of a passive oxide layer as a result of the voltage between the anode and the cathode (a growth of 20 Å/V is obtained for most electrolytes [16] [17]).

4.4 Discussion

The corrosion behaviour of the surface treated Ti alloy subjected to immersion in PBS and bovine serum solution has been characterised using anodic potentiodynamic polarisations. No pit formation was observed in PBS and bovine serum solution because Ti alloys have a high breakdown potential (2 V, SCE) [9].

The passivated sample and the control without immersion showed lower open circuit potentials (E_{corr}) than the aged sample, which had a noble value. This corrosion

behaviour is possible because the passivated and the control surfaces initially produce higher metal ion release from the surface than the aged surface, which has been demonstrated in previous work [18] [19]. The previous TEM [18] [20] results also have proven that the aged surface has more stable inert oxide layers due to the homogeneous rutile surface than the passivated sample, which might include heterogeneous or amorphous phases (TiO, Ti_2O_3, Ti_3O_5, anatase and rutile) (Table 4-3) and some defect points (in *Figure 3-1(c) and (d)*).

Table 4-3 Identification of oxide layers of P and A by TEM [18]

Passivated Oxide (P)	
d-spacing (Å)[1]	Identity of ring
5.498	TiO
3.41	An[2]/Ti_3O_5
2.92	TiO
2.46	Ru[3]/TiO/Ti_3O_5
2.08	Ru/Ti_3O_5
1.86	An/Ti_3O_5
1.71	An/Ti_3O_5/Ti_2O_3
1.48	An/TiO
Aged Oxide (A)	
d-spacing (Å)	Identity of ring
2.47	Ru
2.20	Ru
1.96	Ru
1.70	Ru
1.62	Ru
1.45	Ru
1.37	Ru
1.34	Ru

1. The d-spacing for the main diffraction rings are shown along with the oxides to which they correspond
2. An: anatase
3. Ru: rutile.

The control sample possesses a complex duplex microstructure (α and β phases) on the surfaces as demonstrated in *Chapter 3, AFM morphology* (*Figure 3-1(a)*). This complex system may affect the open circuit potential, for example due to the solubility

of Ti, Al and V ions [21]; therefore it was difficult to explain the corrosion behaviour of the control sample and interpret the different corrosion behaviour between the control, and the passivated and the aged samples according the present data. However, after 240 hours immersion, the effect of the bovine serum solution on the current density was obvious, this is possibly related to the potential difference produced between two phases (α and β) on surface, and between these two phases and proteins [14] [22].

When the passivated samples are immersed in PBS or bovine serum solution, the oxide thickness may increase with time [23], causing a reduction in current density in the passive region compared to the sample P without immersion. Immersion in bovine serum solution is more complex than in PBS, not only O_2 or OH^- can react with oxide layers, but also other ions, such as Cl^-, Ca^{2+}, HPO_4^{2-} or $H_2PO_4^{2-}$ (in PBS) and proteins (in bovine serum solution), etc. These reactions may cause these ions, e.g. Cl^-, Ca^{2+}, HPO_4^2 or proteins to penetrate or migrate to the matrix of the oxide layer and change the microstructure of oxide layer [24]. Indeed, this new microstructure consisting of a metal/protein/hydroxide form possibly restricts metal dissolution [21], which is consistent with the reduction in current density in the passive region observed for the immersed samples. However, when the potential reached ~342 mV the current density clearly increased for the sample P undergoing long-term (240 hours) immersion in bovine serum solution. This suggests that as soon as the driving force (applied potential) is higher than the chemical binding energy between metal/protein/hydroxide, part of the new-formed oxide layers will be broken. This induces metal ion containing species to be released from oxide layers resulting in a current density increase. The surface chemistry of this oxide layers has been investigated in *Chapter 3, Figure 3-4 (XPS analyses)*, e.g., the O/Ti ratio of the passivated surface varied from 103.87 (1 h), then 52.31 (10 h) and to 19.60 (240 h)[iii]. The significant change of O/Ti ratio with time, which suggested a dynamic surface, could be related to the remarkable difference in the corrosion behaviour of the passivated sample after 240 hours bovine serum immersion compared to the aged samples (O/Ti ratio: 15.93 (1 h), then 12.12 (10 h) and to 7.64

[iii] For the passivated surface, this ratio is from 1-3 nm depth profile; 3-5 nm depth profile: 40.64 (1 h), 23.78 (10 h) and 9.9 (240 h), and 5-7 nm depth profile: 23.84 (1 h), 10.39 (10 h) and 7.6 (240 h).

(240 h)[iv]). These potential curves also suggest that the bovine serum solution affects the corrosion behaviour of the passivated sample more than PBS. This was also previously suggested by Merritt and Brown [25] [26].

The aged sample (A) prior to immersion exhibited a constant current density in the passive region until reaching the potential of ~562mV (Figure 4-2 (c)). In addition, it showed a broader passive region than P and C. In fact, the current densities in the passive region are quite similar among samples prior to and after immersion. It is believe that the original aged oxide layer is stable and *Chapter 3* also shows the aged surface consists of hydroxylated groups which may enhance the reaction with proteins and form stable layers. Even though, an increased current density above the potential of ~ 360 mV was observed, this potential was still more noble for sample A immersed in bovine serum 240 hours than compared to that of the control and the passivated samples. This suggests that the interaction between the aged surface and the organic compounds results in a more stable complex than that of the passivated and the control samples.

The present results show that (1) bovine serum solution has a greater effect on the corrosion behaviour of Ti-6Al-4V than PBS solution during long-term immersion and (2) the corrosion behaviour of the aged surface is less affected by bovine serum solution than the passivated and the control samples. This behaviour can be explained in terms of the surface properties and the reaction between proteins and surfaces. From the view of surface properties, generally speaking, the more atomic defects or amorphous phases (Table 4-3) there are in the oxide, especially the passivated samples, the less able the oxide film is to prevent migration of ionic species and the lower the kinetic barrier is to corrosion. These atomic defects include vacancies, which are missing atoms in the oxide crystal and impurity atoms with different valance states within the oxide crystal [1]. In addition, the passivated surface also has higher roughness (*Ra*: 1.14 ± 0.092) than the aged surface (*Ra*: 0.60 ± 0.174) (in *Chapter 3*). The high roughness not only causes a high metal ion release rate (or high current density) but also allows proteins to embed in the valleys. Evidence for this has been

[iv] For the aged surface, this ratio is from 1-3 nm depth profile; 3-5 nm depth profile: 13.20 (1 h), 9.4 (10 h) and 7.11 (240 h), and 5-7 nm depth profile: 12.90 (1 h), 9.4 (10 h) and 6.4 (240 h).

observed in the AFM work (*Figures 3-1* and *3-2*). Therefore, the passivated surface has more amorphous phases, some defect points, high roughness and less hydroxylated groups so that it is unable to form a stable chemical reaction between oxide layers and proteins. When the applied potential increased to a certain level, the new-formed oxide layers are easier to break down than those of the aged surface and cause metal ion release (i.e. increase current density). On the contrary, the aged surface consists of more hydroxylated groups enhance the chemical reaction between the oxide layer and proteins to form stable complexes (in *Chapter 3*).

If we consider the contribution of proteins to the corrosion process, proteins can interact with the corrosion mechanism (M_{corr}) in a number of ways. For example, ($M_{corr}1$) proteins can bind to metal ions to form proteins/metals (or organometallic oxides) complexes and transport them away from metal/solution interface thus encouraging further dissolution, or ($M_{corr}2$) proteins may adsorb onto the metal surface thus restricting the diffusion of oxygen to the surface making it more difficult for the metal to repassivate (i.e. new-formed oxide layers). Both of these mechanisms might be expected to reduce the corrosion resistance of the alloy [21]. It is also possible that ($M_{corr}3$) the protein adsorption on the surface restricts metal ion dissolution. Before the applied potential approaches the point where the current density increases, the protein/oxide layer complexes are able to diminish the metal ion dissolution (according to $M_{corr}3$ and $M_{corr}2$) and have a constant current density in the passive region results. However, when the applied potential is higher than the point where the current density increases, $M_{corr}1$ may become the dominant mechanism, encouraging dissolution and $M_{corr}2$ may also make a contribution. These mechanisms could possibly explain why the treated samples with 240 hours bovine serum solution immersion demonstrated an obvious change in current density (Figure 4-2). In addition, proteins adsorb on surface, forming colonies that constitute physical anomalies on a metal surface, resulting in the formation of local cathodes and anodes. Under aerobic conditions, the areas under the adsorbed proteins become anodic and the surrounding areas become cathodic [14]. The adsorbed proteins produce the difference in potential at the interface and consequently results in increasing higher corrosion currents [21].

The possible interface reactions of PBS/Ti substrate and bovine serum solution/Ti substrate immersed in the simulated physiological environment (before corrosion) are

demonstrated in the following reactions[v]: at a pH of 7.4 (PBS) or 7.89 (bovine serum solution), albumin has a negative charge since its point of zero charge (PZC) is about pH 4.7-4.9. Titanium has a negatively charged surface; Ca ions would have a bridging effect in the electrostatic adsorption of albumin to titanium [13] [27] [28].

In PBS (pH: 7.4):

Ti oxide surface ($\ominus$, negative charge) = Ca^{2+} ($\oplus$, positive charge)

(Reaction 4-1)

In bovine serum solution (pH: 7.8):

Ti oxide surface ($\ominus$, negative charge) = Ca^{2+} ($\oplus$, positive charge) = Albumin ($\ominus$, negative charge)

(Reaction 4-2)

The interface reaction formed not only new oxide layers after immersion, but also the adsorption of proteins or inorganic ions onto the surface [29] [30]. This can result in potential differences developing between metal and protein producing an electric current and therefore corrosion. In addition, it is known that the existence of orthophosphates (HPO_4^{2+}) in solution, like PBS, can contribute to the formation of a protective film, if the solution has a sufficient calcium concentration in solution, like bovine serum solution [31]. Based on these suggestions, we may explain why the current density increases before the potential approaches the breakdown potential in this study. In addition, it is interesting to find that the control samples showed clear curves (Figure 4-2(a)). In the contrary, the passivated and the aged samples expressed obvious instability around the open potential (E_{corr}) and passive region. This phenomenon suggests that various surface properties, such as surface phases, oxide thickness or roughness etc., cause different reaction between surfaces and inorganic ions/organic proteins and in turn to affect the stability of the potential curve. For these remaining questions, future work has to be done before any conclusion to be drawn.

[v] The figure is presented in *Chapter 2 Literature review, Figure 2-2.*

Even though the physiological bioelectric potentials[vi] [32] are unable to reach the potential (range of 250 ~ 360 mV) where the current density increases in this study, living bone tissue is still able to release so-called "strain-related potentials" [33] [34] during typical loading conditions, e.g., walking or jumping. For example, it may be possible for the cyclically stressed femur to generate potentials on the order of ±100 mV while in contact with the implant's surface. These potential pulses may help to encourage depassivation. Also, it has been suggested that these pulses may interfere with normal bone regeneration and be a factor in the osteolysis (bone deterioration) frequently observed around the implant [33].

Summary

The corrosion resistance is one of the most important characteristics for biomedical materials, because it concerns not only the device's lifetime but also their potential adverse effects the human body. Thus, it was necessary to evaluate it as part of a comprehensive study of the treated surfaces. The results obtained suggest that the aged Ti-6Al-4V possessed a much better corrosion resistance and a more stable passive oxide film than the other treatments as expected. It has also been shown that bovine serum solution has a greater effect than PBS on treated Ti-6Al-4V samples. Therefore, the adsorption of an organic testing medium as a simulated physiological environment would appear appropriate as it simulated a worse case scenario in terms of corrosion. Having assessed the corrosion performance of these mechanisms, it is now necessary to assess biocompatibility in cell culture since the response of osteoblast to the alloy critical to the performance (acceptance/rejection) of the material in the body.

[vi] Magnitude of physiological bioelectric potentials (mV): Bone: -2 to +7.6, cartilage: -1 to +22, muscle: 1 to +12, nerves (via remote electrode): -0.4 to +1.4 and nerves (transmembrane): -90 to +35. These potentials at least in principle can polarise implant surfaces or portions of implant surfaces in ways that could significantly affect corrosion behaviour.

(a)

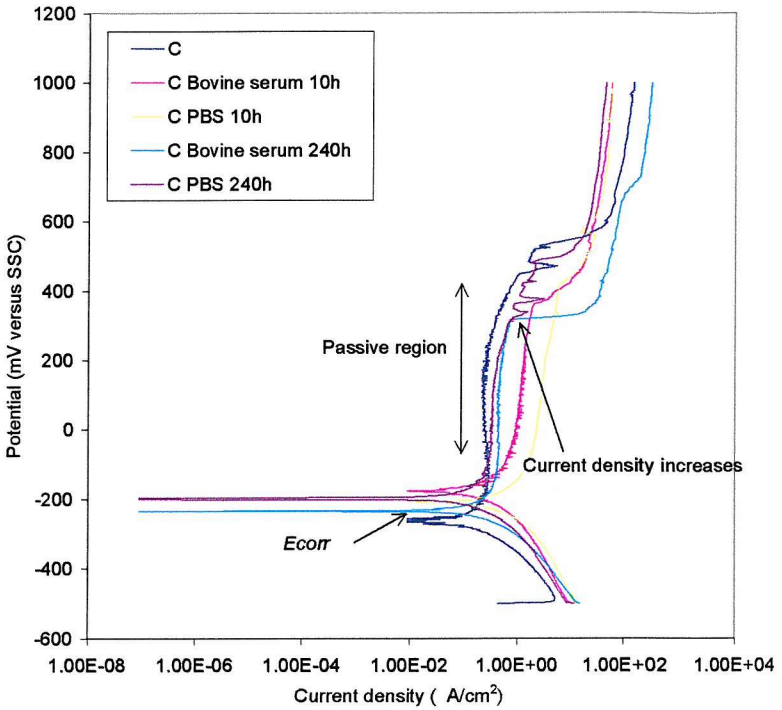

(b)

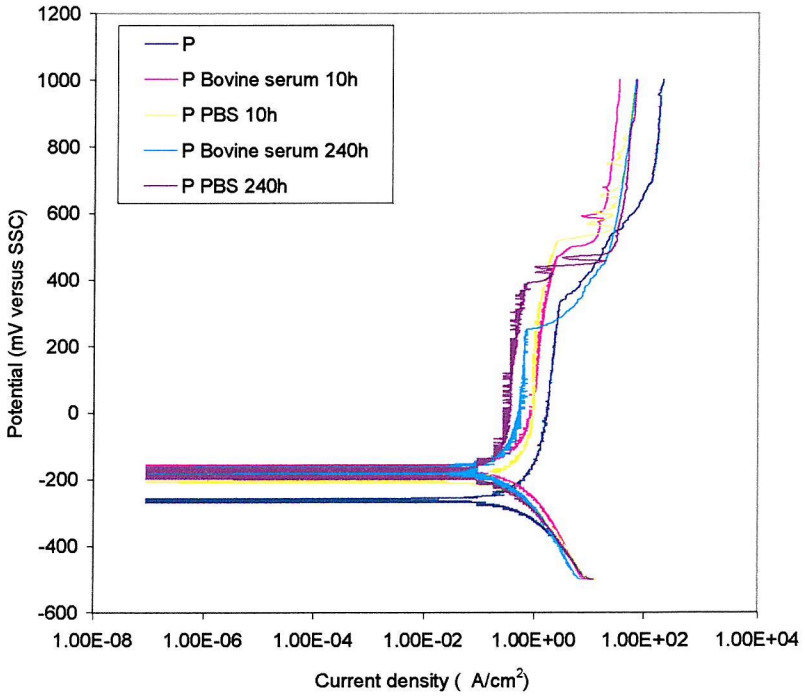

Figure 4-2 The potentiodynamic anodic polarisation curves for various treated Ti-6Al-4V. (a) Control (C), (b) the passivated sample (P) and (c) the aged sample (A). Scan rate: 0.5 mV/S, temperature: ambient temperature.

(c)

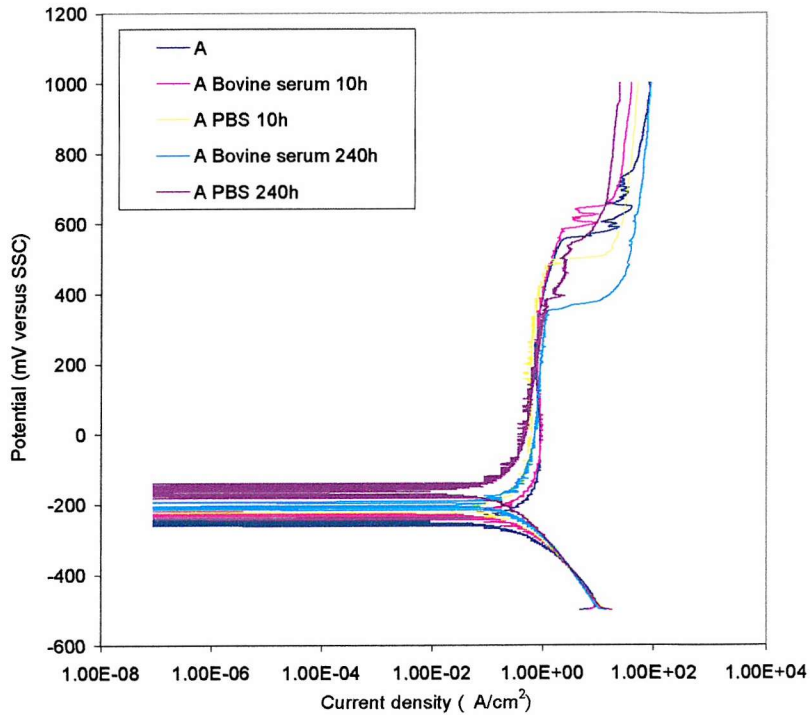

Figure 4-2 (*continued*)

References

1. Jacobs, J.J., J.L. Gilbert, and R.M. Urban, *Corrosion of metal orthopaedic implants.* Journal of Bone and Joint Surgery-American Volume, 1998. **80A**(2): p. 268-82.
2. Jones, F.H., *Teeth and bones: applications of surface science to dental materials and related biomaterials.* Surface Science Reports, 2001. **42**(3-5): p. 79-205.
3. Sittig, C., et al., *Surface characterization of implant materials c.p. Ti, Ti-6Al-7Nb and Ti-6Al-4V with different pretreatments.* J Mater Sci Mater Med, 1999. **10**(1): p. 35-46.
4. Black, J., *Does Corrosion Matter.* Journal of Bone and Joint Surgery-British Volume, 1988. **70**(4): p. 517-20.
5. Souto, R.M. and G.T. Burstein, *A preliminary investigation into microscopic depassivation of passive titanium implant materials in vitro.* J Mater Sci Mater Med, 1996. **7**: p. 337-43.
6. Sundararajan, T., et al., *Surface characterization of electrochemically formed passive film on nitrogen ion implanted Ti6Al4V alloy.* Materials Transactions Jim, 1998. **39**(7): p. 756-61.
7. Pouilleau, J., et al., *Structure and composition of passive titanium oxide films.* Mater Sci Eng B, 1997. **47**: p. 235-43.
8. Azumi, K., N. Yasui, and M. Seo, *Changes in the properties of anodic oxide films formed on titanium during long-term immersion in deaerated netural solutions.* Corros Sci, 2000. **42**: p. 885-96.
9. Cai, Z., et al., *In vitro corrosion resistance of titanium made using different fabrication methods.* Biomaterials, 1999. **20**(2): p. 183-90.
10. Souto, R.M. and G.T. Burstein, *Study of corrosion processes with electrochemical noise measurements.* Materials science forum, 1998. **298-292**: p. 799-806.
11. Burstein, G.T. and R.M. Souto, *Observations of localised instability of passive titanium in chloride solution.* Electrochemica Acta, 1995. **40**(12): p. 1881-8.
12. Clark, G.C. and D.F. Williams, *The effects of proteins on metallic corrosion.* J Biomed Mater Res, 1982. **16**(2): p. 125-34.

13. Ellingsen, J.E., *A study on the mechanism of protein adsorption to TiO2.* Biomaterials, 1991. **12**(6): p. 593-6.
14. Characklis, W.G. and K.C. Marshall, *Biofilms*. 1990, New York: Wiley. xvii, 796.
15. Kobayashi, E., et al., *Mechanical properties and corrosion resistance of Ti-6Al-7Nb alloy dental castings.* Journal of Materials Science-Materials in Medicine, 1998. **9**(10): p. 567-74.
16. Khan, M.A., R.L. Williams, and D.F. Williams, *In-vitro corrosion and wear of titanium alloys in the biological environment.* Biomaterials, 1996. **17**(22): p. 2117-26.
17. Sundgren, J.E., P. Bodo, and I. Lundstrom, *Auger electron spectroscopic studies of the interface between human tissue and implants of titanium and stainless steel.* J Colloid Interface Sci, 1986. **110**(1): p. 9-20.
18. Browne, M. and P.J. Gregson, *Surface modification of titanium alloy implants.* Biomaterials, 1994. **15**(11): p. 894-8.
19. Ku, C.-H., M. Browne, and P.J. Gregson. *Chemical and morphological changes of surface treated titanium alloy implants in vitro.* in *Cell and Materials Meeting*. 1999. Davos, Switzerland: Cell and Materials.
20. Wisbey, A., et al., *Effect of surface-treatment on the dissolution of titanium-based implant materials.* Biomaterials, 1999. **12**(5): p. 470-3.
21. Khan, M.A., R.L. Williams, and D.F. Williams, *The corrosion behaviour of Ti-6Al-4V, Ti-6Al-7Nb and Ti-13Nb-13Zr in protein solutions.* Biomaterials, 1999. **20**(7): p. 631-7.
22. Denny, A.J., *Principles and prevention of corrosion*. 2nd ed. 1996, NJ, USA: Prentice Hall.
23. Effah, E.A.B., P.D. Bianco, and P. Ducheyne, *Crystal-Structure of the Surface Oxide Layer on Titanium and Its Changes Arising from Immersion.* Journal of Biomedical Materials Research, 1995. **29**(1): p. 73-80.
24. Ciolac, S. and E. Vasilescu, *The corrosion behaviour of some titanium alloys in physiological environment. Short term "in vitro" studies.* Revue Roumaine De Chimie, 1999. **44**(5): p. 431-8.
25. Brown, S.A. and K. Merritt, *The effects of serum proteins on corrosion rates in vitro.* Clinical Applications of Biomaterials, 1982: p. 195-202.

26. Brown, S.A. and K. Merritt, *Fretting Corrosion in Saline and Serum.* Journal of Biomedical Materials Research, 1981. **15**(4): p. 479-88.

27. Lima, J., et al., *Interactions between calcium, phosphate, and albumin on the surface of titanium.* Journal of Biomedical Materials Research, 2001. **55**(1): p. 45-53.

28. Wassell, D.T.H. and G. Embery, *Adsorption of bovine serum albumin on to titanium powder.* Biomaterials, 1996. **17**(9): p. 859-64.

29. Hanawa, T., *In vivo metallic biomaterials and surface modification.* Mater Sci Eng A, 1999. **267**: p. 260-6.

30. Hanawa, T., K. Asami, and K. Asaoka, *Repassivation of titanium and surface oxide film regenerated in simulated bioliquid.* Journal of Biomedical Materials Research, 1998. **40**(4): p. 530-8.

31. Wranglen, G., *An introduction to corrosion and protection of metals.* 1985, London, UK: Chapman and Hall. 168.

32. Bundy, K.J., *Corrosion and other electrochemical aspects of biomaterials.* Crit Rev Biomed Eng, 1994. **22**(3-4): p. 139-251.

33. Douglas, J.W., *The Characterization of Particulate Debris Obtained from Failed Orthopaedic Implants - 5. Mechanical metallurgy and passivation of titanium implant alloys (http://www-engr.sjsu.edu/cme/materials/projects/srproject/index.htm).* 1993, College of Materials Engineering, San José State University.

34. Hsieh, Y.F. and C.H. Turner, *Effects of loading frequency on mechanically induced bone formation.* Journal of Bone and Mineral Research, 2001. **16**(5): p. 918-24.

Chapter 5 Biological Interaction with Metal Oxides

Part A Cellular approach[i]

5.1 Introduction

The interaction between solid surfaces and biological systems are critically important to many areas of medicine, technology and research. In general, only the surface of an implant is in direct contact with the host tissue, and thus this portion of the material plays a central role in determining its biocompatibility. The surface of material can change with time, and is often distinctly different from the bulk properties, because of oxidation and contamination. Although the surface clearly plays an important role in implant/cell interactions, the relationships between surfaces of the implant, its reactivity with tissue constituents, and long-term integrity and clinical efficacy are still poorly understood [1] [2].

Ti-6Al-4V alloy has become one of the most used biomaterials due to its excellent corrosion resistance, good mechanical properties and low toxicity [3]. Its corrosion resistance is due to the oxide film, which forms spontaneously on exposure to air. However, when the alloy is implanted into a complicated and aggressive physiological *in vivo* environment, the oxide stability may be affected, resulting in increased metal ion release [4]. Elevated levels of metal ions have been reported in the serum of patients with both well functioning and failed total joint replacements [5]. In addition, aluminium (Al) has well documented toxic effects in the serum or urine of patients who

[i] This article has been accepted by *Biomaterials, 2001.*/

had a total hip replacement made of titanium-based alloy [6]. Moreover, several *in vitro* studies have been carried out with a variety of cell lines to test metal ion toxicity, which is suspected of playing a significant role in cell behaviour. Titanium ions have been shown to influence mineral formation and osteoid nodules in rat calvaria cultures [7]. It has been demonstrated that Ti-6Al-4V ion solution can affect the normal differentiation of bone marrow stroma cells to mature osteoblasts *in vitro* [8]. Therefore, decreasing the metal ion release could be a method to increase the biocompatibility of Ti alloy.

In our previous work, it has been shown that a simple thermal treatment, ageing in deionised distilled boiling water, improves the dissolution resistance of Ti-6Al-4V alloy compared to conventional passivation treatments [9]. In the present study, the biocompatibility of the aged surface has been evaluated in comparison to the control and the passivation treatments. Short-term and long-term *in vitro* tests were performed with two osteoblastic cell lines corresponding to immature and mature cells. In the first instance, the biocompatibility of the aged titanium alloy was evaluated *in vitro* via short-term tests, which assessed cell viability, cell proliferation and cell morphology. Secondly, quantification of the ageing treatment took place via long-term *in vitro* tests, which measured FN production, ALP activity and TP content.

5.2 Materials and Methods

5.2.1 Ti alloy surface preparations

Distal sections of forged Ti-6Al-4V alloy femoral stems from the Ti-Mod Freeman hip replacement were supplied by Finsbury Instruments (Leatherhead, Surrey, UK). The hip stems were cut into discs in 4 mm^2 and 10 mm^2 and 1 mm thickness. The samples were first wet-ground with 120, 600, 1200, 2400 and 4000 grit silicon carbide abrasive paper (Struers, UK) at approximately 150 rpm, then polished with 6, 3 and 1 μm diamond solution (Microcloth Buehler, UK) on a clean polishing cloth (Microcloth Buehler, UK) and finally with colloidal silica polishing suspension (0.06 μm, Mastermet Buehler, UK). Following polishing, the samples were cleaned in 1% Triton

solution for 1 hour and rinsed in deionised distilled water (MilliQ water, 18 MOhm water). This treatment was used as a control (C). The practice for surface preparation of surgical implants involves a nitric acid passivation treatment (P) based on the ASTM F86 protocol using 30% nitric acid for 1 hour [10]. A third treatment (the ageing treatment, A) consisted of the passivated treatment followed by ageing in boiling deionised distilled water (MilliQ water) for 10 hours. The successive steps of the three surface treatments are shown in Table 5-1.

Table 5-1 The successive steps of surface treatments for the control (C), the passivated (P) and the aged (A) Ti-6Al-4V

	Control (C)	Passivated (P)	Aged (A)
Surface preparation	-Polished -Cleaning in 1% Triton for 1 hour -Rinsing in deionised distilled water (MilliQ water)	-Polished -Cleaning 1% Triton for 1 hour -Rinsing in deionised distilled water -30% nitric acid for 1 hour -Rinsing in deionised distilled water	-Polished -Cleaning 1% Triton for 1 hour -Rinsing in deionised distilled water -30% nitric acid for 1 hour -Rinsing in deionised distilled water -10 hours in boiling deionised distilled water
Sterilisation	-Immersed in 100% ethanol for 10 min -Air-dried -Exposed under UV light for 30 min on each side -Rinsing in PBS before immersion		

Finally, the discs were rinsed several times with sterile, endotoxin-free PBS before cells were seeded. As a preliminary experiment, the endotoxin assay using Limulus Amebocyte Lasate (BioWhittaker, Emerainville, France) revealed that no contamination of lipopolysaccharides (LPS)[ii] [11] [12] [13] was present on the surface of the treated samples. Measurement of LPS contamination is very important because

[iiii] LPS is a complex glycolipid composed of a hydrophilic polysaccharide portion and a hydrophobic domain known as lipid A that is responsible for most of the LPS-induced biological effects. One of the many known functions of LPS is the stimulation of bone resorption by osteoclast. Although it has not been fully elucidated how LPS is involved in this process, there was evidence that LPS failed to activate osteoclats directly. In contrast, LPS can stimulate osteoblasts to secrete IL-1, IL-6, GM-CSF and PGE2.

LPS may stimulate osteoblasts to secrete interleukin 1 (IL-1), IL-6, granulocyte-macrophage colony-stimulating factor (GM-CSF) and prostaglandin E2 (PGE2) which induce bone resorption [11]. These three treated surfaces, the control (C), the passivated (P) and the aged (A) were then examined in the biocompatibility tests.

5.2.2 Cell culture

Two human osteoblast-like cell lines obtained from American Tissue Culture Collection (Manassas, VA, USA) were tested: (i) an immature osteoblast (MG-63) and (ii) a mature osteoblast (SaOS-2)[iii] [14]. We used two cell lines in our tests because cellular response depends on the local environment and state of maturation of responding cells [15]. The osteoblastic cell lines were cultured in Dulbecco's modified Eagle's medium (DMEM) (Sigma, Buchs, Switzerland) containing 10% fetal bovine serum (Sigma), 1% PSF (100 x, 10,000 U/ml Penicillin, 10,000 µg/ml Streptomycin and 25 µg/ml Fungizone®) (GibcoBRL, Life Technologies, Basel, Switzerland) under a humidified 5% CO_2 air atmosphere at 37°C.

Samples of 4 mm^2 were used for cell proliferation assessment in 96 well cell culture plates and 10 mm^2 samples for cell viability, ALP activity, FN and TP production in 24-well cell culture plates. Cells were seeded on to each sample at 5,000 cells/well in 96-well plates and 100,000 cells/well in 24-well plates. These biochemical assays can provide the information concerning that osteoblastic cells response to the various surface treatments.

MG-63 cells were used for cell viability and proliferation measurements of the treated Ti-6Al-4V implants at 12 hours, 24 hours and 72 hours. SaOS-2 cells have been demonstrated to express high steady-state levels of ALP activity [16]. SaOS-2 cell line was used for ALP, TP and FN assay on the control, the passivated and the aged

[iii] Transformed SaOS-2 and MG-63 cells derived from human osteosarcomas have been used in studying interactions with implant biomaterials. An immortalised cell line is relatively easier to maintain over a period of time with many passages without a loss of phenotypic expression. The MG-63 cells is considered more as an immature osteoblast than the SaOS-2 with respect to their ALP production. Therefore, we used MG-63 for early experiment as in this case, immature osteoblasts would be in contact with the implant in the body and we used SaOS-2 for long-term experiments to be in a situation more "similar" to the implant being for some time in the body.

samples at weeks 1, 2, 3 and 4. The medium was changed every 3-4 days. The medium (DMEM with 10% serum) was removed two days before each time point (at weeks 1, 2, 3 and 4) and cells were washed 3 times with PBS to avoid the effects of compositions from serum on the biochemical assays. The cell culture was then incubated with serum free medium for 2 days before biochemical assays.

5.2.3 Biochemical assays

5.2.3.1 Cell viability/proliferation[iv]

To assay cell viability, cells were collected by trypsinisation with 1% trypsin for 5 minutes. The collected cells were double stained with 25 μg/ml fluorescein diacetate (Sigma) in PBS and 20 μg/ml propidium iodide (Sigma) in PBS in aluminium-covered tubes for 5 minutes [17]. Live cells appear green and dead cells appear red under epifluorescent illumination (blue filter of 450-490 nm and green filter of 510-560 nm which allowed visualisation of the green and red fluorescing cell, respectively). Cell viability tests were performed twice for each point and at least 200 cells were counted in epifluorescent mode in a Nikon Microphot-FXA microscope (Nikon, Tokyo, Japan). Cell viability was defined as the ratio of viable cells to the total number of cells and presented in percentage (%) for three treatments (C, P and A). To assay cell proliferation, cells were treated with CellTiter 96® AQ_{ueous} Assay (Promega Corp., WI, USA). The assay is based on the reduction of a tetrazolium compound {3-(4,5-dimethylthiazol-2-yl)-5-(3-carboxymethoxyphenyl)-2-(4-sulfophenyl)-2H-tetrazolium, inner salt; MTS} to a coloured formazan product by viable cells (or cell metabolic activity). The absorbance at 490 nm on plate reader is directly proportional to the cell proliferation. The cell proliferation of the passivated (P) and the aged (A) samples was normalised by the control (C).

[iv] Viability and cytotoxicity assay are principally used to enumerate the proportion of live and dead cells in a population. Proliferation assays are primarily designed to monitor the growth rate of a cell population or to detect daughter cells in a growing population (http://www.probes.com/handbook).

5.2.3.2 Total protein measurement[v]

A solution of 0.5 ml 1% Triton-X in MilliQ water H_2O (18 MOhm water) was used to lyse cells. The lysate was sonicated for 30 seconds at 40 W. The total protein was measured in the cell lysate with DC (Detergent Compatible) Protein Assay Kit (Bio-Rad Lab, CA, USA).

5.2.3.3 Alkaline phosphatase activity

ALP level is considered to reflect osteoblastic activity and is thought to play a major role in bone formation and mineralisation [18]. The enzyme activity within the lysate was measured with a commercial Kit (Sigma ALP-10, cat. no.245). One unit of ALP activity is defined as that amount of enzyme, which produces 1 μmole of *p*-nitrophenol (PNP) per minute. The total protein was used to normalise the ALP activity.

5.2.3.4 Fibronectin measurement

FN is one of the most abundant extracellular matrix components in many tissues and has been shown to be present in early bone formation [19]. A commercially available Human Fibronectin ELISA kit (Biomedical Tech Inc., Stoughton, MA, USA) was used to measure FN within the lysate. The FN production was normalised by the total protein.

5.2.3.5 Statistical analysis

The viability and proliferation of MG-63 are presented at each time point (12, 24, and 72 hours) (Figure 5-1 and Figure 5-2, respectively) corresponding to the mean ± standard error of three independent analyses. The ALP activity and FN normalised by TP of SaOS-2 are presented at each time point (1, 2, 3 and 4 weeks) (Figure 5-3 and

[v] The detailed experimental procedure for TP, ALP, FN and cell morphology are described in *Appendices, Biochemical assays and Cell morphology.*

Figure 5-4, respectively) corresponding to the mean ± standard error of 4 independent analyses performed in duplicates. ANOVA was applied to determine the statistical significance of the differences observed between groups. p values smaller than 0.05 were considered significant.

5.2.4 Cell morphology

Cell morphology studies can provide information concerning the cell initial interaction with the treated Ti-6Al-4V implant and cell-cell contact. In order to approach this purpose, SaOS-2 cells were seeded on to each sample (10 mm^2) at a concentration of 2,000 cells/ml in 24-well tissue culture plates for 24 hours and 7 days incubation. Cells were then fixed with 1% glutaraldehyde (Sigma) in PBS, treated with 1% Triton X-100, 2 mg/ml sodium borohydride (Sigma) in PBS and stained with 4 μg/ml rhodamin-phalloidin (Sigma) for actin microfilaments. A Nikon Eclipse TE300 inverted epifluorescence microscope enabled cells to be visualised. A Standard filter set (510 nm) was used for rhodamin-phalloidin. Images were acquired with a Micromax PB1300 cooled CCD camera (Roper Scientific, Trenton, NJ) and image processing was performed using a MetaMorph imaging system (Universal Imaging Corporation, Westchester, PA). The cell morphology and particularly the actin filament organisation were visually examined.

5.3 Results

5.3.1 Cell viability/Proliferation

There was no significant difference between the three different treated samples (C,P and A) for the cell viability of MG-63 during the test (Figure 5-1). The aged samples had significantly higher cell proliferation compared to the control samples at 72 hours (Figure 5-2). Although the aged samples had higher cell proliferation than the passivated samples at 72 hours, no statistical difference was found.

5.3.2 Alkaline phosphatase activity

The ALP activity of the control sample was statistically higher than the passivated and the aged samples at week two (Figure 5-3). At week four, the aged sample induced a statistically higher ALP production than the passivated and the control samples. In addition, the ALP activity of the aged sample also showed significant higher than the passivated sample at week four.

5.3.3 Fibronectin study

No FN activity was detected at week one (Figure 5-4). FN activity was observed after the week two and reached a peak at week three before decreasing at week four. There was no significant difference between the three surface treatments.

5.3.4 Cell morphology

After 24 hours, bundles of actin filaments (stress fibres) were found and cells had an angular shape on the three different treated surfaces. Focal adhesion and some small stress fibres were also revealed at the periphery (Figure 5-5). After 7 days, cell-cell contact was visualised for the osteoblasts on these three surface treatments (Figure 5-6). No major difference was visually found between the three surface treatments.

5.4 Discussion

In this study, we investigated the effect of metal ions on osteoblastic cell behaviour cultured on the surface treated Ti-6Al-4V alloy. More specifically, biocompatibility tests were performed on Ti-6Al-4V surfaces, which had a simple, cost-effective ageing surface treatment applied to reduce metal ion dissolution.

In short-term *in vitro* tests (24 hours), cell viability/proliferation and cell morphology demonstrated that there was no evidence of cell toxicity in response to the various treated Ti-6Al-4V surfaces. Moreover, the cell morphology of SaOS-2 clearly showed that focal adhesion sites localised at the periphery and bundles of actin filaments spanned the entire cell (Figure 5-5). These observations allowed us to conclude that cells attached to the treated surfaces at 24 hours as already demonstrated in literature [20]. In addition, it may suggest that in short-term at 24 hours cell viability/proliferation and cell morphology tests are unable to discriminate the effects of various surface treatments on cell behaviour. Therefore, a longer period test is necessary in this study.

Differences between osteoblasts behaviour became apparent only since 72 hours with a significant difference in proliferation between the aged and the passivated samples (Figure 5-2). The proliferation measurement was based on cellular reduction of MTS and was dependent on the reduced pyridine nucleotides NADH and NADPH, i.e. finally on mitochondrial activity. The cellular damage in mitochondria inevitably results in loss of the ability of the cell to maintain and provide energy for metabolic cell function and growth [21]. Decrease in cell proliferation suggests that metal ion release may indeed affect mitochondrial activity. Nevertheless, this hypothesis needs to be further confirmed.

It has been found that by affecting their proliferation, osteoblasts may delay the time course of their differentiation stages e.g. [22]. In the present study, we showed that metal ion release from the different surface treatments affected the cell proliferation. Therefore, it seems reasonable to assume that the different surface treatments may shift the time course of differentiation stage. A delay in the peak measurement of ALP activity was noted on the aged and the passivated samples compared to the control sample (Figure 5-3). Even though results comparisons between two different cell lines should be handled carefully, it seems that the decrease of MG-63 proliferation and the delay in the peak measurement of SaOS-2 ALP activity agrees with the assumption mentioned that surface treatment could delay the differentiation pathway of the osteoblasts. A similar result has been demonstrated in a previous study [23].

No FN was detected at week one. Other proteins such as collagen may play a major role in the cell attachment to the different samples instead of FN at week one e.g. [20]. It may also be possible that the metal ion release from the samples affected the initial production of FN. A previous study has demonstrated that FN was not involved in the adhesion of osteoblasts to uncoated Ti alloy at 24 hours [24]. Moreover, the integrin α_5- which is a major adhesion receptor of osteoblasts interacting with FN [25] [26]- was not detected in cell cultured on polished or rough Ti-6Al-4V at 12 hours while it was detected for cell cultured on polystyrene [27]. Despite results of the study by Sinha et al. (1996) were obtained at 12 hours while present FN results were obtained at week one, they could support the hypothesis that proteins other than FN were involved in the osteoblast adhesion to Ti alloy. The production of FN observed after two weeks could then probably be due to cell-cell contact e.g. [28]. The increasing FN production at week two and three could also contribute to cell spreading configuration maintaining the survival of mature osteoblasts [29]. Therefore, FN may play an important role in cell adhesion at the initial stage (very early stage before week one) and be involved in bone formation during the process of cell differentiation [30] [31] [32].

Previous work in our group has demonstrated that the various surface treatments alter the metal ion release behaviour [9] [33] and surface composition (in *Chapter 3*) of the Ti-6Al-4V alloy. An established model[vi] was used to describe the kinetics of Al ion dissolution by Browne et al. [9], the release of Al ions was about 0.84 μM for the ageing treatment and about 5.55 μM for the passivation treatment after 7 days. The osteoblast cultured on the aged surface experienced therefore, a much lower concentration of Al ions for the test duration[vii] [34] [35] [36] [37]. The kinetics of the metal ion release, especially for Al, could explain the differences in cell behaviour, which were observed only in long-term *in vitro* study. Indeed, results of ALP peak activity at week two for the control treatment compared to the passivated and the aged treatments was in agreement with a previous study using a similar Al ion concentration [38]. It should be noted also that the only difference in terms of surface composition between the different Ti-6Al-4V surface treatments was the presence of vanadium for

[vi] This established model is described in *Appendices, Metal ion release kinetics.*

[vii] *In vivo*, typical plasma Al concentrations are in the range of 0.37 μM, Al^{3+} can bind to serum proteins, notably transferring, albumin and to smaller moleculars such as citrate and phosphate.

the control treatment (in *Chapter 3*). It may be possible therefore, that vanadium also has an impact on osteoblast differentiation by maturing the osteoblasts faster. Further experiments on this particular hypothesis need to be performed before a definitive conclusion can be drawn.

It has been shown that surface roughness influenced the cell behavior [15]. We have used XPS and AFM techniques to examine the surface properties of the treated Ti-6Al-4V surfaces (in *Chapter 3*). A difference in roughness (R_a) between the passivated and the aged samples could only be observed at a small scale (1 μm^2). The area average R_a was about 0.99 nm (C), 1.29 nm (P) and 0.56 nm (A). Therefore, at the cell level, the roughness could be considered as similar between samples and could not explain the differences in osteoblasts behaviour. Moreover, the different characteristics of Al and Ti oxide layers can explain the higher impact of Al than Ti on cell behaviour *in vitro* or *in vivo*. Ti oxide surfaces are normally terminated by acidic and basic hydroxyl groups, which are readily resolved into bridged and terminal configurations (in *Chapter 3*, *Figure 3-5*). These two sites are chemically considerably more distinct on the Ti surface than Al surface [39]. This amphoteric surface, coupled with the inherently low solubility of titanium, make the surface considerably more corrosion resistant than a similar oxide film on aluminium. On the contrary, the high solubility of the alkalis (like aluminium) creates a basic solution when water is present at the oxide surface and accelerates the conversion of oxide into hydroxide, ultimately disrupting the oxide film and resulting in attack of the underlying metal. Therefore, the composition and structure of the surface causing Al ions released from Ti-6Al-4V seems to be a major component capable of interacting with osteoblastic cells by affecting cell proliferation and ALP activity [8] [40].

Biocompatibility tests such as those performed in this study can only quantify particular aspects of cell behaviour. The cell reaction to an implant is however a very complex situation and can only be partially understood using standard biological assays. In order to have a comprehensive description of the cell-implant interaction with surface treated Ti alloy, functional genomic studies may be performed [41]. This will form the basis of the next part of this Chapter.

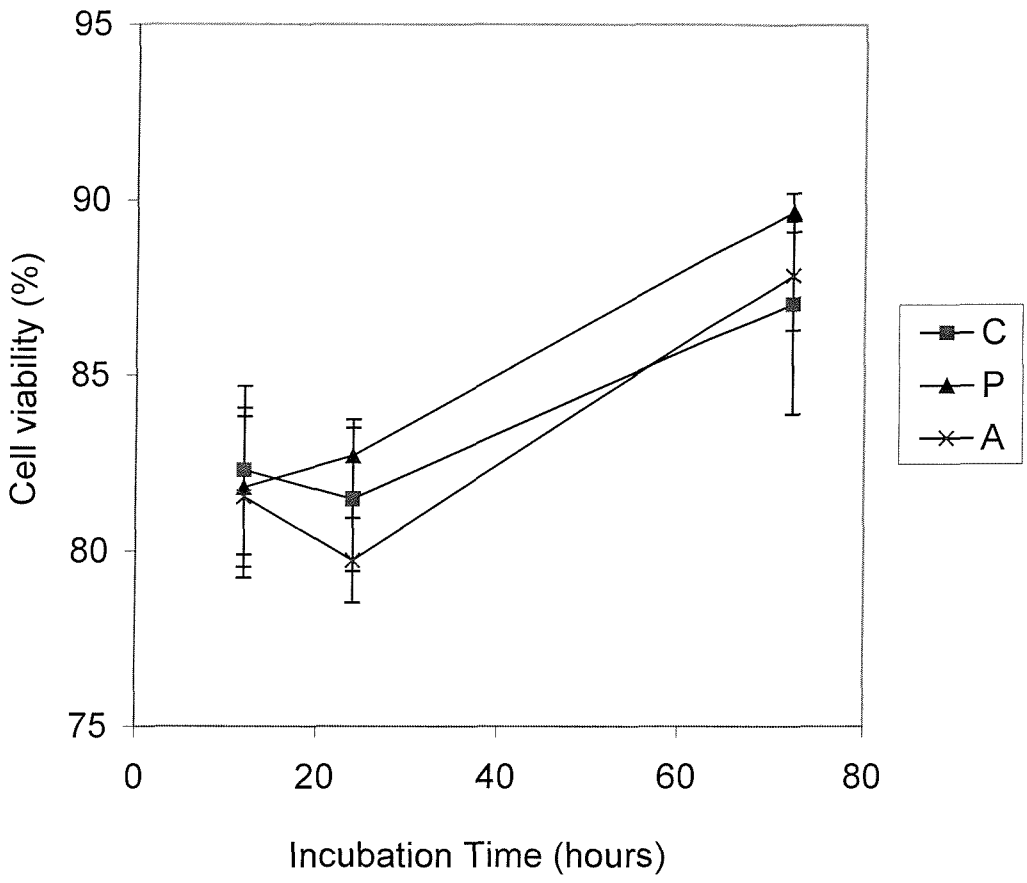

Figure 5-1 Viability of MG-63 cell on the treated Ti-6Al-4V samples. C: the control sample, P: the passivated sample and A: the aged sample.

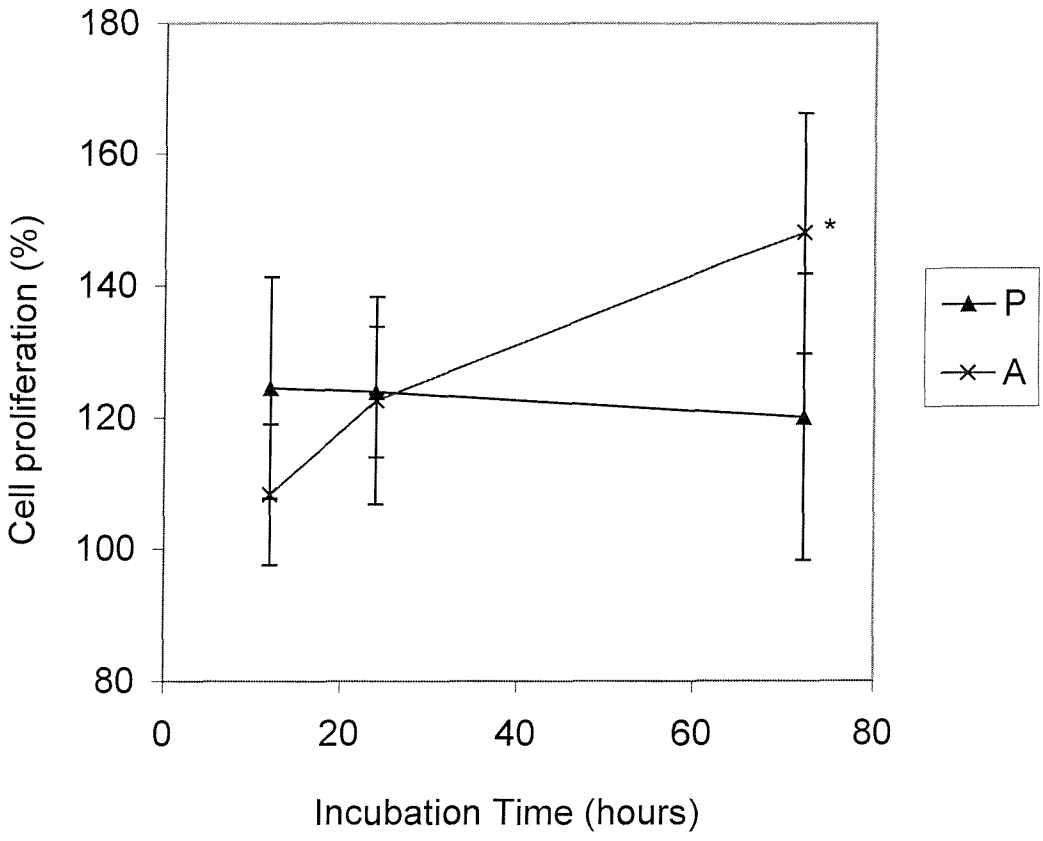

Figure 5-2 Proliferation of MG-63 cell on the treated Ti-6Al-4V samples. P: the passivated sample and A: the aged sample. *: Significant difference C versus A, $p \leq 0.05$. C: the control sample, used to normalise P and A, is not shown in the figure.

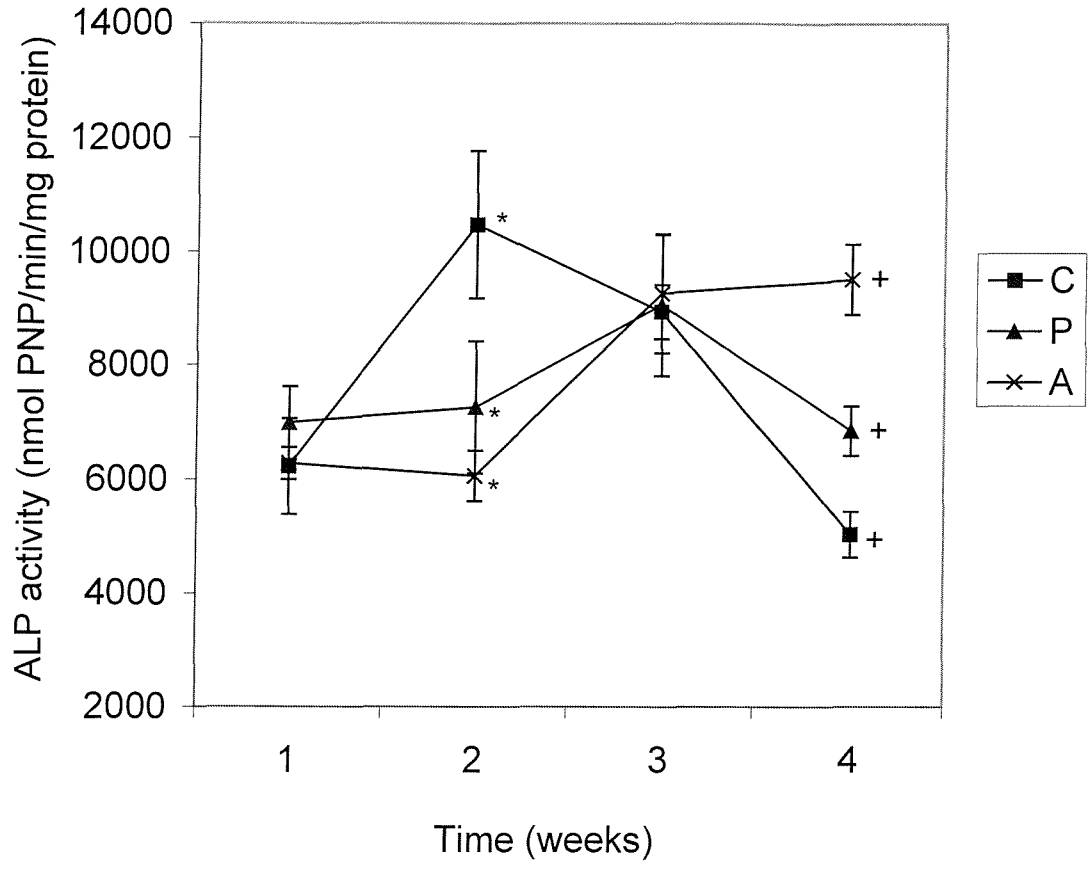

Figure 5-3 ALP activity of SaOS-2 cell on the treated Ti-6Al-4V samples. C: the control sample, P: the passivated sample and A: the aged sample. At week 2, there was a significant difference between C versus P and C versus A (*, $p \leq 0.05$). At week 4, there was a significant difference between C versus A, and between P versus A (+, $p \leq 0.05$).

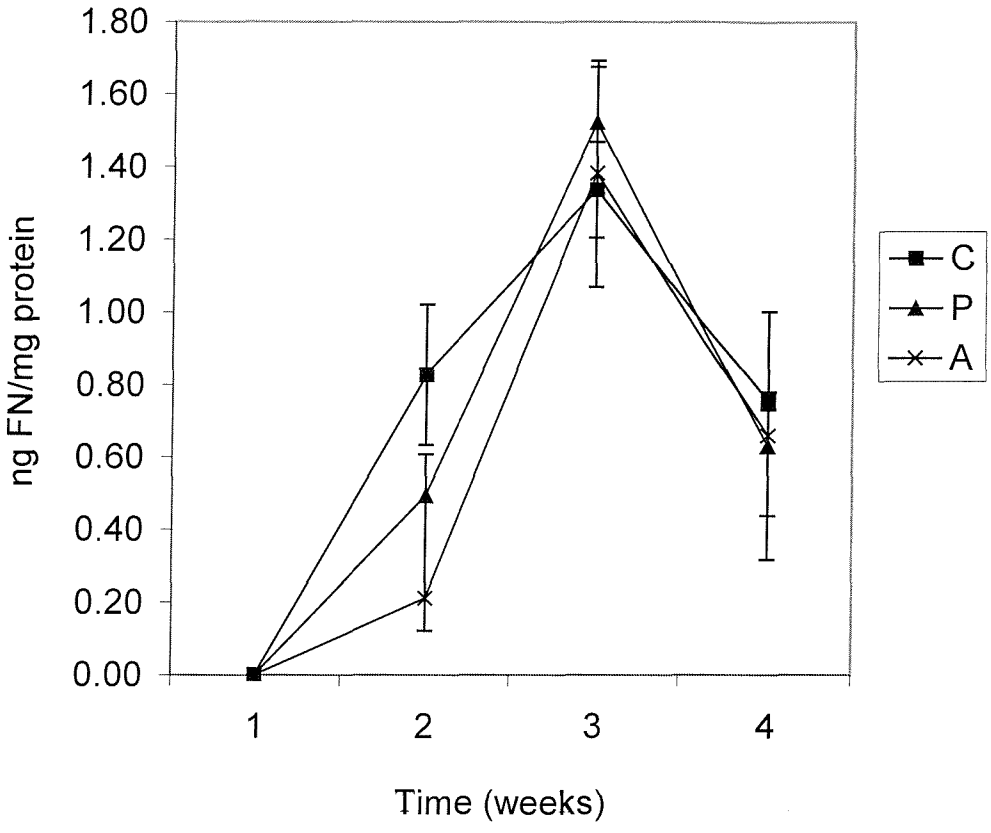

Figure 5-4 Fibronectin activity of SaOS-2 cell on the treated Ti-6Al-4V samples. C: the control sample, P: the passivated sample and A: the aged sample. FN activity was not detectable at week 1.

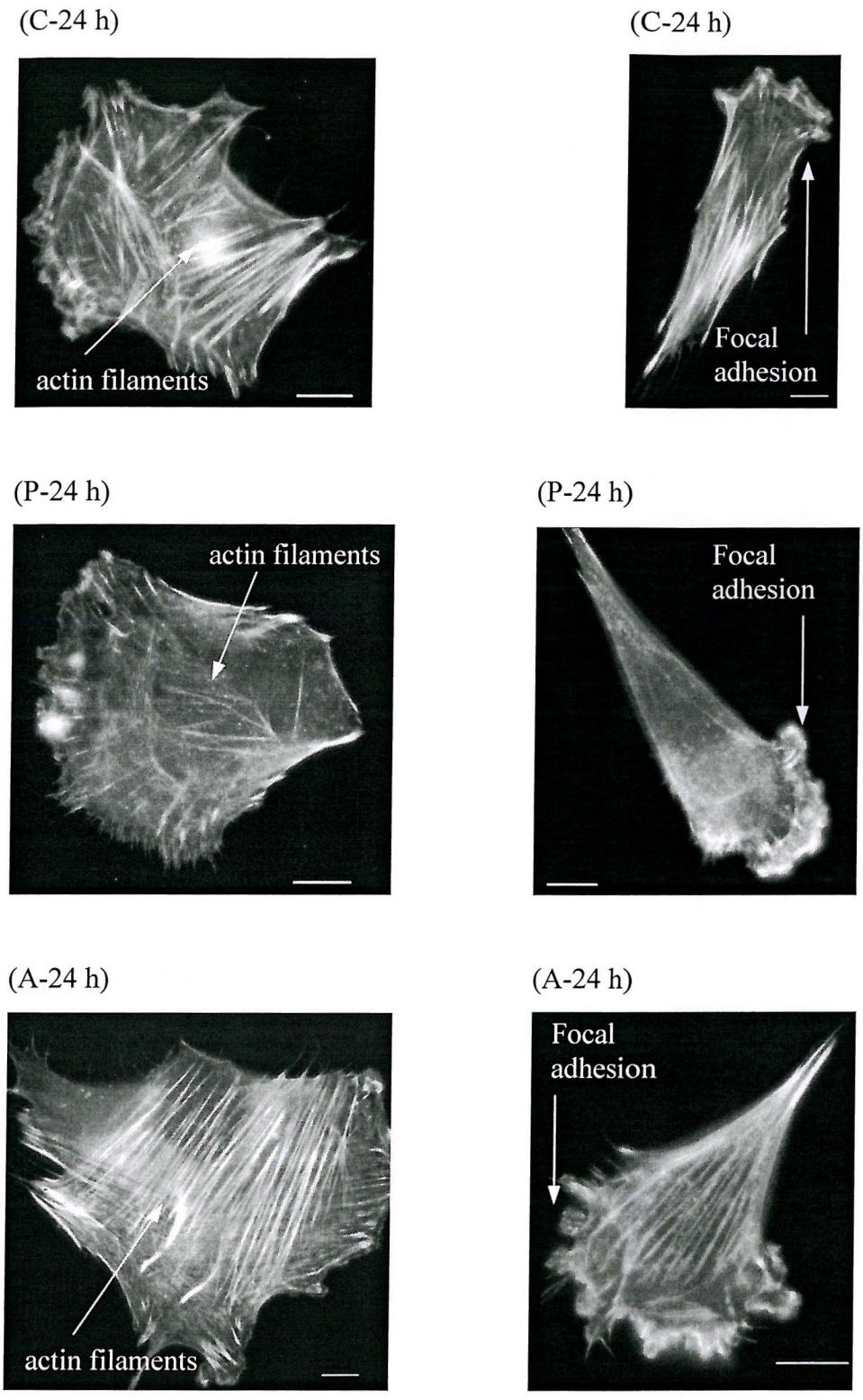

Figure 5-5 SaOS-2 cell morphology on the treated Ti-6Al-4V samples at 24 hours. Scale bar: 10 μm. C: the control sample, P: the passivated sample and A: the aged sample. C-24h: SaOS-2 seeded on the control sample for 24 hours. P-24h: SaOS-2 seeded on the passivated sample for 24 hours. A-24h: SaOS-2 seeded on the aged sample for 24 hours.

(C–7d)

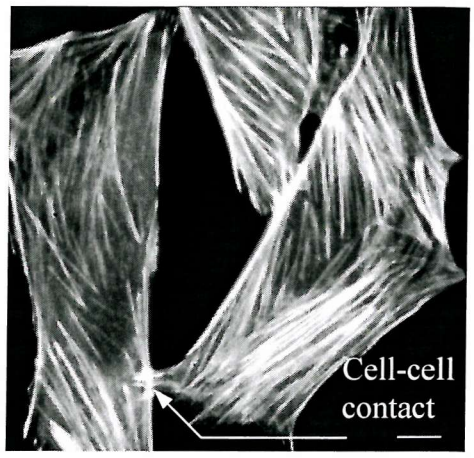

(P–7d)

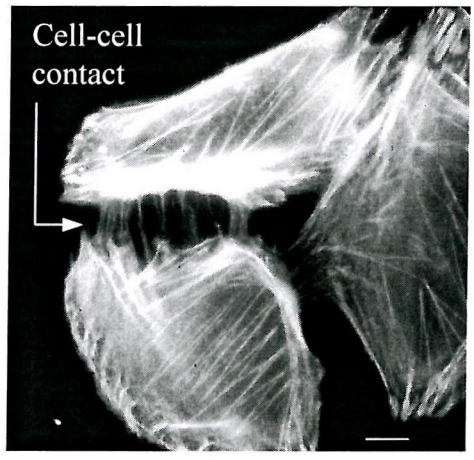

(A-7d)

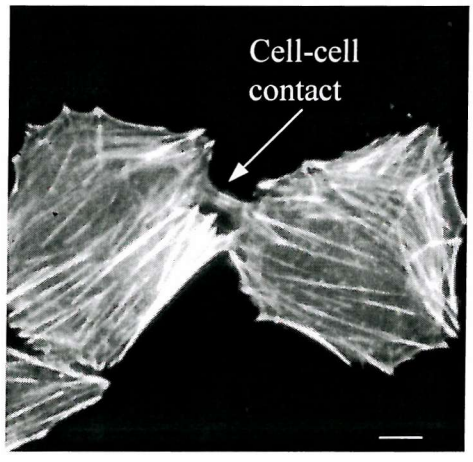

Figure 5-6 SaOS-2 cell morphology on the treated Ti-6Al-4V samples at 7 days. Scale bar: 10 μm. C: the control sample, P: the passivated sample and A: the aged sample. C-7d: SaOS-2 seeded on the control sample for 7 days. P-7d: SaOS-2 seeded on the passivated sample for 7 days. A-7d: SaOS-2 seeded on the aged sample for 7 days.

Part B Functional genomic approach

5.5 Introduction

It is now evident that osteoblast differentiation is a multistep series of events modulated by a sequence of gene expression that initially supports proliferation and the sequential expression of genes associated with the biosynthesis, organisation and mineralisation of the bone extracellular matrix [42]. In Part A, cell proliferation and differentiation have been examined for biocompatibility purposes as well as several proteins (markers) of different maturation stages. These measurements furnish important information on the biocompatibility of the various treated Ti alloy samples. However, only a small number of variables can simultaneously be measured. It is crucial to understand the osteoblast-implant interactions, because these affect cell proliferation, differentiation and bone resorption (osteolysis) [43]. The balance between bone formation and bone resorption around the prosthesis during remodelling determine the long-term success or failure of these implants [44]. In order to gain a broader insight into the biocompatibility of Ti alloy, quantification of gene expression on a large scale is introduced in this study.

Genomics include studies of genome mapping, gene sequencing, gene function and gene expression. Using cDNA microarray technology, it is possible to achieve large-scale analysis of gene expression in a single experiment. These technologies allow novel approaches to complex biomedical problems ranging from basic research in fundamental cellular structure and processes to applied research in pathogenesis, and therapy [45] [46]. Since this method was developed in 1995, it has been applied to a variety of studies, such as, the discovery of novel genes associated with osteoblast differentiation [47]. The discovery of novel genes is important in biology since it can find new targets for drug development. For example, the inhibition of the formation or

activity of osteoclasts on OPG/RANKL/RANK[viii] pathway could be a promising approach to treat osteoporosis [48]. Furthermore, the Genomic study has also been used to investigate the effect of the ionic products of Bioglass© 45S5 dissolution on the gene expression profile of human osteoblast (hOB) [49].

Recently it has been found that particulate wear debris of Ti or Ti alloys can be involved in periprosthetic osteolysis [50] [51]. However, information on the surface treated Ti-6Al-4V alloys directly affecting gene expression of osteoblasts is limited [52]. The first goal of this study is to extensively investigate the osteoblast gene expression that follows osteoblast attachment to the Ti-6Al-4V alloys using the cDNA microarray technology. The second goal is to identify genes, involved with osteolysis, which are differentially expressed when cells are exposed to the various treated Ti-6Al-4V alloys.

5.6 Materials and Methods

5.6.1 Ti alloy surface preparations

Forged Ti-6Al-4V alloy hip stems were cut into discs 10 mm in diameter and 1 mm thickness. The three treated surfaces, the control (C), the passivated (P) and the aged (A), were examined for the functional genomic study. The successive steps of the three surface treatments and the cleaning schedule are described in Table 5-1.

5.6.2 Cell culture

Human osteoblasts (hOB) were isolated from piece of bone femur obtained during total hip arthrophasty of a female patient (62 years) following a procedure previously described [53]. The osteoblastic cells were cultured in Dulbecco's modified Eagle's

[viii] Abbreviations: OPG: osteoprotegerin, RANKL: receptor for activator of nuclear factor-κB ligand and RANK: receptor for activator of nuclear factor-κB.

medium (Sigma, Buchs, Switzerland) containing 10% fetal bovine serum (FBS) (Sigma), 1% PSF (100 x, 10,000 U/ml Penicillin, 10,000 µg/ml Streptomycin and 25 µg/ml Fungizone®) (GibcoBRL, Life Technologies, Basel, Switzerland) under a humidified 5% CO_2/air atmosphere at 37°C. Osteoblasts were used at passages lower than 4. The osteoblasts, at a concentration of 382,000 cells/cm^2 (300,000 cells/ml), were seeded on each sample (surface area: 0.785 cm^2). In order to have enough cells for the genomic study, 6 samples of each treated surface were used (total cells number: 1.62×10^7)[ix].

5.6.3 Genomic study

Genefilters (GF211 Research Genetics, Huntsville, AL) were used to monitor the expression of 12,626 genes. The collected RNA from the cells (5 µg of total RNA per condition) was processed according to the manufacturer's recommendations[x]. The Pathways™ software, developed by Research Genetics was used to acquire for the microarray data. Quantification of the gene expression of cells in contact with the three treatments was performed at 24, 48 and 120 hours. Normalisation of gene expression and data analysis was performed using Excel and 2HAPI, a web-base bioinformatics, software (http://array.sdsc.edu). The microarray data analysis system 2HAPI are able to display a table of genes and corresponding information from different databases (PubMed, Genecards, Genebank, Unigene, Entrez, etc.).

The kinetics of gene expression for hOB incubated with the aged Ti-6Al-4V was only measured at 4, 24, 48 and 120 hours (Table 5-2). The gene expression of cells incubated for 4 hours on the aged sample (A_4) was chosen as a reference. 58 genes were selected and classified in 6 groups according to adhesion, signal pathway and transcription factors, growth factors and cytokines, differentiation, mineralisation and apoptosis. This selection represents a panel of major genes expressed by osteoblasts [54] [55]. The cellular functions of the chosen genes are described in Table 5-4.

[ix] Total cells number: 300,000 cells/ml x 6 (samples) x 3 (treatments) x 3 (time points)

[x] The detail analysis procedure is described in website: http//genomics.ucsd.edu/genefilter_pr.html.

28 genes were specifically analysed in Table 5-2 to compare the difference in gene expression between different surface treatments. The results are presented in the ratio of P/A and C/A (Table 5-3).

For both analyses, the difference in gene expression is based on the experimental finding that up-regulation by a ratio higher than 2.5-fold or down-regulation by a ratio lower than 0.4-fold (=1/2.5) has to be reached to be considered as significant [56] [57]. Sample control was analysed twice ($C_{24(1)}$ and $C_{24(2)}$) with two filters and showed good reproducibility of the analysis.

5.7 Results

The results presented in Table 5-2 are intended to evaluate of the gene modulation of the aged Ti-6Al-4V implants, while Table 5-3 is used to compare gene expression with respect to the different surface treatments. Sample A_{24} did not have enough RNA for the analysis.

5.7.1 Kinetics of genes modulation by the aged Ti-6Al-4V implants (Table 5-2)

From a quantitative point of view, in comparison to A_4, A_{48} has 213 up-regulated genes and 5 down-regulated genes; A_{120} has 247 up-regulated genes and 5 down-regulated genes by using 2HAPI software. 58 genes were selected and described in the following groups:

Cell adhesion

Integrin α_3, integrin α_5, integrin α_6, integrin β_1, integrin β_5 and fibronectin were expressed by the isolated hOB, but did not show a significant difference compared to the reference (A_4), except for collagen alpha-2 type I which was up-regulated 4.4-fold at 48 hours and 3.48-fold at 120 hours.

Signal pathways and transcription factors

Focal adhesion kinase (FAK) and mitogen-activated protein (MAP) kinases were down-regulated at 48 and 120 hours. c-*jun* showed a 0.43-fold decrease and c-*fos* was up-regulated 2.23-fold for A_{48}. Protein tyrosine kinase (PTK9) showed a 0.5-fold decrease at 48 hours. PTK receptor was up-regulated 3.20-fold at 48 hours and increased with time. Stem cell tyrosine kinase 1 (STK-1) was up-regulated 10.10-fold at 48 hours but undetected at 120 hours.

Growth factors and cytokines

The most important and effective growth factors of bone, fibroblast growth factors (FGFs), insulin-like growth factor (IGF-1), transforming growth factor-β (TGF-β) and bone morphogenetic proteins (BMPs) have been examined. FGF-5 was up-regulated 5.85-fold and increased to 6.37-fold at 120 hours. Keratinocyte growth factor (KGF = FGF-7) was up-regulated 2.8-fold at 120 hours. Insulin-like growth factor (IGF-1) was up-regulated 4.38-fold at 48 hours and not detected at 120 hours. Transforming growth factor-β induced gene (BIGH3) and platelet-derived growth factor (PDGF-A) were detected, but did not show significant modulation. Most of the BMPs were not detected (BMP-2A, BMP-3 and BMP-5, supplementary information; and data not shown) or down-regulated (BMP-1, BMP-2B and BMP-4). Genes, which have been proved to be involved in the process of osteoporosis, such as FGF-2 (= basic fibroblast growth factor, or bFGF) and interleukin 1 alpha (IL-1α) were either absent or down-regulated compared to reference A_4. The expression of proinflammatory mediators including IL-6 and prostaglandin E-2 (PGE-2) was not detected (supplementary information; and data not shown).

Differentiation stage

No significant value of core-binding factor runt domain alpha subunit 1 (cbfa1), indian hedgehog (IHH) and homeodomain (BAPX1) was observed, except alkaline phosphatase (ALP) with an 1.22-fold increase at 48 hours and an 1.45-fold increase at 120 hours.

Mineralisation stage

SPARC/osteonectin, osteopontin (OPN), and biglycan (bone matrix glycoproteins), which are required for bone matrix formation, were detected. SPARC had a 1.76-fold

increase, OPN showed a 0.86-fold decrease and biglycan showed a 1.42-fold increase at 48 hours. Sialoprotein precursor (IBSP) was absent.

Apoptosis

TNF-related apoptosis-inducing ligand (TRAIL), TRAIL-R3, human nuclear transcription factor-kappa B (NF-κB) binding subunit (NF-κB1), NF-κB p65 (= Rel A), receptor activator of NF-κB (RANK), apoptosis-related protein (TFAR15), apoptosis specific protein, osteoprotegerin ligand (TRANCE or RANKL) and colony-stimulating factors (CSF-1, CSF-2 and CSF-3) were absent or decreased. NF-κB1 showed a 0.85-fold decrease at 48 hours and 0.92-fold decrease at 120 hours. NF-κB p65 showed a 0.69-fold decrease at 48 hours and 0.83-fold decrease at 120 hours. Apoptosis-related protein TFAR15 showed a 0.52-fold decrease at 48 hours and a down-regulation 0.41-fold at 120 hours. Bcl-xL was up-regulated 6.42-fold at 48 hours and up-regulated 10.08-fold at 120 hours. Bax isoform (alpha, beta, gamma and delta) decreased with time.

5.7.2 Comparison of gene expression with respect to the different surface treatments (Table 5-3)

In order to determine any difference in gene expression of hOB due to the different treated surfaces, 28 genes were selected based on Table 5-2 and described in the following groups:

Adhesion

Collagen α-2 type I expression increased by 1.45-fold and 1.18-fold for samples P_{48} and C_{48} compared to A_{48}, and decreased by 0.70-fold and 0.74-fold for samples P_{120} and C_{120} compared to A_{120}.

Signal pathways and transcription factors

FAK was up-regulated 4.25-fold and 6.63-fold for samples P_{48} and C_{48} compared to A_{48}. MAPK6 was up-regulated 2.59-fold for sample C_{48} compared to A_{48}. C-*jun* increased by 1.84-fold for samples P_{48} and C_{48}, then decreased with time. C-*fos* expression was down-regulated 0.27-fold for sample C_{48} and increased with time for

samples P and C. PTK9 was up-regulated 3.26-fold for sample C_{48} compared to A_{48}. Serine/threonine kinases (STK-1) did not show different expression between samples.

Growth factors and cytokines

IGF-I expression decreased by 0.58-fold for sample P_{48} and increased by 1.45-fold for sample C_{48}. FGF-5 decreased at 48 hours and increased at 120 hours for samples P and C compared to sample A. Keratinocyte growth factor (KGF = FGF7) expressed an up-regulation of 4.90-fold and 7.07-fold for samples C_{48} and P_{48}. FGF-2 (bFGF) expressed an up-regulation by 3.19-fold for sample C_{48} and by 2.40-fold for P_{48}.

Differentiation stage

ALP-1 was absent or marginal (M) for samples P and C during the test.

Mineralisation stage

SPARC/osteonectin and biglycan expressed by ~0.95-fold decrease for samples P_{48} and C_{48} compared to sample A_{48}.

Apoptosis

NF-κB1 increased 1.51-fold and 1.31-fold for samples P_{48} and C_{48}, respectively, then decreased at 120 hours. NF-κB p65 (Rel A) decreased with time. TFAR15 was up-regulated 2.75-fold and 2.56-fold for samples P_{48} and C_{48}. Bcl-xL was absent for samples P_{48} and C_{48}. It was down-regulated 0.14-fold for sample C_{120} and decreased 0.90-fold for sample P_{120}. Bax isoform (alpha, beta, and delta) increased with time and also increased for samples P_{120} and C_{120} compared to sample A_{120}.

5.8 Discussion

cDNA microarray technology is used to obtain a high-throughput of information on gene expression. This is a very powerful method, which allows the user to extensively compare the cell behaviour in different situations. However, there are some drawbacks to this technology, one of the major problems is its reproducibility [58]. Dealing with such a significant amount of data (we used a filter containing 12,626 genes) inevitably

generates problems of accuracy and reproducibility of the results. In order to have confidence in the results, we have performed the analysis of one sample (C_{24}) twice with two Genefilters. Although not identical, a comparison of results showed a good agreement of the gene expression values between the two filters. Indeed, it has to be mentioned that the purpose of running a cDNA microarray analysis is to gain a large view of differentially expressed genes between different situations. This information is then analysed and used in future experiments to specifically target the genes, which were found modulated with the microarray. This was the philosophy followed in this study. We first built a database of gene expression in various situations (the different treated titanium surfaces) with the cDNA microarray technology. We then analysed the database to look for differentially expressed genes. We ended up with a list of genes of interest whose expression has to be precisely quantified in future studies using real time reverse transcription polymerase chain reaction (RT-PCR).

5.8.1 Kinetics of genes modulation by the aged Ti-6Al-4V implants

In the cell adhesion group, the expression of different integrin subunits was detected. However, only collagen alpha-2 type I expression was significantly up-regulated compared to the reference, A_4. This suggests that the possible ligands contributing to the interaction between cells and the aged treated Ti-6Al-4V were mainly directed by collagen (linked with $\alpha_3\beta_1$ [27]) after 48 hours. The level of integrin α_5, α_6, β_1, β_5 and fibronectin did not change significantly with increasing time during the test. This is probably due to the fact that the maximum modulation of cell adhesion genes is an early event, which was not highlighted by measurements performed after 24 hours.

FAK and MAPK were down-regulated at 48 hours. These genes are thought to have important roles in signal transduction, proliferation and differentiation. Expression of these genes is related with integrin expression in a time course of events according to the Pathway 5-1 [59].

Integrins (at cell membrane) → FAK → MAPK signalling cascade (at cytoplasm) → c-*jun* and c-*fos* (at cell nucleus) → Proliferation → Differentiation

(Pathway 5-1)

In parallel, it has been demonstrated that osteoblasts cultured on Ti-6Al-4V produce FAK and MAPK (protein) within 24 hours [43]. According to our results, down-regulation of FAK and MAPK at 48 hours would not contradict the Pathway 5-1, especially if integrins were not modulated which was the case at 48 hours. c-*jun* expression of osteoblasts cultured on Ti-6Al-4V was also shown to be expressed before c-*fos* [43]. In our experiment, we noted a down-regulation of c-*jun* and an up-regulation of c-*fos* at 48 hours, which is then in accordance with the time course of events for c-*jun* and c-*fos* expression. It seems then reasonable to predict that the osteoblast adhesion process on the aged Ti-6Al-4V followed the Pathway 5-1. To confirm this, RT-PCR measurements could be performed at a very early stage (30 minutes to 4 hours following the cell seeding on the titanium surfaces) to quantify the expression of genes expressed before c-*fos* in the Pathway 5-1.

The expression of PTK, which belongs to another pathway of signal transduction [59], decreased over time. Indeed, PTK has been showed to follow the Pathway 5-2 in macrophages when metallic particles were present [60].

Surface membrane receptors binding particles → Protein tyrosine kinase and Serine/Threonine kinase → NF-κB → Releasing TNF/IL-6

(Pathway 5-2)

The osteoblasts also possess an inflammatory signalling response similar to Pathway 5-2 [61]. Following the decrease of PTK, we did not observe any modulation of NF-κB or IL-6. It is possible that either the concentration of metal ions released from the aged sample is unable to stimulate the PTK pathway in osteoblasts or the induced signal pathway is different between particles and ions.

FGF-5 and IGF-I were up-regulated at 48 hours. FGF-2 (bFGF) was down-regulated at all time points. These results are in agreement with the observation of an up-regulation for the collagen alpha-2 type I. Indeed, it has been demonstrated that IGF-I can increase type I collagen production while FGF-2 (bFGF) can inhibit its synthesis in osteoblastic cells [62]. In addition, the absence of IL-1, IL-6 or PGF_2 was also consistent with the

up-regulation of collagen as these cytokines could have an inhibitory effect on collagen expression [51] [63].

Surprisingly, BMPs, which induce cartilage and bone formation [64], were absent or down-regulated. Genes involved in osteoblast differentiation process, such as cbfa1, IHH and Bapx1 [65] were also absent. The isolated hOB cells used in this study may be too mature to express these genes [66]. This has to be confirmed in our future work.

ALP was detected with an 1.22-fold increase at 48 hours and 1.34 at 120 hours. It has been shown that the gene expression of type I collagen peaks earlier than that of ALP or osteocalcin [67]. Therefore, it is possible that an up-regulation of ALP or osteocalcin would arise after the 120 hours of the tests.

There was no significant difference for the chosen genes involved in the mineralisation process over time. Osteonectin and biglycan, which are related to mineralisation [62], were constantly detected at all time points suggesting that the aged Ti-6Al-4V surface did not impair the mineralisation process over time.

Several genes involved in the apoptosis process, such as TRAIL, TRAIL-R3, NF-κB1, NF-κB p65, TFAR15, RANK, TRANCE and CSFs [68] [69] [70] were not detected or had their expression decreased. In addition, the up-regulation of Bcl-xL, which is an inhibitor of apoptosis [71], increased with time. Conversely, the expression of Bax, which can accelerate apoptosis [71], decreased with time. These results could indicate that the aged Ti-6Al-4V did not stimulate the activation of apoptosis at 120 hours. The survival of osteoblasts could be therefore enhanced.

Without the expression of NF-κB, or CSFs, osteoblasts are unable to secrete different cytokines such as IL-1 or IL-6 involved in the differentiation and apoptosis of osteoclasts [68] [70] [72]. This confirms the previous observation of IL-1 or IL-6 expressions not being detected in our experiment. Based on the genes studied in this experiment, no stimulating effect of osteoblasts on osteoclasts differentiation or activation through cytokine expression seems involved in the 120 hours of the experiment.

5.8.2 Comparison of gene expression with respect to the different surface treatments

Considering the genes involved in signal transduction, FAK was up-regulated 4.25-fold for sample P_{48} and 6.63-fold for sample C_{48} while MAPK6 was up-regulated 2.59-fold for sample C_{48} compared to A_{48}. c-*jun* increased and c-*fos* decreased for samples P_{48} and C_{48} compared to A_{48}. In addition, c-*jun* decreased with time while c-*fos* increased. All these modulations seem to indicate that samples P and C shift or delay the time course of gene expression in the Pathway 5-1 compared to the sample A. If we extrapolate the event in the Pathway 5-1, we should then observe a decrease of proliferation for the samples C and P compared to A. Indeed, this is what we found in Part A, where we showed (however with different cell lines) that the proliferation decreased with surface treatments P and C compared to A. It could then be reasonably assumed that the decrease of cell proliferation, which is an important parameter for biocompatibility, is caused by a modulation of the Pathway 5-1 depending on the surface treatments used. It also has been suggested that Al may be altering the timing/regulation of the proliferation/differentiation transition point [38]. The possible explanation of decrease cell proliferation is a good demonstration of the usefulness of cDNA microarray technology. The data provided by this technique enables us to explore different hypotheses to understand the cell reaction under a particular stimulus.

The expression of PTK9 was differentially modulated according to the surface treatments with an up-regulation for C_{48} and P_{48} compared to A_{48}. In our previous work[xi] [33] [73], we showed that the control Ti-6Al-4V releases the highest amount of metal ions followed by the passivated Ti-6Al-4V, then the aged Ti-6Al-4V. The up-regulation of PTK followed exactly the same classification function with the highest up-regulation of PTK for control Ti-6Al-4V followed by passivated Ti-6Al-4V compared to the aged Ti-6Al-4V at 48 hours. It seems then that the up-regulation of PTK is directly related to the amount of ions released. According to the Pathway 5-2, the ageing treatment would then be more favourable by inducing less inflammatory reaction than the passivation or the control treatment.

[xi] The details are described in *Appendices, Metal ion release kinetics*.

Interestingly, among the growth factors, KFG showed a significant up-regulation for samples P_{48} and C_{48} compared to A_{48}. KGF, a stroma-derived member of the FGF family (also referred to as FGF-7), plays an important role in the epithelial repair process [74] and in inflammatory process [75] [76]. FGF-2 (bFGF), reported to stimulate bone resorption through osteoclastogenesis [77], was also up-regulated for samples P_{48} and C_{48} in our result. A previous study has showed that human KFG is 39% identical to FGF-2 [78]. Both proteins share similar biological functions [79] [80]. Until now, no correlation between KGF[xii] [81] and osteoblasts has been reported in literature. It has been demonstrated that KGF may be influenced, at least in part, by modulation of apoptosis mediators [82] [83]. Therefore, it could be interesting to find out if the expression of KGF affects osteoblastgenesis or osteoclastogenesis.

The increase of FGF-2 expression may cause the formation of a fibrous tissue around the implant [84] [85] [86]. Fibrous tissue around the implant bone may serve as a conduit for particles transport [15]. It has been suggested that fibroblast activation coupled with the biologic response of macrophages to wear debris may have a synergistic effect on the etiology of periprosthetic osteolysis [84]. Quantification of FGF-2 and FGF-7 modulation by RT-PCR would then be a very interesting future work. In contrast to the expression of KGF and FGF-2, IGF-I and FGF-5 modulation decreased for samples P_{48} and C_{48} compared to sample A_{48}, then increased at 120 hours. The delay in the expression of downstream genes such as IGF-I and FGF-5 could be a similar effect as the one influencing the shift in the signal Pathway 5-1.

Recently, it has been demonstrated that particles or ions[xiii] may induce apoptosis of osteoblasts [50] [87] [88]. Several signals or mechanisms have been shown to be involved in cell's apoptotic machinery[xiv]. Here several possible apoptosis pathways in relation to the metal ion dissolution from the treated surfaces are presented.

[xii] KGF dose not stimulate fibroblast growth.

[xiii] Stea el al., have demonstrated that apoptotic cells were presented in a higher percentage in tissue sections where metal particles were present (24% apoptotic cells) if compared to areas where no wear (6%), or plastic wear (2.8%) or ceramic wear (1.5%).

[xiv] The details are described in *Appendices*, *The mechanisms of apoptosis*.

NF-κB binding subunit (NF-κB1, p105), which is the precursor of the p50 subunit of NF-κB [89], was increased by 1.51-fold and 1.31-fold for samples P_{48} and C_{48} compared to A_{48}. p65 (Rel A), a subunit of NF-κB, showed a 1.04-fold increase for sample C_{48}. The NF-κB binding complexes are composed of either NF-κB1 and Rel A homodimers or NF-κB1/Rel A heterodimers [58]. The expression of p105 (NF-κB1) and p65 (Rel A) did not induce TNF/IL-6 (data not shown) expression according to Pathway 5-2 likely because of the insufficient level of NF-κB binding complexes. Interestingly, TFAR15[xv] (apoptosis-related protein 15, programmed cell death 10) was activated for samples P_{48} and C_{48} and may influence cell apoptosis. Until now only a few papers have described this gene e.g., [90]. It has been found that TFAR15, which showed up-level mRNA and protein expression induced by growth factor withdrawal, might also take some part as an apoptotic regulator. Therefore it will be particularly intriguing to elucidate the role of TFAR15 in osteoblasts apoptosis in future work.

No modulation of Bcl-xL was detected for samples P_{48} and C_{48} compared to A_{48} while it was down-regulated for P_{120} and C_{120} compared to A_{120}. The gene expression of Bax isoform (alpha, beta, and delta) increased with time. Apoptosis could then be initiated in association with the high ratio of Bax to Bcl-xL. Indeed, it has been demonstrated that the inhibition of Bcl-xL, resulted in an altered ratio of Bax to Bcl-xL and subsequently to mitochondria-mediated cell death [91] [92] [93]. Bax (at the protein level) can target mitochondrial membranes to trigger cell death (or apoptosis) (Pathway 5-3) [94] [95] even when caspases are inactivated [96]. Based on these observation, osteoblasts may undergo more apoptosis on the passivated and the control Ti-6Al-4V samples at 120 hours than on the aged treatment according to Pathway 5-3 as a result of increased apoptotic factors expression.

Bax → (ICE-like proteases independent pathway) → mitochondria (↓$\Delta\Psi$, ↑ROS, DNA condensation, cytosolic vaculation, membrane permeability) → cell death

(Pathway 5-3)

[xv] TFAR 15 is one of apoptosis associated genes, currently under review and without approved symbols (Please see the website: http://www.hugo-international.org/users/hester/apop.html)

Literature Aliases	Proposed Symbol	Genbank ID	Location	Citation PMID	LocusLink ID
TFAR15	PDCD10	AF022385	?	?	11235

Where,
ICE-like proteases independent pathway: or called caspase-independent death via channel-forming activity
ICE-like proteases: interleukin 1β-converting enzyme-like proteases
$\Delta\Psi$: mitochondrial membrane potential
ROS: reactive oxygen species (for example O_2^-) [97]
(Many Bcl-2 family proteins reside in the mitochondrial outer membrane)

Furthermore, it has been demonstrated that the lower corrosion resistance of titanium when peroxide (H_2O_2) is present in literature [98]. The influence of H_2O_2 generated by an inflammatory response to the high rate of titanium oxidation/corrosion *in vivo*[xvi] [97] [99] [100] [101]. Therefore, The production of ROS (reactive oxygen species) from mitochondria (Pathway 5-3) could be a potential risk not only to induce apoptosis but also to cause the high rate of titanium oxidation/corrosion *in vitro or in vivo* [102]. In addition, from the point of view of metal ion properties and their physiological impact, it is reasonable to consider that the metal ion (atomic radii of Ti, Al and V[xvii] are 2, 1.82 and 1.92 Å, respectively [103] [104]) play an important role in the modulation of Bax expression. If metal ion complexes can penetrate the ion channel (size: ~10 Å) [105] located in the extra-cellular membrane into the cytoplasm, it is possible that metal ions may directly affect the function of Bax and Bcl-2 (xL) in outer mitochrondrial membrane (intrinsic pathway) [106] but not via the nucleus. The possible mechanism is that Bcl-2 family (at the protein level) may have a conformational change in outer mitochrondrial membrane, where they could form large channels or pores of an estimated 1.5-nm diameter (also called porin or voltage-dependent anion channel (VDAC)) [107]. Thus, this outer membrane should be freely permeable to ions and most metabolites [96]. This possible apoptotic activation is different from the extrinsic pathway via receptor, for example TRAIL receptor in extra-cellular membrane [106].

[xvi] An intracellular dismutation of O_2^- catalysed by superoxide dismutase (SOD) produced H_2O_2, which has a much longer lifetime and higher permeability again the cell membrane than O_2^-. The titanium surface is hyperoxidised by H_2O_2, which may induce the release of titanium ions.

[xvii] It would appear that free aluminium is not likely to be readily available in physiological situations. The free Al^{3+} concentration is already low due to hydrolysis < 10^{-5} (pH = 5), 10^{-8} (pH = 6), 10^{-11} (pH = 7), and 10^{-14} (pH = 8). For example, dissolution constants K_D (pH = 7) of Al^{3+} complexes, $Al(OH)^{2+}$: 3.16E-09 (-log K_D = 8.5) and $Al(HPO_4)^+$: 2.0E-10 (-log K_D = 9.7). Therefore, Al^{3+} will bind proteins to form complexes. For example, the fetal bovine serum (FBS) used in several of the experiments presented in Kasai's work contained 175.5 mg/dL transferrin which could bind up to 4.5 μM Al. The physical properties of these metals are described in *Appendices*.

The p53 tumour suppressor gene is another important apoptotic gene [108]. Interestingly, our results showed that the expression of p53 binding protein (TP53BP2) and insulin-like growth factor binding protein 3 (IGF-BP3) decreased with time, while IGF-I increased with time. It has been demonstrated that IGF-BP3 was transcriptionally activated by p53 and transactivation of IGF-BP3 was capable of binding to and inhibiting IGF-I [109] [110]. Although TP53BP2 may effect the expression of IGF-I at 48 hours, the expression of TP53BP2 (p53) was diminished at 120 hours reduced the effect on IGF-I in our result, it seems that TP53BP2 (p53) is unable to induce further apoptotic program by means of p53-dependent apoptosis[xviii] [108] [111].

Based on the genes selected, we could propose a general pathway for the cell reaction according to the surface treatments used:
(1) Metal ion release changes the time course of gene expression in the FAK pathway.
(2) Once the accumulation of metal ions released from the Ti surface exceeds a threshold value, the apoptosis process may be activated and cell growth is diminished.
(3) PTK up-regulation is also induced by metal ion release. This up-regulation could be involved in the apoptosis process via the initial metal ion penetration of the ion channels and may not be due to the phagocytosis of ions. (4) The expression of Bcl-2 family may suggest that metal ions induce the apoptosis process through the Pathway 5-3.

Summary

For the first part of this work (Part A), short-term (24 hours) *in vitro* experiments demonstrated that different Ti-6Al-4V surface treatments had negligible effects on the measured parameters. Cell viability remained unaffected and cell morphology expressed rich actin filaments. In longer *in vitro* experiments (from 72 hours until 4

[xviii] p53-dependent apoptosis: cells respond to DNA damage by increasing their production of p53. p53 is a potent inducer of apoptosis. The p53 network is normally "off". It is activated ("on" switch) only when cells are stressed or damaged such as DNA breaks, UV light and oncogenes (Oncogenes are analogous to the accelerators in a car. They stimulate appropriate cell growth under normal condition.).

weeks), the difference in the kinetics of metal ion dissolution between treatments is more important and consequently a higher cell proliferation on the aged sample and an accelerated peak of ALP activity on the control sample were observed. FN production was not affected by the different surface treatments. Based on our previous metal ion release studies and surface analyses, Al ions release kinetics as well as presence of vanadium ions may play a major role in influencing the osteoblasts behaviour.

For the second part of this work (Part B), the significant gene expression of collagen, FAK, MAPK, FGF-5, IGF-I and Bcl-xL (Table 5-2) demonstrated that human osteoblastic cells were active on the aged Ti-6Al-4V implants. The lack of IL-1, IL-6, prostaglandin E-2 (PGF_2), NF-κB and tumour necrosis factor-alpha (TNF-α) suggest that the aged samples are less capable to induce bone resorption mediators compared to the passivated and the control samples.

The mechanisms that initiate signalling pathways (FAK, MAPK, PTK) and growth factors (KGF, FGF-2) with the surface treatments (P and C) remain unknown. However, it is reasonable to assume that the metal ions released (or metal ions/proteins complexes) are involved in the activation of these genes according to the findings in Table 5-3. Although several apoptotic genes were expressed during the test, none of them continuously increased with time, except Bax. It seems to suggest that the Bax expression plays a significant role in the effects of metal ions on apoptosis. The Bax increasing expression with time would be compatible with the possibility of cell death (apoptosis) via Pathway 5-3, concomitant with the increase in metal ion release.

Considering the experimental design, it has been found that most of the significant modulation took place before 48 hours (Table 5-3). Therefore, future genomic studies in this area should be performed in short-term tests (48 hours or less) to find out the critical point of gene expression and upstream genes in the pathways.

cDNA microarray technology is a powerful method for the large-scale analysis of genes expression. It allows the user not only to identify potential genes involved in cell reaction to particular stimuli, but also to explore different pathways that could fit the observed gene modulations. However, independent techniques, such as RT-PCR, need to be used to further confirm the results obtained by cDNA microarray technology. The

effects of metal ions on signal pathways or apoptosis processes could then be confirmed. It should also be mentioned that gene expression quantification (regardless of the method used) brings only an indication of possible cell reaction at the transcription level. Quantification from transcription to translation and finally to protein function should be performed using different techniques such as immunochemistery, or methods such as Western blot.

Table 5-2 Gene expression of the aged samples for different incubation times (58 genes)

Acc[xix]	Gene name	A_4[xx]	ac	A_{48}	ac	A_{120}	ac
	Adhesion						
U70312	Homo sapiens integrin binding protein Del-1 (Del1) mRNA (vitronectin sequence homology, amino acid tumour cells, cultured)	1[xxi]	P[xxii]	1.32	P	0.98	P
M59911	Human integrin alpha-3 chain mRNA	1	P	0.87	P	1.76	P
X06256	Human mRNA for integrin alpha 5	1	P	0.81	P	0.69	P
X53586	Human mRNA for integrin alpha 6	1	P	0.93	P	0.84	P
X07979	Human mRNA for integrin beta 1	1	P	0.55	P	0.79	P
M35011	Human integrin beta-5 mRNA	1	P	0.80	P	0.79	P
X53002	Human mRNA for integrin beta-5	1	P	0.68	P	0.61	P
X02761	Human mRNA for fibronectin (FN precursor)	1	P	1.10	P	1.26	P
M10905	Human cellular fibronectin mRNA	1	P	1.14	P	1.42	P
J03464	Human collagen alpha-2 type I mRNA	1	P	**4.40**	**P**	**3.48**	**P**
	Signal pathway and transcription factors						
L13616	Human focal adhesion kinase (FAK) mRNA	1	P	**0.16**	**M**	0.73	P
Z11695	H.sapiens 40 kDa protein kinase related to rat ERK2 (MAPK1 (mitogen-activated protein kinase 1), MAPK2)	1	P	0.52	P	0.72	P
X80692	Cluster Incl X80692:H.sapiens ERK3 mRNA (MAPK6 (mitogen-activated protein kinase 6))	1	P	0.49	P	0.41	P
AF002715	Cluster Incl AF002715:Homo sapiens MAP kinase kinase kinase (MTK1) mRNA, complete cds	1	P	**0.33**	**P**	0.46	P
D87116	Human mRNA for MAP kinase kinase 3b	1	P	**0.22**	**P**	**0.23**	**P**
J04111	Human c-jun proto oncogene (JUN), clone hCJ-1	1	P	0.43	P	0.63	P
V01512	Human cellular oncogene c-*fos*	1	P	**2.23**	**P**	1.52	P
U02680	Human protein tyrosine kinase mRNA (PTK9)	1	P	**0.50**	**P**	0.63	P
M59371	Human protein tyrosine kinase (PTK) mRNA (EPHA2) (MeSH term[xxiii]: protein tyrosine kinase receptors, cell surface sequence homology)	1	A	**3.20**	**P**	**9.09**	**P**
AF015254	Homo sapiens serine/threonine kinase (STK-1) mRNA	1	A	**10.10**	**P**	-	A
	Growth factors and cytokines						
M37825	Human fibroblast growth factor-5 (FGF-5) mRNA	1	M	**5.85**	**P**	**6.37**	**P**
M60828	Human keratinocyte growth factor (KFG = FGF-7) mRNA (3853 bp)	1	A	1.33	P	**2.80**	**P**
X03563	Human gene for insulin-like growth factor I (MeSH terms: base composition evolution insulin, IGF-I, IGF-II)	1	A	4.38	p	-	A
M77349	Human transforming growth factor-beta induced gene product (BIGH3) mRNA	1	P	1.31	P	0.82	P
X06374	Human mRNA for platelet-derived growth factor PDGF-A	1	P	1.41	P	1.83	P
M22488	Human bone morphogenetic protein 1 (BMP-1) mRNA	1	A	0.79	P	-	A

[xix] acc is the Genebank accession number.

[xx] The first row: A_4 means the aged sample in 4 hours incubation, the same principle for other symbols.

[xxi] All the data are normalised by standard A_4 (=1). Negative values are considered to be zero. "-" means absent. The value in bold type means significant expression (≥ 2.5 fold: up-regulation; ≤ 0.4-fold: down-regulation).

[xxii] The ac (code): A: absent, P: Present, M: marginal. A are not taken into account, only P is used for analysis.

[xxiii] MeSH terms: (Me)dical (S)ub (H)eadings. MeSH is a vocabulary of medical and scientific terms assigned to most documents in PubMed by a team of experts (http://www.nlm.nih.gov/mesh/meshhome).

M22489	Human bone morphogenetic protein 2A (BMP-2A) mRNA	1	A	-	A	-	A
M22490	Human bone morphogenetic protein-2B (BMP-2B) mRNA	1	P	0.76	M	-	A
U43842	Homo sapiens bone morphogenetic protein-4 (hBMP-4) gene	1	P	**0.43**	P	0.57	P
M27968	Human basic fibroblast growth factor (bFGF) mRNA	1	P	0.52	P	0.61	P
M28983	Homo sapiens interleukin 1 alpha (IL-1) mRNA	1	A	-	A	-	A
	Differentiation genes						
J04948	Human alkaline phosphatase (ALP-1) mRNA	1	A	1.22	P	1.34	P
L40992	Homo sapiens (clone PEBP2aA1) core-binding factor, runt domain, alpha subunit 1 (CBFA1) mRNA, 3 end of cds	0	A	-	A	-	A
L38517	Homo sapiens indian hedgehog protein (IHH) mRNA, 5' end	1	A	-	A	-	A
AF009801	Homo sapiens homeodomain protein (BAPX1) mRNA	1	A	-	A	-	A
	Mineralisation genes (bone matrix compoments)						
J03040	Human SPARC/osteonectin mRNA	1	P	1.76	P	1.49	P
J04765	Human osteopontin mRNA	1	P	0.86	P	-	A
J04599	Human hPGI mRNA encoding bone small proteoglycan I (biglycan)	1	P	1.42	P	1.82	P
J05213	Homo sapiens **sialoprotein** precursor (IBSP) mRNA	0	A	-	A	-	A
	Apoptosis						
U37518	Human TNF-related apoptosis inducing ligand TRAIL mRNA	1	P	-	A	-	A
AF014794	Homo sapiens TNF related TRAIL receptor (TRAIL-R3) mRNA	1	A	-	A	-	A
M58603	Human NF-κB DNA binding subunit (NF-kappa-B) mRNA (NF-κB1)	1	P	0.85	P	0.92	P
L19067	Human NF-κB transcription factor p65 subunit mRNA (Rel A)	1	P	0.69	P	0.83	P
AF018253	Homo sapiens receptor activator of nuclear factor-kappa B (RANK) mRNA	1	A	-	A	-	A
AF022385	Homo sapiens apoptosis-related protein TFAR15 (TFAR15) mRNA	1	P	0.52	P	**0.41**	**P**
Y11588	H.sapiens mRNA for apoptosis specific protein	1	A	-	A	-	A
AF053712	Homo sapiens osteoprotegerin ligand mRNA (= TNF-related activation-induced cytokine =TRANCE)	0	A	-	A	-	A
M37435	Human macrophage-specific colony-stimulating factor (CSF-1) mRNA (= M-CSF)	1	P	0.90	P	0.56	P
M13207	Human granulocyte-macrophage colony-stimulating factor (CSF-1) gene (= CSF-2 = GM-CSF)	0	A	-	A	-	A
X03656	Human gene for granulocyte colony-stimulating factor (G-CSF = CSF-3)	1	A	-	A	-	A
M14745	Human bcl-2 mRNA (BCL2 (B-cell CLL/lymphoma 2))	1	A	-	A	-	A
M13994	Human B-cell leukemia/lymphoma 2 (bcl-2) proto-oncogene mRNA encoding bcl-2-alpha protein (BCL2 (B-cell CLL/lymphoma 2))	0	A	-	A	0	A
M13995	Human B-cell leukemia/lymphoma 2 (bcl-2) proto-oncogene mRNA encoding bcl-2-beta protein	1	A	-	A	-	A
Z23115	H.sapiens bcl-xL mRNA	**1**	**P**	**6.42**	**P**	**10.08**	**P**
L22473	Human Bax alpha mRNA	1	P	1.12	P	0.68	P
L22474	Human Bax beta mRNA	1	P	1.32	P	-	A
L22475	Human Bax gamma mRNA	1	P	0.47	P	-	A
U19599	Human Bax delta mRNA	1	P	0.99	P	0.67	P

Table 5-3 Different gene expressions between samples (28 genes)

acc	Gene name	P_{48}/A_{48}	C_{48}/A_{48}	P_{120}/A_{120}	C_{120}/A_{120}
	Adhesion				
J03464	Human collagen alpha-2 type I mRNA	1.45	1.18	0.70	0.74
	Signal pathways and transcription factors				
L13616	Human focal adhesion kinase (FAK) mRNA	**4.25**	**6.63**	1.04	1.22
Z11695	H.sapiens 40 kDa protein kinase related to rat ERK2 (MAPK1 (mitogen-activated protein kinase 1), MAPK2)	2.32	2.17	0.85	0.76
X80692	Cluster Incl X80692:H.sapiens ERK3 mRNA (MAPK6 (mitogen-activated protein kinase 6))	2.48	**2.59**	1.60	1.01
AF002715	Cluster Incl AF002715:Homo sapiens MAP kinase kinase kinase (MTK1) mRNA	1.14	1.14	0.93	0.69
D87116	Human mRNA for MAP kinase kinase 3b	1.14	1.46	0.86	1.24
J04111	Human c-jun proto oncogene (JUN), complete cds, clone hCJ-1	1.84	1.85	1.09	0.69
V01512	Human cellular oncogene c-fos	0.78	**0.27**	1.91	0.42
U02680	Human protein tyrosine kinase (PTK9) mRNA	2.16	**3.26**	1.54	0.81
AF015254	Homo sapiens serine/threonine kinase (STK-1) mRNA	1.30	0.89	0.84	1.48
	Growth factors and Cytokines				
X03565	Human IGF-I mRNA for insulin-like growth factor I	0.58	1.45	2.13	1.47
M37825	Human fibroblast growth factor-5 (FGF-5) mRNA	0.55	0.78	1.80	1.06
S81661	Keratinocyte growth factor (KGF = FGF-7)	**4.90**	**7.07**	0.79	0.62
M60828	Human keratinocyte growth factor (KFG) mRNA	2.41	**2.51**	0.88	0.67
M27968	Human basic fibroblast growth factor (bFGF) mRNA	2.40	**3.19**	1.02	1.13
	Differentiation				
J04948	Human alkaline phosphatase (ALP-1) mRNA	(-) A	(0.86) M	(-) A	(-) A
	Mineralisation				
J03040	Human SPARC/osteonectin mRNA	0.95	0.94	0.90	1.34
J04599	Human hPGI mRNA encoding bone small proteoglycan I (biglycan)	0.93	0.94	0.84	1.25
	Apoptosis				
M58603	Human nuclear factor kappa-B DNA binding subunit (NF-kappa-B) mRNA (NF-κB1)	1.51	1.31	0.98	0.88
L19067	Human NF-kappa-B transcription factor p65 subunit mRNA (Rel A)	0.97	1.04	0.86	0.87
AF022385	Cluster Incl AF022385:Homo sapiens apoptosis-related protein TFAR15 (TFAR15) mRNA	**2.75**	**2.56**	1.95	1.20
Z23115	H.sapiens bcl-xL mRNA	(-) A	(-) A	0.90	**0.14**
L22473	Human Bax alpha mRNA	**0.25**	(-) A	2.25	1.99
L22474	Human Bax beta mRNA	0.44	1.23	0.77	1.30
U19599	Human Bax delta mRNA	0.75	0.75	1.72	1.63
U09477	Human clone 53BP1 p53-binding protein mRNA, partial cds (TP53BP1 (tumour protein p53-binding protein, 1))	(-) A	(-) A	(-) A	(-) A
U58334	Human Bcl2, p53 binding protein Bbp/53BP2 (BBP/53BP2) mRNA (TP53BP2 (tumour protein p53-binding protein, 2))	1.31	1.14	0.80	1.01
M35878	Human insulin-like growth factor-binding protein-3 gene (IGFBP3)	1.18	1.08	0.65	0.96

Table 5-4 The cellular functions of the chosen genes (based on GeneCards; website: http://bioinfo.weizmann.ac.il/cards/ and [112])

Gene	Genecard	Cellular function
Integrin α_3	ITGA3	Acts a receptor for fibronectin, laminin and collagen
Integrin α_5	ITGA5	Integrin alpha-5/beta-1 is a receptor for fibronectin and fibrinogen. It recognizes the sequence R-G-D in its ligands
Integrin α_6	ITGA6	Integrin alpha-6/beta-4 may mediate adhesive and/or migratory functions of epithelial cells. On platelets, integrin alpha-6/beta-1 functions as a laminin receptor
Integrin β_1	ITGB1	Associates with alpha-1 or alpha-6 to form a laminin receptor, with alpha-2 to form a collagen receptor, with alpha-4 to interact with vcam-1, with alpha-5 to form a fibronectin receptor and with alpha-8. Integrins recognize the sequence r-g-d in their ligand
Integrin β_5	ITGB5	Integrins are a large family of cell surface glycoproteins that mediate cell to cell and cell to matrix adhesion
Fibronectin	FN1	Fibronectins bind cell surfaces and various compounds including collagen, fibrin, heparin, DNA, and actin. fibronectins are involved in cell adhesion, cell motility, opsonization, wound healing, and maintenance of cell shape
Collagen α-2 type I	COL1A2	Type I collagen is a member of group I collagen (fibrillar forming collagen)
FAK	PTK2	Activation of focal adhesion kinases (FAK) may be an early step in intracellular signal transduction pathways. This tyrosine-phosphorylation is triggered by integrin interactions with various extracellular matrix (ecm) adhesive molecules and by neuropeptide growth factors. Potential role in oncogenic transformations resulting in increased kinase activity
MAPK	MAPK1	Phosphorylates microtubule-associated protein-2 (map2). Myelin basic protein (MBP), and elk-1; may promote entry in the cell cycle
c-jun	JUN	Transcription factor that binds and recognize the enhancer DNA sequence: TGA(C/G)TCA
c-fos	FOS	Nuclear phosphoprotein, which forms a tight but non- covalently linked complex with the c-jun/ap-1 transcription factor. c-fos has a critical function in regulating the development of cells destined to form and maintain the skeleton. It is thought to have an important role in signal transduction, cell proliferation and differentiation
PTK	PTK9	-
PTK-receptor	EPHA2	Receptor for members of the ephrin-a family. Binds to ephrin-a1, -a3, -a4 and -a5
STK-1	STK12	-
FGF-2	FGF2	The heparin-binding growth factors are angiogenic agents *in vivo* and are potent mitogens for a variety of cell types *in vitro*. There are differences in the tissue distribution and concentration of these 2 growth factors
FGF-5	FGF5	This oncogene is expressed in neonatal brain. FGF-5 can transform NIH 3T3 cells
FGF-7	FGF7	Growth factor active on keratinocytes. Possible major paracrine effector of normal epithelial cell proliferation
IGF-I	IGF1	The insulin-like growth factors, isolated from plasma, are structurally and functionally related to insulin but have a much higher growth-promoting activity
TGF-β	TGFBI, BIGH3	Binds to type I, II, and IV collagens. This adhesion protein may play an important role in cell-collagen interactions. In cartilage, may be involved in endochondral bone formation
BMPs	BMP4	Induces cartilage and bone formation
PDGF-A	PDGFA	Platelet-derived growth factor is a potent mitogen for cells of

		mesenchymal origin. Binding of this growth factor to its affinity receptor elicits a variety of cellular responses. It is released by platelets upon wounding and plays an important role in stimulating adjacent cells to grow and thereby heal the wound
IL-1α	IL1A	Produced by activated macrophages, il-1 stimulates thymocyte proliferation by inducing il-2 release, b-cell maturation & proliferation, & fibroblast growth factor activity. IL-1 proteins are involved in the inflammatory response, being identified as endogenous pyrogens, and are reported to stimulate the release of prostaglandin and collagenase from synovial cells
IL-6	IL6	It plays an essential role in the final differentiation of b-cells into ig-secreting cells, it induces myeloma and plasmacytoma growth, it induces nerve cells differentiation, in hepatocytes it induces acute phase reactants
PGE-2	PTGER1	Receptor for prostaglandin E2 (PGE2). The activity of this receptor is mediated by G-Q proteins which activate a phosphatidylinositol-calcium second messenger system. May play a role as an important modulator of renal function. Implicated the smooth muscle contractile response to PGE2 in various tissues
Cbfa1	RUNX2	Osteoblast-specific transcription factor
IHH	IHH	Intercellular signal essential for a variety of patterning events during development. Binds to the patched (PTC) receptor, which functions in association with smoothened (SMO), to activate the transcription of target genes. Implicated in endochondral ossification: may regulate the balance between growth and ossification of the developing bones. Induces the expression of parathyroid hormone-related protein (PTHRP) (by similarity)
BAPX1	BAPX1	Homeo box-containing gene,Drosophila bagpipe homolog, involved in mesodermal and skeletal development
ALP	ALPPL2	Catalytic activity: an orthophosphoric monoester + h(2)o = an alcohol + orthophosphate (at a high ph optimum)
SPARC	SPARC	Appears to regulate cell growth through interactions with the extracellular matrix and cytokines. Binds calcium and copper, several types of collagen, albumin, thrombospondin, PDGF and cell membranes. There are two calcium binding sites; a acidic domain that binds 5 to 8 Ca^{2+} with a low affinity and a ef-hand loop that binds a Ca^{2+} ion with a high affinity
OPN	SPP1	Binds tightly to hydroxyapatite. Appears to form an integral part of the mineralized matrix. Probably important to cell-matrix interaction
Biglycan	BGN	Found in the extracellular matrices of several connective tissues, specially in articular cartilages. The two glycosaminoglycan chains attached to biglycan can be either chondroitin sulfate or dermatan sulfate
IBSP	IBSP	Binds tightly to hydroxyapatite. Appears to form an integral part of the mineralized matrix. Probably important to cell-matrix interaction. Promotes Arg-Gly-Asp-dependent cell attachment
TRAIL	TNFSF10	Induces apoptosis
NF-κB1	NFKB1	p105 is the precursor of the p50 subunit of the nuclear factor NF-kappa-b, which binds to the kappa-b consensus sequence 5'-ggrnnyycc-3', located in the enhancer region of genes involved in immune response and acute phase reactions. The precursor protein itself does not bind to DNA
NF-κB p65	RELA	p65 is a subunit of the nuclear factor kappa-b, a second messenger, which activates the transcription of a number of genes in multiple tissues. The inhibitory effect of i-kappa-b upon NF-kappa-b in the cytoplasm is exerted primarily through the interaction with p65. p65 shows a weak DNA-binding site which could contribute directly to

		DNA binding in the NF-kappa-b complex
OPG	TNFSF11	Tumour necrosis factor superfamily, member 11 TNFRSF11A (RANK) and OPG (osteprogerin ligand), localized in T cells bone marrow stromal cells, hypertrophic chondrocyte, stimulated by IL1B and TNFRSF11B,expressed in bone, brain, heart, kidney, skeletal muscle, skin, cooperating with prostaglandin, mediating osteoclastognesis and bone loss through systemic activation of T cells, regulating lymph node organogenesis lymphocyte development and interactions between T cells and dendritic cells, activating the antiapoptotic serine threonine kinase AKT/PKB through a signal complex involving TRAF6 and SRC
RANK	TNFRSF11A	
TRANCE	TNFSF11	
TFAK15	PDCD10	-
CSFs	CSF1	Granulocyte/macrophage colony-stimulating factors are cytokines that act in hematopoiesis by controlling the production, differentiation, and function of 2 related white cell populations of the blood, the granulocytes and the monocytes-macrophages
Bcl-2	BCL2 (B-cell CLL/lymphoma 2)	Prolongs the survival of hematopoietic cells in the absence of required growth factors and also in the presence of various stimuli inducing cellular death. Bcl2 blocks apoptosis because it interferes with the activation of caspases by preventing the release of cytochrome c. might function in an antioxidant pathway to prevent apoptosis at sites of free radical generation such as mitochondria
Bcl-xL	BCL2L1	Dominant regulator of apoptotic cell death. The long form displays cell death repressor activity, whereas the short isoform (-xS) promotes apoptosis
Bax	BAX	Accelerates programed cell death by binding to, and antagonizing the apoptosis repressor bcl-2 or its adenovirus homolog e1b 19k protein. Induces the release of cytochrome c, activation of caspase-3, and thereby apoptosis
TP53BP2	TP53BP2	Impedes cell cycle progression at G2/M
IGF-BP3	IGFBP3	IGF-binding proteins prolong the half-life of the IGFs and have been shown to either inhibit or stimulate the growth promoting effects of the IGFs on cell culture. They alter the interaction of IGFs with their cell surface receptors

References

1. Nanci, A., et al., *Chemical modification of titanium surfaces for covalent attachment of biological molecules.* J Biomed Mater Res, 1998. **40**(2): p. 324-35.
2. Ratner, B.D., *Molecular design strategies for biomaterials that heal.* Macromol Symp, 1998. **130**: p. 327-35.
3. Williams, D.F., *Titanium and titanium alloys.* 1981, Boca Raton, FL: CRC Press.
4. Callen, B.W., R.N. Sodhi, and K. Griffiths, *Examination of clinical surface preparations on titanium and Ti-6Al-4V by X-ray photoelectron spectroscopy and nuclear reaction analysis.* Progress in surface Science, 1995. **50**(1-4): p. 269-79.
5. Amstutz, H.C., et al., *Metal on metal total hip replacement workshop consensus document.* Clin Orthop, 1996(329 Suppl): p. S297-303.
6. Jacobs, J.J., et al., *Release and excretion of metal in patients who have a total hip- replacement component made of titanium-base alloy [see comments].* J Bone Joint Surg [Am], 1991. **73**(10): p. 1475-86.
7. Liao, H., T. Wurtz, and J. Li, *Influence of titanium ion on mineral formation and properties of osteoid nodules in rat calvaria cultures.* J Biomed Mater Res, 1999. **47**(2): p. 220-7.
8. Thompson, G.J. and D.A. Puleo, *Ti-6Al-4V ion solution inhibition of osteogenic cell phenotype as a function of differentiation timecourse in vitro.* Biomaterials, 1996. **17**(20): p. 1949-54.
9. Browne, M., P.J. Gregson, and R.H. West, *Characterization of titanium alloy implant surfaces with improved dissolution resistance.* J Mater Sci Mater Med, 1996. **7**: p. 323-9.
10. ASTM, *Medical devices; Emergency medical services.* Vol. 13.01. 1999, Pennsylvania, USA: American Society for Testing and Materials.
11. Kikuchi, T., et al., *Gene expression of osteoclast differentiation factor is induced by lipopolysaccharide in mouse osteoblasts via toll-like receptors.* Journal of Immunology, 2001. **166**(5): p. 3574-9.

12. Nair, S.P., et al., *Bacterially induced bone destruction: Mechanisms and misconceptions.* Infection and Immunity, 1996. **64**(7): p. 2371-80.
13. Amano, S., et al., *Functional role of endogenous CD14 in lipopolysaccharide-stimulated bone resorption.* Journal of Cellular Physiology, 1997. **173**(3): p. 301-9.
14. Ahmad, M., M. McCarthy, and G. Gronowicz, *An in vitro model for mineralization of human osteoblast-like cells on implant materials.* Biomaterials, 1999. **20**(3): p. 211-20.
15. Boyan, B.D., et al., *Effect of titanium surface characteristics on chondrocytes and osteoblasts in vitro.* Cells and Materials, 1995. **5**(4): p. 323-34.
16. Rodan, S.B., et al., *Characterization of a human osteosarcoma cell line (Saos-2) with osteoblastic properties.* Cancer Res, 1987. **47**(18): p. 4961-6.
17. Jones, K.H. and J.A. Senft, *An improved method to determine cell viability by simultaneous staining with fluorescein diacetate-propidium iodide.* J Histochem Cytochem, 1985. **33**(1): p. 77-9.
18. Laitinen, M., et al., *The role of transforming growth factor-beta on retarded osteoblastic differentiation in vitro.* Life Sci, 1999. **64**(10): p. 847-58.
19. Cowles, E.A., et al., *Mineralization and the expression of matrix proteins during in vivo bone development.* Calcif Tissue Int, 1998. **62**(1): p. 74-82.
20. Gronowicz, G. and M.B. McCarthy, *Response of human osteoblasts to implant materials: integrin-mediated adhesion.* J Orthop Res, 1996. **14**(6): p. 878-87.
21. Kowaltowski, A.J., R.F. Castilho, and A.E. Vercesi, *Mitochondrial permeability transition and oxidative stress.* Febs Letters, 2001. **495**(1-2): p. 12-15.
22. Noda, M., *Cellular and molecular biology of bone.* 1993, San Diego: Academic Press. xxi, 567.
23. Stein, G.S. and J.B. Lian, *Molecular mechanisms mediating proliferation/differentiation interrelationships during progressive development of the osteoblast phenotype.* Endocr Rev, 1993. **14**(4): p. 424-42.
24. Geissler, U., et al., *Collagen type I-coating of Ti6Al4V promotes adhesion of osteoblasts.* J Biomed Mater Res, 2000. **51**(4): p. 752-60.
25. Webster, T.J., et al., *Specific proteins mediate enhanced osteoblast adhesion on nanophase ceramics.* J Biomed Mater Res, 2000. **51**(3): p. 475-83.
26. Schneider, G. and K. Burridge, *Formation of focal adhesions by osteoblasts adhering to different substrata.* Exp Cell Res, 1994. **214**(1): p. 264-9.

27. Sinha, R.K. and R.S. Tuan, *Regulation of human osteoblast integrin expression by orthopedic implant materials.* Bone, 1996. **18**(5): p. 451-7.

28. Hynes, R.O., *Cell adhesion: old and new questions.* Trends Cell Biol, 1999. **9**(12): p. M33-7.

29. Chen, C.S., et al., *Geometric control of cell life and death.* Science, 1997. **276**(5317): p. 1425-8.

30. Damsky, C.H., *Extracellular matrix-integrin interactions in osteoblast function and tissue remodeling.* Bone, 1999. **25**(1): p. 95-6.

31. Globus, R.K., et al., *Fibronectin is a survival factor for differentiated osteoblasts.* J Cell Sci, 1998. **111**(Pt 10): p. 1385-93.

32. Moursi, A.M., R.K. Globus, and C.H. Damsky, *Interactions between integrin receptors and fibronectin are required for calvarial osteoblast differentiation in vitro.* J Cell Sci, 1997. **110**(Pt 18): p. 2187-96.

33. Browne, M. and P.J. Gregson, *Surface modification of titanium alloy implants.* Biomaterials, 1994. **15**(11): p. 894-8.

34. Andress, D.L., *Blood aluminium in renal osteodystrophy*. 2nd ed. Primer on the metabolic bone diseases and disorders of mineral metabolism, ed. M.J. Favus. 1993, New York: Raven Press.

35. Favarato, M., C.A. Mizzen, and D.R. McLachlan, *Resolution of Serum Aluminum-Binding Proteins by Size-Exclusion Chromatography - Identification of a New Carrier of Aluminum in Human Serum.* Journal of Chromatography-Biomedical Applications, 1992. **576**(2): p. 271-85.

36. Elsebae, A.K.H., et al., *Binding of Aluminum to Human Serum Transferrin, Human Serum- Albumin and Rat Serum-Proteins.* Journal of Environmental Science and Health Part B-Pesticides Food Contaminants and Agricultural Wastes, 1994. **29**(2): p. 303-21.

37. Ohman, L.O. and R.B. Martin, *Citrate as the Main Small-Molecule Binding Al3+ in Serum.* Clinical Chemistry, 1994. **40**(4): p. 598-601.

38. Bellows, C.G., J.N. Heersche, and J.E. Aubin, *Aluminum accelerates osteoblastic differentiation but is cytotoxic in long-term rat calvaria cell cultures.* Calcif Tissue Int, 1999. **65**(1): p. 59-65.

39. Metson, J.B., et al., *X-Ray Photoelectron-Spectroscopy Applications to Corrosion and Adhesion at Metal-Oxide Surfaces.* Colloids and Surfaces a-Physicochemical and Engineering Aspects, 1994. **93**: p. 173-80.

40. Thompson, G.J. and D.A. Puleo, *Effects of Sublethal Metal-Ion Concentrations on Osteogenic Cells Derived from Bone-Marrow Stromal Cells.* Journal of Applied Biomaterials, 1995. **6**(4): p. 249-58.

41. Pioletti, D.P., et al., *Functional genomic analysis of osteoblasts contacted by orthopedic implant particles.* J. Bone Min. Res., 2001.

42. Lian, J.B. and G.S. Stein, *Osteoblast biology.* Osteoporosis, ed. R. Marcus, D. Feldman, and J. Kelsey. 1996, San Diego: Academic Press. xxiv, 1373.

43. Krause, A., E.A. Cowles, and G. Gronowicz, *Integrin-mediated signaling in osteoblasts on titanium implant materials.* J Biomed Mater Res, 2000. **52**(4): p. 738-47.

44. Sohrabi, A., et al., *Proinflammatory cytokine expression of IL-1beta and TNF-alpha by human osteoblast-like MG-63 cells upon exposure to silicon nitride in vitro.* J Biomed Mater Res, 2000. **50**(1): p. 43-9.

45. Brazma, A. and J. Vilo, *Gene expression data analysis.* Febs Letters, 2000. **480**(1): p. 17-24.

46. Brazma, A., et al., *One-stop shop for microarray data - Is a universal, public DNA- microarray database a realistic goal?* Nature, 2000. **403**(6771): p. 699-700.

47. Carulli, J.P., et al., *High throughput analysis of differential gene expression.* J Cell Biochem, 1998. **286**(Suppl. 30-31): p. 14.

48. Rodan, G.A. and T.J. Martin, *Therapeutic Approaches to Bone Diseases.* Science, 2000. **289**(5484): p. 1508-14.

49. Xynos, I.D., et al., *Gene-expression profiling of human osteoblasts following treatment with the ionic products of Bioglass (R) 45S5 dissolution.* J Biomed Mater Res, 2001. **55**(2): p. 151-7.

50. Pioletti, D.P., et al., *The cytotoxic effect of titanium particles phagocytosed by osteoblasts.* J Biomed Mater Res, 1999. **46**(3): p. 399-407.

51. Vermes, C., et al., *The effects of particulate wear debris, cytokines, and growth factors on the functions of MG-63 osteoblasts.* J Bone Joint Surg Am, 2001. **83**(2): p. 201-11.

52. Swiontkowski, M.F., et al., *Cutaneous metal sensitivity in patients with orthopaedic injuries.* Journal of Orthopaedic Trauma, 2001. **15**(2): p. 86-9.

53. Beresford, J.N., et al., *Production of Osteocalcin by Human-Bone Cells-Invitro - Effects of 1,25(Oh)2d3, 24,25(Oh)2d3, Parathyroid-Hormone, and*

Glucocorticoids. Metabolic Bone Disease & Related Research, 1984. **5**(5): p. 229-34.

54. Stein, G.S., et al., *Transcriptional control of osteoblast growth and differentiation.* Physiol Rev, 1996. **76**(2): p. 593-629.
55. Bidwell, J.P., et al., *Nuclear matrix proteins and osteoblast gene expression.* J Bone Miner Res, 1998. **13**(2): p. 155-67.
56. Corbeil, J., *Personal communications.* 2001.
57. Xynos, I.D., et al., *Bioglass 45S5 stimulates osteoblast turnover and enhances bone formation In vitro: implications and applications for bone tissue engineering.* Calcif Tissue Int, 2000. **67**(4): p. 321-9.
58. Vermes, C., et al., *Particulate wear debris activates protein tyrosine kinases and nuclear factor kappa Beta, which down-regulates type I collagen synthesis in human osteoblasts.* Journal of Bone and Mineral Research, 2000. **15**(9): p. 1756-65.
59. Cowles, E.A., L.L. Brailey, and G.A. Gronowicz, *Integrin-mediated signaling regulates AP-1 transcription factors and proliferation in osteoblasts.* J Biomed Mater Res, 2000. **52**(4): p. 725-37.
60. Nakashima, Y., et al., *Signaling pathways for tumor necrosis factor-alpha and interleukin-6 expression in human macrophages exposed to titanium-alloy particulate debris in vitro.* Journal of Bone and Joint Surgery-American Volume, 1999. **81A**(5): p. 603-15.
61. Glant, T.T. and J.J. Jacobs, *Response of three murine macrophage populations to particulate debris: bone resorption in organ cultures.* J Orthop Res, 1994. **12**(5): p. 720-31.
62. Bilezikian, J.P. and L.G. Raisz, *Principles of bone biology.* 1996, San Diego: Academic Press. xxi, 567.
63. Sun, J.S., et al., *Effect of anti-inflammatory medication on monocyte response to titanium particles.* Journal of Biomedical Materials Research, 2000. **52**(3): p. 509-16.
64. Reddi, A.H., *Bone and cartilage differentiation.* Curr Opin Genet Dev, 1994. **4**(5): p. 737-44.
65. Karsenty, G., et al., *Cbfa1 as a regulator of osteoblast differentiation and function.* Bone, 1999. **25**(1): p. 107-8.

66. Ducy, P., *CBFA1: A molecular switch in osteoblast biology.* Dev Dyn, 2000. **219**(4): p. 461-71.

67. Pockwinse, S.M., et al., *Expression of cell growth and bone specific genes at single cell resolution during development of bone tissue-like organization in primary osteoblast cultures.* J Cell Biochem, 1992. **49**(3): p. 310-23.

68. Jilka, R.L., et al., *Osteoblast programmed cell death (apoptosis): modulation by growth factors and cytokines.* J Bone Miner Res, 1998. **13**(5): p. 793-802.

69. Suliman, A., A. Lam, and R. Datta, *Intracellular mechanisms of TRAIL: apoptosis through mitochondrial-dependent and -independent pathways.* Oncogene, 2001. **20**(17): p. 2122-33.

70. Schwarz, E.M., et al., *Tumor necrosis factor-alpha/nuclear transcription factor-kappa B signaling in periprosthetic osteolysis.* Journal of Orthopaedic Research, 2000. **18**(3): p. 472-80.

71. Lynch, M.P., et al., *Apoptosis during bone-like tissue development in vitro.* J Cell Biochem, 1998. **68**(1): p. 31-49.

72. Hofbauer, L.C., et al., *The roles of osteoprotegerin and osteoprotegerin ligand in the paracrine regulation of bone resorption.* J Bone Miner Res, 2000. **15**(1): p. 2-12.

73. Ku, C.-H., M. Browne, and P.J. Gregson. *Chemical and morphological changes of surface treated titanium alloy implants in vitro.* in *Cell and Materials Meeting.* 1999. Davos, Switzerland: Cell and Materials.

74. Werner, S., *Keratinocyte growth factor: A unique player in epithelial repair processes.* Cytokine & Growth Factor Reviews, 1998. **9**(2): p. 153-65.

75. Maas-Szabowski, N., H.J. Stark, and N.E. Fusenig, *Keratinocyte growth regulation in defined organotypic cultures through IL-1-induced keratinocyte growth factor expression in resting fibroblasts.* Journal of Investigative Dermatology, 2000. **114**(6): p. 1075-84.

76. Szabowski, A., et al., *c-jun and JunB antagonistically control cytokine-regulated mesenchymal-epidermal interaction in skin.* Cell, 2000. **103**(5): p. 745-55.

77. Manabe, N., et al., *Involvement of fibroblast growth factor-2 in joint destruction of rheumatoid arthritis patients.* Rheumatology, 1999. **38**(8): p. 714-20.

78. Finch, P.W., et al., *Human KGF is FGF-related with properties of a paracrine effector of epithelial cell growth.* Science, 1989. **245**(4919): p. 752-5.

79. Sher, I., et al., *Identification of residues important both for primary receptor binding and specificity in fibroblast growth factor-7.* Journal of Biological Chemistry, 2000. **275**(45): p. 34881-6.

80. Sher, I., et al., *Mutations uncouple human fibroblast growth factor (FGF)-7 biological activity and receptor binding and support broad specificity in the secondary receptor binding site of FGFs.* Journal of Biological Chemistry, 1999. **274**(49): p. 35016-22.

81. Rubin, J.S., et al., *Purification and Characterization of a Newly Identified Growth- Factor Specific for Epithelial-Cells.* Proceedings of the National Academy of Sciences of the United States of America, 1989. **86**(3): p. 802-6.

82. Fehrenbach, H., et al., *Alveolar epithelial type II cell apoptosis in vivo during resolution of keratinocyte growth factor-induced hyperplasia in the rat.* Histochemistry and Cell Biology, 2000. **114**(1): p. 49-61.

83. Jost, M., et al., *Epidermal growth factor receptor-dependent control of keratinocyte survival and Bcl-x(L) expression through a MEK- dependent pathway.* Journal of Biological Chemistry, 2001. **276**(9): p. 6320-6.

84. Manlapaz, M., W.J. Maloney, and R.L. Smith, *In vitro activation of human fibroblasts by retrieved titanium alloy wear debris.* J Orthop Res, 1996. **14**(3): p. 465-72.

85. Aspenberg, P. and J.S. Wang, *The bone conduction chamber, materials and growth factors.* Cells and Materials, 1995. **5**(4): p. 337-44.

86. Archibeck, M.J., et al., *The basic science of periprosthetic osteolysis.* Journal of Bone and Joint Surgery-American Volume, 2000. **82A**(10): p. 1478-89.

87. Scott, R.S., et al., *Phagocytosis and clearance of apoptotic cells is mediated by MER.* Nature, 2001. **411**(6834): p. 207-11.

88. Stea, S., et al., *Apoptosis in peri-implant tissue.* Biomaterials, 2000. **21**(13): p. 1393-8.

89. Roebuck, K.A., et al., *Down-regulation of procollagen alpha1[I]] messenger RNA by titanium particles correlates with nuclear factor kappaB (NF-kappaB) activation and increased rel A and NF-kappaB1 binding to the collagen promoter.* J Bone Miner Res, 2001. **16**(3): p. 501-10.

90. Wang, W., H.T. Liu, and Y.M. Zhang, *cDNA cloning and expression of an apoptosis-related gene, human TFAR15 gene.* Sci China Ser C, 1999. **42**(3): p. 323-9.

91. Boise, L.H., et al., *bcl-x, a bcl-2-related gene that functions as a dominant regulator of apoptotic cell death.* Cell, 1993. **74**(4): p. 597-608.

92. Oltvai, Z.N., C.L. Milliman, and S.J. Korsmeyer, *Bcl-2 heterodimerizes in vivo with a conserved homolog, Bax, that accelerates programmed cell death.* Cell, 1993. **74**(4): p. 609-19.

93. Zhang, L., et al., *Role of BAX in the apoptotic response to anticancer agents.* Science, 2000. **290**(5493): p. 989-+.

94. Xiang, J.L., D.T. Chao, and S.J. Korsmeyer, *BAX-induced cell death may not require interleukin 1 beta- converting enzyme-like proteases.* Proceedings of the National Academy of Sciences of the United States of America, 1996. **93**(25): p. 14559-63.

95. Gajewski, T.F. and C.B. Thompson, *Apoptosis meets signal transduction: Elimination of a BAD influence.* Cell, 1996. **87**(4): p. 589-92.

96. Green, D.R. and J.C. Reed, *Mitochondria and apoptosis.* Science, 1998. **281**(5381): p. 1309-12.

97. Mu, Y., et al., *Metal ion release from titanium with active oxygen species generated by rat macrophages in vitro.* J Biomed Mater Res, 2000. **49**(2): p. 238-43.

98. Fonseca, C. and M.A. Barbosa, *Corrosion behaviour of titanium in biofluids containing H2O2 studied by electrochemical impedance spectroscopy.* Corrosion Science, 2001. **43**(3): p. 547-59.

99. Tengvall, P., H. Elwing, and I. Lundstrom, *Titanium Gel Made from Metallic Titanium and Hydrogen-Peroxide.* Journal of Colloid and Interface Science, 1989. **130**(2): p. 405-13.

100. Sun, Z.L., J.C. Wataha, and C.T. Hanks, *Effects of metal ions on osteoblast-like cell metabolism and differentiation.* Journal of Biomedical Materials Research, 1997. **34**(1): p. 29-37.

101. Halliwell, B. and J.M.C. Gutteridge, *Free radicals in biology and medicine.* 2nd ed. The chemistry of oxygen radicals and other oxygen-derived species. 1989, Oxford: Oxford University. 22-226.

102. Pan, J., et al., *Variation of oxide films on titanium induced by osteoblast-like cell culture and the influence of an H2O2 pretreatment.* Journal of Biomedical Materials Research, 1998. **40**(2): p. 244-56.

103. Rowatt, E., et al., *An examination of the binding of aluminum to protein and mineral components of bone and teeth.* Journal of Inorganic Biochemistry, 1997. **68**(4): p. 235-8.

104. Kasai, K., M.T. Hori, and W.G. Goodman, *Transferrin Enhances the Antiproliferative Effect of Aluminum on Osteoblast-Like Cells.* American Journal of Physiology, 1991. **260**(4): p. E537-E543.

105. Benjamin, L., *Genes VII.* 7th ed ed. 2000, Oxford: Oxford University Press.

106. Nicholson, D.W., *From bench to clinic with apoptosis-based therapeutic agents.* Nature, 2000. **407**(6805): p. 810-6.

107. Hengartner, M.O., *The biochemistry of apoptosis.* Nature, 2000. **407**(6805): p. 770-6.

108. Vogelstein, B., D. Lane, and A.J. Levine, *Surfing the p53 network.* Nature, 2000. **408**(6810): p. 307-10.

109. Buckbinder, L., et al., *Induction of the Growth Inhibitor Igf-Binding Protein-3 by P53.* Nature, 1995. **377**(6550): p. 646-9.

110. Wilson, J.W., C. Booth, and C.S. OPotten, *Apoptosis genes.* 1998, Norwell: Kluwer Academic Publishes. 5-35.

111. Allday, M.J., et al., *DNA-Damage in Human B-Cells Can Induce Apoptosis, Proceeding from G(1)/S When P53 Is Transactivation Competent and G(2)/M When It Is Transactivation Defective.* Embo Journal, 1995. **14**(20): p. 4994-5005.

112. Ho, N.C., et al., *A skeletal gene database.* J Bone Miner Rer, 2000. **15**(11): p. 15254-64.

Chapter 6 Conclusions

The present study has been approached from a materials science perspective and a biological perspective. It has been demonstrated that the ageing treatment offers advantages in terms of metal ion dissolution and bioactivity over the ASTM-F86 passivation procedure for Ti-6Al-4V. The passivation treatment results in the elimination of vanadium from the surface layers. The high metal ion release from the passivated sample is attributed to the less stable outer oxide layer, which induces a high rate of oxide layer formation as demonstrated by the significant change in O/Ti ratio of the passivated sample. The porous nature of the passivated surface appears to allow proteins to embed in the oxide surface and alter the microstructure. In contrast, the aged oxide layers are more stable, dense and also possess good biocompatibility due to the increased number of the hydroxylated groups. After immersion the concentration of hydroxylated groups on the aged oxide surface decreases, this is possibly due to a reaction with the deprotonated carboxyl group of amino acids; the adsorption of such species is reflected in the significant increase in surface roughness after one hour immersion compared to the passivated surface.

It has also been demonstrated that the grit-blasting and heating cycle associated with the plasma-spraying HA coating treatment changes the surface properties, and this may further affect the metal ion release behaviour. This is thought to be due to a number of processes such as, the decrease in concentration of the hydroxylated groups on both the passivated and the aged surfaces during heat treatment, the increase of Al_2O_3 particles on the Ti-6Al-4V surface during grit-blasting treatment, and the cracked, amorphous phase HA surface, which can form a possible transport pathway for metal ion release.

Potentiodynamic tests were additionally undertaken to understand the nature of the passive film. It was shown that the aged Ti-6Al-4V exhibits better corrosion resistance than other standard treatments, and bovine serum solution has a greater effect on the

corrosion (or dissolution) behaviour of the treated Ti-6Al-4V surfaces than PBS. Indeed, the corrosion resistance of an implant material not only influences its functional performance and durability, but also governs biocompatibility.

From a biological perspective, the biocompatibility tests show that the various surface treatments, which exhibit different metal ion release kinetics, influence the cell proliferation (i.e. metabolic activity) and alkaline phosphatase (ALP) activity of osteoblast cells in long-term tests (≥ 72 hours). The aged Ti-6Al-4V surface shows higher cell proliferation than the passivated and the control Ti-6Al-4V at 72 hours. The peak of ALP activity appears earlier at week two for the control surface compared to the passivated and the aged surfaces. The early increase in ALP activity for the control sample could be a compensatory effect of decreased osteoblasts proliferation.

Recent advances in genomic technology, such as cDNA microarray technology, allow us to precisely determine the gene expression of osteoblast cells on the treated Ti-6Al-4V from a vast amount of gene expression data. It was found that the control and the passivated samples delay or shift the time course of gene expression of the focal adhesion kinase (FAK) pathway, which is involved in cell proliferation and differentiation, compared to the aged sample. In particular, the Bax increasing expression with time for samples P and C would be compatible with the possibility of cell death (apoptosis). Therefore, the Bax pathway (via mitochondria) may play an important role in the apoptotic cell death, especially for metal ion release, based on the results of cell proliferation (i.e. metabolic activity), gene expression of the Bcl-2 family, and the literature. Accordingly the ageing treatment shows better biocompatibility than the passivated treatment.

The present research has demonstrated the chemical and biological advantages of applying the ageing treatment to titanium based implant materials that possess a titanium oxide surface film. This treatment is not intended to replace the well-established ATSM standard passivation procedure. Rather the ageing treatment would provide a simple, inexpensive adjunct to the standard passivation procedure of titanium alloy implants.

Chapter 7 Future work

7.1 Surface properties

Different surface treatments have been used in this study to enhance biocompatibility. One is the simple thermal ageing treatment to enhance the oxide stability in order to reduce the metal ion dissolution; another is the commonly used method of HA-coating on the treated Ti-6Al-4V by plasma-spraying to enhance ossintegration. However, some adverse effects have been noted due to the plasma-spraying process; this was evident from the present results and also in the literature. Therefore, an extra process (or post treatment) could be introduced to reduce these side effects. For example, the post-heat treatment after plasma-spraying can be used to improve the HA crystallinity for HA-coated titanium substrates and produce a thickened, dense rutile layer at the interface which prevents Ti atoms diffusing into the coatings and inhibits the Ti-catalysed decomposition of apatite [1].

In addition, it is very important to develop a surface property with active bio-functionality, which will in turn enhance biocompatibility. Therefore, it would be useful to precisely control the surface properties of the treated surface so that it might be specially recognised by biomolecules (proteins) or cells and trigger normal healing pathways (or normal cell cycle) [2]. Based upon this hypothesis, there are several particularly intriguing works to be continued in the future. By considering the possible structure of proteins or cells, we can modify the surface structures to help proteins to recognise them, and further enhance cell adhesion, and cells can receive signals that instruct them to enter the active segments of the cell cycle [3] [4]. For example, nanobiotechnology or self-assembly may be possible to improve the biocompatibility without causing adverse effects. Self-assembly can create ordered surface structures and strategies to place recognition sites on surfaces by random arrays of groups and by templates. In addition, another method, colloidal lithography [5] is a quick and

relatively simple method to prepare nanostructure model biomaterials surfaces to create uniform nanostructure over large surface areas [6]. If possible, a surface of a well established orthopaedic implant alloy (Ti alloy, Cr-Co alloy, or stainless steel) could be processed to have a geometric structure with a periodicity of certain size of holes. The mineralisation could be spontaneously initiated resulting in an osteoinduction of the surface [7]. This could also solve the problem of the creation of a fibrous tissue surrounding the implant [8]. This type of surface should enhance cell adhesion and proper cell function [2]. In order to approach these goals, biocompatibility (cellular and genomic) tests are necessary to examine the cell response to these active bio-function or bio-mimic surfaces. Moreover, advances in surface analytical techniques ensure excellent interface resolution will be possible between oxide layers and biomolecules or cells *in situ* in the future.

7.2 Biocompatibility (cellular and genomic) tests

According to the present results, we have examined few proteins (markers) for biocompatibility tests and several genes with significant expression by using the microarray data analysis system supplied by UCSD. The functional genomic study is not only able to establish a set of new quantitative test methods to examine osteoblastic cell proliferation, differentiation and mineralisation due to their significant expression but also to be the inductor of apoptosis, tumour or cancer, etc., to interpret the effect of the treated implant on cell cycle (intracellular signalling pathways). For example, in order to prove that metal ion release modulates the expression of these interested genes, such as TFAR15, KFG, etc., and also causes Bax (BcL-2 family) to affect the function of mitochondria according to Pathway 5-3, several methods can be used to confirm their roles in cell cycle (or apoptosis): (1) Using a known metal ion concentration (for example $AlCl_3$[i]) [9] [10] to examine the effects of metal ions on the gene expression (or mitochondria), (2) using Inductively Coupled Plasma Mass Spectroscopy (ICP-MS) [11] [12] [13] to measure the concentration of metal ion release from implants. (3) confocal microscopy or epifluorescence microscopy is necessary to identify cell or

[i] *In vivo*, typical plasma Al (Al^{3+}) concentrations are in the range of 0.37 μM.

mitochondria[ii] morphology. (4) A final method involves examining biophysical reactions in mitochondria. For example, the anti-oxidative substances like superoxide dismutase (SOD)[iii] can be used to reduce the production of reactive oxygen intermediate (ROI)[iv] or reactive oxygen species (ROS) to test whether metal ions cause apoptosis via Pathway 5-3 [14] [15] [16] [17] [18]. For practical reasons, (1) and (2) are able to measure the factors which cause apoptosis in cell populations, and (3) and (4) are able to assay apoptosis in individual cells[v]. An independent technique, RT-PCR, needs to be used to correlate the aforementioned tests. These tests can determine the gene expression (usually several hundreds of genes) of osteoblasts in direct contact with a metallic substrate or metal ion solution, which may be different from the reaction between osteoblastic cells and wear particles.

This work can approach two goals:

(1) The genocompatibility tests can be used to improve the existing biocompatibility test for biomaterials.

(2) Medical purposes - particles and metal ions play an important role in bone resorption (osteoporosis or osteolysis). These technologies, such as DNA microarray, offer a systematic approach for searching for effective targets, such as apoptotic genes, for drug discovery and diagnostics.

7.3 Summary

Based upon the present results and future work, we are hopefully able to have a precise description of cell-implant interface interactions via the understanding of the surface properties and the cell mechanism. This understanding allows a new methodology for examining biocompatibility. It is believed that the advance in this biotechnology

---

[ii] Useful information, probes for mitochondria (http://www.probes.com/handbook/).

[iii] It has been demonstrated that SOD (200U/ml) is able to decrease particle- and fibre-induced the expression of NF-Bp50/p105 mRNA expression.

[iv] Superoxide can not only set up a chain reaction of chemical destruction in the body and destroy microorganisms but it also has an important function in the immune response (e.g., by means of NF-κB activation).

[v] Other apoptosis assay methods (*Guide to Cell Proliferation and Apoptosis Methods*) can be found in http://biochem.roche.com/.

(cDNA microarray) can help material scientists develop new biomaterials, or assess currently used materials, and understand the interface interaction more closely.

References

1. Weng, J., et al., *Integrity and thermal decomposition of apatite in coatings influenced by underlying titanium during plasma spraying and post-heat-treatment.* J Biomed Mater Res, 1996. **30**(1): p. 5-11.
2. Ratner, B.D., *The engineering of biomaterials exhibiting recognition and specificity.* Journal of Molecular Recognition, 1996. **9**(5-6): p. 617-25.
3. Brune, H., et al., *Self-organized growth of nanostructure arrays on strain-relief patterns.* Nature, 1998. **394**(6692): p. 451-3.
4. Keser, M. and S.I. Stupp, *Genetic algorithms in computational materials science and engineering: simulation and design of self-assembling materials.* Computer Methods in Applied Mechanics and Engineering, 2000. **186**(2-4): p. 373-85.
5. Hanarp, P., et al., *Nanostructured model biomaterial surfaces prepared by colloidal lithography.* Nanostructured Materials, 1999. **12**(1-4): p. 429-32.
6. Hanarp, P., et al., *Nanoporous thin films for biomaterials applications.* Abstracts of Papers of the American Chemical Society, 2000. **219**: p. 211-COLL.
7. Pioletti, D.P., et al., *Functional genomic analysis of osteoblasts contacted by orthopedic implant particles (submitted).* J Bone Min Res, 2000.
8. Sutherland, D.S., et al., *Surface-Analysis of Titanium Implants.* Biomaterials, 1993. **14**(12): p. 893-9.
9. Yui, S., et al., *Growth-inhibitory and apoptosis-inducing activities of calprotectin derived from inflammatory exudate cells on normal fibroblasts: Regulation by metal ions.* Journal of Leukocyte Biology, 1997. **61**(1): p. 50-7.
10. Stea, S., et al., *Apoptosis in peri-implant tissue.* Biomaterials, 2000. **21**(13): p. 1393-8.
11. Kunze, J., et al., *ICP-MS determination of titanium and zirconium in human serum using an ultrasonic nebulizer with desolvator membrane.* Atomic Spectroscopy, 1998. **19**(5): p. 164-7.
12. Kunze, J., et al., *Use of ultrasonic nebulizer with desolvator membrane for the determination of titanium and zirconium in human serum by means of*

inductively coupled plasma-mass spectroscopy. Fresenius Journal of Analytical Chemistry, 2000. **366**(2): p. 165-6.

13. Kunze, J., et al., *Determination of titanium and zirconium wear debris in blood serum by means of HNO3/HF pressurized digestion using ICP optical emission spectrometry.* Fresenius Journal of Analytical Chemistry, 1998. **361**(5): p. 496-9.
14. Baeuerle, P.A., R.A. Rupec, and H.L. Pahl, *Reactive oxygen intermediates as second messengers of a general pathogen response.* Pathologie Biologie, 1996. **44**(1): p. 29-35.
15. Schmidt, K.N., et al., *Induction of Oxidative Stress by Okadaic Acid Is Required for Activation of Transcription Factor Nf-Kappa-B.* Journal of Biological Chemistry, 1995. **270**(45): p. 27136-42.
16. Muller, J.M., R.A. Rupec, and P.A. Baeuerle, *Study of gene regulation by NF-kappa B and AP-1 in response to reactive oxygen intermediates.* Methods-a Companion to Methods in Enzymology, 1997. **11**(3): p. 301-12.
17. Muller, J.N., et al., *Hypoxia induces c-fos transcription via a mitogen-activated protein kinase-dependent pathway.* Journal of Biological Chemistry, 1997. **272**(37): p. 23435-9.
18. Oettinger, R., et al., *Production of reactive oxygen intermediates by human macrophages exposed to soot particles and asbestos fibers and increase in NF-kappa B p50/p105 mRNA.* Lung, 1999. **177**(6): p. 343-54.

Appendices

1. Double layer (or electrical double layer) [1]

The electrical double layer is a region where no electron transfer reactions occur at the electrode and the solution is composed only of electrolyte (assumed in the 1850's by Helmholtz). The interactions between the ions in solution and the electrode surface were assumed to be electrostatic in nature and resulted from the fact that the electrode holds a charge density. The interface remains neutral and the charge held on the electrode is balanced by the redistribution of ions close to the electrode surface. The attracted ions are assumed to approach the electrode surface and form a layer balancing the electrode charge, the distance of approach is assumed to be limited to the radius of the ion and a single sphere of solvation round each ion. The overall result is two layers of charge (the double layer) and potential drop occurring in a linear manner.

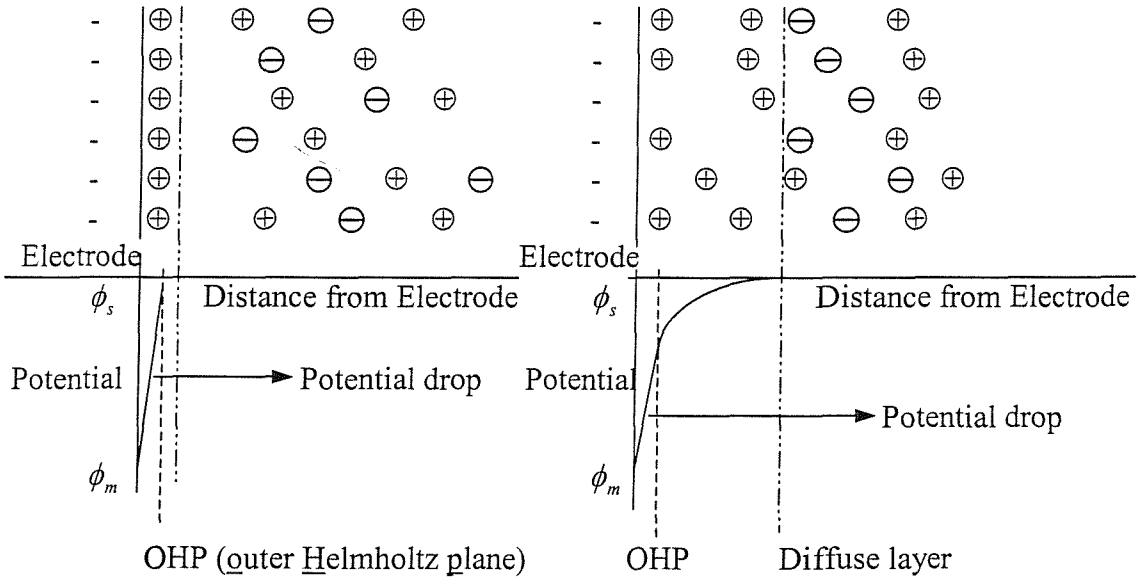

(A) Helmholtz's model (B) Stern's model

Figure 1 The electrical double layer.

2. XPS [2]

Angle dependent

The effect of sample orientation with respect to the analyser can be determined by considering a flat surface model (Figure 2). If 95% of the signal arises from a depth into the solid of 3λ then the depth sampled, d, is given by the equation:

$$d = 3\lambda \sin\theta \qquad \text{(Equation 1)}$$

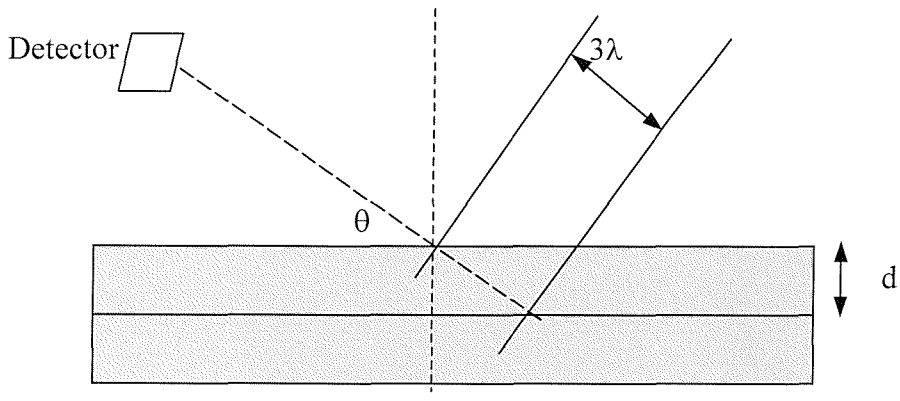

Figure 2 Angle dependent XPS.

where θ is the angle between the sample surface and the analyser accetance plane and λ is the inelastic mean free path of the emitted photoelectrons. Thus at θ = 90° the sample surface is perpendicular to the line of acceptance of the analyser, and d is the maximum sampling depth of 3λ. At θ = 0° the sample surface is parallel to the line of the accaptance of the analyser and hence d = 0 and so no signal would be obtained. In summary, as θ tends to 0° the outermost surface species account for a proportion of the signal detected. λ varies from sample to sample, an estimate of the sampling depth is said to be ~10 monolayers at the standard analysis angle (35°).

Definitions

Binding energy (BE): Binding energy in the atom of the escaping electron.

BE difference: The difference of the peak positions.

Full width at half maximum (FWHM): The observed peak of a given photoelectron peak is determined by the lifetime of the core hole, instrumental resolution and satellite features. The deeper the orbital has the shorter the core lifetime and the larger the intrinsic peak width (Γ). Similarly, the value of Γ for a given orbital (e.g., 1s) increases as the atomic number of the element increases [3].

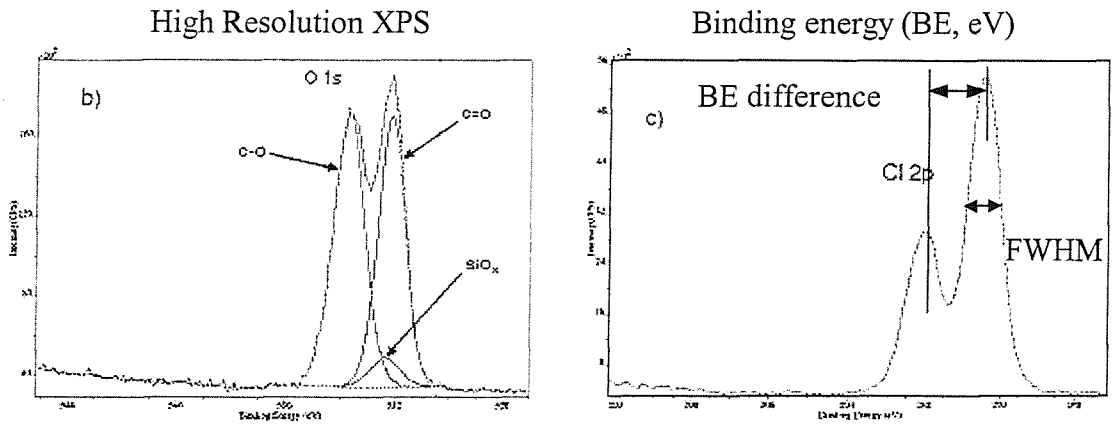

Figure 3 XPS spectra[i].

Typical XPS data for titanium oxide (Table 1)

Table 1 Reference values for O 1s, Ti 2p, N 1s, Al 2p and V 2p peaks of XPS [4], [5]

Binding Energy (eV)	Chemical Species	Unimplanted passivated	Implanted passivated	As implanted
Oxygen				
529.8	TiO_2			
530	TiO_2			
530.1	TiO_2			
530.4	TiO_2			
530.7	TiO_2			
531.2	Physisorbed OH			

[i] The images are copied from the website: http://www.kratos.com/.

531.3	$TiO_{1.65}$			
531.5	$TiO_{1.35}$			
531.7	Physisorbed OH			
~531.6	Physisorbed OH			
531.8	$TiO_{0.9}$			
531.8	$TiO_{1.0}$, Ti_2O_3, and O-OH			
531.9	Physisorbed OH			
531-533	C=O and C-OH			
~533.1	Chemisorbed H_2O			
Titanium				
458.9	TiO_2	458.8($2p_{3/2}$)	458.8	458.8
459.0	TiO_2			
458.7	TiO_2			
459.1	TiO_2			
456.9-457.3	Ti-N-O		457.0	
457.6	Ti-N-O			
456.3±0.2	Ti-N-O			
454.4	TiN			
455.2	TiN			
456.9	TiN_x			
457.0	Ti_2O_3			
557.8	Ti_2O_3			
453.8	Ti			
456.4	TiN_xO_{1-x}			456.5
Nitrogen				
396.6	N-Ti	-		
397.2	N-Ti			
396.75±0.2	N-Ti			
399.5	N-O			399.9
400.2	N-O		400.1	399.9
396.6	N-O			
400.3±0.1	N-O			
397.2	N-implanted		398.6	398.5
400.6	N-C			400.7
402	NH_4^+			
402.8	N_2			
403.3±0.4	Dissolved N			
Aluminium				
74.5	Al_2O_3	74.5	74.5	
74.7	Al_2O_3			
73.9±0.05	AlN			
72.8±0.05	Al			
Vanadium				
516.9($2p_{1/2}$)	V_2O_5			
524.3($2p_{3/2}$)	V_2O_5			
516.2($2p_{1/2}$)	V_2O_5			
523.5($2p_{3/2}$)	VO_2			

515.7($2p_{1/2}$)	VO_2			
523.3($2p_{3/2}$)	V_2O_3			
512.4($2p_{1/2}$)	V			
515.9($2p_{3/2}$)	V	519.9	519.9	
516.1	V oxide	516.2	517.6	521.2
		523.0	522.4	522.8

Table 1 (*Continued*)

3. AFM[ii]

The Force-Distance Curve

In order to measure the adhesion between two surfaces or the hardness of a sample surface, one can use information derived from the "Force-Distance Curve" produced by an AFM. This curve represents a measurement of the force exerted on the AFM cantilever (with force constant, k) by the sample surface as the distance between the sample and the fixed end of the cantilever is ramped. There are several pieces of information, which can be derived from the force-distance curve:

ab: the probe and sample are not in contact but are moving towards each other; no information content.

bc: "jump to contact", it is due to an attractive pull on the cantilever. The attraction between the probe and sample are electrostatic, patch charge and van der Waals forces. The force distance along *bc* can be converted to a cantilever displacement ($F = -kD$).

cd: shows the upwards motion of the cantilever in response to the sample motion after they are in contact.

de: reverses the situation in segment *cd*. If both segments are straight and are parallel to each other, there is no additional information content. If they are not parallel, the difference in the in- and out-going curves gives information on plastic deformation of the sample, or elastic deformation, which has a response time slower than the withdrawal rate of the probe.

[ii] Based on AFM User's Manual, Version 3.05 TopoMetrix.

ef: records the motion of the cantilever from its neutral deflection position as it is deflected downwards until the spring force of the cantilever equals the adhesion of the surfaces for each other.

fg: shows the jump of the cantilever away from the surface

gh: the probe and sample are not in contact and moving away from each other.

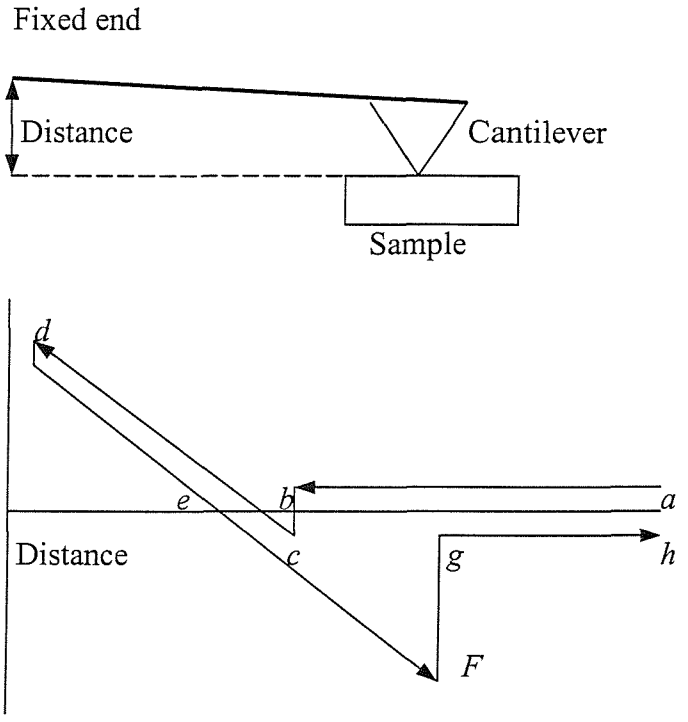

Figure 4 Force-Distance curve.

4. Roughness (R_a)

A particularly useful parameter for the characterisation of surface is the surface roughness (R_a) parameter. An understanding of this parameter is clear from the arithmetic mean ($\overline{Z}$) of the surface, defined as the sum of all height values divided by the number of the data points (N):

$$\overline{Z} = \frac{1}{N}\sum_{i=0}^{N} Z_i \qquad \text{(Equation 2)}$$

so that R_a, the arithmetic mean of the deviations in height from the profile mean value can be defined thus:

$$R_a = \frac{1}{N}\sum_{i=0}^{N} | Zi - \overline{Z} | \qquad \text{(Equation 3)}$$

Thus, when examining the effect of surface morphology on cellular attachment, the R_a or RMS values obtained by section analyses may be more useful than whole area surface roughness measurement [3]. Normally, the total roughness of the surface of the thin films comes from two origins, i.e., the initial roughness of the substrate, and the deposition process of the film. Osseointegration is strongly dependent on the surface roughness of the implant. Therefore, the surfaces of the implants are often deliberately roughened at the micrometer level to increase the osseointegration. If a film were deposited on the surface of such an implant, the initial roughness would be affected by the film deposition methods and film thickness.

5. Metal ion release kinetics

Uncoated Ti-6Al-4V (passivation and ageing treatments)

According to the previous result in our group, the metal ion dissolution mechanisms [4] are presented in the following equations. A linear relationship between metal ion release and square root of time is followed for the passivated treatment (Eq.4). The aged sample exhibits two-stage dissolution kinetics (Eq.5 and Eq.6). An additional mechanism is occurring after approximately 25 hours (Eq.6).

$$Y = 5.4e^{-2} + 7.4e^{-3}X \qquad \text{Equation 4}$$

$$Y = 4.2e^{-3} + 3.3e^{-3}X (X \leq 25^{1/2} h) \qquad \text{Equation 5}$$

$$Y = 2.1e^{-2} + 1.3e^{-4}X(X \geq 25^{1/2}h) \qquad \text{Equation 6}$$

Where:
Y is ion release ($\mu g/cm^2$) and X is square root time ($h^{1/2}$).
The equations originally were used only in bovine serum solution without cells.
(For the details, please refer to Dr. Browne Martin's PhD thesis [5].)

Coated Ti-6Al-4V

Previous work has investigated the metal ion dissolution kinetics of HA-coated/uncoated specimens (Table 2) [6].

Surface treated Ti-6Al-4V (control, passivation and ageing treatments)

Al ions released into the bovine serum solution from various surface treated Ti-6Al-4V during tests were measured by using electrothermal atomic absorption spectrophotometry [7] [8] (Zeeman 4100 ET-AAS) (Table 3).

Case study

Table 4 shows that ion concentration not only varies according to patient (the reason for the large scatter) but also by the type of ion and the location in which it is measured.

Table 2 Kinetics behaviour for aluminium ion release into bovine serum from HA-coated/uncoated specimens

Surface treatment	Rate constant ($\mu g/cm^2/s^{1/2}$)
Nitric acid passivated, HA coated	2.43×10^{-4}
Nitric acid passivated, no HA coating	2.52×10^{-4}
Aged, HA coated	1.80×10^{-4}
Aged, no HA coating	7.17×10^{-4}

Table 3 Al concentration in bovine serum solution from various surface treated Ti-6Al-4V

	Aluminium (Al) analysis of aqueous samples							
Empty tubes (1 ml 0.1%Nitric acid)	e1	e2	e3	e4	e5	Mean		
Al ion (μg/l)	3.8	1.7	2.1	2.6	3.9	-		
DDH_2O	dd1	dd2	dd3	dd4	dd5			
	2.7	1.8	0.8	1	1	-		
	Aluminium analysis of bovine serum samples							
Bovine serum (blank)	b1	b2	b3	b4	b5	Mean		
Total Al ion (μg/l, mean)	35.3	40.4	37.2	37.8	40.1	38.16		
Stdev	0	0.5	0.1	0.4	1.1			
Immersion time	1 h	2 h	5 h	10 h	50 h	100 h	200 h	400 h
Control	C1	C2	C5	C10	C50	C100	C200	C400
Total Al ion (μg/l)	45.8	45.8	-	46.6	50.8	52.1	57.4	53
Metal ion (ng/ml) (Total-38.16)	7.64	7.64	-	8.44	12.64	13.94	19.24	14.84
Metal ion release (μg/cm^2)	0.007464	0.007464	-	0.008246	0.012349	0.01362	0.018798	0.014499
Passivation (30% nitric acid)	P1	P2	P5	P10	P50	P100	P200	P400
Total Al ion (μg/l)	44	44.5	44	50.3	50.5	62.1	51.6	50.8
Metal ion (ng/ml) (Total-38.16)	5.84	6.34	5.84	12.14	12.34	23.94	13.44	12.64
Metal ion release (μg/cm^2)	0.005706	0.006194	0.005706	0.011861	0.012056	0.02339	0.013131	0.012349
Ageing treatment	A1	A2	A5	A10	A50	A100	A200	A400
Total Al ion (μg/l)	40.4	38.7	37.5	38.2	40.4	42.4	44.1	40.5
Metal ion (ng/ml) (Total-38.16)	2.24	0.54	-0.66	0.04	2.24	4.24	5.94	2.34
Metal ion release (μg/cm^2)	0.002189	0.000528	-0.00064	3.91E-05	0.002189	0.004143	0.005803	0.002286

Table 4 Metal ion concentrations (determined by atomic absorption spectrophotometry) in various regions surrounding cementless implants (control baseline values in parentheses)[iii]

	Ion Concentrations (μg/l)		
Tissue Type	Ti	Al	V
Synovial Fluid	556±882 (13±22)	654±743 (109±158)	62±95 (5±1)
Capsule	1540±1238 (723±1217)	2053±1064 (951±586)	288±133 (122±123)
Fibrous Membrane	20813±26467 (N/A)	10581±9764 (N/A)	1027±702 (N/A)
Blood	67±62 (17±60)	218±233 (13±4)	23±31 (6±4)

[iii] This table is cited from (http://www.engr.sjsu.edu/).

	Ion Concentrations (μg/l)			
Tissue Type	Co	Cr	Mo	Ni
Synovial Fluid	588±427 (5±3)	385±232 (3±4)	58±53 (21±8)	32±16 (5±2)
Capsule	821±451 (25±17)	3329±2890 (133±63)	447±247 (17±8)	5789±2535 (3996±6237)
Fibrous Membrane	2229±1583 (N/A)	12554±8055 (N/A)	1524±1399 (N/A)	13234±10074 (N/A)
Blood	20±25 (0.1-1.2)	110±150 (2-6)	10±4 (0.5-1.8)	29±29 (2.9-7)

Table 4 (*Continued*)

6. Biochemical assays

Total Protein

The total protein is measured in cell lysate with DC (Detergent Compatible) Protein Assay Kit (Bio-Rad Lab, CA, USA). For lower concentrations (5-250 μg/ml) of protein, the microarray procedure is used in a microtiter format as follows:

1. Preparation of protein standard
   Rehydrate with 20ml MQ H_2O to obtain a solution of 1.5 g/l (bovine plasma gamma globulin) and dilute it with 1% Triton-X in MQ water to the range of 5-250 μg/ml
2. Preparation of working solution
   Mix 20 μl of reagent S to 1 ml of reagent A = working solution reagent A'
3. Pipette 20 μl samples and standards into 96-WP in duplicate
4. Add 10 μl working solution reagent A' into each well
5. Add 80 μl of reagent B into each well
6. 15 min later, read absorbance at 650-750 nm
7. Make a standard curve and calculate the protein concentration

Fibronectin (FN)

The FN is measured in cell lysate with a commercially available Human Fibronectin ELISA kit (Biomedical Tech Inc.) (Stoughton, MA, USA).

1. Dilute «Diluent Buffer Concentration (BT-702)» with water to a volume of 150 ml and store at 4°C before use
2. Prepare standards (2000, 500, 250, 100, 50 and 25 ng/ml) by using «the fibronectin stock solution (BT-701)»
3. Do determinations in duplicate, 2 blank, 2Bmax and 2 for each of 6 standards
4. Pipette 150 µl diluent buffer into blank and 100 µl into the Bmax wells
5. Pipette 100 µl standards, controls and unknowns wells
6. Pipette 50 µl of the fibronectin antiserum (BT-703) into all wells except blanks. Mix gently, cover with Parafilm and incubate at 37°C for 1 h
7. Add 50 µl fibronectin tracer (BT-704) to all wells, mix gently, cover with Parafilm and incubate at 37°C for 1 h
8. Dissolve PNPP (BT-706), 4 mg/ml in Diethanolamine buffer (BT-705). Prepare it before use. Put 200 µl per well
9. Aspirate all wells. Wash with diluent buffer and aspirate 3 times by multichannel washer.
10. Remove excess liquid and add 200 µl substrate solution per well, mix and incubate at 37°C for 1 h, then measure absorbance at 400-410 nm
11. The FN production is normalised by the total protein

ALP activity

1. Add 100 µl of ATP solution into 96 WP in duplicate
2. Incubate the plate at 37°C
3. Put the samples at the room temperature
4. Add 2 µl of samples to the wells containing ALP test solution for 5 minutes
5. Measure absorbance at 405 nm at 37°C
6. Calculate the ALP concentration as follows:

$$\text{ALP activity (units/L)} = \frac{\delta A \times TV \times 1000}{18.45 \times SV \times LP} = \delta A \times 2764.2$$

Where,
ALP activity: one unit of activity is defined as that amount of enzyme, which produce one µmole of *p*-nitrophenol (mw: 139.1) per minute

δA: change in absorbance per min at 450 nm (abs of 2min–initial abs)/2
TV: total sample volume (102 μl)
SV: sample volume (2 μl)
18.45: millimolar absorptivity of *p*-nitrophenol at 450 nm
LP: light path (1 cm)

7. Cell morphology

SaOS-2 cells are seeded on to each sample (10 mm^2) at 2,000 cells/ml in 24-well tissue culture plates for 24 hours and 7 days incubation.

1. Fix cells with 1% glutaraldehyde (Sigma) in PBS in 24-well plates for 10 minutes and then wash by PBS three times. Do not let cell dry
2. Treat with 1% Triton X-100 to soften the cell membrane, then wash by PBS three times
3. Put samples into 2 mg/ml sodium borohydride ($NaBH_4$, Sigma) in PBS (prepare $NaBH_4$ before using) for 5 – 10 minutes twice
4. Shake well plates to remove bubble and wash by PBS to remove bubble
5. Stain cells (actin microfilaments) with 4 μg/ml rhodamin-phalloidin (Sigma) for 20 minutes (see figure)
6. A Nikon Eclipse TE300 inverted epifluorescence microscope enabled cells to be visualised. A Standard filter set (510 nm) was used for rhodamin-phalloidin. Images were captured using a Micromax PB1300 cool CCD camera (Roper Scientific, Trenton, NJ) and a Metamorph imaging system (Universal Imaging, Westchester, PA)

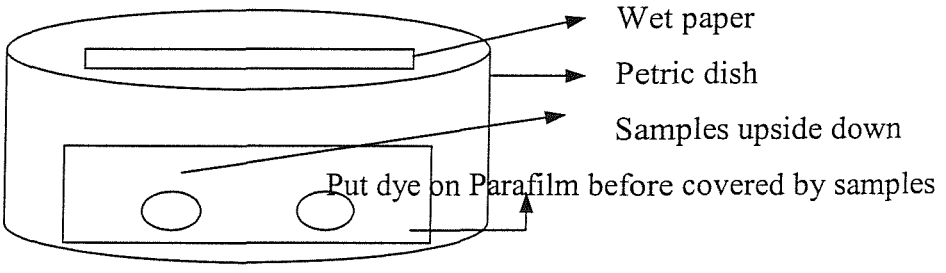

Figure 5 The staining procedure.

8. Genomic study

Experimental conditions

1. Seed 300,000 osteoblasts on each sample, C, P, A samples
2. Repeat 6 times each sample
3. At 24, 48 and 120 hours for C, P, A samples + collect 1 sample at T_0 (4 hours) for A as a standard
4. Collect cells by trysinisation
5. Spin down, discard supernatant
6. Resuspend the cells in 1 ml PBS at 37°C, vortex
7. Spin down, discard supernatant
8. Resuspend the cells in 250 µl PBS at 37°C, vortex
9. Add 75 µl Trizol LSs
10. Freeze at –8°C before GeneFilter analysis

GeneFilter analysis

The GeneFilter protocol is settled up by "Centre for AIDS Research, UCSA (http://genomics.ucsd.edu/genefilter_pr.html)". The following protocol is a slight modification of that suggested by the manufacturer of the GeneFilters (Research Genetics) and a full list of GeneFilter types available for purchase can be found at Research Genetics.

(A) GeneFilter Pre-hybridisation

1. If GeneFilter is new (has never been hybridized), it must first be washed in boiled 0.5% SDS for 5 minutes at room temperature. Then rinse it a few times in ddH_20
2. The filter membrane is placed in a hybridisation roller tube with the DNA side facing the interior of the tube so that the DNA is not touching the glass
3. For pre-hybridisation, the filter is placed in a hybridisation roller bottle with the spotted cDNA side facing the interior of the bottle so that the cDNA is not touching the surface. The following blocking reagents are added to the tube containing the filter: 5.0 µg Cot-1 DNA and 5 µg Poly dA in 5 ml of MicroHyb

hybridisation solution (all from Research Genetics). Pre-hybridise the GeneFilter at 42 °C for 2-3 hours; meanwhile, prepare the probe

(B) Probe Preparation

1. In a 1.5 ml microcentrifuge tube place the following
   a. 5 μg total RNA suspended in 8.0 μl DEPC-treated water
   b. 2.0 μl Oligo dT (1 μg/μl 10-20 per mixture)
2. Heat at 70 °C for 10 minutes and briefly chill on ice
3. Add 6 μl 5X First Strand Buffer (Life Technologies)
4. Add 1 μl 0.1M DTT
5. Add 1.5 μl dNTP mixture containing dATP, dGTP, dTTP at 20 mM
6. Add 1.5 μl Reverse Transcriptase
7. Add 10 μl ^{33}P-dCTP (Amersham, 10 mCi/ml)
8. Incubate for 2-3 hours at 42 °C in a water bath

(C) Purify the probe by passage through a Bio-Spin 6 Chromatography Column (BioRad)

1. QS the probe to 100 μl with water
2. Pass the probe through the column (devoid of buffer) three times, each time adding the probe back to the top of the column and IEC centrifuging at 1000 x g at room temp

(D) Quantify ^{33}P incorporated by measuring 1 μl of purified probe in 5 ml LS fluid (total should be approximately 1.0 x 108 cpms). Denature the purified probe for 3 minutes in a heating block at 100°C. Pipette the entire probe into the roller bottle containing the GeneFilter membrane and the prehybridisation solution

Hybridise overnight at 42 °C in a hybridisation oven (such as that from Hybaid, Inc.) at 5-7 rpm.

(E) Wash the Filter

The washes are done twice at 50 °C in 2X SSC, 1% SDS for 20 minutes and once at room temperature in 0.5X SSC, 1% SDS for 15 minutes. The radioactivity of the filter should be monitored in between washes to avoid washing away the signal completely. Using a Geiger counter, monitor the cpms and don't wash signal below 3000 cpms.

(F) Expose GeneFilter to Phosphorscreen

The GeneFilter is wrapped in plastic and placed in a phosphorimager cassette overnight (approximately 16 hours) and scanned at 50 micron resolution using a Storm 680 Phosphoimager.

(G) Analysis and Stripping

The resulting image is imported in to Pathways image analysis software and normalisation is performed according to the manufacturer's (Research Genetics) procedure.

(H) Stripping the GeneFilter of Probe

The membrane is stripped on a horizontal shaker in boiled 1% SDS several times until no signal is detected by Geiger counter. The GeneFilter can then be reused up to 5 times.

DNA microarray technology [9] [10]

A microarray is a glass slide, onto which single-stranded DNA molecules are attached at fixed locations (spots). There may be tens of thousands of spots on an array, each related to a single gene. Microarrays exploit the preferential binding of complementary single-stranded nucleic acid sequences. There are several variations of microarray technologies each used in a specific way. One of the most common experimental platforms is used for comparing mRNA abundance in two different samples (or a sample and a control). RNA from the sample and control extracted and labelled with two different fluorescent labels, e.g. red dye for the RNA from the sample population and a green dye for that from the control population. Both extracts are washed over the microarray. Gene sequences from the extracts hybridise to their complementary sequences in the spots. A laser is used to excite the array and measure the relative abundance of the hybridised RNA. If the RNA from the sample population is in abundance, the spot is red. If the RNA from the control population is in abundance, the spot is green. If sample and control bind equally, the spot is yellow, while if neither binds, it is not fluoresce and appear black. Thus, from the fluorescence intensities and colours for each spot, the relative expression levels of the genes in the sample and control populations can be estimated.

Gene expression data analysis

The following spreadsheet (Table 5) is the description of one gene from the raw data (database in http://array.sdsc.edu). The samples are A4h, A24h (failed), A48h and A120h, C24h, C48h, and C120h and finally P24h, P48h and P120h. The average difference values correspond to the level of mRNA. Negative values should be considered to be zero. Average difference values of 25 or more are believable. The absolute call stand for P: present, A: absent and M: marginal. Obviously P is believable. For most microarray technology platforms only the ratio of the backgroup-subtracted signals of the given sample and the control is meaningful (please see *Tables 5-2 and 5-3*). If the spot intensity is low, the ratio of these numbers may be high, but the measurement may not be reliable [9].

Table 5 The spreadsheet of genomic study

acc	Y08200 (**accession code**)
Description	Y08200 /FEATURE= /DEFINITION=HSRABGTRA Homo sapiens mRNA for rab geranylgeranyl transferase, alpha-subunit
a2_4h_ad	4229 (**average difference value**)
a2_4h_ac	P (**the absolute call: present**)
a2_48h_ad	3353
a2_48h_ac	M (**marginal**)
a2_120h_ad	3646
a2_120h_ac	A (**absent**)
p2_24h_ad	3944
p2_24h_ac	A
p2_48h_ad	3550
p2_48h_ac	A
p2_120h_ad	3712
p2_120h_ac	A
ca2_24h_ad	3532
ca2_24h_ac	P
cb2_24h_ad	3323
cb2_24h_ac	A
c2_48h_ad	4236
c2_48h_ac	P
c2_120h_ad	4227
c2_120h_ac	P

The useful websites for genomic study [11]

1. Online Mendelian Inheritance in Man (OMIM) 1999 OMIM, National Center for Biotechnology Information, National Library of Medicine. http://www.ncbi.nlm.nih.gov/Omim.

   OMIM, containing over 10,000 entries, offers textual and reference information on human genes and genetic disorders as well as fostering links to the Entrez database of the NCBI, thereby providing access to Medline articles and sequence information.
2. National Center for Biotechnology Information (NCBI) 1999 PubMed. NCBI, National Library of Medicine. http://www.ncbi.nlm.gov/PubMed.
3. National Center for Biotechnology Information (NCBI) 1999 Unigene. NCBI, National Library of Medicine. http://www.ncbi.nlm.gov/web/Unigene.

   The Unigene system is designed to gather clusters containing sequences of well-characterised genes novel ESTs representing newly discovered genes. It also gives information on chromosomal localisation of a specific gene or EST and its tissue expression.
4. National Center for Biotechnology Information (NCBI) 1999 LocusLink. NCMI, National Library of Medicine. http://www.ncbi.nlm.nih.gov/LocusLink. LocusLink provides information about genetic loci, official nomenclature, aliases, sequences accession, phenotypes, map information, and related web sites.
5. Weizmann Institute (WI) 1999 Genecard. Weizmann Institute of Genome and Bioinformatics. http://bioinformatics.weizmann.ac.il/cards.
6. EMBL 1999 Swiss-Prot. Outstation European Bioinformatics Institue. http://www.ebi.ac.uk/Swiss-Prot.
7. National Center for Biotechnology Information (NCBI) 1998 Entrez. NCBI, National Library of Medicine. http://ncbi.nlm.gov/Entrez.
8. National Center for Biotechnology Information (NCBI) 1999 dbEST. NCBI, National Library of Medicine. http://www.ncbi.nlm.nih.gov/dbEST/dbEST summary html.

9. The mechanisms of apoptosis: ICE-like proteases (caspases) dependent pathways vs ICE-like proteases independent pathways

Given the variety of key events in apoptosis, it has been shown that several signals or mechanisms are involved in a cell's apoptotic machinery, such as Fas (=Apo1/CD95, the best characterised death receptor (surface receptor) and belongs to the TNF receptor gene family) [12] [13], Apo2L/TRAIL [13], caspase activation [14] [15], Bcl-2 family [16] [17], etc. In *Chapter 5*, a possible pathway (*Pathway 5-3*), which is a ICE-like proteases (caspases) independent pathway, may involve in apoptosis due to the existence of metal ions. In addition, there is another pathway, ICE-like proteases (caspases) dependent pathways (for example, Pathways 1, 3 and 4), may also cause apoptosis.

Surface membrane receptors binding particles → Protein tyrosine kinase and Serine/Threonine kinase → NF-κB → Releasing TNF/IL-6

(Pathway 1)

Bax → (ICE-like proteases independent pathway) → Mitochondria (↓$\Delta\Psi$, ↑ROS, DNA condensation, cytosolic vaculation, membrane permeability) → cell death

(Pathway 2 = *Pathway 5-3*)

Bcl-2 (in intracellular membrane) —⊗— (pro-apoptotic subfamilies: Bax, Bik block the anti-apoptotic function of Bcl-2) → Apaf-1 → Caspase-9 → Apoptosis

(Pathway 3)

Where,
Apaf-1: apoptotic protease activating factor
Caspase-9: CASP9, apoptosis-related cysteine protease

Fas/CD95 (death receptor in plasma membrane) → FADD (adaptor)→ Caspase-8 → Apoptosis

(Pathway 4)

Where,
CD95: Fas, TNFRSF6 (tumor necrosis factor receptor)
FADD: Fas (TNFRSF6)-associated via death domain
Caspase-8: CASP8, Mach, apoptosis-related cysteine protease

In our results, gene expressions of Fas (CD95) and Apo2L/TRAIL were not detected (supplementary information; and data not shown). It seems that these apoptosis signalling was not involved during tests, except the increased Bax expression (apoptotic member of the bcl-2 family) was observed. Even though, several investigations have demonstrated that particles[iv] strongly affect the NF-κB signalling pathway [18] [19] [20], it may be not the case for metal ions. The signal pathways could be different between particles and ions [18] [21].

Moreover, Bcl-2, anti-apoptosis can be diminished by Bax, the (over-) expression of Bax can activate Apaf-1, caspase-9 and finally cause apoptosis (Pathway 3) [16]. This is a caspase-dependent pathway. However, Apaf-1 was absent and caspase-9 was not found from our data.

Fas-induced apoptosis requires the activation of ICE-like proteases (caspases) dependent pathway (Pathway 5-5). Based on our findings, as no Fas, Apo2L/TRAIL, caspases, or IL/TNF was detected, it is then possible that the pro-apoptosis involved at 120 hours is due to the Bax expression [16]. Bax (at the protein level) may target mitochondrial membranes to induce cell death by a caspases-independent pathway. Therefore, we considered that Bax pathway (ICE-like proteases independent) is possible one to cause apoptosis due to metal ion release.

[iv] In the literature, different size particles have been used, for example, small phagocytosable size, approximately 0.5 to 3 μm in diameter and big size: 21-85 μm in diameter.

Apoptosis triggered by external signals (cells)

Apoptosis triggered by internal signals (mitochondria)

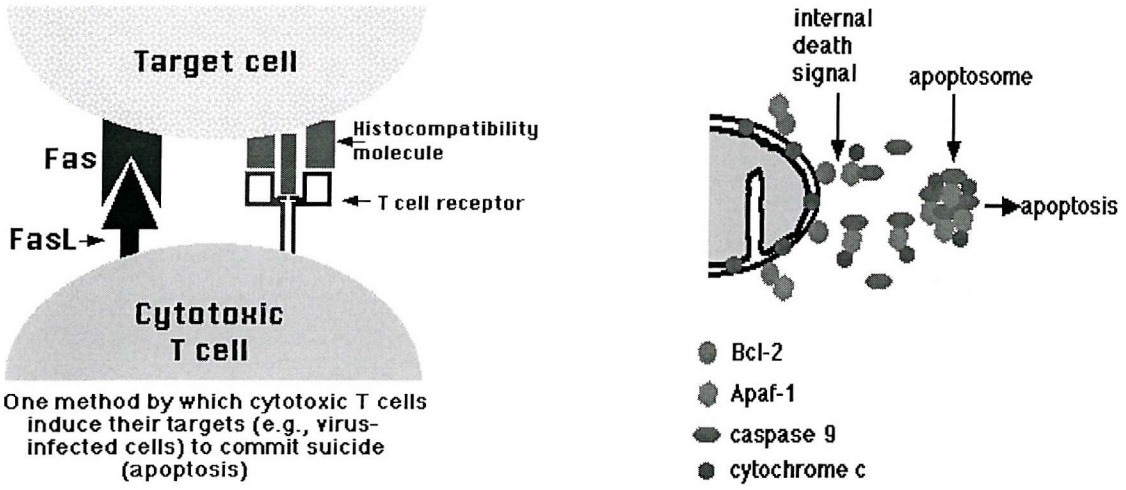

Figure 6 The mechanisms of apoptosis[v].

[v] Kimball's Biology Pages, Author: Dr. John W. Kimball.
Website: (http://www.ultranet.com/~jkimball/BiologyPages/W/Welcome.html).

10. The physical properties of (1) Ti alloys: Ti, Al, V, (2) Transition metals in metalloproteins: Cu, Fe, Zn, and (3) Metal ion channel: Ca, K, Na and Cl

(1) Ti alloys

Ti - Titanium

Atomic number	-	22	Density	g/ml	4.5
Atomic weight	u	47.9	Melting point	K	1943
Bonding radius	Å	1.32	Boiling point	K	3562
Atomic radius	Å	2	Heat of vaporization	kJ/mol	421
Ionisation Potential	V	6.82	Heat of fusion	kJ/mol	15.45
Electronegativity	-	1.54	Specific heat	J/gK	0.52
Electrical conductivity		0.024	Thermal conductivity		--
The oxide is amphoteric			Crystal are hexagonal		
Electron configuration: [Ar] $3d^2$ $4s^2$					

Al – Aluminum

Atomic number	-	13	Density	g/ml	2.7
Atomic weight	u	26.98154	Melting point	K	933.25
Bonding radius	Å	1.18	Boiling point	K	2740
Atomic radius	Å	1.82	Heat of vaporization	kJ/mol	293.4
Ionisation Potential	V	5.986	Heat of fusion	kJ/mol	10.79
Electronegativity	-	1.61	Specific heat	J/gK	0.9
Electrical conductivity		0.382	Thermal conductivity		0.5
The oxide is amphoteric			Crystal are face centred cubic		
Electron configuration: [Ne] 3s2 3p1					

V - Vanadium

Atomic number	-	23	Density	g/ml	5.8
Atomic weight	u	50.9415	Melting point	K	2175
Bonding radius	Å	.22	Boiling point	K	3682
Atomic radius	Å	1.92	Heat of vaporization	kJ/mol	447.02
Ionisation Potential	V	6.74	Heat of fusion	kJ/mol	20.9
Electronegativity	-	1.63	Specific heat	J/gK	0.49
Electrical conductivity		0.04	Thermal conductivity		--
The oxide is amphoteric.			Crystal are body centred cubic.		
Electron configuration: [Ar] $3d^3$ $4s^2$					

(2) Transition metals in metalloproteins

Cu – Copper

Atomic number	-	29	Density	g/ml	8.96
Atomic weight	u	63.546	Melting point	K	1357.6
Bonding radius	Å	1.17	Boiling point	K	2836
Atomic radius	Å	1.57	Heat of vaporization	kJ/mol	300.3
Ionisation Potential	V	7.726	Heat of fusion	kJ/mol	13.05
Electronegativity	-	1.9	Specific heat	J/gK	0.38
Electrical conductivity		0.593	Thermal conductivity		0.94
The oxide is mildly basic			Crystal are face centred cubic		
Electron configuration: [Ar] $3d^{10}$ $4s^1$					

Fe - Iron

Atomic number	-	26	Density	g/ml	7.86
Atomic weight	u	55.847	Melting point	K	1809
Bonding radius	Å	1.17	Boiling point	K	3135
Atomic radius	Å	1.72	Heat of vaporization	kJ/mol	349.6
Ionisation Potential	V	7.87	Heat of fusion	kJ/mol	13.8
Electronegativity	-	1.83	Specific heat	J/gK	0.44
Electrical conductivity		0.1	Thermal conductivity		0.18
The oxide is amphoteric			Crystal are body centred cubic		
Electron configuration: [Ar] $3d^6$ $4s^2$					

Zn - Zinc

Atomic number	-	30	Density	g/ml	7.14
Atomic weight	u	65.38	Melting point	K	692.73
Bonding radius	Å	1.25	Boiling point	K	1180
Atomic radius	Å	1.53	Heat of vaporization	kJ/mol	115.3
Ionisation Potential	V	9.394	Heat of fusion	kJ/mol	7.322
Electronegativity	-	1.65	Specific heat	J/gK	0.39
Electrical conductivity		0.167	Thermal conductivity		0.27
The oxide is amphoteric			Crystal is hexagonal		
Electron configuration: [Ar] $3d^{10}$ $4s^2$					

(3) Metal ion channel

Ca - Calcium

Atomic number	-	20	Density	g/ml	1.55
Atomic weight	u	40.08	Melting point	K	1112
Bonding radius	Å	1.74	Boiling point	K	1757
Atomic radius	Å	2.23	Heat of vaporization	kJ/mol	153.6
Ionisation Potential	V	6.113	Heat of fusion	kJ/mol	8.54
Electronegativity	-	1	Specific heat	J/gK	0.63
Electrical conductivity		0.218	Thermal conductivity		0.3
The oxide is a strong base			Crystal are face centred cubic		
Electron configuration: [Ar] $4s^2$					

K - Potassium

Atomic number	-	19	Density	g/ml	0.86
Atomic weight	u	39.0983	Melting point	K	336.35
Bonding radius	Å	2.03	Boiling point	K	1032
Atomic radius	Å	2.77	Heat of vaporization	kJ/mol	79.87
Ionisation Potential	V	4.341	Heat of fusion	kJ/mol	2.334
Electronegativity	-	0.82	Specific heat	J/gK	0.75
Electrical conductivity		0.143	Thermal conductivity		0.23
The oxide is a strong base			Crystal are body centred cubic		
Electron configuration: [Ar] $4s^1$					

Na – Sodium

Atomic number	-	11	Density	g/ml	0.97
Atomic weight	u	22.98977	Melting point	K	371
Bonding radius	Å	1.54	Boiling point	K	1156
Atomic radius	Å	2.23	Heat of vaporization	kJ/mol	96.96
Ionisation Potential	V	5.139	Heat of fusion	kJ/mol	2.598
Electronegativity	-	0.93	Specific heat	J/gK	1.23
Electrical conductivity		0.218	Thermal conductivity		0.32
The oxide is a strong base			Crystal are body centred cubic		
Electron configuration: [Ne] $3s^1$					

Cl – Chlorine

Atomic number	-	17	Density	g/ml	0.000317
Atomic weight	u	35.453	Melting point	K	172.16
Bonding radius	A	0.99	Boiling point	K	239.1
Atomic radius	A	0.97	Heat of vaporization	kJ/mol	10.2
Ionisation Potential	V	12.967	Heat of fusion	kJ/mol	3.203
Electronegativity	-	3.16	Specific heat	J/gK	0.48
Electrical conductivity		--	Thermal conductivity		2e-05
The oxide is a strong acid.			Crystals are orthorhombic.		
Electron configuration: [Ne] $3s^2$ $3p^5$					

References

1. *The electrical double layer (http://bath.ac.uk/~chsacf/sloarton/electro)*, in *Electrochemistry Refresher*, University of Bath.
2. Coultas, S., *Investigation of serum immersed surfaces using angle dependent XPS Analysis report*. 1999, CSMA Limited: Manchester, UK.
3. Campbell, P.A., et al., *Vacuum plasma sprayed hydroxyapatite coatings on titanium alloy substrates: surface characterization and observation of dissolution processes using atomic force microscopy.* J Vac Sci Technol B, 1996. **14**(2): p. 1167-72.
4. Browne, M., P.J. Gregson, and R.H. West, *Characterization of titanium alloy implant surfaces with improved dissolution resistance.* J Mater Sci Mater Med, 1996. **7**: p. 323-9.
5. Browne, M., *Surface modification of titanium alloy implants*, in *Department of Engineering Materials*. 1995, University of Southampton: Southampton, UK. p. 98.
6. Browne, M. and P.J. Gregson, *Effect of mechanical surface pretreatment on metal ion release.* Biomaterials, 2000. **21**(4): p. 385-92.
7. Einhauser, T.J., T.G. Pieper, and B.K. Keppler, *Titanium determination in human blood plasma by ICP-OES, longitudinally, and transversally heated Zeeman ETAAS.* Journal of Analytical Atomic Spectrometry, 1998. **13**(10): p. 1173-6.
8. Hirata, S., Y. Umezaki, and M. Ikeda, *Determination of Chromium(Iii), Titanium, Vanadium, Iron(Iii), and Aluminum by Inductively Coupled Plasma Atomic Emission- Spectrometry with an Online Preconcentrating Ion-Exchange Column.* Analytical Chemistry, 1986. **58**(13): p. 2602-6.
9. Brazma, A. and J. Vilo, *Gene expression data analysis.* Febs Letters, 2000. **480**(1): p. 17-24.
10. Celis, J.E., et al., *Gene expression profiling: monitoring transcription and translation products using DNA microarrays and proteomics.* Febs Letters, 2000. **480**(1): p. 2-16.
11. Ho, N.C., et al., *A skeletal gene database.* J Bone Miner Rer, 2000. **15**(11): p. 15254-64.

12. Krammer, P.H., *CD95's deadly mission in the immune system.* Nature, 2000. **407**(6805): p. 789-95.
13. Ashkenazi, A. and V.M. Dixit, *Death receptors: Signaling and modulation.* Science, 1998. **281**(5381): p. 1305-8.
14. Green, D.R. and J.C. Reed, *Mitochondria and apoptosis.* Science, 1998. **281**(5381): p. 1309-12.
15. Wei, M.C., et al., *Proapoptotic BAX and BAK: A requisite gateway to mitochondrial dysfunction and death.* Science, 2001. **292**(5517): p. 727-30.
16. Adams, J.M. and S. Cory, *The Bcl-2 protein family: Arbiters of cell survival.* Science, 1998. **281**(5381): p. 1322-6.
17. Hengartner, M.O., *The biochemistry of apoptosis.* Nature, 2000. **407**(6805): p. 770-6.
18. Vermes, C., et al., *Particulate wear debris activates protein tyrosine kinases and nuclear factor kappa Beta, which down-regulates type I collagen synthesis in human osteoblasts.* Journal of Bone and Mineral Research, 2000. **15**(9): p. 1756-65.
19. Nakashima, Y., et al., *Signaling pathways for tumor necrosis factor-alpha and interleukin-6 expression in human macrophages exposed to titanium-alloy particulate debris in vitro.* Journal of Bone and Joint Surgery-American Volume, 1999. **81A**(5): p. 603-15.
20. Roebuck, K.A., et al., *Down-regulation of procollagen alpha1[I]] messenger RNA by titanium particles correlates with nuclear factor kappaB (NF-kappaB) activation and increased rel A and NF-kappaB1 binding to the collagen promoter.* J Bone Miner Res, 2001. **16**(3): p. 501-10.
21. Archibeck, M.J., et al., *The basic science of periprosthetic osteolysis.* Journal of Bone and Joint Surgery-American Volume, 2000. **82A**(10): p. 1478-89.